Factors impacting tissue compliance in the human left atrium and its effect on radiofrequency ablation success.

Rebecca Jane Norton

Submitted in fulfilment of the requirements of the Degree

Queen Mary, University of London

First iteration September 2018

Updated May 2022

An EPSRC Engineering and Physical Sciences Research Council supported project

Statement of Originality

I, Rebecca Norton, confirm that the research included within this thesis is my own work or that where it has been carried out in collaboration with, or supported by others, that this is duly acknowledged below and my contribution indicated. Previously published material is also acknowledged below.

I attest that I have exercised reasonable care to ensure that the work is original, and does not to the best of my knowledge break any UK law, infringe any third party's copyright or other Intellectual Property Right, or contain any confidential material.

I accept that the College has the right to use plagiarism detection software to check the electronic version of the thesis.

I confirm that this thesis has not been previously submitted for the award of a degree by this or any other university.

Signature:

Date: 22 May 2022

Acknowledgements

To say completing this PhD has been challenging, would be the understatement of the century!

I was asked during it if I could be proud of what I have done, it may not be perfect but what research ever is however I can honestly say that I am proud of what I have done. To submit this thesis against all odds is one of the happiest moments of my life.

During this time the world has changed in ways that no one could ever of imagined and I can look back and say I have been right in the thick of it. Alongside preparing this thesis for submission I have also worked in ITU, I worked the night of the Westminster attack, during the Grenfell Tower disaster, the London bridge/borough market attack and most recently the COVID-19 pandemic. I have seen things that no one should ever have to see that will remain with me for as long as I shall live. I have looked after friends and colleagues as well as patients, something that no one should ever have to do. Except there was no-one else!

The reason I initially applied to be a part of this research project was because of its impact on the population, not only due to it being the most commonly sustained cardiac arrythmia but that it hugely increases the risk of debilitating morbidities such as stokes. I had not been directly affected by any of the morbidities caused by Atrial fibrillation but I had looked after numerous patients who had and wanted to play a part in trying to reduce this risk, however small that may be. Whilst in London carrying out my research that all changed, first my Grandfather had a stroke, then my farther had two strokes, followed by my father in Law. These events made me even more determined to complete my research.

No matter how determined or how strong I appeared on the outside all of these events were taking their toll and completing this PhD seemed more and more impossible. It may have taken longer than I intended however it has now been submitted, that is why I am extremely proud. This could not of been done without the help and support every step of the way from my supervisor, Hazel Screen.

She has seen me at my worst and shown me that no matter what things are not always as bad as they seem. To her I owe everything, thank you Hazel.

I would to thank my other supervisors, Ross Hunter and Wen Wang, for their guidance and faith in my abilities. I could not have asked for more dedicated supervisors, whose support has allowed me to develop as a researcher. Their enthusiasm, depth of knowledge and ability to stay on top of things despite their busy schedules never ceases to amaze me. They are my inspiration.

I would like to thank the Engineering and Physical Sciences Research Council for funding this research project and thank all the collaborators involved. Thank you to the electrophysiology laboratory team at St Bartholomew's Hospital who were exceptionally helpful during my research cases, namely Waqas Ullah and Shohreh Honarbakhsh for your guidance and assistance and most importantly I would like to thank the patients who very generously consented to participate in my research.

I would also like to thank the engineering team at Queen Mary University, namely Chris Mole, Douge Thomson, Dennis Ife, Roger Nelson and Dan Neighbour, without their guidance it would have been near on impossible to complete the engineering section of this project.

I would also like to acknowledge all my friends and colleagues at Queen Mary, University of London, who made each day at Queen Mary an enjoyable experience. A big thank you also goes to all of my friends and colleagues not at Queen Mary, those at Mile End Climbing Wall, who have been understanding and supportive during this crazy period of my life, and to Camilla Cullen, for making this PhD look incredible. Thank you all for keeping me sane!

Finally, I would like to dedicate this thesis to family for their constant love and support. I will forever be grateful.

Abstract

Atrial fibrillation (AF), synchronized atrial contraction in lost decreasing cardiac output and increasing atrial pressure and is thought to be associated with low left atrial (LA) compliance. Management of AF is through the permanent destruction of abnormal cardiac tissue responsible for cardiac arrhythmogenesis, whilst avoiding collateral tissue injury forms the cornerstone of catheter ablation therapy. Although the acceptance and performance of catheter ablation has increased worldwide, there is still a relatively low success rate of 70% for first-time AF ablation.

Atrial compliance allows the atria to react in response to homeostatic change as well as atrial fibrillation being associated with low compliance (so is ablation) with more extensive ablations with more touches though to reduce LA compliance.

It is unclear what clinical implications LA compliance has on patients who underwent radiofrequency catheter ablation, although several attempts have been made to measure compliance of the left atrium each of these have had their limitations.

The hypothesis of this thesis was that AF, a multifactorial disease associated with degenerative disease, may contribute to reduced LA compliance.

There have been several ways to estimate compliance in the past each with their limitations. This thesis aims to determine a suitable measure of compliance from data collected from patients with both paroxysmal and persistent atrial fibrillation as standard as part of the radiofrequency ablation procedure. Once a suitable measure for compliance was determined, to preliminary test this measure in a small pilot study to determine factors that could reduce compliance. Finally, in the same cohort of patients begin to explore the impact of fibrosis through voltage on the measure of compliance calculated.

Additionally, an attempt will be made to develop a mechanical tissue measurement rig in order to recreate force measurements used as part of the compliance measure ex-vivo, for an in-depth look at the variability in mechanical properties of left atrial tissue in porcine atria.

List of Tables

List of Figures

List of Abbreviations

2D-ST	Two-dimensional speckle-tracking imaging
3D	Three-dimensional
ABL	Ablation
ACL	Advanced Catheter location
AF	Atrial Fibrillation
AFCL	Atrial Fibrillation Cycle Length
AFFIRM	Atrial Fibrillation Follow-Up Investigation of Rhythm Management
Ang II	Angiotensin II
ANP	Atrial Natriuretic Peptide
ANS	Autonomic Nervous System
Ao	Aorta
AP	Action Potential
AP-1	Activator protein-1
APD	Action Potential Duration
AT	Atrial Tachycardia
AV	Atrioventricular Node
AW	Anterior Wall
BCS	Body Coordinate System
beta-AR	norepinephrine activates beta-adrenoceptors
Ca2+	Calcium
CaMKII	Calmodulin-dependant protein kinase II
CCI	Charlston Comorbidity index
CF	Contact Force
CFs	Cardiac Fibroblasts
CMs	Cardiomyocytes

CS	Coronary Sinus
CSQ	Calsequestrin
CTGF	Connective tissue growth factor
DADs	Delayed after depolarizations
DAG	Diacylglycerol
DECAAF	Delayed Enhancement– MRI determinant of successful Catheter Ablation of Atrial Fibrillation
DE-MRI	Delayed Enhancement Magnetic Resonance Imaging
EA	Electroanatomical
EADs	Early After Depolarisations
EAM	Electroanatomical Mapping
ECG	Electrocardiogram
ECM	Extracellular Matrix
ECS	Elixhauser Comorbidity Score
EGM	Electrogram
Endo Cs/IW	Combined Coronary Sinus & Inferior Wall
EP	Electrophysiology
ERK 1/2	Extracellular signal-related kinase 1/2
ERP	Effective Refractory Period
ETI	Electrode Tissue Interface
FAM	Fast Anatomical Mapping
Frc	Force Tag
GP	Ganglionic Plexi
Grb2	Growth factor receptor binding protein 2
HB	His bundle
HF	Heart Failure
HR	Heart Rate
IAS	Interatrial Septum

IC	Intracardiac
ICa,L	L-type calcium current
IK,ACh	Acetylcholine-activated inward-rectifier potassium current
Ik1	Inward rectifying potassium currents
IK2P	Two-pore domain potassium current
IKs	Slow delayed rectifier potassium current
Ikur	Ultrarapid delayed rectified potassium current
INCX	Sodium-calcium-exchanger type 1 current
IP3	Inositol 1,4,5-trisphosphate
Ito	Transient-outward potassium current
IVC	Inferior Vena Canae
IW	Inferior Wall
JAK	Janus kinase
JNK	c-Jun N-terminal kinase
LA	Left Atrium
LAA	Left atrial appendage
LAAC	Left Atrial Appendage Closure
LAP	Left Atrial Pressure
Lapp	Left atrial pulse pressure
LAW	Left atrial wall
LIPV	Left Inferior Pulmonary Vein
LLR	Left Lateral Ridge
LLW	Left Lateral Wall
LPV	Left Pulmonary Vein
LSPV	Left Superior Pulmonary Vein
LV	Left Ventricle
LVEF	Left Ventricular Ejection Fraction
MAPK	Mitogen-activated protein kinase

MEK 1/2	Mitogen-activated/ERK kinase 1/2
MI	Myocardial Infarction
MMP	Matrix metalloproteinase
MRI	Magnetic Resonance Imaging
MV	Mitral Valve
MVI	Mitral value Isthmus
NF-κB	Nuclear factor-κB
NHS	National Health Service
PA	Pulmonary Artery
PAF	Paroxysmal Atrial Fibrillation
PBS	Phosphate buffered saline solution
PDGF	Platelet-derived growth factor
PDGFR	PDGF receptor
PeAF	Persistent Atrial Fibrillation
PIP2	Phosphatidylinositol bisphosphate
PKC	Protein kinase C
PLB	Phospholamban
PLC	Phospholipase C
PP2A	Protein serine/threonine phosphatase 2A
PT	Pulmonary Trunk
PTP	Phosphotyrosine phosphatase
PV	Pulmonary Vein
PVI	Pulmonary Vein Isolation
PW	Posterior Wall
QoL	Quality of Life
RA	Right Atrium
RAA	Right atrial appendage
RAAS	Renin–angiotensin–aldosterone system

RACE	Rate Control and Rhythm Control in Patients with recurrent persistent atrial fibrillation
RAFW	Right atrial free wall
RAS	Right atrial septum
RCFA	Radiofrequency catheter ablation
RECK	Reversion-inducing cysteine-rich protein
RF	Radiofrequency
RFCA	Radiofrequency catheter ablation
RIPV	Right Inferior Pulmonary Vein
RLW	Right Lateral Wall
RPV	Right Pulmonary Vein
RRN	Remote Robotic Navigation
RSPV	Right Superior Pulmonary Vein
RV	Right Ventricle
RyR2	Type-2 Ryanodine Receptor
S	Strain
SA	Sinoatrial Node
SEC	Spontaneous Echo Contract
SERCA2a	Sarcoplasmic Reticulum Calcium-ATPase 2a
Shc	src homologous and collagen protein
SMAD	SMA- and MAD-related proteins;
SOS	Son of sevenless protein
SR	Sinus Rhythm
SR	Sarcoplasmic Reticulum
Srate	Strain Rate
STAT	Signal transducers and activators of transcription
SVC	Superior Vena Cavae
TAK1	TGF-β1–activated kinase 1
TF	Transcription factor

TGF-β1	Transforming growth factor-β1
TGF-βR	TGF-β receptor
TIMP	Tissue inhibitor of matrix metalloproteinase.
TOCCATA	Touch+™ for Catheter Ablation
TV	Tricuspid Valve
WACA	Wide Area Circumferential Ablations
WL	wavelength
αβ	Integrin receptor α- and β-subunits
ΔP	Change in pressure
ΔV	Change in volume

Chapter 1:

Introduction

Atrial Fibrillation

Background

Atrial fibrillation (AF) is the most commonly sustained cardiac arrhythmia [1] contributing to the mortality, morbidity, and reduced quality of life of millions of individuals [1] [2]. One large population-based study [3] estimated that around one in four Europeans have a lifetime risk of developing AF with 100,000 to 200,000 people, specifically in the UK, risk developing AF every 12 months [4]. For most people affected AF can be described as a chronic disease that begins with sporadic short-lasting episodes (a recurrence of ≥2) of an irregular and often abnormally fast heart rate. This is the result of chaotic atrial cell depolarization causing a loss of organised atrial contractile function and asymmetrical ventricular rates that for most spontaneously convert back to normal sinus rhythm within 7 days (paroxysmal AF) [5]. In this study the continuous monitoring results of over 13,000 individuals diagnosed with paroxysmal AF were reviewed and found to have significant variability in the frequency, duration, and timing of paroxysmal AF episodes [5]. A recent study found that the most common patient-reported triggers of AF are alcohol, caffeine, exercise, lack of sleep [6]. Some symptomatic patients go on to develop persistent AF whereby the episodes of paroxysmal AF become progressively longer-lasting and more stable. These may require electrical or pharmacological cardioversion to restore normal heart rhythm. If this continues to progress the success rate of rhythm-control therapy reduces eventually resulting in therapy-resistant permeant AF. This is not always the case though. The progression of AF is variable with one systematic review finding that out of over 27,000 patients less than 10 patients progressed to permanent AF [7], with another finding that some patients even regressed over time [8].

In the majority of patients AF is a manifestation of atrial remodelling [9] also known as atrial cardiomyopathy produced by a wide range of comorbidities and risk factors. Recognised AF-promoting factors include: advancing age with a number of studies suggesting less than 1% of individuals under the age of 60 are affected, increasing to 10% of individuals over the age of 80 [10]

[11] [12], heart failure (HF), hypertension, and valvular heart disease, especially mitral valve dysfunction [13]. Gender is also thought to have an effect on an individual's likelihood of developing AF [14] [4]. The incidence of atrial fibrillation was found to be greater in men than in women, however this difference was reduced with advancing age. Women with AF over the age of 75 had an increased risk of an embolism and long-term mortality [15]. Although this sample consisted of a primarily Western Caucasian cohort, additional work conducted in a multi-ethnic population in Birmingham, England found that there was a similar risk of developing AF across the globe [16]. There is increasing awareness about obesity and metabolic syndrome, alcohol consumption, sleep apnea, and endurance exercise emerging as potential risk factors of AF [13]. With the list of potential AF risk factors ever increasing it is no surprise that fewer and fewer patients are considered to have lone AF [17].Previous work has shown that in idiopathic AF patients, where no one heart disease can be documented by clinical examination or by laboratory investigations often develop cardiovascular disease at a younger age, with a more severe disease profile compared with healthy sinus rhythm-control patients, suggesting the presences of comorbidities [18]. A recent retrospective study of AF patients with the mean age 46 years found that only 11% of patients were free of AF risk factors or comorbidities, whereas 44% had hypertension and 25% had a family history of AF [19].

The prevalence of AF is expected to increase significantly over the upcoming years, with NHS England forecasting that the incident rate could so much as double over the next 25 years [12] as a result of an ageing population and an increased longevity resulting from improved medical care for the ever-growing list of risk factors including chronic cardiac conditions which predispose AF [20]. AF is not only a danger to our health but is a huge expenditure for the National Health Service (NHS) [12], with one report estimating that approximately 1% of all NHS expenditures are the result of AF [21]. In 2008, the Office of Health Economics estimated that the direct cost of atrial fibrillation was over £2.2 billion each year [12]. It emphasised that 5.7 million bed delays that year were as a direct result of primary or secondary diagnosis of AF, setting the NHS back £1,873 million, with a further

£205 million spent on outpatient costs (electrocardiograms, monitoring anti-coagulant treatment, and post-discharge attendance), and £124 million on other inpatient costs [12].

Mechanisms of Atrial Fibrillation

Molecular and Cellular Overview

In atrial fibrillation (AF), the normal regular impulses generated by the sinoatrial node in the right atrium of the heart are overwhelmed by disorganised ectopic/triggered electrical impulses, which usually originate in the roots of the pulmonary veins (PVs). Although the exact cause of AF is often unclear, there are a number of different pathophysiological processes thought to promote atrial fibrillation (AF), below is an overview of these (Figure 1).

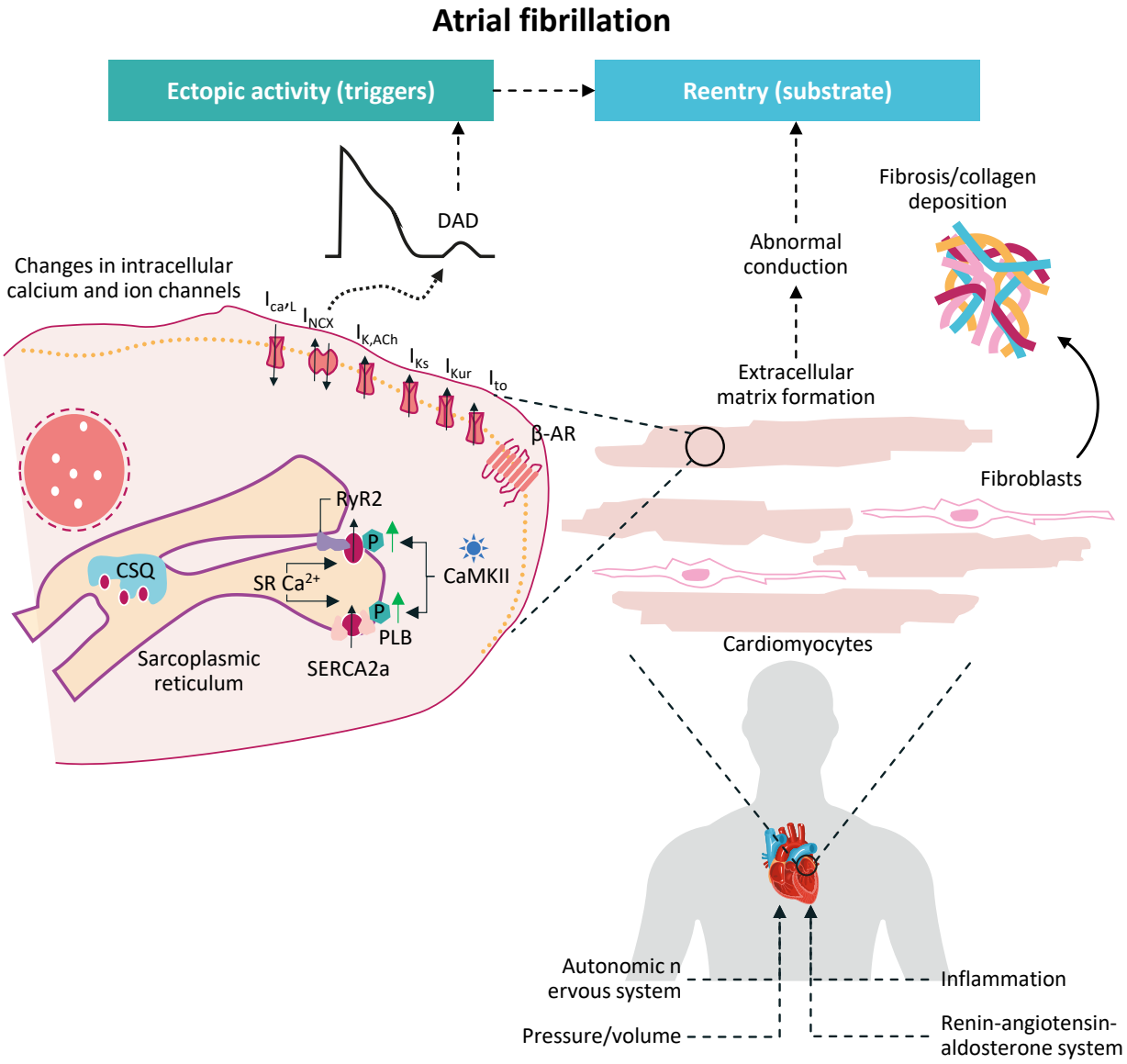

Figure 1: Major pathophysiological mechanisms underlying AF - promoting ectopic activity and reentry. Intracellular calcium changes in the sarcoplasmic reticulum (SR) occur due to phosphorylation [by calcium-/calmodulin-dependant protein kinase II (CaMKII)] of important calcium-handling proteins, such as the SR calcium-ATPase 2a (SERCA2a) and the type-2 ryanodine receptor (RyR2), which are regulated by numerous proteins, including calsequestrin (CSQ) and phospholamban (PLB). Together with mechanisms involving several ion currents, including the acetylcholine-activated inward-rectifier potassium current (IK,ACh), the transient-outward potassium current (Ito), the ultrarapid delayed rectified potassium current (IKur), the slow delayed rectifier potassium current (IKs), the L-type calcium current (ICa,L), and the sodium-calcium-exchanger type 1 current (INCX), these intracellular calcium changes contribute to delayed afterdepolarizations (DADs), ectopic activity, and reentry. During stimulation of the autonomic nervous system (ANS), norepinephrine activates beta-adrenoceptors (beta-AR), which regulate several cellular mechanisms. Fibroblasts contribute to extracellular matrix formation by fibrosis and collagen deposition creating a substrate for reentry. Both mechanisms are modulated by ANS dysfunction, inflammation, pressure/volume changes, and activation of the renin/angiotensin/aldosterone system. Adapted *from [22]*

Ectopic/triggered activity refers to impulses that form outside of the sinoatrial node, usually originating in the roots of the pulmonary vein, these are disorganised impulses overwhelm those normally generated by the sinoatrial node. This ectopic activity can result from abnormal automaticity and early or delayed afterdepolarizations (EADs and DADs, respectively). EADs are helped by excessive prolongation of repolarization duration, which allows for the L-type calcium channels to recover from their initial inactivation and produce a secondary depolarization during the action potential (AP). Ectopic activity only occurs when the depolarization is sufficiently strong to activate the neighbouring cardiomyocytes. Ectopic/triggered activity can result in unidirectional block and initiate reentry. Reentry is deemed to be the predominate AF-maintaining mechanism and refers to the continuous self-excitation of cardiac tissue. There are many forms of reentry that have previously been discussed such as, anatomical reentry localised around a fixed substrate as well as functional reentry, which can be stable or meander through the tissue. Most forms of reentry tend to be promoted by a short and/or heterogeneous effective refractory period (ERP) [23] and slow, heterogeneous conduction. Previous animal models have shown that, the complexity of electrical activity in more advanced forms of AF increases with electrical as well as structural remodelling and that this to some extent is as a result of AF itself [24]. Moreover, the more recent computational works of Gharaviri et al. [25] modelled the complex three-dimensional nature of reentry in AF, with increased epicardial fibrosis resulting in increased epi-/endocardial dissociation, epicardial breakthroughs, and AF complexity.

Although the exact cause of AF is often unclear, for many years three major hypotheses have been proposed: multiple random propagating wavelets, focal electrical discharges and localised re-entry activity with fibrillary conductance [26] [27] [28] [29].

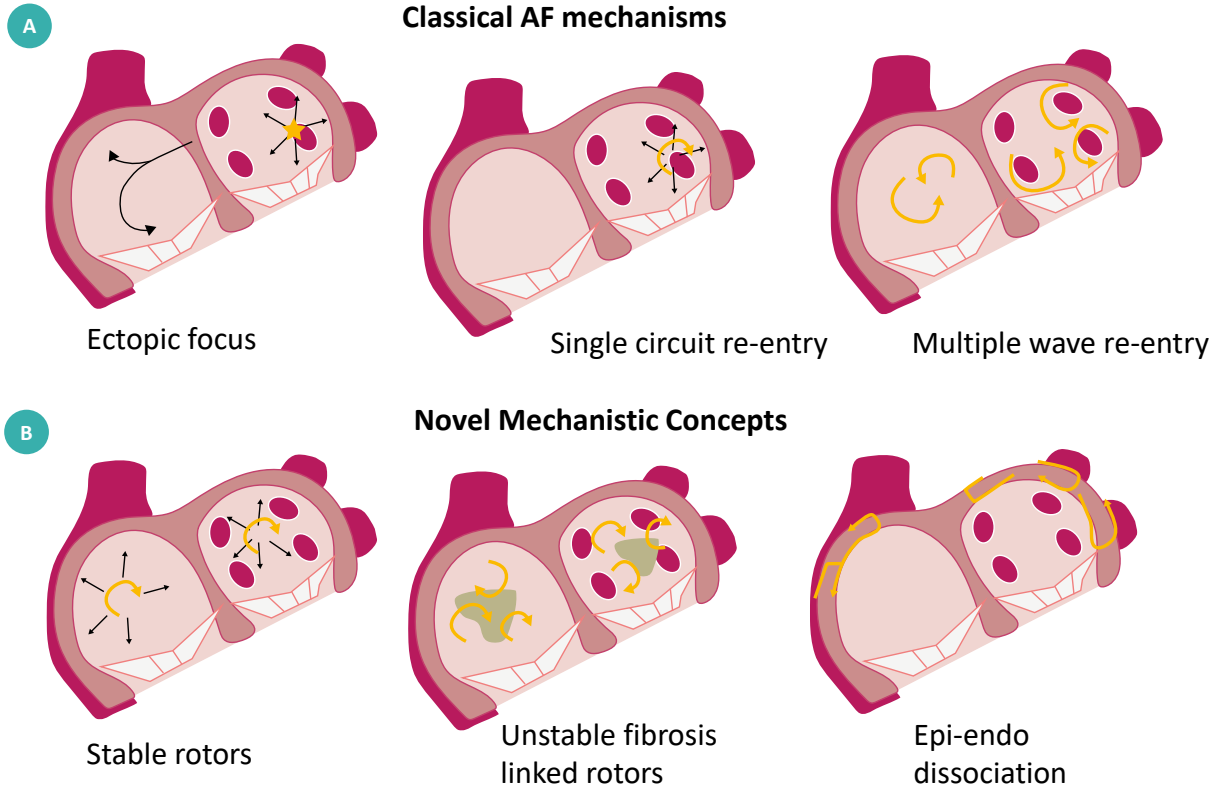

Figure 2: Mechanisms of AF. A) Classical AF mechanisms including: (a) initiation from an ectopic focus; (b) automatic or triggered activity, single circuit re-entry and (c) multiple wavelet re-entry. B) More recently proposed AF mechanisms including: (a) stable rotors; (b) unstable fibrosis-linked rotors (with areas of fibrosis shown in grey) and (c) epicardial-endocardial dissociation. Adapted from [22].

Multiple Wavelet Hypothesis

Developed by Moe et al, the multiple wavelength hypothesis was widely accepted as the dominant AF mechanism until the late 1980s [30]. According to this hypothesis, AF results from the presence of multiple independent wavelets occurring simultaneously and propagating randomly throughout the left and right atria. This model suggests that the number of wavelengths at any point in time depends on atrial conductance velocity, refractory period, and excitable mass. Continuation of AF requires the presence of a multiple independent wavelets (more than 20), support of this statement came in the form of the surgical maze procedure, whereby atria that had been severely ablated causing them to become compartmentalised were unable to sustain multiple, randomly propagating wavelets [31].

This made the multiple wavelet hypothesis the most widely accepted by clinical electrophysiologists, preferential to slowed conductance, shortened refractory periods, and increased atrial mass. Greater spatial dispersion of refractoriness stimulates continuation of AF by heterogeneous conduction delay and block. Experimental and clinical results suggest however, that although sustained AF may occur by randomly propagating wavelets in some cases, atrial refractory periods and cycle lengths do not seem to distribute randomly. Morillo et al. demonstrated this in their experiment on canine atria, in which they found that the atrial fibrillation cycle length (AFCL) was significantly shorter in the left atrium (LA) compared to the right atrium (RA), and an area in the posterior LA was consistently found to have a shorter AFCL [32]. These results were later confirmed by the work of van Loon et al. on equine atria [33].

Focal Triggers Hypothesis

Haissaguerre et al. observed that AF is often triggered by a focal source and that ablation of that source can eliminate AF [34] [35] [36]. In 1994 three patients successfully underwent one of the first catheter ablation procedures targeting AF [34]. In each of the three patients, AF was determined to arise from a “focal source”. The successful treatment of these three patients with catheter ablation suggests that in some patients, AF may result from a focal trigger and that ablation of that trigger could eliminate AF. Previous work in animal models supported this, demonstrating that AF could be induced by local administration of aconitine (an alkaloid from the root of aconitum plants that activates voltage-gated sodium channels) that triggered a rapid focal atrial tachycardia (AT) [37]. This type of “focal AF” was also reverted into normal sinus rhythm by isolation of the site of aconitine-induced focal AT from the remainder of the atria. In a subsequent report of 45 patients with frequent drug-refractory episodes of AF, Haissaguerre et al. found that a purely right-sided linear ablation approach resulted in an extremely low long-term success rate [38]. They also found that linear lesions were often arrhythmogenic due to gaps in the ablation lines, and that many patients were ultimately reverted back to normal sinus rhythm with ablation of a single rapidly firing ectopic

focus. These ectopic foci were located at the orifices of the left or right superior pulmonary veins (PVs) or near the superior vena cava (SVC) (Figure 2 and Figure 3) The latter observation led them to systematically attempt to revert paroxysmal AF back to normal sinus rhythm by mapping and ablating individual foci of ectopic activity [34] [35] [36]. Others have confirmed the importance of a focal trigger in the development of AF, and it is now established that the PVs appear to be a crucial trigger that initiate AF.

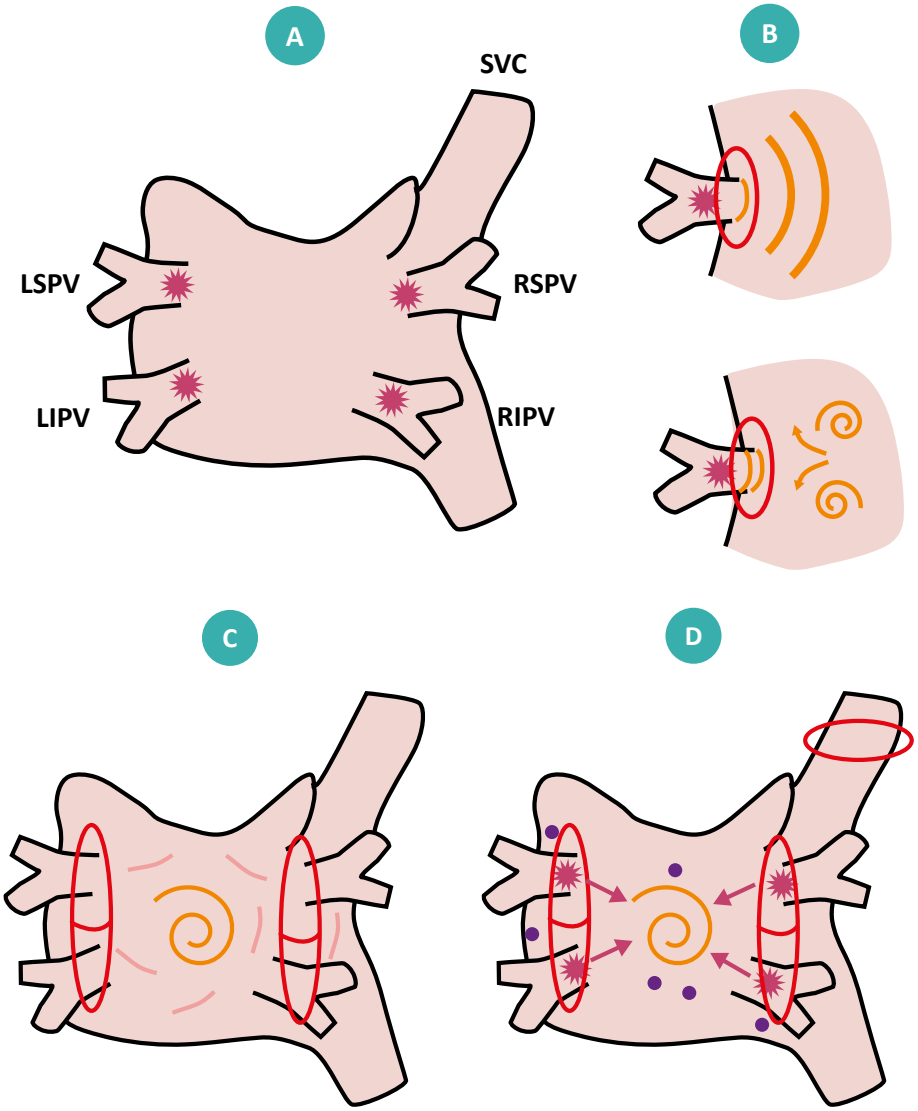

Figure 3: Focal triggers leading to initiation of re-entry. A schematic drawing that illustrates the manner in which focal triggers lead to the initiation of re-entry (rotors), eventually leading to additional focal triggers and perpetuation of re-entry. Includes common ablation strategies in paroxysmal and long-standing/persistent AF. (A) Active triggers arising from the atrial myocardium within the PVs are shown in red. Abrupt changes of fiber orientation along the PV antrum (the junction between the left atrium and pulmonary veins) and posterior LA wall favouring anatomic re-entry or high frequency rotors are also shown. (B) The two most common approaches for paroxysmal AF; segmental PV isolation for electric disconnection of triggers within the veins, and circumferential ostial PV isolation (one-by-one linear ablation of the PVs). (C) Simultaneous isolation of the ipsilateral PVs, encircling the antrum and additional linear lesions between the superior and inferior PVs. (D) Combinations of more than two techniques are usually necessary for a successful outcome in long-standing or persistent AF. These approaches include (i) PV isolation; (ii) isolation of the thoracic veins and non-PV triggers; (iii) additional linear lesions such as 'mitral isthmus' line connecting the mitral valve and the lesion encircling the LIPV, a 'roof' line connecting the lesions encircling the left and right PVs, a 'right atrial isthmus' line, and an 'anterior' line connecting the roof line to the mitral annulus anteriorly; (iv) ablation complex fractionated activity; and (v) ablation of the autonomic plexuses. LAA, left atrial appendage; LIPV, Left inferior pulmonary vein; LSPV, Left superior pulmonary vein; RIPV, Right inferior pulmonary vein; RSPV, Right superior pulmonary vein; SVC, Superior vena cava. Adapted from *[39] [40] [41]*.

Pulmonary Veins (PVs) Hypothesis

Nathan et al [42] in 1966, was the first to draw attention to the presence of sleeves of cardiac tissue that extend onto the PVs (Figure 3). Investigation of the autonomic and electrophysiological properties of the PVs remained limited however, until the importance of PV triggers in the development of AF was appreciated decades later. It is now known that myocardial muscle fibers extend from the LA into all four PVs for up to 3cm. The fibers are thickest at the proximal ends (1-1.5mm), gradually decreasing distally as they interdigitate with the PV tissue [43] [44] [45].

PV focal firing is believed to both initiate AF and strongly influence the maintenance of the arrhythmia once initiated, however, the mechanisms by which it does this are poorly understood. The locations of the precursors of the conduction system are determined during the looping process of the heart tube during embryonic development [46] [47]. Cell markers common to precursors of specialized conductance tissue derived from the heart tube have been found within myocardial sleeves [48], and the presence of P cells, transitional cells, and Purkinje cells has been demonstrated in human PVs [49] [50]. PV-sleeve cardiomyocytes have discrete ion channel and action potential properties that predispose them to arrhythmogenesis [49] [50]. They have small background inward rectifying potassium currents (Ik1), which are thought to favour spontaneous automaticity [50], also reducing their coupling to atrial tissue, a property common to pacemaker structures which favour spontaneous automaticity [51]. Honjo et el. found that exposure to Ca2+ caused by treatment with ryanodine brought about Ca2+-dependent arrhythmia mechanisms [52], a response hypothesised by others to occur due to cells of melanocyte origin [53]. In a series of studies by three separate research groups, in isolated rabbit and canine cardiomyocytes, PVs were found to display abnormal automaticity, which brought about arrhythmic activity when manipulated, resulting in enhanced Ca2+ loading [52] [53] [54]. In a further study, on dissociated pulmonary vein arrhythmias, Weerasooriya found that the cardiomyocyte properties observed by the Honjo, Patel and

Wongcharoen groups may result in the electrical activity within the PVs that is usually observed after electrical disconnection of the PVs from the atrium [51].

Other studies have provided further evidence to suggest that the PVs and also the posterior LA are preferred sites of re-entrant arrhythmias [55] [56] showing shorter action potential durations of the PVs compared to the atrium [49] due to larger delayed rectifier K+ currents as well as smaller inward Ca2+ currents in the PVs [54] [57]. In addition, PVs demonstrate conductance abnormalities that promote re-entry due to abrupt changes in fiber orientation as well as Na+ channel inactivation by reduced resting potentials due to small Ik1 [49], [56] However, another study by Kalifa et al. [58] that assessed the effect of increasing intra-atrial pressure on PV activation, found that as LA pressure was increased above 10cm H_2O, the LA-PV junction became the source of dominant rotors. Using a multielectrode basket catheter to carry out electrophysiological evaluation of PVs has revealed effective refractory period heterogeneity and anisotrophic conduction properties within the PV and at the PV-LA junction, which could provide a substrate for re-entry [59].

Spontaneous Pulmonary Veins Firing

The atria receive autonomic input from both the central autonomic nervous system (ANS) (pre-ganglionic) and the intrinsic cardiac autonomic nervous system [60] [61]. Included in the intrinsic cardiac ANS are clusters of ganglia, known as ganglionated plexi (GP), which are located within the ligament of Marshall in specific epicardial fat pads. The GP receive signals from the central (extrinsic) ANS and contains afferent neurons, post-ganglionic efferent parasympathetic and sympathetic neurons, and numerous interconnecting neurons that provide communication within and between the GP. Animal models, stimulating the vagosympathetic trunk (“vagus nerve”) showed that AF could be sustained provided there was pacing or other stimuli to initiate AF [62] [63]. Scherlag et al. found that by stimulating the GP, they could cause it to produce short repetitive bursts of rapid, irregular firing in the neighbouring PV, initiating sustained AF [64]. In another study by the Patterson group, it was found that the same pause-dependent initiation pattern and intracardiac electrograms (EGM)

used on the GP by Scherlag produced during focal firing within the PVs, closely resembled the firing patterns recorded in the PVs of patients suffering with paroxysmal AF [65]. Both sympathetic and parasympathetic stimulation of the GP is required to activate focal firing in the PVs [66] [67] [68]. Parasympathetic stimulation shortens the action potential duration (and effective refractory period) in atrial and PV myocytes, and sympathetic stimulation increases calcium loading and automaticity. Combined, they cause pause-induced early after depolarisations (EADs) and generated activity in PV and atrial myocytes. It is thought that the mechanism of triggered firing could be the cause of a very short action potential duration combined with increased calcium release during systole, which in turn leads to high intracellular calcium levels during and after repolarization. These findings suggest that the activation of the sodium/calcium exchanger is caused by high calcium concentration, which lead to an inward current, EADs, and triggered firing [63] [66] [69]. PV myocytes have shorter action potential durations and are more sensitive to autonomic stimulation than atrial myocytes, which elucidates the prevalence of focal firing in the PVs of patients with paroxysmal AF and the cessation of focal firing by ablation of the autonomic GP [70].

Electrical remodelling

A reduction in the L-type calcium current ($I_{Ca,L}$) along with an increase in potassium currents, including the inward-rectifier potassium current (I_{K1}), slow delayed rectifier potassium current (I_{Ks}), and two-pore domain potassium current (I_{K2P}) are predominately used to determine re-entry-promoting ERP shortening, a distinctive sign of the presence of AF [29] [71] [72]. Electrical remodelling is largely a consequence of AF, however in some cases mutations within cardiac ion channels have been seen to promote electrical remodelling. A number of animal models have shown that with rapid atrial pacing used to replicate the presence of AF atrial remodelling occurs within a matter of days, however, they have also shown that this form of remodelling can be reversed when sinus rhythm is restored [73] [74]. In support of this, one large population-based study in humans with paraoxysmal AF who were in sinus rhythm at the time of atrial tissue

collection, showed that the duration of repolarization remained unchanged [75] , the same was seen in Heart Failure (HF) patients without history of AF who are at increased risk of developing AF [76]. Another study of 17 patients with long-standing persistent AF demonstrated that the shortened effective refractory period associated with Chronic AF was reversible upon cardioversion, further supporting this [77].

Structural Remodelling

Structural remodelling of the atria is believed to be a major component of the initiation and persistence of AF [78] and is promoted by a wide range of signalling molecules (Figure 4). Remodelling of the atria is progressive, caused by excess pressure and volume, underlying risk factors such as age, hypertension, heart failure and AF itself [79] [80]. Although structural remodelling is progressive, some studies have observed initial structural changes after a week in AF [81].

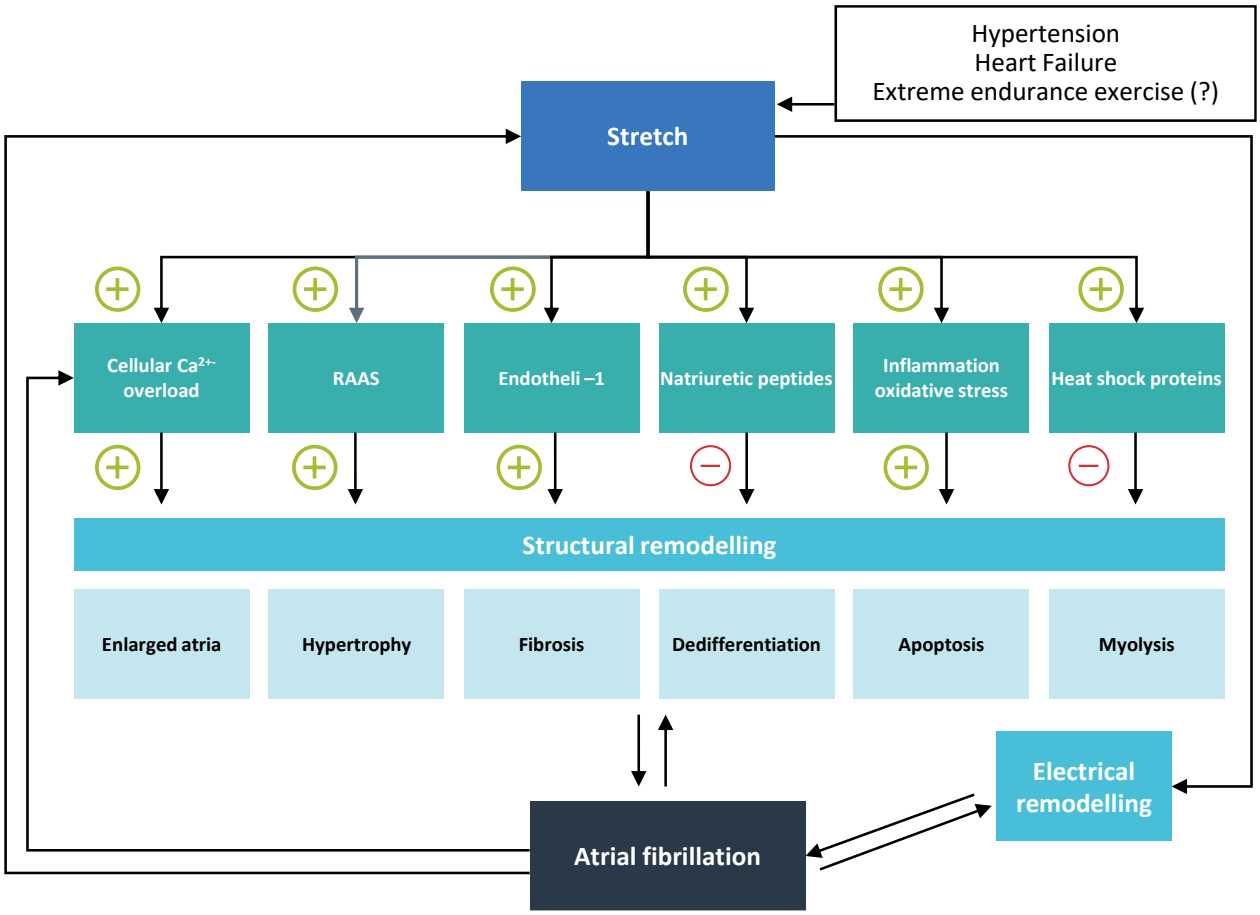

Figure 4: Flow chart showing the series of events caused by stretch. Hypothetical scheme of stretch induced by hypertension, heart failure and possibly extreme endurance exercise leading to calcium overload, activation of the renin–angiotensin–aldosterone system (RAAS) and release of different factors, resulting in structural remodelling and finally in AF. Adapted from [78].

Table 1 below is a summary of the structural remodelling that have been reported in studies containing human models with of AF with or without underlying disease, including with it the duration of time in AF of the experimental model. A schematic representation of this structural remodelling can be seen in Figure 5.

Reference	Underlying cardiac disease	n	Biopsy	Duration (months)	Type of Structural Remodelling
Frustaci et al. (1997) [82]	Paroxysmal lone AF	Ctrl: 11, AF: 12	RAS	3–108	Hypertrophy, Fibrosis, Cell death, Myolysis, +Inflammation
Thiedemann and Ferrans (1977) [83]	Valve disease	Ctrl: 4, AF: 10	LAW	6–396	Enlarged atria, Hypertrophy, Fibrosis, Cell death, Myolysis,
Anne et al. (2005) [84]	Mitral valve disease	Ctrl: 10, AF: 9	RAA,LAA	46.8 ± 15.6	Enlarged atria, Hypertrophy, Fibrosis, Myolysis, =MMP2,9 activity, =MMP1, TIMP1,2,4 protein , = AT1R, AT2R, TNFα protein
Han et al. (2008) [85]	Mitral valve replacement	Ctrl: 17, AF: 15	RA	48.9 ± 42.1	Enlarged atria, Cell death, +NOS2, 3nitrotyrosine =NOS3
Eiras et al. (2006) [86]	Coronary artery disease, valve disease	Ctrl: 9, AF: 16	RAA	>3	Enlarged atria, Hypertrophy, −Kinetics of force redevelopment, +Dedifferentiation
Aimé-Sempé et al. (1999) [87]	Coronary artery disease, valve disease or congenital heart defects	Ctrl: 35, AF: 17	RAA	1–240	Enlarged atria, Hypertrophy, Fibrosis, Cell death, Myolysis
Rucker-Martin et al. (2002) [88]	Coronary artery disease, valve disease or congenital heart defects	Ctrl: 14, AF: 10	RAA	n.a.	Enlarged atria, Fibrosis, Myolysis , +Dedifferentiation
Polyakova et al. (2008) [89]	Coronary artery disease, valve disease, atrial septal defect, dilated cardiomyopathy	Ctrl: 24, AF: 24	RAA, RAFW	12–240	Enlarged atria, Fibrosis, +MMP2,9 protein, +TIMP1,2, RECK protein, =TIMP3,4 protein, +TGFβ1 protein
Ke et al. (2008) [90]	Coronary artery disease, paroxysmal lone AF, mitral valve disease	Ctrl: 13, AF: 14	RAA, LAA	−	, =Cardiac Troponin T,I,C, +Calpain activity
Ke et al. (2008) [90]	Coronary artery disease, persistent lone AF, mitral valve disease	Ctrl: 13, AF: 17	RAA, LAA	0.1–56	Enlarged atria, Myolysis , −Cardiac troponin T, I, C, +Calpain activity

Table 1: Atrial structural remodelling in AF, data from human tissue biopsies. RAS, right atrial septum; RA, right atrium; RAA, right atrial appendage; RAFW, right atrial free wall; LAW, left atrial wall; LAA, left atrial appendage. +, increased compared with control; −, no changes compared with control; n.a., not available. Column others: +, increased compared with control; −, reduced compared with control; =, no changes compared with control. RECK, reversion-inducing cysteine-rich protein with Kazal motifs [82] [83] [84] [85] [86] [87] [88] [89] [90].

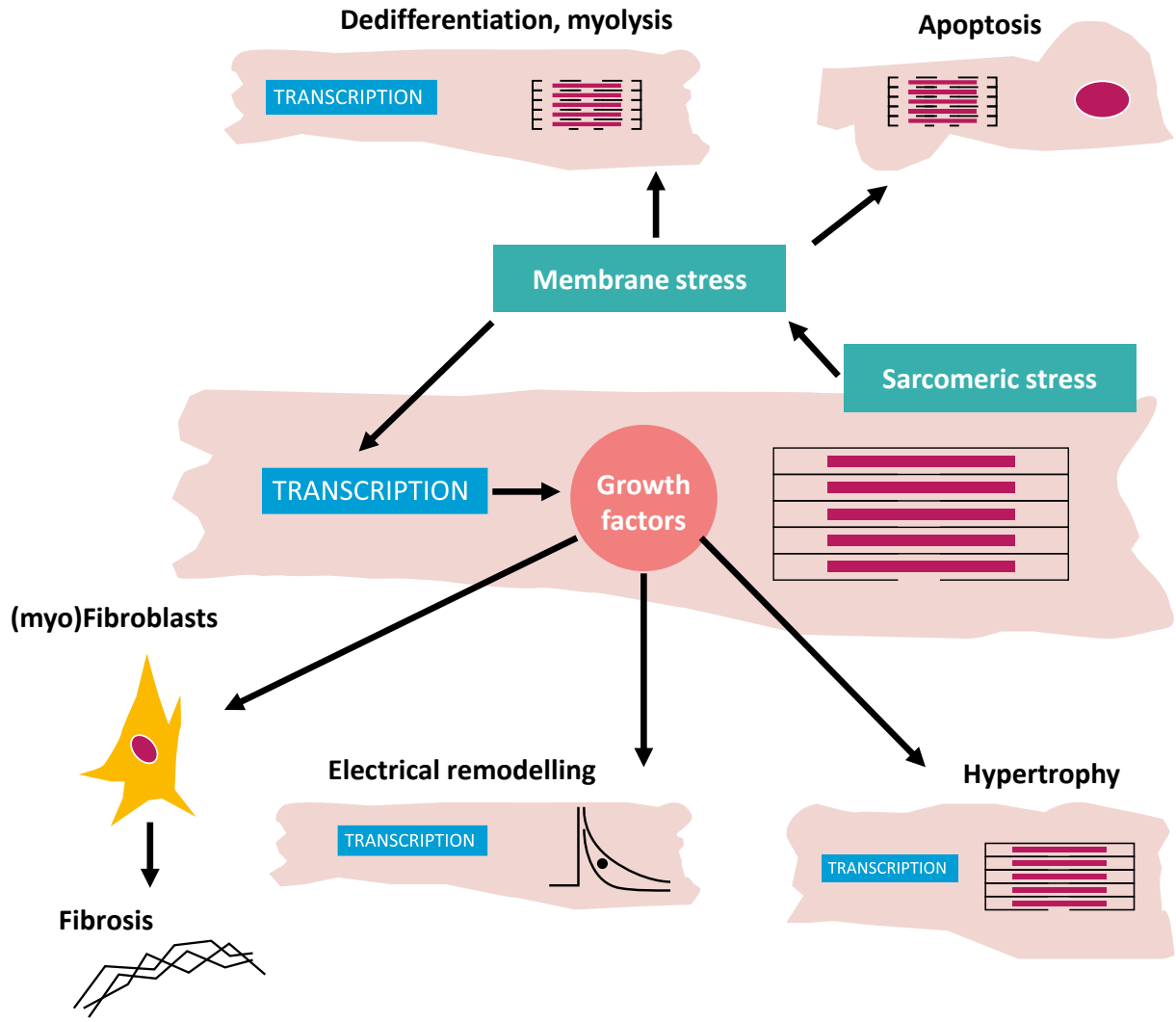

Figure 5: Different characteristics of cardiomyocyte remodelling which are induced by stretch. It is unclear which cellular department (sarcomere, cell membrane) senses stretch but this leads to induction of signal transduction that ultimately leads to increased expression and/or secretion of growth factors, structural remodelling including dedifferentiation, myolysis, apoptosis, fibrosis and hypertrophy, and also electrical remodelling. The growth factor actions could thus be intracrine, autocrine, or paracrine. Adapted from [78] .

Atrial structural remodelling is a major component of the vulnerable substrate for AF [78], atrial dilation results in a larger substrate that can more easily maintain reentry. It also results in increased atrial stretch, which further promotes structural remodeling [78]. Fibrosis is one of the characteristics of structural remodelling, there are different types of fibrosis (replacement, interstitial, endomysial) all of which have been seen in both animal models and patients with AF [91]. Fibrosis is caused by the formation of excessive extracellular matrix due to the proliferation and differentiation of fibroblasts into procollagen-secreting myofibroblasts as well as elastic and collagen fibres. A schematic overview of the factors involved in the build-up of extracellular matrix can be

seen in Figure 6, replacement and endomysial fibrosis have been associated with reentry-promoting alterations in impulse conduction [91] [92].

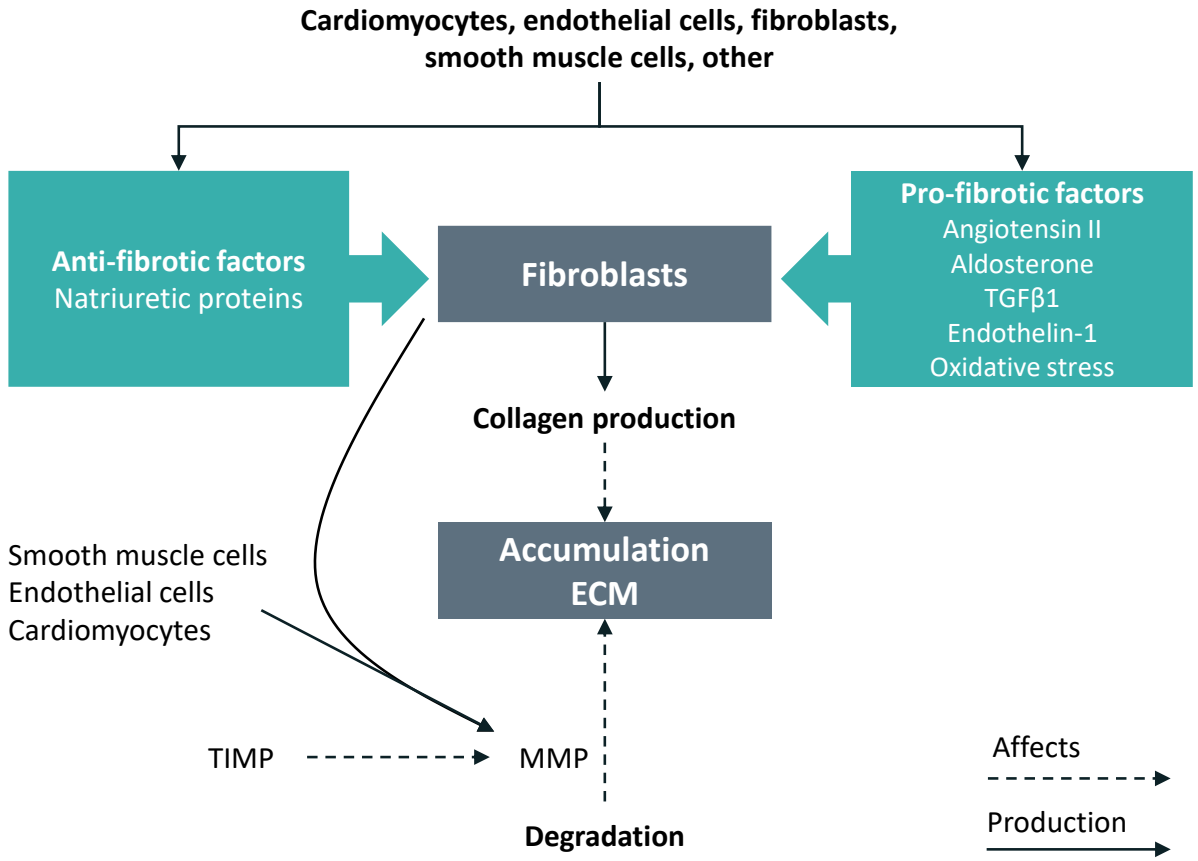

Figure 6: Accumulation of the extracellular matrix. MMP, matrix metalloproteinase; TIMP, tissue inhibitor of metalloproteinases; ECM, extracellular matrix; TGFβ1, transforming growth factor β1. Adapted from [78].

In response to increasing LA pressure, a greater change in the atrial volume is noted in non-hypertensive compared to hypertensive rats and greater stiffness is also observed in left atrial tissue strips taken from the latter rats [93]. In canine studies, a regional difference in the compliance of the left atrium was observed, with the appendage having a lower elastic modulus (higher compliance) than the left atrium [94] [95] and following appendectomy, or ligation of the appendage, the mean stiffness of the whole left atrial chamber is increased [95] [96]. The relationship between the left atrial pressure and volume has also been found to be different

depending on whether the left atrial pressure is increasing or decreasing, being greater if the pressure was falling rather than rising [96].

Compliance within the LA may be determined invasively during cardiac catheterisation by measuring an increase in systolic pressure and then dividing it by stroke volume [97]. Another way of clinically assessing if compliance is in range is to compare the dynamic echocardiographic left atrial area, as determined by an automated boundary detection application, with the invasively determined left atrial pressure [98]. It is also possible to determine atrioventricular compliance using echocardiographic assessment of transmitral velocity profiles [99] and in the presence of normal left ventricular compliance, this compliance has been taken as a surrogate of left atrial compliance, and correlates with peak pulmonary systolic and diastolic flow velocity as well as the pulmonary artery systolic pressure [100]. In a post-mortem study of human tissue, an acoustic microscope was used to measure left atrial compliance, and found that the speed of sound through left atrial tissue specimens increased with increasing subject age, this increase was felt to reflect a decrease in the elasticity of the tissue with ageing [101].

There is believed to be a relationship between left atrial compliance and AF. In one study looking at canine hearts it was found that extensibility for a given rise in pressure was larger in the LA during normal sinus rhythm and then after it was induced to fibrillate, reflecting a reduced compliance during AF acutely [102]. Similarly in a human study, using echocardiography and invasive left atrial pressure measurement to measure compliance, left atrial stiffness was higher in patients with atrial fibrillation compared to control patients [103]. A porcine study, also demonstrated that the provocation of AF resulted in a smaller end systolic LA volume, larger end diastolic volume and a reduction in the compliance of both atria [104]. In contrast, there was no difference seen in left atrial compliance of healthy and AF patients with mitral valve stenosis undergoing echocardiographic left atrial compliance assessment [100].

Compliance has been suggested to be lower during AF acutely for a number of reasons [104]; unsynchronised myofiber contractions, which means that some of the microfibers are always

contracting, greater myocardial turgor due to increased blood flow in the atrial myocardium during AF meaning the atria is under a greater initial stretch [105] while increased cytosolic calcium concentrations which alters contractility. Further to this, one would also expect a contribution secondary to the structural remodelling to attribute to and sustain AF.

In AF, the LA loses its contractile contribution to cardiac output. An increase in the stiffness of the left atrium, certainly acutely, may be an important response to this loss as it results in an elevation in the left atrial pressure, allowing for increased blood flow down the higher pressure gradient into the left ventricle and so reducing the decline in stroke volume from the loss of atrial systole [104]. The benefits of understanding this more could result in more effective transmural lesions being made, leading to shorter procedure times and fewer procedures per patient, therefore less risk to the patient and a greater quality of life post procedure.

Atrial compliance is calculated as $\Delta V/\Delta P$, several previous studies have tried to indirectly measure LA volume in both animal [106] and human [107] models using different echocardiographic techniques. In one study ultrasonic external diameter transducers were sutured to the atrial surface to record cross-sectional dimension, with microtip pressure transducer catheters used to record pressure [106]. In another they used real-time two-dimensional echocardiographic imaging with automatic boundary detection to estimate LA area change and catheter-tipped micromanometer to measure LA pressure [107]. However, due to the complexity of the LA geometry it can be difficult to precisely and instantly measure LA volume change and pressure in this way. For this reason, more recently Park et al. quantified LA compliance by directly measuring the LA pulse pressure (LApp) at the beginning of the procedure and assumed minimal change in LA volume [108].

Management of Atrial Fibrillation

AF patients usually seek medical attention because of AF-related symptoms such as myocardial infarction (MI), heart failure (HF) or stroke. Previously it has been treatment of these symptoms that have been motivation for AF therapy. In MI and HF patients a large scale trial (AFFIRM trial) [109]

found that the successful maintenance of sinus rhythm was associated with longer survival of these patients.

Pharmacological management of AF consists of three aspects: Anticoagulation, rate control, and rhythm control, with most patients receiving a combination of treatments [110] (Figure 7).

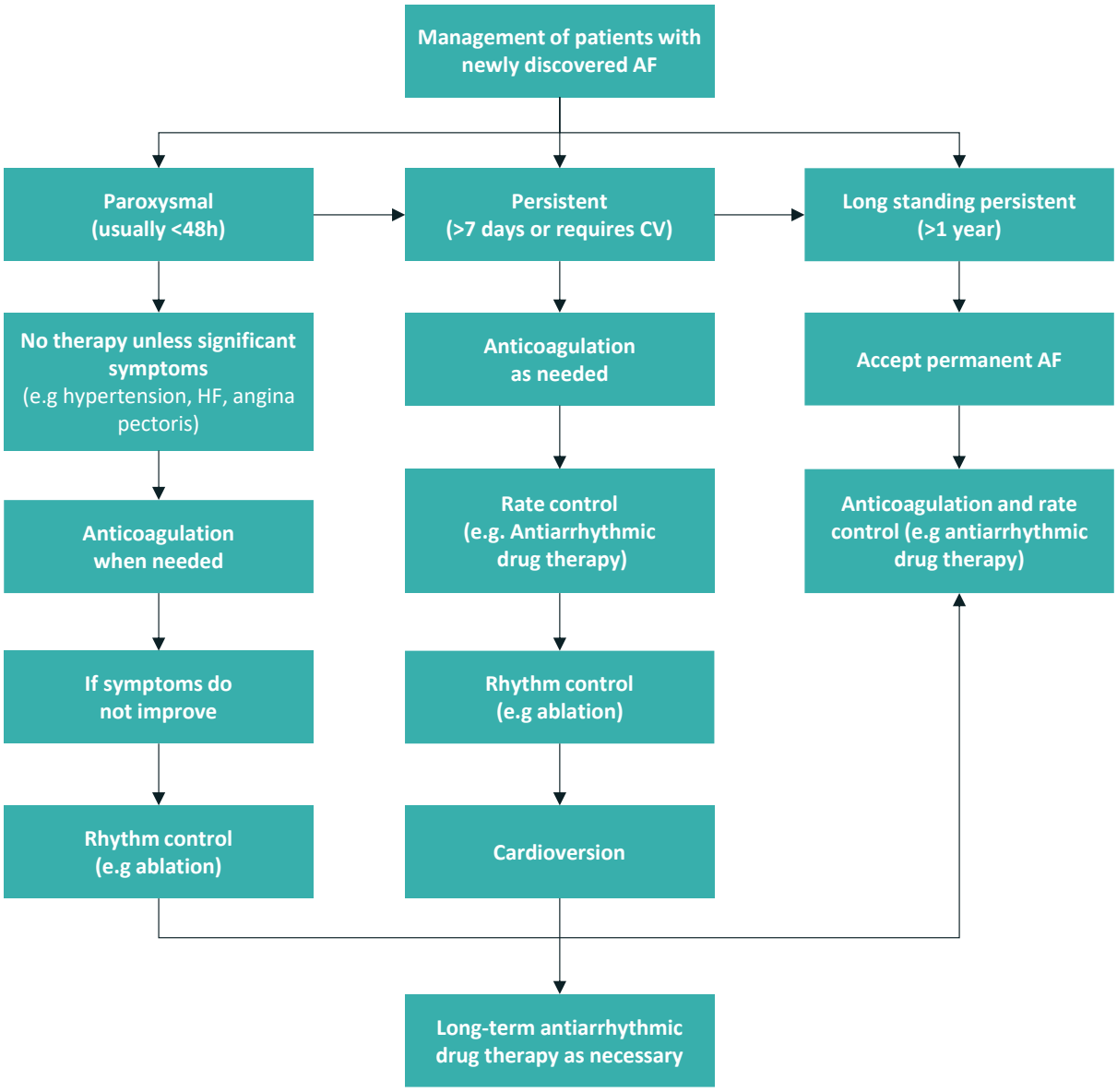

Figure 7: AF Treatment. Arrhythmias tend to progress from paroxysmal (self-terminating, usually with <48h) to persistent (non-self-terminating or requiring cardioversion), long-standing persistent (lasting longer than 1 year) and eventually to Figure 8: AF Treatment. Arrhythmias tend to progress from paroxysmal (self-terminating, usually with <48h) to persistent (non-self-terminating or requiring cardioversion), long-standing persistent (lasting longer than 1 year) and eventually to permanent (accepted) AF. Along the way different treatments are offered to better manage the symptoms of AF, the treatment offered is based on the type of AF. AF, atrial fibrillation; HF, heart failure; CV, cardioversion. Adapted from [111] *[112].*

Atrial Ablation Therapy

The aim of a radiofrequency application during AF ablation is to create transmural lesions to act as a permanent blockade against electrical conduction, eliminating any potential AF drivers. As yet, there is no definitive definition of success for AF ablation surgery, despite recent attempts to define and clarify the treatment endpoints. For the patients a successful procedure would provide them with freedom from symptoms of AF and stroke, for physicians however, in line with recent guidelines [113] this would be defined as freedom from AF, atrial flutter, tachycardia and off antiarrhythmic therapy, but not anticoagulants. Limiting the risk of stroke. At a procedural level, this is best reflected by an improvement in the single procedure success rate for the ablation.

The original procedure of atrial ablation was a surgical one, whereby atrial tissue was incised and the scar tissue that formed following healing, acted to insulate the aberrant pathways [114]. More recently, various energy modalities have been adopted in order to scar the atrial tissue such as: radiofrequency energy, cryoablation energy, ultrasound, and laser ablation modalities. With the advent of trans-arterial catheters, the procedures can now be carried out minimally invasively with lower associated risk than the surgical procedure counterpart [113]. However, despite the well-established procedure, the efficacy of lone ablative procedures is poor with only 51.2% of patients being free from recurrence at five years [115]. The efficacy with multiple procedures is notably improved (77.8%) however, with the high procedure costs of around £8,000 per procedure [116] increasing the efficacy of lone procedure treatments should be an aim for research.

For successful radiofrequency ablation, procedures rely on transmural lesions to fully isolate the regions responsible for triggering and maintaining AF [117]. Recent technological

improvements such as implementation of contact force sensing catheters are hypothesised to help to improve the quality of ablative lesions and lesion formation [113]. However, to best benefit from these advances, the relationships between contact force and the mechanics of left atrial tissue need to be explored further to be fully understood.

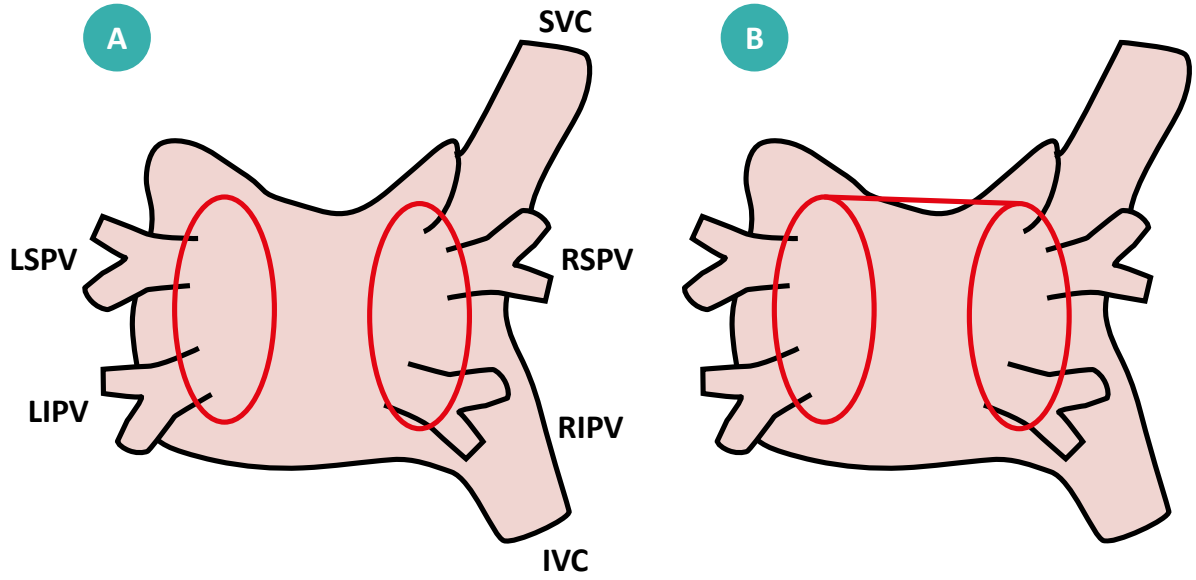

Figure 8: Ablation Therapy Common Lesion Patterns. (A): shows circumferential lesions isolating the pulmonary veins. (B): Pulmonary vein isolation with additional linear lesions. Adapted from [113].

The effectiveness of ablative procedures is supplemented by the technology that has been developed over recent years. Atrial tissue can be electro anatomically mapped prior to ablation, catheters can provide contact force data, newly emerging catheter designs enable circumferential ablation (ablation lesions encircling the pulmonary veins (Figure 8A), and in addition to this, there are many energy modalities available [118] [119] [120]. With all of this additional technology and variation in techniques for ablation, isolating a single best ablation treatment strategy is difficult and many multi-centre studies are being carried out comparing treatment efficacies, based on both the techniques used and patient demographics.

Biophysics of Radiofrequency Catheter Ablation

Catheter-based radiofrequency ablation utilises alternating electrical current to create a tissue lesion through resistive heating (which occurs at the electrode-tissue interface (ETI)), and conductive heating spreading away from the interface point. One method of increasing efficacy is to produce larger volume lesions during ablation. This ensures continuity and transmurality of lesions to make reliable lines of block.

Initial studies demonstrated that lesion size correlates positively with catheter tip temperature [121] [122]. The threshold temperature for tissue viability has been calculated to be between 46.6 and 48.9°C, with tissue temperature being inversely related to the distance from the electrode [121] [123]. If the temperature at the ETI exceeds 100°C then blood boils and a coating of coagulum and char on the electrode forms which electrically insulates the electrode and causes a rise in impedance [124], preventing further delivery of energy to the tissue.

Cooling the catheter tip through irrigation prevents the formation of coagulum and char by reducing the temperature at the ETI, and allows for greater power delivery, resulting in larger lesions compared with non-irrigated catheters [125]. The degree of cooling, as dictated by the rate of irrigation flow, also affects lesion size, with a very high rate associated with a reduced lesion width [126]. A by-product of catheter tip irrigation though is that temperatures deeper in the tissue can rise to the extent that superheating occurs with a sudden explosion of steam (which can be heard as a pop) associated with crater formation and an impedance rise [125].

As one would expect, cooling the catheter tip changes the relationship between the catheter-tip temperature and lesion size: from animal models, there is no correlation

between the ETI temperature or the electrode temperature and the lesion depth or maximal temperature in irrigated ablation, while the converse is true in non-irrigated ablation [125].

The diameter of the catheter also makes a difference: with non-irrigated catheters, larger lesions are caused by catheters with a larger diameter [123], while the converse is true with irrigated catheters [127].

The duration of ablation also affects lesion size. An exponential increase in lesion size with time at a target electrode temperature has been noted with non-irrigated catheters, with a plateau when a steady state of tissue temperature is reached after around sixty seconds [128]. With irrigated catheters, the temperature at deeper levels continues to rise after sixty seconds of contact, indicating that lesion size may also follow this trend [125].

Electrode orientation also affects lesion size [129] [130], with a vertical orientation increasing, and a horizontal orientation reducing lesion sizes with irrigated catheters [129] [130] and the converse the case with non-irrigated catheters in vitro [130].

Ablation Efficacy

As stated previously, an ablation procedure is considered successful if only a single procedure is required to terminate AF, the aim therefore for any radiofrequency catheter ablation procedure is to generate transmural lesions to act as a constant barrier against any electrical conductance that does not originate from the SA node, or eliminated any drivers that could potentially maintain AF. Reddy et al. in the TOCCATA trial [131] compared CF parameters between different ablation cases of patients both with and without a recurrence of symptoms [132](Table 2).

Author	Number of Patients	AF Subtype	Method to judge ablation efficacy	Suboptimal Ablation	Effective Ablation
Reddy (2012)[131]	32	PAF	12 months recurrence of symptoms	CF <20g	CF>20g
Haldar (2013)[133]	40	35% PAF	Acute PV reconnection in a 7 segment model per PV pair	CF 14.5g	CF 19.6g
Kumar (2012)[134]	12	PAF	Acute PV reconnection in a 5 segment model per PV pair	*LPV:* CF 9g, *RPV:* CF 11g,	*LPV:* CF 20g, *RPV:* CF 24g,
Kumar (2012)[134]	20	PAF	EGM criteria for transmurality(160)		CF>16g
Neuzil (2013)[135]	40	PAF	PV reconnection at 3 month protocol-driven restudy in a 5 segment model per PV pair	CF 15.5g Minimum CF 3.6g	CF 19.5g Minimum CF 8.1g
Sohns (2014)[136]	6	PAF	MRI-defined scar in 5mm 2 zones		>1,200g.s

Table 2: Clinical studies assessing ablation efficacy. With respect to catheter contact force: methods used to assess efficacy and cut off values for effective ablation. PAF = Paroxysmal Atrial Fibrillation, CF = Contact Force, PV = Pulmonary Vein, LPV = Left Pulmonary Vein, RPV = Right Pulmonary Vein, EGM = Electrogram [131] [133] [134] [135] [136]

Concluding that, higher CFs were used during the ablation procedures of patients who did not suffer from any AF recurrence. It should not be assumed however, that there is any correlation between increased success rates and efficient individual ablation contact: instead, this would be reflected by the total procedural length being shortened, for example. The aim therefore, to assure efficacy for each ablation procedure should be ensure optimum radiofrequency ablation contact, resulting in shorter procedures and potentially less risk. Moreover, suboptimal applications may in the short run lead procedural success but by resulting in tissue oedema and an incomplete transmural lesion led to long-term failure. It is therefore extremely useful to be able to assess the efficacy of individual radiofrequency ablation contacts.

In preclinical studies, this isn't a problem as the transmurality of each lesion can be assessed histologically [127] [128]. This however cannot be done in clinical studies, instead alternative measures must be used to ascertain the effect of each lesion.

Usually, this is done via electrogram readings, with a reduction of the electrogram signal being the sign of an effective individual ablation contact point and therefore assumed to be a transmural lesion [137]. This statement can be further supported by a number of animal studies using both unipolar and bipolar atrial electrogram attenuation as a means of judging the efficacy and thus the transmurality of ablative lesions [138] [139]. In the bipolar study by Sanchez et al. [139] they concluded that a bipolar signal amplitude drop of ≥ 60% in vitro could be accurately used to determine lesion transmurality. In clinical studies, for ablations tissue lesions to be deemed transmural a ≥80% reduction in electrogram amplitude is expected [140] [141]. Electrode-tissue contact is vital to creating transmural lesions [142], however, in the left atrium there is both smooth and trabeculated tissue, due to its shape holding an ablation catheter in the same stable position for the time needed to create an ablation lesion in trabeculated tissue, if it is even possible to manoeuvre the catheter into the desired place within the tissue is extremely difficult. Tissue mechanics, such as fiber direction as well as tissue thickness could affect electrode-tissue contact by providing too little or too much resistance and therefore reducing the ability to create transmural lesions, this would therefore be something worth exploring.

Changes in electrogram morphology have also been shown to be predictive of transmurality of ablation lesions in a porcine model [143]. This approach is limited clinically in that it has been validated only in sinus rhythm cases, however, one group have used these criteria for bipolar signals to judge ablation efficacy [144].

The most commonly employed model for assessing ablation efficacy is reconnection of the pulmonary vein isolation (PVI) lines which are used to isolate the pulmonary veins from the left atrium [133] [144] [135]. In this approach, the ipsilateral paired PVI line is divided into five to seven segments and efficacy is based on whether that segment reconnects or not. A disadvantage of this method is that target parameters for individual radiofrequency ablation contacts are assessed based on regional response, that is to say the amplitude reduction in that area however, ablation contacts often overlap one another it is therefore difficult to determine which signal corresponds to which ablation contact. Furthermore, in all except one study the operators were blinded to CF measurements, with operators being blinded to only half the cases in the one non-blinded study, which due to a lack of knowledge of CF may unfortunately serve to exaggerate the differences between ineffective and effective ablations as it allows for a greater range of CF to be applied, making it difficult to determine where the actual threshold for effective ablation contacts lies. These studies suggest a mean ablation CF of at least 15g and FTI of >400g which is thought to correlate with a reduced risk of an ablation being in a reconnecting segment.

Cardiac Magnetic resonance imaging (MRI) has been used more recently to assess the transmurality of ablation lesions in clinical cases instead of electrogram attenuation. In one study using delayed enhancement MRI (DE-MRI) LA scar was imaged, in this study a correlation was found between the extent of LA wall scaring and short-term procedural outcome, the greater the amount of scarring the lower the risk of AF recurrence [145]. This same group later suggested that DE-MRI could be used to identify breaks in pulmonary vein isolation lines further supporting their claim by showing that areas of DE-MRI enhancement correlate with areas of electrical scar (R^2=0.57) [146]. However, another group found that

investigators in a blinded analysis using only pre- and post-ablation MRI images were only able to identify ablation points in LA myocardium in only 60% of cases, and that of these points they were unable to distinguish between ostial from circumferential ablation lesions [146], completely contradicting the work of Peters et al. [147] in which they reported that ablated myocardium could be identified in 100% of cases on DE-MRI. MRI may be a useful method for identifying ablation lesion sites however scar should be assigned a definitive signal intensity threshold as this appears to be the reason for the variation in reported identification. More recently an animal study has been carried out with the aim to correlated macroscopic scar volumes with DE-MRI imaging scar volumes, proposed DE-MRI signal intensity have been determined which allow the best approximation of the macroscopic scar volume [148].

Sohns et al. [136] compared contact force parameters with MRI-imaged atrial scar (Table 2), in six patients. For this comparison to happen, the FTI was not taken from a single radiofrequency application, but instead from a subdivision of 1cm zones. They concluded that FTI greater than 1,200g.s resulted in a greater proportion of DE-MRI scar being exhibited across a $5mm^2$ region of myocardium and that for any increase in FT below this value the scar burden within this same region was less. This study therefore suggests the possibility of using cardiac MRI to assess ablation efficacy clinically. One disadvantage of this method though is that the efficacy of an ablation lesion could not be assessed individually but instead at an MRI-zone level (albeit a small zone). This method therefore would be heavily reliant on the extremely accurate registration of each radiofrequency application between the electroanatomic navigation system and the MRI being used only to assess levels of scar. Moreover, it was impossible to account for any overlap in ablation

contact brought about by any form of catheter drift. This may be the reason why the MRI threshold for effective ablation is much higher than the CF thresholds shown in (Table 2). In this context, a better understanding of the mechanical properties of atrial tissue is needed. A better understanding could result in more effective transmural lesions being made, leading to shorter procedure times and fewer procedures per patient.

Current Technologies

Electroanatomical Mapping (EAM) Systems

Most complex arrhythmias are investigated using three-dimensional EAM systems because these are felt to optimally integrate both the anatomical and electrical features of a given arrhythmia in a given patient [149].

Three-dimensional (3D) EAM systems were first introduced in the 1990s as a new and exciting way to investigate regular atrial and ventricular tachycardia. The use of these systems have increased dramatically over recent years due to their ability to display the position of catheters in real time on a computer screen, as well as create detailed 3D reconstructions of the surface anatomy of a given cardiac chamber, whilst also tagging the endocardial or epicardial surface geometry with electrophysiological information, such as activation time (ie the timing of local activation), unipolar or biopolar voltage, amplitude (ie the presence of normal healthy tissue or scar tissue) and the presence of fractionated complex electrograms or late potentials, in cases of atrial fibrillation or ventricular tachycardia [149].

Several studies have shown that, three-dimensional EAM systems reduce radiation exposure as well as improve procedural success when radiofrequency catheter ablation (RFCA) procedures are performed well by well-trained senior operators [150] [151] [152] [153] [154] [155].

Over the years there have been a number of different 3D EAM systems made available each with slightly different properties, these include but are not limited to: CARTO® (Biosense Webster Inc.,

Irvine, CA, USA), a magnetic system with specific catheters; RPM™ (Boston Scientific, Marlborough, MA, USA), which uses ultrasound with dedicated catheters; LocaLisa™ (Medtronic Inc., Minneapolis, MN, USA), uses standard catheters, based on an electrical field; Electroview™ (Bard Electrophysiology, Lowell, MA, USA) which uses simple electrophysiological data annotation on generic models of cardiac chambers already embedded within the system and the Basket™ catheter (Boston Scientific), equipped with a very limited 3D mapping system [156] [157] [158] [159]. Nowadays, CARTO® (Biosense Webster Inc., Irvine, CA, USA) and EnSite NavX (Abbott, Abbott Park, IL, USA) are the most commonly used mapping systems used within clinical practice [160].

The choice of which EAM system is used is largely operator dependent, it may also depend on the availability of the system on the day of the clinical procedure. The clinicians at St. Bartholomew's Hospital tend to use the CARTO® (Biosense Webster Inc., Irvine, CA, USA) EAM system over others, and in this Thesis this was the only EAM system used. The reasons given by the clinicians at St Bartholomew's Hospital for using this system over others is that they believe the three-dimensional geometry is slightly more advanced due to the advanced algorithms used for the mapping. However, one large study that analyzed a total of 1070 consecutive RFCA procedures over an 8-year period for fluoroscopic time stratified by ablation target and mapping system, found that there were no statistically significant differences in acute success rates of either EAM system, nor was there any difference in complication rates as were the radiofrequency and fluoroscopy times [160].

Another reason for given for why clinicians at St Bartholomew's Hospital favored CARTO® (Biosense Webster Inc., Irvine, CA, USA) over others was the feel of the specific catheters linked with the system, CARTO® (Biosense Webster Inc., Irvine, CA, USA) uses specific catheters such as the Thermacool SmartTouch (SF) catheter (non – irrigated catheter) and Thermacool SmartTouch Surround Flow (STSF) catheter (irrigated catheter) which they consider to be less stiff than the TactiCath™ Contact Force Ablation Catheter, the specific catheter for the EnSite NavX (Abbott, Abbott Park, IL, USA).

As the CARTO® (Biosense Webster Inc., Irvine, CA, USA) is arguably one of the most widely used mapping systems, and it is the mapping system of choice at St Bartholomew's Hospital, it will be the focus of the following discussion.

CARTO® (Biosense Webster Inc., Irvine, CA, USA) EAM system

The CARTO system is designed to acquire, analyze and display electroanatomical maps of the human heart as well as provide a display in real-time of the location of the catheter within the 3D cardiac maps constructed. The 3D cardiac reconstructions are based on sample point data taken during the ablation procedure. How these points are acquired will be covered in more detail later on in this chapter. As the points are added to the map, the area from which the point was acquired is displayed on screen. In areas where points have not been collected, they are extrapolated in order for a complete map to be created. Different colours are used to represent timing or voltage. The types of maps that can be created using this EAM system include: (1) local activation time, (2) voltage maps, and (3) propagation maps. Activation maps display local activation times within a given cardiac chamber or chambers in relation to timing of a reference electrogram. Propagation maps visually display the spread of a wave front of activation throughout a cardiac cycle in the form of an animation [161] [162] .

The CARTO® (Biosense Webster Inc., Irvine, CA, USA) EAM system incorporates the use of magnetic localization technology to triangulate the position of miniature location sensors embedded into the tip of a single specialized mapping-ablation catheter [163].

Mapping Technique

Location Reference

Before arrhythmia mapping can take place, a stable location reference must first be established.

Positioned beneath the fluoroscopy table and the patient, a triangular electromagnetic location pad with three separate magnetic coils embedded with the ability to emit ultralow-intensity magnetic fields (5 x 10^{-6} to 5 x 10^{-5} Tesla) is inserted (Figure 9) [163]. The magnetic field strength from each of

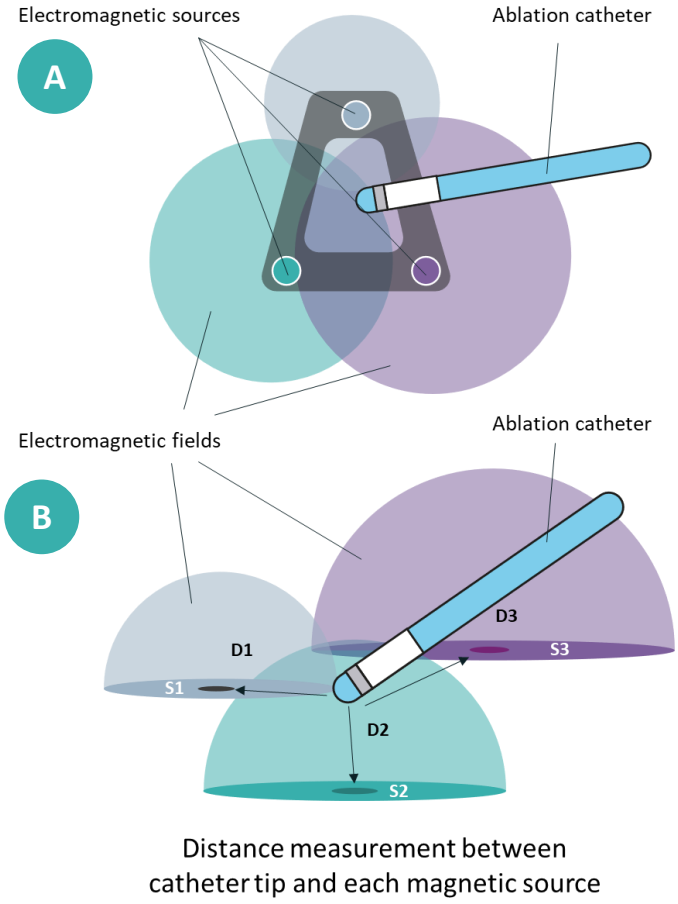

Figure 9: A) Electromagnetic location pad in relation to ablation catheter. Based on information from [163]. B) Schematic diagram of CARTO coils localizing the CARTO catheter

these coils differs and is detected by a location sensor in the specialized mapping catheter. The strength of the fields deteriorates as the move further away from the source (coils).

Two sets of three reference patches attached to the front and back of the patient's thorax, arranged in a triangle formation around the cardiac chamber of interest. If either the location pad or patches become displaced during the procedure, their original location is recorded by CARTO to allow for them to be repositioned, the system also prompts the investigator that there has been a change i.e. the patient's body has moved and prompts them to rebuild the map [161] [164]. A limitation noted by the manufacturer however, is that the system may not be able to detect changes such as

repositioning the patient's head on a pillow or moving the patient's arm without changing the patient's position on the fluoroscopy table. Whereby the relative position between the patches remains the same but the position of the heart relative to the back patches has changed, this map result in an incorrect map (map shift) being generated.

Building the Cardiac Mesh

In order for the clinician to visualize the catheter within the cardiac chamber in order to ensure they create their ablation point within the desired area; they must first create a cardiac mesh. A selection of the reference electrogram, positioning of the anatomical reference, and determination of the window of interest are undertaken. A reference catheter is then guided into the Coronary Sinus (CS) using an electrode recording a prominent atrial electrogram, and ensuring that the ventricular electrogram is not the one picked up by the system. The reason the CS is the area most often selected is due to its stability [165].

A 4mm tip mapping catheter is directed by the use of fluoroscopy to known anatomical points which will later serve as landmarks for the electroanatomical map created. Known anatomic and electrophysiology (EP) landmarks are then tagged, for right atrial (RA) mapping these are the inferior vena cava (IVC), superior vena cava (SVC), CS, His bundle (HB), and tricuspid annulus and for left atrial (LA) mapping these are the mitral annulus and pulmonary veins (PVs) [165]. Once tagged, the catheter is slowly advanced around the chamber walls allowing it to sample sequential points along the endocardium, sequentially acquiring the location of its tip together with the local electrogram (Figures 10, and 11).

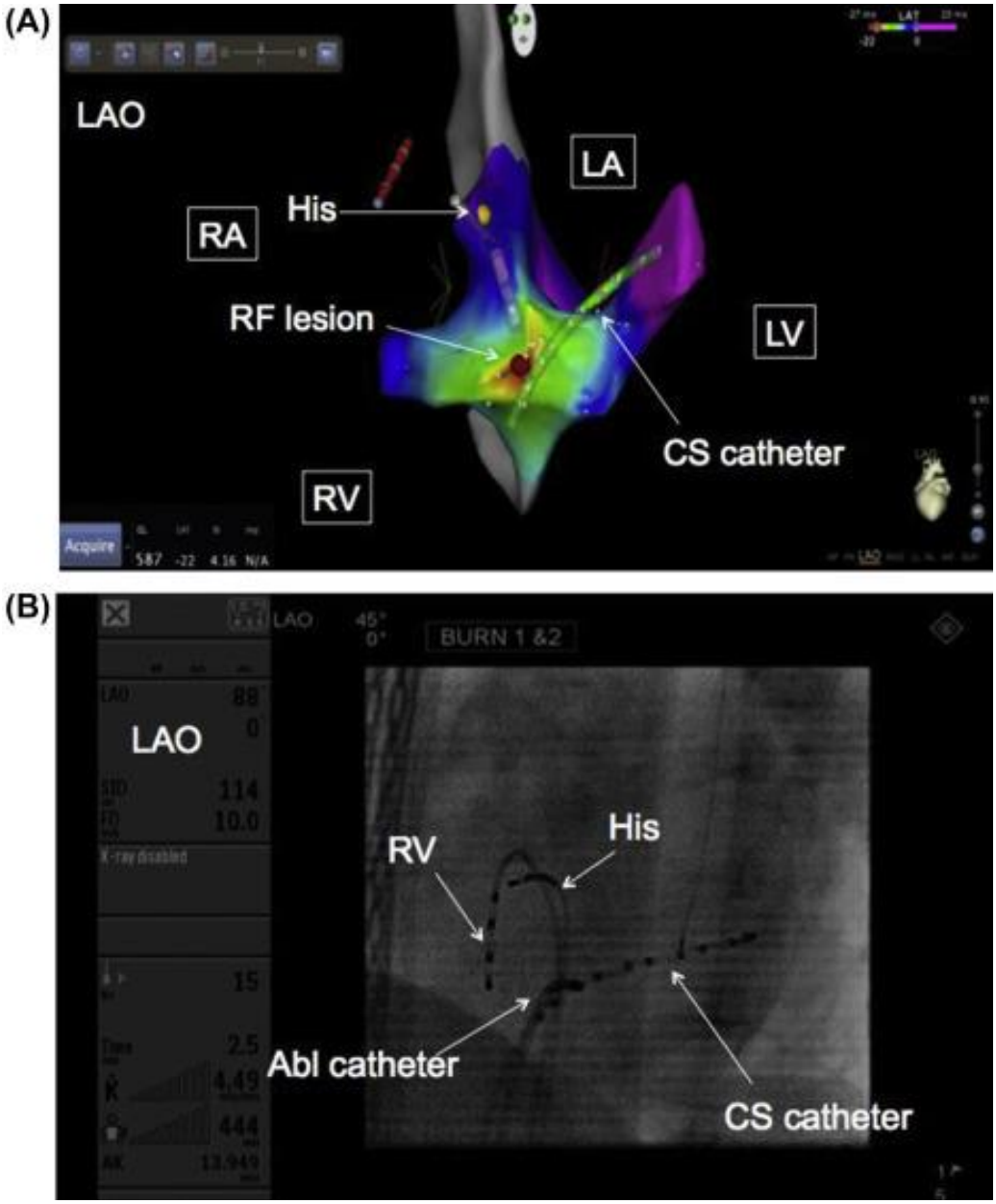

Figure 10: Electroanatomical mapping. (A) Left anterior oblique (LAO) view of electroanatomical activation map with red dot representing successful ablation in the right posteroseptal location. Coronary Sinus (CS), Left Atrium (LA) Left Ventricle (LV), Right atrium (RA) Radiofrequency (RF), Right Ventricle (RV). (B) Fluoroscopic view of similar catheter positions seen in (A).

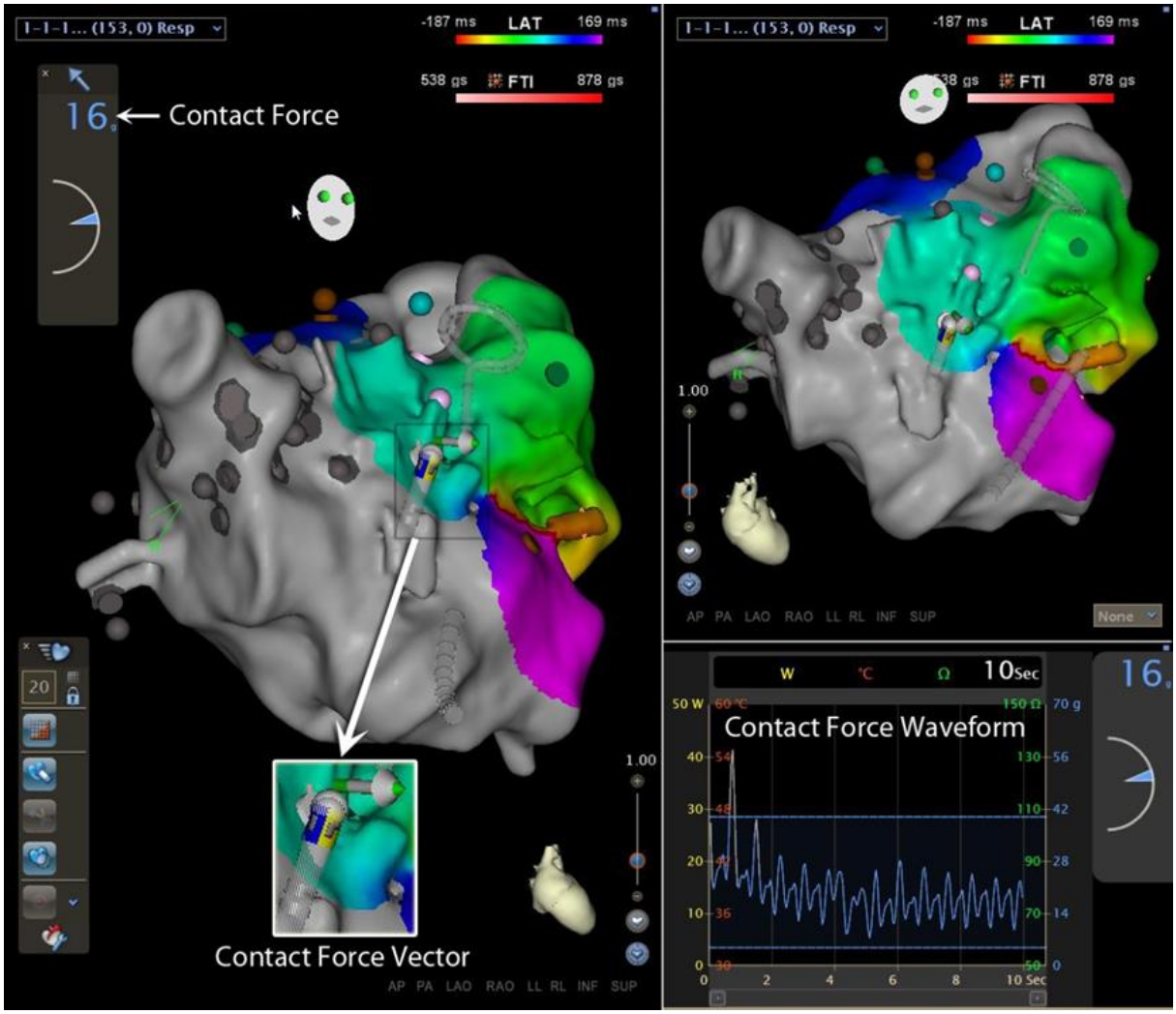

Figure 11: Electroanatomical Mapping Display. The Display of Contact Force Data Measured by the SmartTouch Catheter on the Carto3 Screen. Displayed is a left atrial geometry created using the Carto3 electroanatomic navigation system. Highlighted are the contact force, contact force vector and the contact force waveform for the contact between the catheter and the myocardium.

Catheter Location

The location of the catheter within the cardiac chamber if determined by magnetic and current-based technology, interrogating the field strength of each of the three magnetic coils located triangular electromagnetic location pad and converting this measurement into a distance, allows the EAM system to precisely localize, record and display the catheter-tip position in real time, in three dimensions (x, y, and z) as well as orientation (roll, pitch, and yaw) [161] [162], this is done in conjunction with current-based technology, in order to reduce the risk of distortions at the peripheries of the electrical field caused by extraneous variables resulting in background signals

[164]. A small current is produced by the current-based visualization system, which stems from the three electrodes located in the catheter, and travels to the surface patches located on the front and back of the patients' thorax. The currents generated by each of the different electrodes within the catheter emit a slightly different frequency of current allowing the operator to determine which electrode the current has originated from. Each of the three patches located on the patients' thorax measure the strength of current emitted from each electrode, and from this current-ratio data for each electrode location is produced. From this, the locations of the three electrodes in three-dimensional space can be determined, by indexing the current-ratio data with the magnetic location data from the electromagnetic location pad [164]. With the location of the mapping-ablation catheter being gated to a reliable point in the cardiac cycle and position information recorded relative to the location of an external reference patch affixed to the patients back, some degree of compensation for both cardiac and patient movement is provided [163].

Validation studies including Gepstein et al. [166] have demonstrated the accuracy of magnetic localization in providing location measurements within the heart both to a single point, in vitro and in vivo; as well as in returning to prior ablation sites, and in creating a desired length of ablation line. These measures were highly reproducible with a very little margin for error [167] [168] [169].

Activation Mapping

Activation mapping is carried out to determine the atrial activation sequence with the cardiac chambers. During a LA RCFA procedure, between 80-100 evenly distributed points in the LA are usually taken. The local activation time at each site is determined from the intracardiac biopolar electrogram and is measured in relation to the fixed intracardiac electrogram from the CS (reference) catheter. Points are only added to the map if the stability criteria in space (<2mm) as well as the local activation time requirements (<2 milliseconds) are met. The activation map may

also be used to record sites at which pacing manoeuvres have been performed during the assessment of tachycardia.

Atrial Compliance

Atrial compliance is defined as the ability of the atria to distend and increase in volume in response to increased transmural pressure or to resist recoil towards its original dimensions if a compressing force is applied [170].

This is important in that the atria control ventricular filling, there are three was in which it does this, looking specifically at the left atrium, it controls left ventricular filling: in sinus rhythm, as a reservoir during systole, as a conduit during diastole, and as an active contractile component during late diastole.

In individuals during exercise, for example, this active contractile component (reservoir and conduit) of the left atrium is required to act as a 'booster pump' to accelerate left ventricular filling by helping to maintain increased atrioventricular pressure gradient [171] increase ventricular volume in response to exercise. In previous animal models, a decrease in left atrial compliance is associated with an increase in the conduit function of the left atrium [172], which may in turn affect the left atria's ability to adapt in response to changing haemodynamics.

In atrial fibrillation, synchronized atrial contraction in lost decreasing cardiac output and increasing atrial pressure. This increase in atrial pressure offsets the decline in ventricular stroke volume, and therefore is an important compensatory mechanism. Additionally, in patients with atrial fibrillation, diastolic atrial compliance has been seen to decrease in both right and left atria [173].

Left atrial compliance is also thought to be affected by catheter ablation, with some reports of more extensive radiofrequency catheter ablation as well as multiple ablation procedures, sometimes required for better clinical outcomes in patients with persistent AF reducing compliance [174] [175] [176]. However, it still remains unclear whether left compliance has itself any clinical implications for patients who underwent radiofrequency catheter ablation (RCFA).

Current ways of calculating compliance

There are several ways left atrial compliance has been measured, in general calculated as the ratio of a change in volume (ΔV) to the change in pressure (ΔP) [106] [103]. The challenge with this method is that it is difficult to get an immediate and accurate measurement of left atrial volume or pressure change. Other groups have measured compliance directly by measuring left atrial pulse pressure (LApp) at the beginning of an ablation procedure and assuming minimal change in left atrial volume [108]. A limitation of this is that their definition for reduced left atrial compliance was based on the median value of LApp taken from a highly selective group of patients referred for Atrial Fibrillation catheter ablation.

As well as these invasive methods for measuring left atrial compliance, there have also been a few non-invasive methods [108] [177]. One way was by determining the role of left atrial pressure (LAP) in AF management and to select non-invasive echocardiographic parameters related to LAP. However, although listed as non-invasive, the LAP measurement was taken using a 6-F pigtail catheter (A&A Medical Device Inc, Gyeonggi-do, Republic of Korea) that was inserted into the left atrium via a long sheath (Schwartz left 1, St Jude Medical Inc, Minnetonka, MN) immediately after transseptal puncture, which in itself is invasive. The non-invasive element of the measure was the image parameter, and these measures were not taken at the same time, although usually within a month of each other. Another limitation with this method of measuring compliance is that patients with structural heart disease were not included in this study, which has previously thought to of had an impact on LA compliance [39].

Another non-invasive way of measuring compliance by Hammerstingl et al. [177] was to utilise ultrasound based two-dimensional speckle-tracking imaging (2D-ST). However, again the patient population was highly selective and as all 2D-ST analysis was made using a single analysis software, although others were available their results cannot be generalised to other available 2D-ST software.

Thesis Outline

Little is known about the pathophysiological and clinical implications of compliance. Although as previously described there have been multiple attempts to measure compliance, each of these have had limitations. Measuring left atrial compliance successfully could be useful in better understanding clinical implications of atrial fibrillation, as well as how compliance itself may also contribute to the pathophysiology of atrial fibrillation. Understanding compliance of the left atrium better may also lead to greater ablation success. With that in mind, the project set out to address the following aim.

Aim

The main aim of this project was to develop a suitable measure of compliance in patients with atrial fibrillation undergoing first time ablation procedures.

Considering that atrial fibrillation is a multifactorial disease associated with degenerative processes, including aging, haemodynamic and metabolic factors, once a suitable measure for compliance was determined, to preliminary test this measure in a small pilot study to determine factors that could reduce compliance. Finally, in the same cohort of patients to begin to explore the impact of fibrosis, through voltage on the measure of compliance calculated.

Hypotheses

The overall hypothesis, would be:

Reduced left atrial compliance my contribute to the pathophysiology of atrial fibrillation, and reduced efficacy of ablation procedures.

In this project the focus was to develop a suitable measure of compliance, which could eventually lead in to testing the overall hypothesis above, as no such measure is available yet. Therefore, the hypotheses for this project are as follows:

Hypothesis 1: Low compliance is linked with severity of AF, haemodynamic and metabolic factors.

Hypothesis 2: Low compliance is linked with severity of fibrosis.

Chapter 2:
Developing and testing a suitable measure for compliance in patients undergoing first time ablation procedures

Introduction

Atrial fibrillation (AF) is the most common arrhythmia in clinical practice, with a projected prevalence of six million people by 2050 in the UK [178] [179]. AF occurs when the electrical circuit of the heart is disrupted and the atria contract in a non-synchronous manner [180] [181]. Several studies suggest that AF is self-sustaining; the tachyarrhythmia itself may generate electrophysiological changes that contribute to the condition [180] [182].

AF has been linked to left atrial (LA) remodelling, a time-dependent adaptive regulation of cardiac myocytes to maintain homeostasis against external stressors [183] [184] [185]. Electrical remodelling, in animal studies, has demonstrated that the more frequently AF is induced or the longer AF is maintained the easier it is to induce and sustain AF [186] [187]. A number of clinical studies have shown that even brief episodes of AF may cause significant impairment of atrial contractility and initiate contractile remodelling, thought to be triggered by Ca2+. Further, experimental studies have shown that during AF, cardiomyocytes undergo dramatic structural changes and show signs of degeneration and apoptosis, and initiate structural remodelling [188]. The type and extent of remodelling is thought to be dependent on the strength and duration of exposure to the arrhythmia [189]. There are thought to be two major forms or atrial remodelling that are associated with atrial fibrillation: electrical remodelling and structural remodelling [190]. It has long been recognised that AF alters electrophysiological properties [191] [192]. AF induces electrical remodelling primarily due to the very rapid rate atrial rate associated with AF and the electrical remodelling itself, coining it the term “AF begets AF” [191] [193].

As the main focus of this Thesis was to develop a suitable measure of compliance in patients undergoing first time ablation procedures, the type of remodelling focused on was structural remodelling, which is associated with fibrosis [190]. However, as electrical and structural remodelling are in most cases believe to jointly present in people with AF [194] [195] [190] a brief overview of electrical remodelling will be given. Figure 12 summarises the molecular mechanisms

that underline electrical remodelling of the atria promotion of reentrant AF. Briefly, Electrical remodelling of the atria shortens the atrial refractiveness by decreasing the action potential duration, primarily by the downregulation of I_{caL} [196] but also by increased inward-rectifier K^+ currents such as background current I_{K1} and a constitutively active form of acetylcholine-dependent K^+ current (I_{KACh}) [197] [198] [199]. In addition, electrical remodelling impairs atrial contractility, principally by causing Ca^{2+}-handling abnormalities [200]., which causes atrial dilation [201] that further promotes reentry.

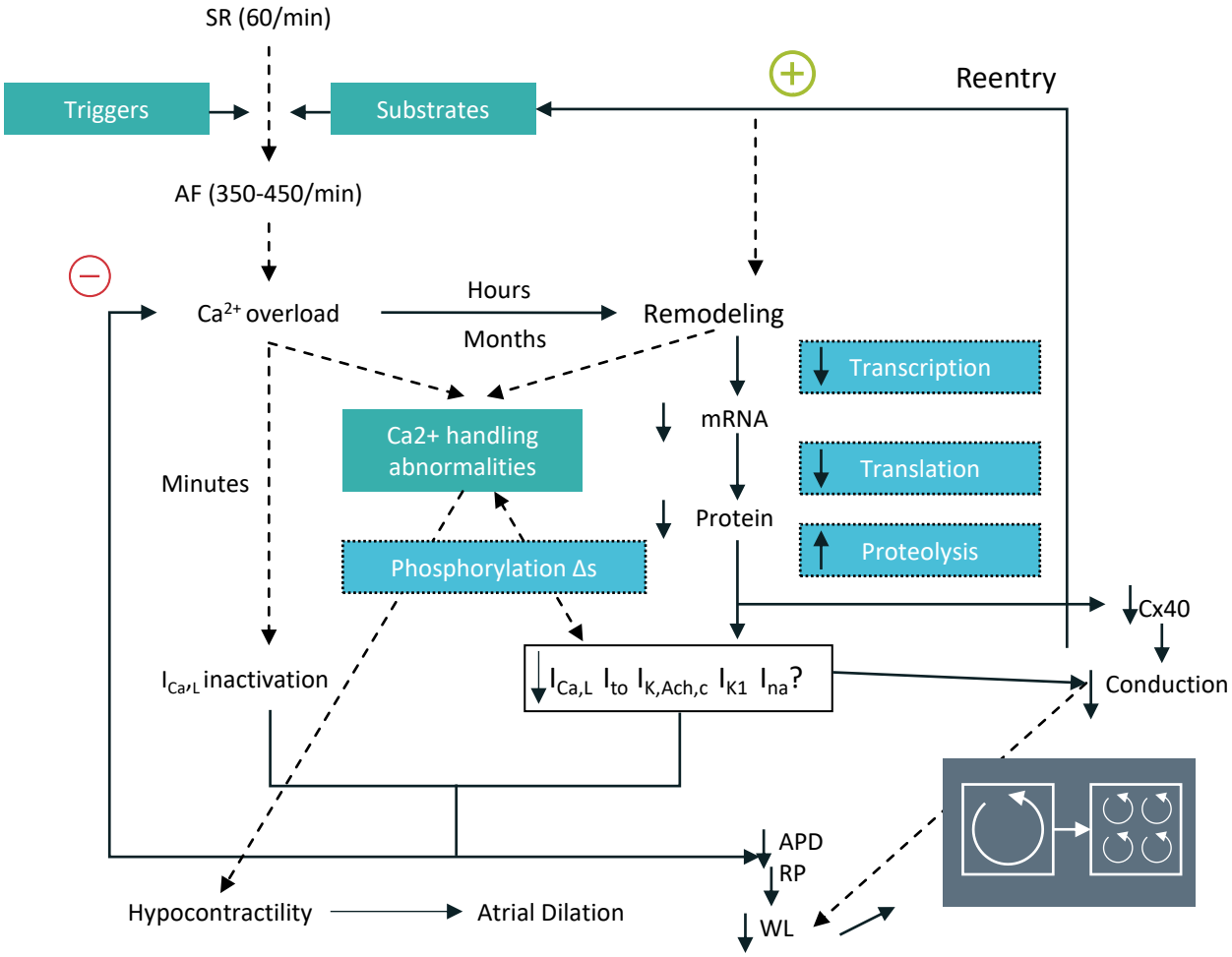

Figure12: Mechanisms underlying electrical remodelling of the atria. Rapid atrial rates increase potentially cytotoxic Ca^{2+} loading. Autoprotective I_{CaL} reductions occur via rapidly developing functional changes (I_{CaL} inactivation) and more slowly developing changes in gene and protein expression. Decreased I_{CaL} reduces Ca^{2+} loading but decreases APD. Diminished APD shortens refractoriness and reduces the wavelength (WL), which allows for smaller and more atrial reentry circuits, thus making AF unlikely to terminate. Atrial tachycardia also increases inward-rectifier currents such as I_{K1} and $I_{KACh,c}$, which further reduces APD and promotes AF. RP indicates refractory period; WL, wavelength. Schematic developed based on [196] [197] [198][199] [200] [201].

Structural remodelling, in particular interstitial fibrosis, is an important contributor to the AF substrate and is believed to reduce atrial tissue compliance by increasing stiffness of the atrial tissue as a result of extracellular matrix remodelling [202]. The regulatory mechanism underlying atrial extracellular matrix remodelling as well as precise signalling pathways that lead to structural changes is thought to vary between different cardiac disease models [203]. There are several secreted factors known to enhance fibrotic tissue development. In addition to their individual effects, they often act together [204]. Angiotensin II and transforming growth factor-β_1 (TGF-β_1) are well-known profibrotic molecules, and recent evidence points to platelet-derived growth factor (PDGF) and connective tissue growth factor (CTGF) also having significant roles in the development of atrial fibrosis [202]. Figure 13 is a summary of the different signalling systems that are involved in atrial fibrosis.

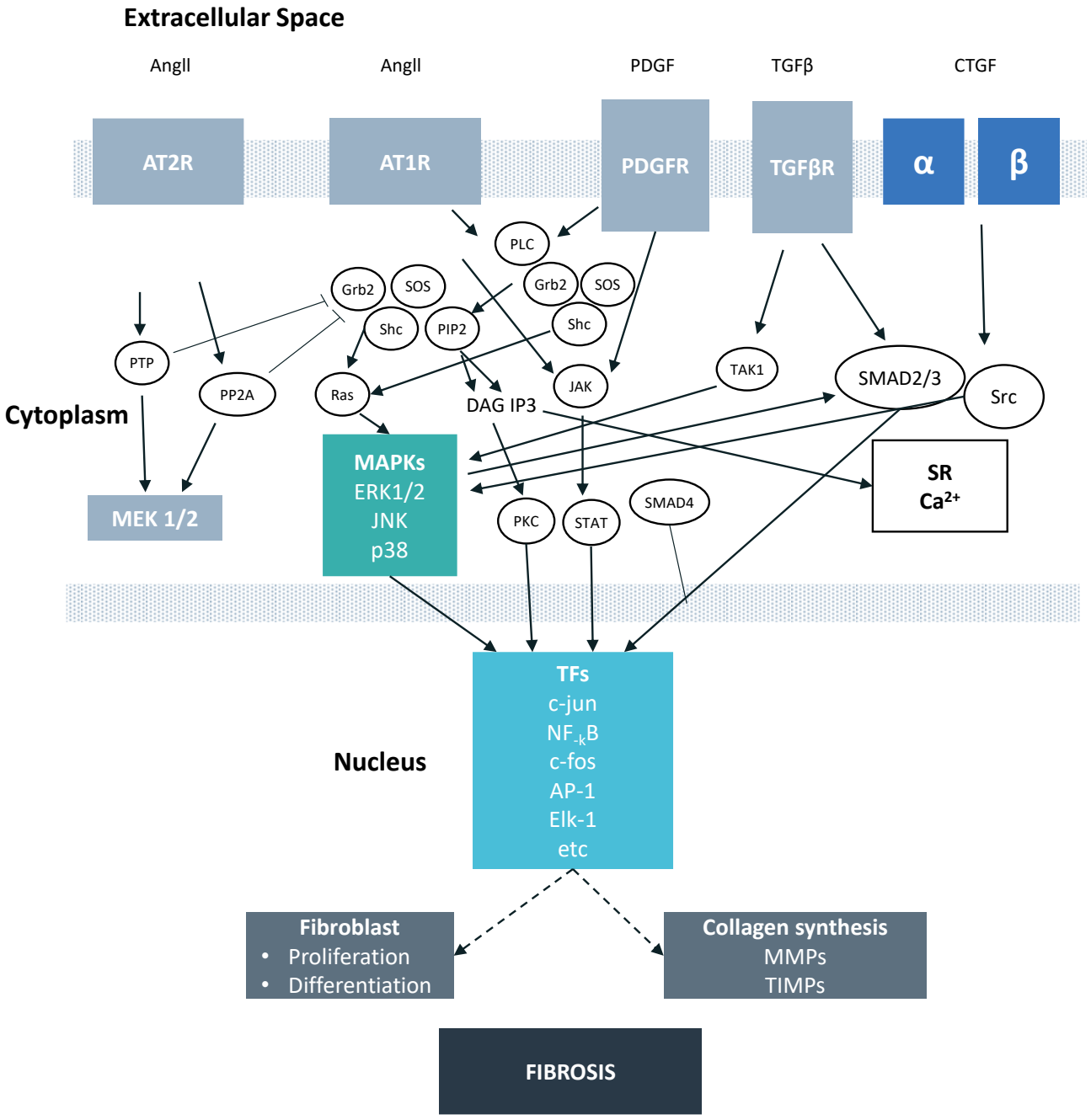

Figure 13: Major profibrotic signalling pathways involved in atrial fibrosis. Interaction between pathways produces positive feedback that is important in fibrosis development. αβ Indicates integrin receptor α- and β-subunits; Ang II, angiotensin II; AP-1, activator protein-1; DAG, diacylglycerol; ERK 1/2, extracellular signal-related kinase 1/2; Grb2, growth factor receptor binding protein 2; JAK, Janus kinase; JNK, c-Jun N-terminal kinase; MAPK, mitogen-activated protein kinase; MEK 1/2, mitogen-activated/ERK kinase 1/2; MMP, matrix metalloproteinase; NF-κB, nuclear factor-κB; PKC, protein kinase C; PDGFR, PDGF receptor; PIP2, phosphatidylinositol bisphosphate; PLC, phospholipase C; PP2A, protein serine/threonine phosphatase 2A; PTP, phosphotyrosine phosphatase; Shc, src homologous and collagen protein; SMAD, SMA- and MAD-related proteins; SOS, son of sevenless protein; STAT, signal transducers and activators of transcription; TAK1, TGF-β1–activated kinase 1; TF, transcription factor; TGF-βR, TGF-β receptor; IP3, inositol 1,4,5-trisphosphate; and TIMP, tissue inhibitor of matrix metalloproteinase. Schematic developed based on [202] [203] [204]

LA compliance, is the ability of the LA to react to haemodynamic changes and is an important determinant of cardiovascular function and pathological physiology [205].

Although, left atrial compliance is thought to be reduced by structural remodelling [206] [207] [208] [209], little data is available on the factors that impact tissue compliance; therefore, the aim of this study was to first calculate a suitable measure of compliance from clinical data obtained from patients attending first time radiofrequency catheter ablation procedures. Once a suitable measure and value for compliance was determined, to preliminary test this measure in a small pilot study to determine factors that could reduce compliance. Finally, in the same cohort of patients to begin to explore the impact of fibrosis, through voltage on the measure of compliance calculated.

3.1.1 Cardiac Catheter Laboratory Setup

Numerous systems are used during an RFCA AF procedure. There are systems to monitor the patient's vital signs (O_2 saturations through pulse oximetry and non-invasive blood pressure) and two different systems to visualize the anatomical structure of the patient's heart, specifically the LA, PVs and LAA. The two imaging systems used within St Bartholemews hospital are fluoroscopy for radiographic visualization and to guide the placement of the CS catheter and trans-septal puncture, and electroanatomic navigation systems for non-fluoroscopic visualization, to guide catheter manipulation during mapping and ablation. An electrogram recording system was also used to record surface ECG and intracardiac electrograms, and to allow for pacing and ablation. Figure 14 and Figure 15 demonstrate the set up at St Bartholomew's Hospital in the cardiac catheter laboratory control room as well as the laboratory itself respectively.

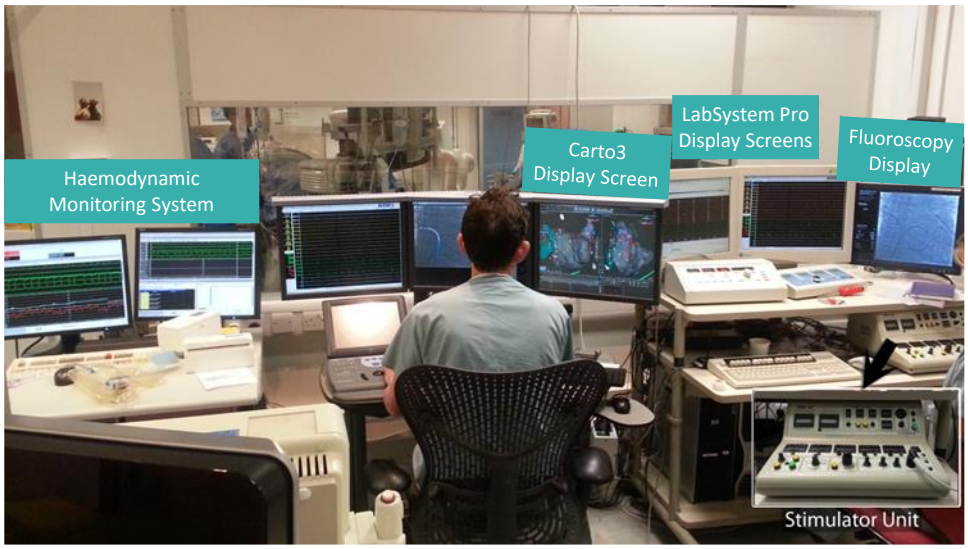

Figure 104: Cardiac Catheter Laboratory Control Room. At St Bartholomew's Hospital. Non-invasive systemic blood pressure as well as invasive pressures is monitored by the haemodynamic monitoring system. The electroanatomic mapping system (Carto3) and fluoroscopy screens as well as the electrogram recording system (LabSystem Pro) are also monitored from the control room.

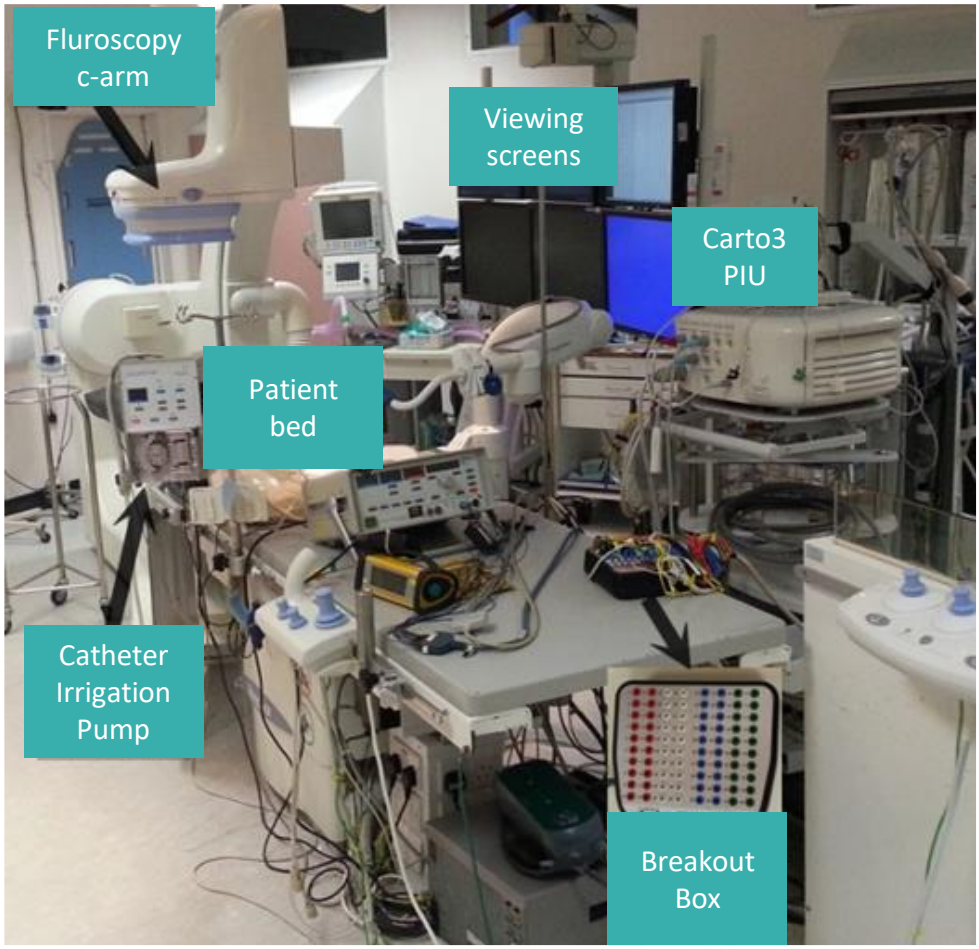

Figure 15: Cardiac Catheter Laboratory. At St Bartholomew's Hospital. Throughout the duration of an AF ablation case, the viewing screens display the same fluoroscopy, electroanatomic mapping, haemodynamic and electrogram data as in the laboratory control room for the operator. The intracardiac electrical signals from the patient pass through the Carto3 Patient Information Unit (PIU) and are fed into the breakout box connector for LabSystem Pro.

Electroanatomic Navigation System

For all clinical procedures in this thesis, the ThermoCool® SmartTouch™ (ST) contact force sensing ablation catheter from Biosense Webster Inc. was used.

The catheter tip electrode of the ThermoCool® SmartTouch™ Catheter range from Biosense Webster (Diamond Bar, CA, USA) is mounted on a precision spring permitting a small amount of electrode deflection (Figure 16).

Figure 16: Thermocool SmartTouch Catheter. On the left side of the image is a cartoon representation of the distal end of the catheter and on the right side, a photograph of a catheter. Cartoon taken from [238].

The SmartTouch catheter integrates with the Carto3 platform. During a case, the magnitude of contact force and its vector are displayed in real-time on the Carto3 display screen as well as the contact force waveform (Figure 17).

For the SmartTouch catheter, the reported sensitivity by the manufacturer is less than 1g of contact force. Comparison data has previously been published comparing the SmartTouch catheter with another widely used contact force sensing catheter (TactiCath™ Contact Force Ablation Catheter,

Abbott), which showed that the aforementioned catheter was highly sensitive and accurate with a mean error rate of ≤1g [211].

Carto3

The Carto3 system incorporates an amalgam of magnetic location technology and current-based visualization to localize catheters within the heart.

The system itself is based on three foundations:

1. ECG – it has the ability to receive body surface signals and up to 78 intracardiac (IC) electrogram channels
2. Location – the system itself is based of two location technologies:
    a. Magnetic location – based on electromagnetic fields generated by the location pads
    b. Advanced Catheter location (ACL) – location based of the three chest and three back patches attached to the patient
3. Mapping – used to build maps of the heart chamber, there are three methods of mapping available, electroanatonical (EA) mapping, Fast anatomical mapping (FAM) and ultrasound catheter mapping. Multiple maps can also be combined, for example EA points can be added to the FAM reconstruction, or the reconstruction created by ultrasound contours.

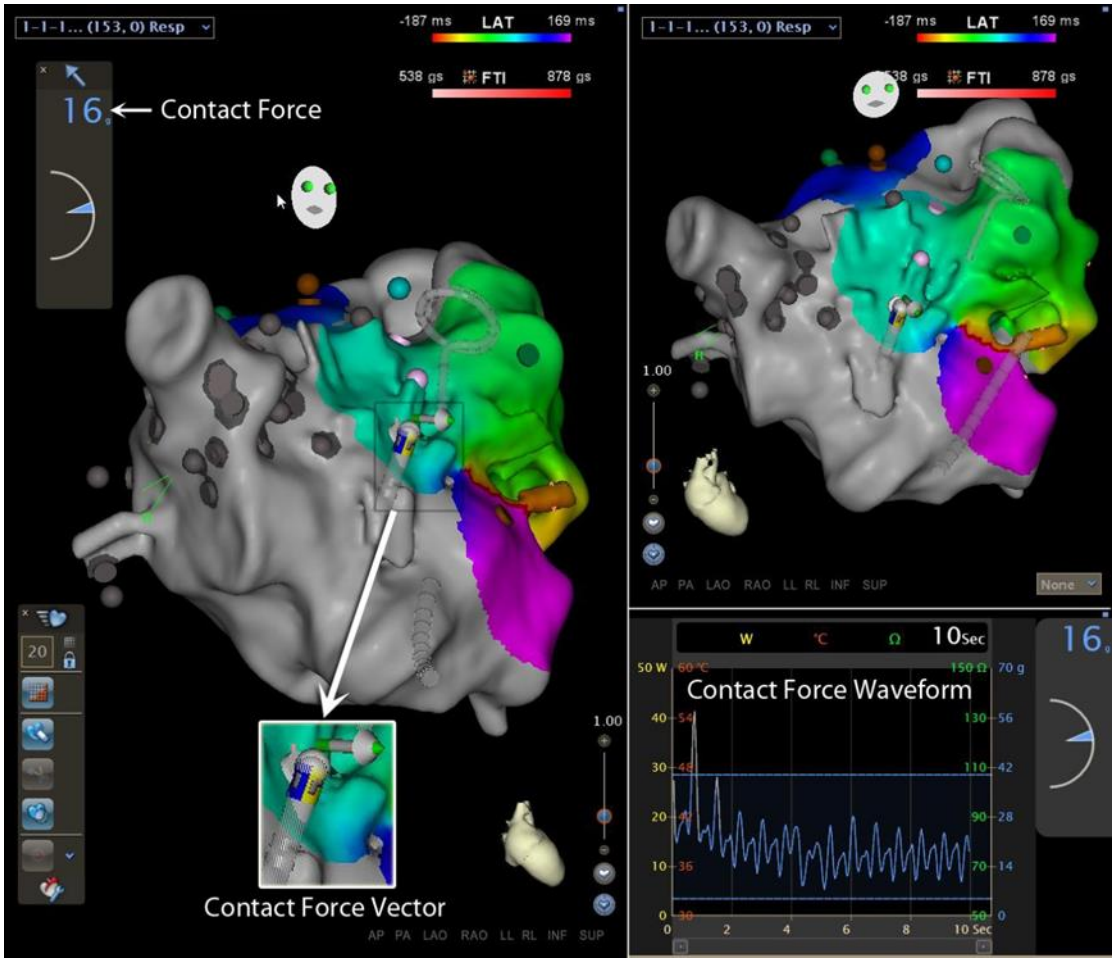

Figure 17: Electroanatomical Mapping Display. The Display of Contact Force Data Measured by the SmartTouch Catheter on the Carto3 Screen. Displayed is a left atrial geometry created using the Carto3 electroanatomic navigation system. Highlighted are the contact force, contact force vector and the contact force waveform for the contact between the catheter and the myocardium.

The magnetic component of the electroanatomic navigation system utilizes a miniature passive magnetic field sensor, which is located in the distal element of the ablation catheter. Beneath the patient a locator pad is inserted, this produces ultralow magnetic fields from three coils [212], the strength of these fields at the location of the sensor deteriorates as they move further away from the source, enabling the operator to determine the distance from each source coil in the location pad. The reported manufacturer mapping accuracy zone is between 12.7 – 46cm above the location Pad. Within this zone, mapping results using the SmartTouch Catheter have an average accuracy of 1mm (Figure 18).

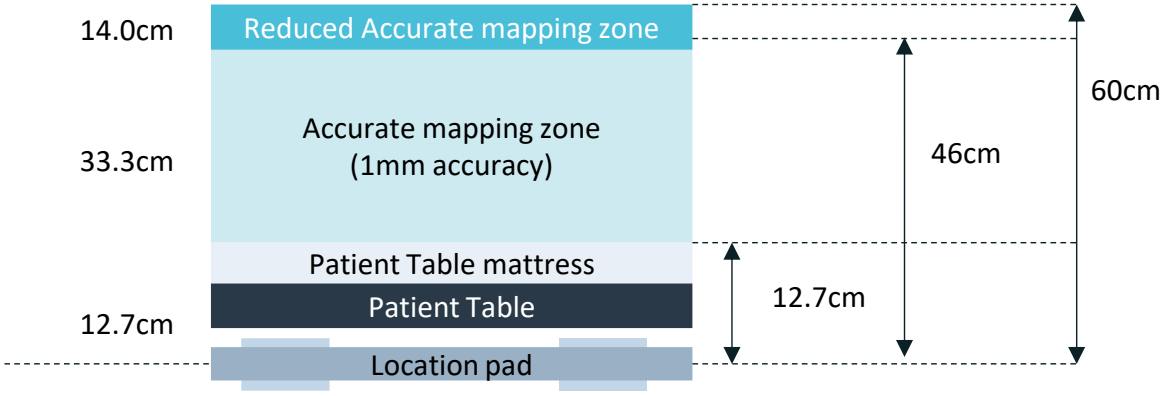

Figure 18: Schematic of the Mapping catheter accuracy zone, based on the set-up at St Bartholemews Hospital, with information from the manufacturers guide.

Gepstein et al. [212] in a previous study demonstrated the accuracy of magnetic localization in providing location measurements within the heart both in vitro and in vivo; these measures were highly reproducible with a very little margin for error.

The current component of the electroanatomic navigation system uses two sets of three reference patches attached to the front and back of the patient's thorax, arranged in a triangle formation around the LA (Figure 19), based on high-frequency, low-power current emissions from every electrode connected to the system. A proprietary algorithm then calculates the position of each electrode based on the relative measured current. The recorded accuracy of this advanced catheter location (ACL) technology alone is 3mm. The current-based technology must be used in conjunction with the magnetic technology, as this not only improves the accuracy of the ACL but is also used to calibrate the current-based technology, in order to reduce the risk of distortions at the peripheries of the electrical field caused by extraneous variables resulting in background signals [213]. The magnetic component of the electroanatomic navigation system utilises magnetic fields generated by a location pad placed under the patient table (Figures 18 and 19), the manufacturer reported mean magnetic-based location accuracy of the Carto3 system is 1mm.

A small current is produced by the current-based visualization system, which stems from the three electrodes located in the catheter, and travels to the surface patches located on the front and back of the patients' thorax. The currents generated by each of the different electrodes within the

catheter emit a slightly different frequency of current allowing the operator to determine which electrode the current has originated from. Each of the three patches located on the patients' thorax measure the strength of current emitted from each electrode, and from this current-ratio data for each electrode location is produced. From this, the locations of the three electrodes in three-dimensional space can be determined, by indexing the current-ratio data with the magnetic location data [213].

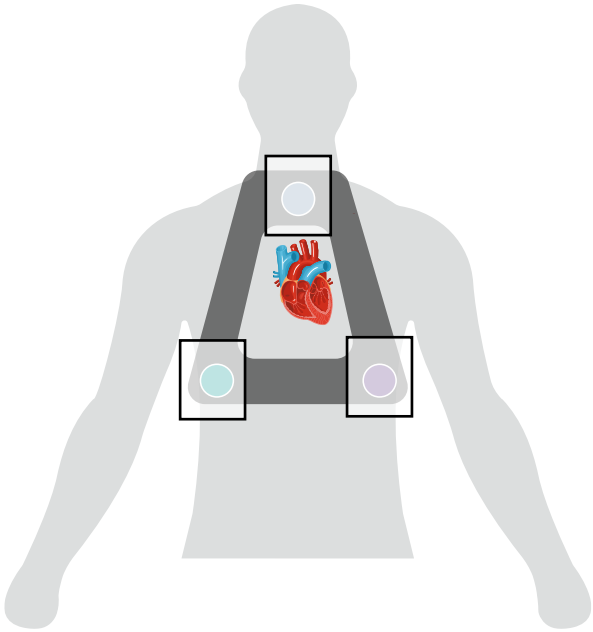

Figure 19: Schematic showing the six surface patches attached to the patient. Rectangles signify the patches attached to the front of the patient's chest, below the coloured circles indicate the three patches attached to the back of the patient, and below that the triangular location pad, situated below the patient table. The heart should be located in the centre.

The system has a number of safety features built in to prevent incorrect placement of the catheter, if the Carto3 system detects severe distortion to the magnetic field, the 'Acquire' button allowing the operator to acquire mapping points is disabled an error message appears, and catheter visualisation disappears. Therefore, mapping is not available, this is in order to prevent incorrect placement of the catheter. Carto3 also has the ability to create a virtual location reference, or body coordinate system (BCS) using the position of the back patches relative to each other and the location pad, this enables the system to determine the initial location reference. The system is then able to monitor this location reference throughout the study for any changes. Depending on the type of movement the system can adjust, these movements are termed "compensated move", whereby the system

detects movement of all back patches as a unit, the distance between patches remains the same. If a "non-compensated move" is detected by the system, when the movement of back patches have changed and the system expects it's due to the patient, the system is unable to adjust it will prompt the operator to start a new map. If a patch(s) is not stuck to the body correctly the system again will alert the operator.

The Biosense Webster Carto3 system has the ability to generate large amounts of separate data export case files per RFCA case. These files include data on cardiac geometries collected, namely the LA and LAA, the locations of the electrodes within these geometries, contact force data, electrogram and ablation biophysical data. All CF data, magnitude and application direction vector data is collected at 20Hz.

Carto 3 in addition to the data collected above, is also capable of exporting location data for each electrode and passive magnetic sensor, however, this data is limited to a 2.5 second collection time, of which 2 seconds is collected retrospectively and 0.5 seconds is collected prospectively to a point being acquired, at a sampling rate of 60Hz.

Throughout the duration of the RFCA procedure, the Carto3 system records CF data and biophysical data, that includes: the temperature of the catheter at its tip (^{o}C – both distally and proximally), the ablation power (W) and impedance power (Ω), all at a sampling rate of 10Hz.

The later part of this study was to both valid the compliance measure calculated by looking at the effect of fibrosis, as a measure of voltage on the measure of compliance. With the overall hypothesis that the greater the level of fibrosis, the lower the compliance. In order to do so bipolar voltage data was required for analysis, however, one limitation of the Carto3 system is that at the time of this research was it was not possible to export data files containing voltage data, for that reason screenshots were taken of the Carto display retrospectively (Figure 20). Points acquired during procedure are automatically tagged by the system to highlight when the point was acquired, if it was before ablation it was tagged with CF (Contact Force) or during ablation (ABL). The point number (#) was used to match the point with the corresponding area within the left atrium.

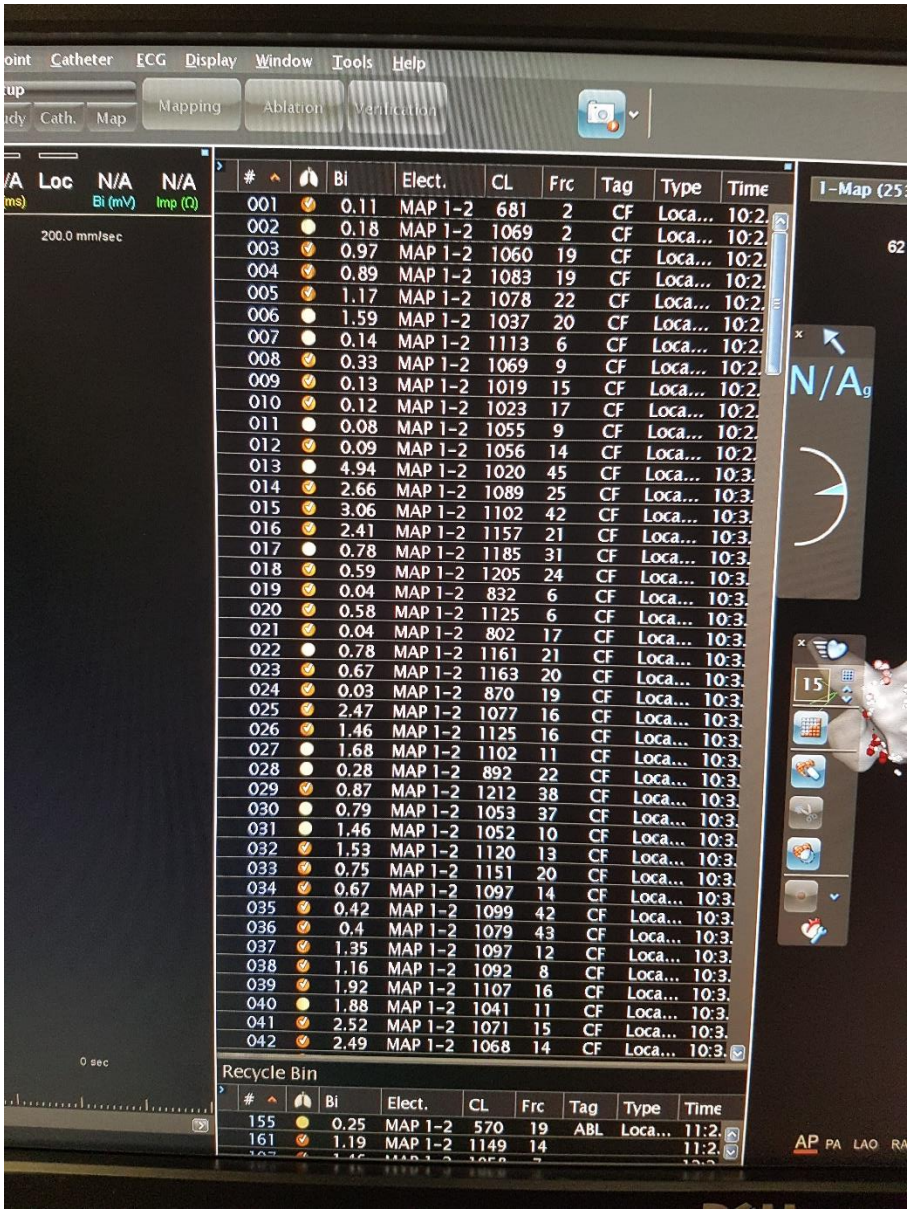

Figure 20: Screenshot taken of the Carto display. Displaying bipolor and force data as well as type of point acquired.

Methods

Study Institution and Personnel

Patients were recruited exclusively from the Barts Heart Centre, St Bartholomew's Hospital, part of the Barts Health NHS Trust, the largest NHS trust, which serves a population of over 2.5 million people in east London and the rest of the United Kingdom. All clinical studies were approved by the institutional Cardiac Peer Review Committee and by National Research Ethics Committee London – West London (reference 11/LO/1861).

All of the studies were designed by the author and Dr Ross Hunter, with all ablation procedures being conducted by Dr Ross Hunter, Professor Richard Schilling and Dr Waqas Ullah. All data was analysed by the author.

Patient and Procedure

The study population includes adults with AF who underwent first time RFCA, performed on clinical grounds. For most, this meant that treatment with at least one anti-arrhythmic drug had failed to revert their hearts back into a normal sinus rhythm.

Patients with an inability or unwillingness to consent to enrolment, who were less than 18 years of age, had contraindications to anticoagulation or transoesophageal echocardiography, or had contraindications to AF ablation such as unresolved intracardiac thrombus, were deemed unfit to enrol on to the research being conducted by an independent research council and thus excluded from the study.

The study population was composed of 36 patients who underwent first-time catheter ablation of either paroxysmal or persistent AF at a single institution. All patients gave written informed consent. The Left Atrium (LA) was divided into 11 sections: Left Pulmonary vein (LPV), Right Pulmonary vein (RPV), Left Atrial Appendage (LAA), Coronary Sinus (Cs) and Inferior wall (IW), combined to be Endo Cs/IW, Anterior Wall (AW), Septum, Posterior Wall (PW), Roof, Mitral value Isthmus (MVI), Left Lateral Wall (LLW), Right Lateral Wall (RLW). Evenly spaced groups of mapping points were

prospectively taken across the LA. No ablation was performed in these regions until mapping was completed. At each location, three to four 8s recordings of CF were taken with the catheter in a stable location, with a minimum CF of 1g and a maximum CF of 40g. None of the study CF points overlapped.

Only when all CF points were acquired from each of the desired areas within the LA, was the ablation procedure performed. All ablation procedures were performed under conscious sedation, a Thermacool SmartTouch (SF) catheter (Biosense Webster, Inc, CA) was used to measure tissue contact force, at a sample rate of 20 Hz. Remote robotic navigation (Sensei Robotic Catheter System, Hansen Medical, Inc, CA) was used in over 60% of procedures, the decision on use was based solely on operator discretion. Tissue CF and electrogram characteristics were recorded using the Carto3 electro-anatomic mapping system (Biosense Webster, Inc). All ablation procedures were temperature controlled, with the internal temperature limited to 48^{o}C, and power limited to 30W. The CF was limited to between 5g and 40g for all procedures. Ablations showing signs of macro displacement of the ablation catheter were excluded from the analysis. None of the study ablations overlapped, and once they were completed within a lesion set, any added ablations were at the operator's discretion

The Carto3 electroanatomic mapping system (Biosense Webster Inc.) recorded CF, location data and voltage data.

Catheter tip and electrode location data were recorded over a 2.5s window for end point, sampled at 60Hz. Displacement of the catheter tip was referenced to the averaged location of the 20 electrode poles of a circular Pulmonary Vein (PV) catheter, positioned in a PV.

Establishing and calculating a suitable measure of compliance

Catheter displacement (displacement (mm)/ contact force (g)) was deemed an appropriate measure of compliance.

To calculate this value, the LA was divided into 11 sections: LPV, RPV,LAA, EndCs/IW, AW, Septum, PW, Roof, MVI, LLW, RLW (Figure 21). A Thermocool SmartTouch catheter (Biosense Webster Inc., Diamond Bar, CA, USA) was used to prospectively map evenly spaced groups, each containing at least four points, across the different sections of the LA, captured across the x,y,z plane. This was also collected by the circular PV catheter, positioned in a PV which would later be used as a reference point (control).

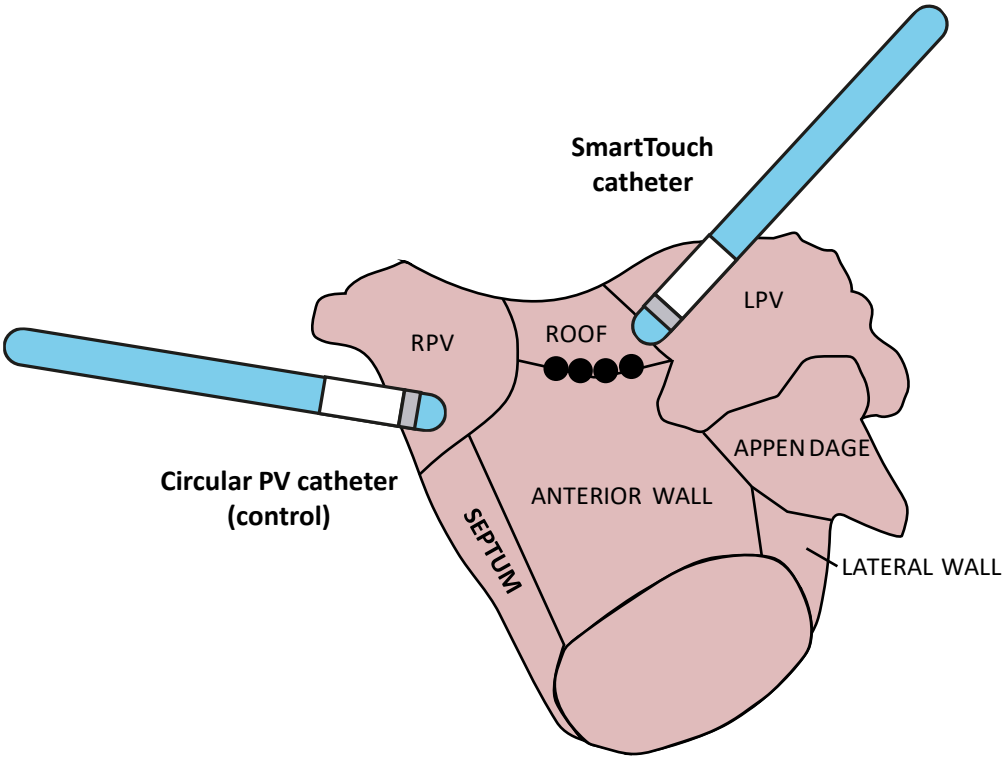

Figure 21: Left atrium divided into segments for the purpose of data collection. LPV = left pulmonary vein, RPV = right pulmonary vein, LAA = left atrial appendage, CS = coronary sinus, IW = inferior wall, AW = anterior wall, PW = posterior wall, MVI = mitral valve isthmus LLW = left lateral wall RLW = Right lateral wall RLW . Displaying the location of the PV catheter (control) and ablation catheter Thermocool SmartTouch catheter (Biosense Webster Inc., Diamond Bar, CA, USA), used to collect all contact force and displacement points. Black circles indicate the group set of points used to develop the compliance measure (mm/g).

Location data as it was captured was automatically tagged by the system to highlight that it was taken prior to ablation (CF) and manually by the operator with the aid of CARTO3 on screen mapping software which visually displays the catheter within an atrial mesh built using the fast anatomical mapping (FAM) method to highlight which location within the Atria the point had been taken from.

At the end of each procedure the location data was exported from the Carto3 system, these exported files were all in .txt format. Data from each catheter at each point was collected in a separate text file (Figure 22) which meant that for each patient there were over 300 files for both the mapping catheter and PV catheter. In order to import these all into excel as one sheet a custom Matlab Script was written.

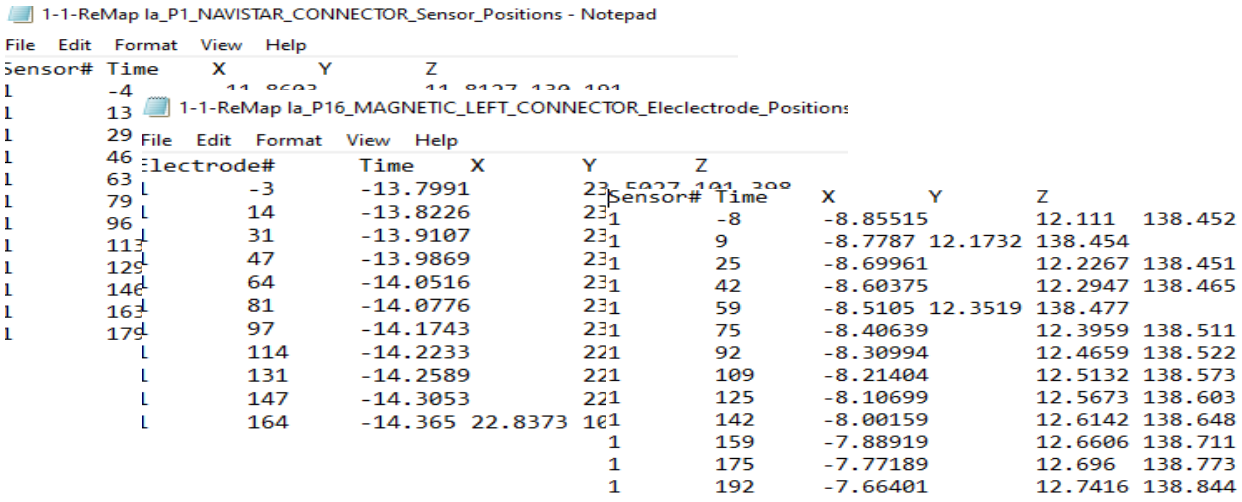

Sensor#	Time (ms)	X	Y	Z
1	5	21.1298	25.9182	95.933
1	22	21.1636	25.8995	95.9143
1	39	21.1937	25.8778	95.8934
1	55	21.2396	25.8583	95.869
1	72	21.271	25.8464	95.8522
1	89	21.3109	25.8325	95.818
1	105	21.3504	25.814	95.7924
1	122	21.383	25.8042	95.772
1	139	21.4126	25.7965	95.7406

Figure 22: Examples of .txt files exported from Carto3 for analysis. It file contains location data in the x,y,z plane for a single point within the LA. Part of a Carto3 location data export for a point. The X, Y and Z co-ordinates for the position of the mapping catheter magnetic location sensor at each time point are given. Here the sensor number refers to the location sensor for the catheter.

Once imported into Excel each point within each area was manually added to the group of points collected from the same area, based on the tag given to the point at the time of the procedure. The vector of each x,y,z plane point of the PV and Thermocool SmartTouch catheter (Biosense Webster Inc., Diamond Bar, CA, USA) were calculated using the Cartesian distance formulae ([P1P2]√(X2-X1)2 + (Y2-Y1)2 + (Z2-Z1)2). As circular PV catheter was the control, reference point for the displacement of the Thermocool SmartTouch catheter (Biosense Webster Inc., Diamond Bar, CA, USA) and should remain in a relatively stable position within the PV, if the absolute distance between vector points taken in PV were greater than 7mm (over twice the length of the catheter tip electrode) they and the corresponding set of vector points recorded by the Thermocool SmartTouch catheter (Biosense Webster Inc., Diamond Bar, CA, USA) were excluded, as highlighted in red (Figure 23).

						ST or STFS Catheter						Lasso Catheter					
Pt	Location	Point	Hansen=	SR(in SR	ST=1 STS	Sensor#	Time	X	Y	Z	3D space	Sensor#2	Time2	X2	Y2	Z2	3D space2
2		348				1	-5	-43.7872	-10.9082	118.47	0.0222865	1	-5	0.622535	3.70133	171.015	0.0078776
2		348				1	12	-43.7697	-10.8944	118.467	0.0223188	1	12	0.623486	3.69351	171.036	0.0155505
2		348				1	28	-43.78	-10.8746	118.477	0.0154013	1	28	0.624284	3.67798	171.064	0.0319439
2		348				1	45	-43.7802	-10.8592	118.491	0.016876	1	45	0.635659	3.64813	171.104	0.0248044
2		348				1	62	-43.7786	-10.8424	118.504	0.0193313	1	62	0.644618	3.625	171.147	0.0333299

Map Cath Location Data					PV Cath Locaton Data			
MeanX	MeanY	MeanZ	Displacement MapCath (mm)	Normalisation by lowest value	MeanX2	MeanY2	MeanZ2	Displacement PV Cath (mm)
-27.66874	-4.634935	112.64096	0		5.63532862	-6.9167496	113.113809	
-30.98206	-2.821984	111.95554	3.838574127	-12.32645192	3.25337054	-1.9658123	113.389751	5.5010589
-25.52981	-5.017853	114.4046	2.798578589	-13.36644745	4.96665507	-8.2537645	112.857069	6.538917121
-29.44839	-3.041692	113.14854	2.44196453	-13.72306151	4.37444792	-3.1022363	113.008169	5.187656854
-21.57114	-18.40227	101.31090	18.843848	2.678821957	6.33287946	-8.4021274	116.734419	6.768252611
-23.89994	-16.56568	100.49807	17.4354951	1.270469059	2.88901424	-0.6189862	116.849954	8.511806074
-22.24969	-14.20598	100.80643	16.1563387	-0.008687342253	2.38263290	-3.7151177	116.607282	3.146639798
-22.66556	-13.42915	100.03390	16.16502604	0	0.42061685	-1.1033407	115.6389	3.407146932

Figure 23: Location data collected in the x,y,z plane (Columns titled: MeanX, MeanY, MeanZ), downloaded directly from Carto and imported into Excel. Converted to a location vector point using the Cartesian distance formulae (Columns titled: Displacement Map Cath (mm), Displacement PV Cath (mm) The red box in the Displacement PV Cath (MM) column highlights a data point to be excluded (>7mm), the lighter pink box in the Displacement MapCath (mm) column highlights the corresponding mapping catheter point that would also be exclude due to the PV rule.

The PV catheter was only used as a sense check, once the mapping points collected using the Thermocool SmartTouch catheter (Biosense Webster Inc., Diamond Bar, CA, USA) had been excluded based off the rule above, the mapping catheter became the only focus in terms of data for calculating displacement.

The first point of each group of vector points taken using the mapping catheter was made zero and this was deemed the baseline vector point (Figure 24). After removing mapping vector point due to the PV rule above, if there were less than two additional vector points from the baseline this entire group of points was removed, two groups of four points (baseline + 3) have been highlighted by the blue squares below in Figure 24.

Figure 24: Displays the patient number, the location within the LA (Area) the vector point came from, manually tagged during the procedure and double checked using both the image export + meta data exported from Carto as well as the exported .txt files, group the point came from (CF Group) tagged by Carto, the point number within that group assigned by Carto, the mean contact force at that location (RmCF (mean Contact) downloaded directly from Carto, PV Displacement (mm), highlighted purple as this was the control data in this column was not used for any analysis, and the location data collected from the Thermocool SmartTouch catheter (Map Cath Displacement (mm)). These points are also vector location points, the two blue squares around the groups of four values separate the two groups of points within the same area of the LA. The first point of each group is made zero as this is the baseline point.

					CONTROL		
Patient Number	Area	CF Group	Point	RmCF (mean contact)	PV Displacement (mm)	Map Cath Displacement (mm)	
14	LPV	4	13	17.33718419	4.025056141	0	
14	LPV	4	14	19.15986631	2.941891196	1.269245186	
14	LPV	4	15	27.12981063	6.107662078	3.348169339	
14	LPV	4	16	27.18097188	5.912232066	1.484555191	
14	LPV	5	20	19.97211444	2.442656464	0	
14	LPV	5	19	27.24982569	2.979955753	2.407184018	
14	LPV	5	17	39.50666063	4.504075334	1.301464956	
14	LPV	5	18	40.60692625	3.946995817	3.137997719	

Contact force data can also be seen in Figure 24, as with was the case with the displacement data, the contact force data was exported from Carto3 in .txt file format, each point had a separate .txt file, containing force data as well as the angle of the catheter Figure 25. Each .txt file had multiple CF values for a single location point, therefore to get a sing mean CF value for each point and to import this data into Excel another custom MatLab script was written.

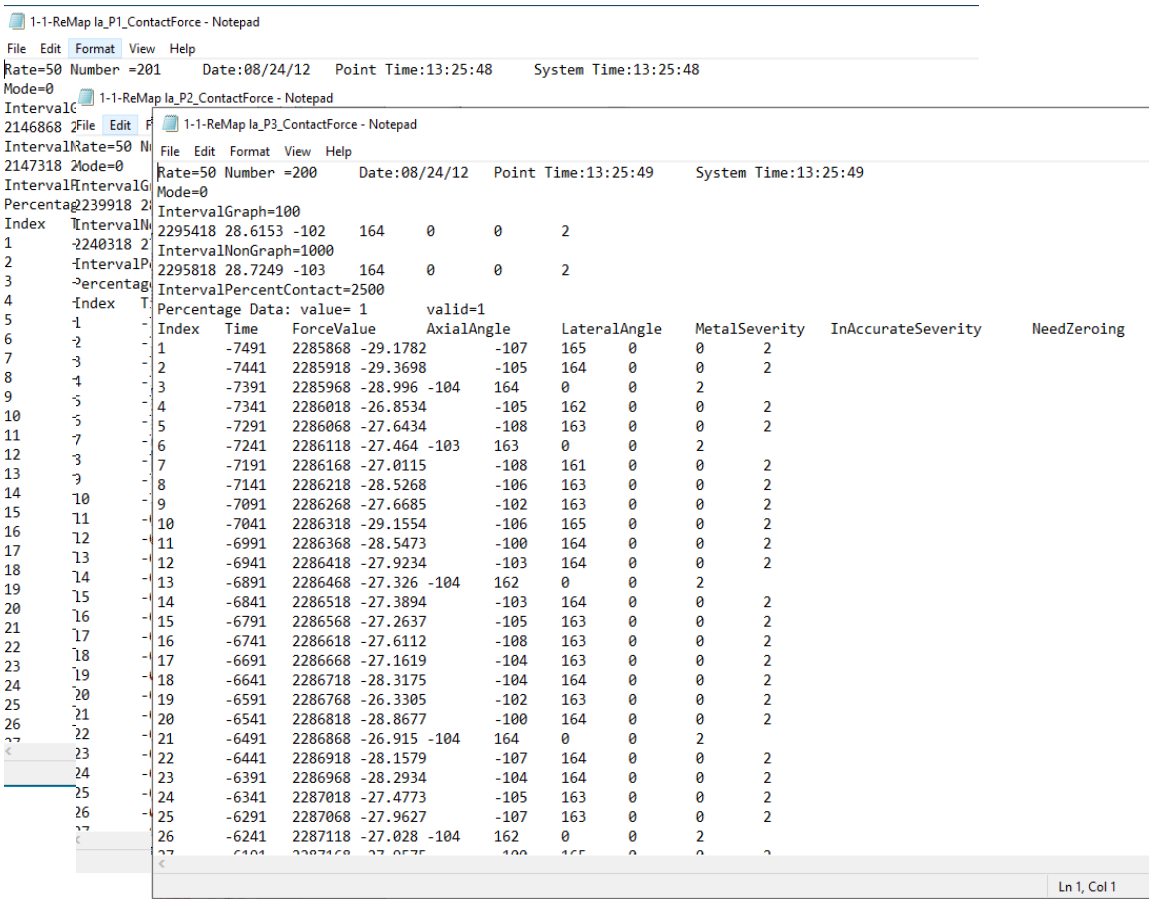

1-1-ReMap Ia_P1_ContactForce - Notepad

File Edit Format View Help

Rate=50 Number =201 Date:08/24/12 Point Time:13:25:48 System Time:13:25:48

Mode=0

1-1-ReMap Ia_P2_ContactForce - Notepad

1-1-ReMap Ia_P3_ContactForce - Notepad

File Edit Format View Help

Rate=50 Number =200 Date:08/24/12 Point Time:13:25:49 System Time:13:25:49

Mode=0

IntervalGraph=100

2295418 28.6153 -102 164 0 0 2

IntervalNonGraph=1000

2295818 28.7249 -103 164 0 0 2

IntervalPercentContact=2500

Percentage Data: value= 1 valid=1

Index	Time	ForceValue	AxialAngle	LateralAngle	MetalSeverity	InAccurateSeverity	NeedZeroing
1	-7491	2285868 -29.1782	-107	165	0	0	2
2	-7441	2285918 -29.3698	-105	164	0	0	2
3	-7391	2285968 -28.996 -104	164	0	0	2	
4	-7341	2286018 -26.8534	-105	162	0	0	2
5	-7291	2286068 -27.6434	-108	163	0	0	2
6	-7241	2286118 -27.464 -103	163	0	0	2	
7	-7191	2286168 -27.0115	-108	161	0	0	2
8	-7141	2286218 -28.5268	-106	163	0	0	2
9	-7091	2286268 -27.6685	-102	163	0	0	2
10	-7041	2286318 -29.1554	-106	165	0	0	2
11	-6991	2286368 -28.5473	-100	164	0	0	2
12	-6941	2286418 -27.9234	-103	164	0	0	2
13	-6891	2286468 -27.326 -104	162	0	0	2	
14	-6841	2286518 -27.3894	-103	164	0	0	2
15	-6791	2286568 -27.2637	-105	163	0	0	2
16	-6741	2286618 -27.6112	-108	163	0	0	2
17	-6691	2286668 -27.1619	-104	163	0	0	2
18	-6641	2286718 -28.3175	-104	164	0	0	2
19	-6591	2286768 -26.3305	-102	163	0	0	2
20	-6541	2286818 -28.8677	-100	164	0	0	2
21	-6491	2286868 -26.915 -104	164	0	0	2	
22	-6441	2286918 -28.1579	-107	164	0	0	2
23	-6391	2286968 -28.2934	-104	164	0	0	2
24	-6341	2287018 -27.4773	-105	163	0	0	2
25	-6291	2287068 -27.9627	-107	163	0	0	2
26	-6241	2287118 -27.028 -104	162	0	0	2	

Ln 1, Col 1

Figure 25: Examples of Contact Force .txt files exported from Carto3.

Once all data was added to excel the following exclusion criteria was used:

- >40mm (change in position (mm))
- At least 2 points in addition to baseline point
- < 1g or > 40g force for each point from baseline (change in CF (g)

The remaining position (displacement) points (mm) were plotted against contact force (g) on a graph, this was done for each of the 11 areas in the LA (LPV, RPV, LAA, Endo Cs/Iw, AW, Septum, PW,

Roof, MVI, LLW, RLW) in each of the 36 individuals included in this trial. A final graph was plotted for each individual of all of the points across the LA.

A trendline was then added to each graph, this trendline was forced through zero to allow for a single Y-value to be given. As the trendline was forced through zero, the R^2 value was also added to give an idea of how robust the points were in comparison to the trendline.

The trendline gave the Stiffness value for each patient for each area (Change in position (mm) (x-axis) / Change in CF (g) (y-axis), compliance is the inverse of this therefore Compliance was calculated using the calculation Compliance = 1/Stiffness. Figure 26 shows an example of this process.

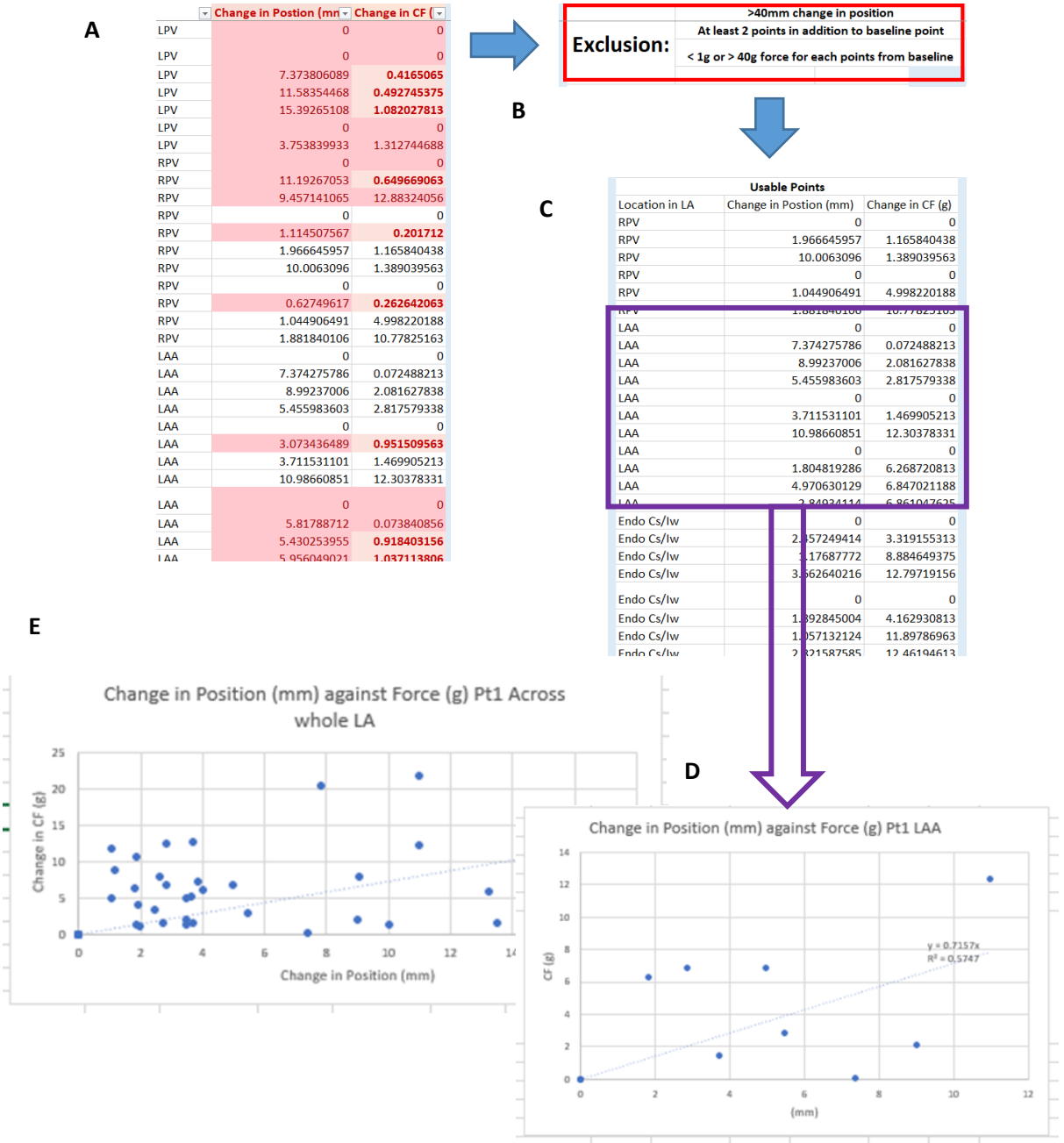

Figure 26: Process of data collection for compliance measure A) shows the change in position (mm) data next to the change in contact force data (g), it displays the baseline value followed by the either the mean change in CF (g), as calculated above, or the location vector for a singular point within a given area within the LA of a single patient. The lighter red box highlights values for exclusion based on the exclusion criteria (for the Change in position >40cm, change in CF <1g >40g) as displayed in B) using the conditional formatting tools within Excel to highlight. The darker red boxes highlight either the corresponding data set in the opposing field, ie if the light red box is in the CF column, the dark red box would be in the adjacent field of the change in position column. Or if after excluding the point there are less than two points from the baseline point that group of points is all highlighted by darker red boxes for exclusion. The remaining non-filled boxes display the data for inclusion. C) is an extract of the remaining usable points for that patient. The Purple box highlights the data that was used to plot D). D) shows the trendline forced through zero, displayed on the graph is also the y -value, the stiffness value, and the R^2value. The stiffness (y-value) is converted to compliance by inversing (1/stiffness) and the R^2value is used through as a means of displaying how robust the trendline value is in relation to all other points. E) shows the same as D) except rather than isolating a certain region within the LA all points obtained for that patient within the LA are plotted and the y and R^2 value recorded.

The R^2 of each trendline was then colour coded (Figure 27):

Males	Females (slightly lighter for the female cohort)
Green ≥ 0.7	Green ≥ 0.7
Yellow <0.7 but >0.5	Yellow <0.7 but >0.5
Red ≤ 0.5	Red ≤ 0.5

Figure 27: R^2 value colour points

The number of each different colour point were then counted (red n=48, yellow n=80 and green n=190), showing that you could be confident in the points around the trendline.

Each patient had multiple compliance values; however, no patient had a value for each of the 11 areas within the left atrium. For that reason, it was decided for all data analysis (except for when comparing compliance within different areas of the LA) the value for compliance used would be 1/stiffness (trendline) value calculated from plotting all points across all 11 areas of the LA within a single patient (Figure 28: highlighted in blue) rather than the average of each individual displacement value for each area (Figure 28: highlighted in purple).

For each of the following graphs used to display the change in compliance based on different factors the same traffic like colour scheme depicting the R^2 value was used.

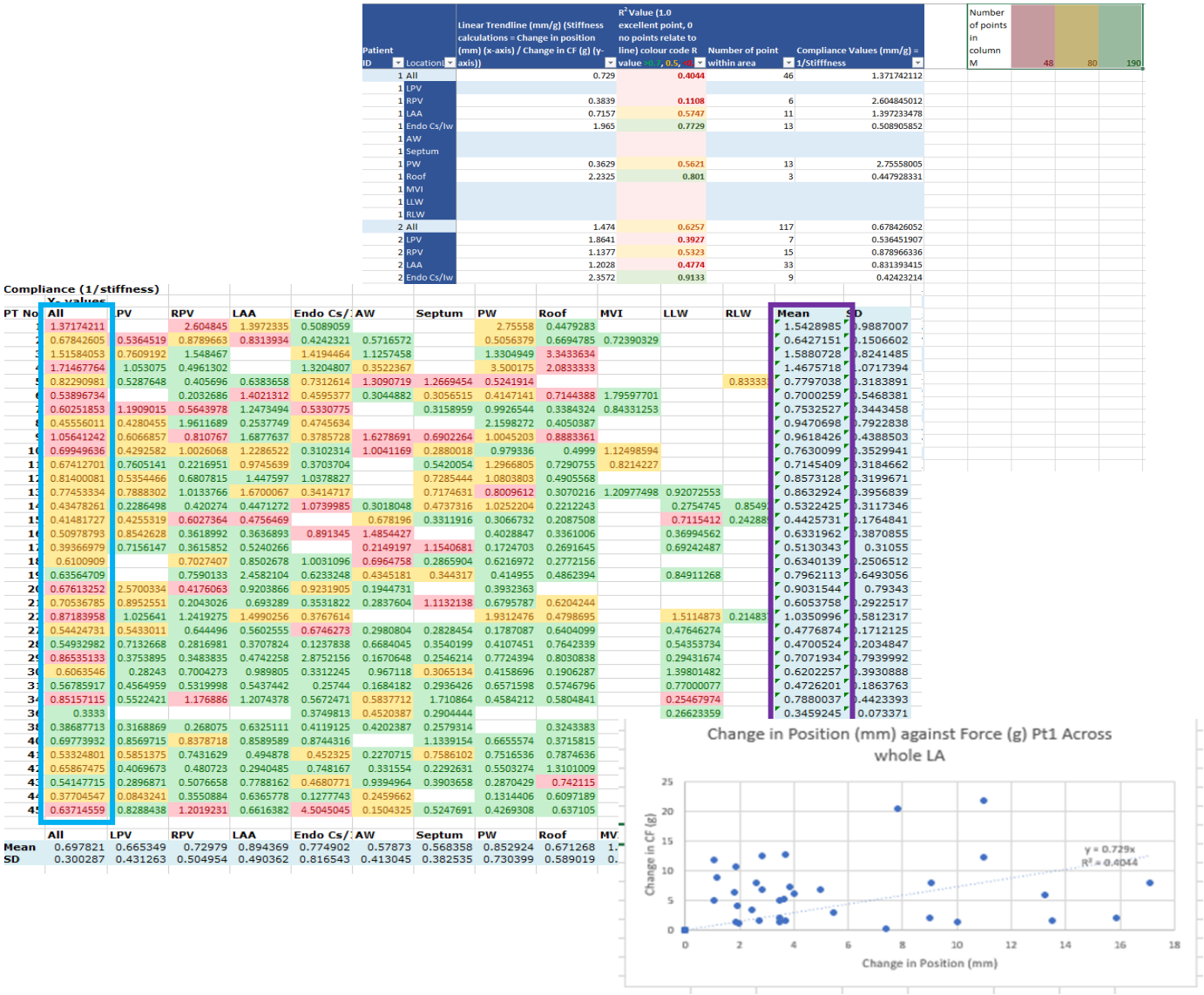

Figure 28: Visual extract of the data used to calculate the compliance for a patient.

Acquiring Voltage data for fibrosis comparisons

Endocardial Bipolar voltage (mV) measured by point-by-point contact mapping collected by the ThermoCool® SmartTouch™ Biosense Webster (Diamond Bar, CA, USA), was used as measure of fibrosis for this project. Using the criteria used by the author with input for the Electrophysiology team at St Bartholemews Hospital, Normal tissue = ≥0.5mV, mild atrial fibrosis = <0.5 but >0.1mV, severe atrial fibrosis = ≤0.1mV. Of the 36 patients included in this cohort, bipolar data was acquired from 29.

Screenshots were taken from the Carto3 system as described previously in *Electroanatomic Navigation System,* as shown in Figure 29, Figure 30 is a schematic example of this data. All bioplar data included in this analysis was collected before any ablation took place.

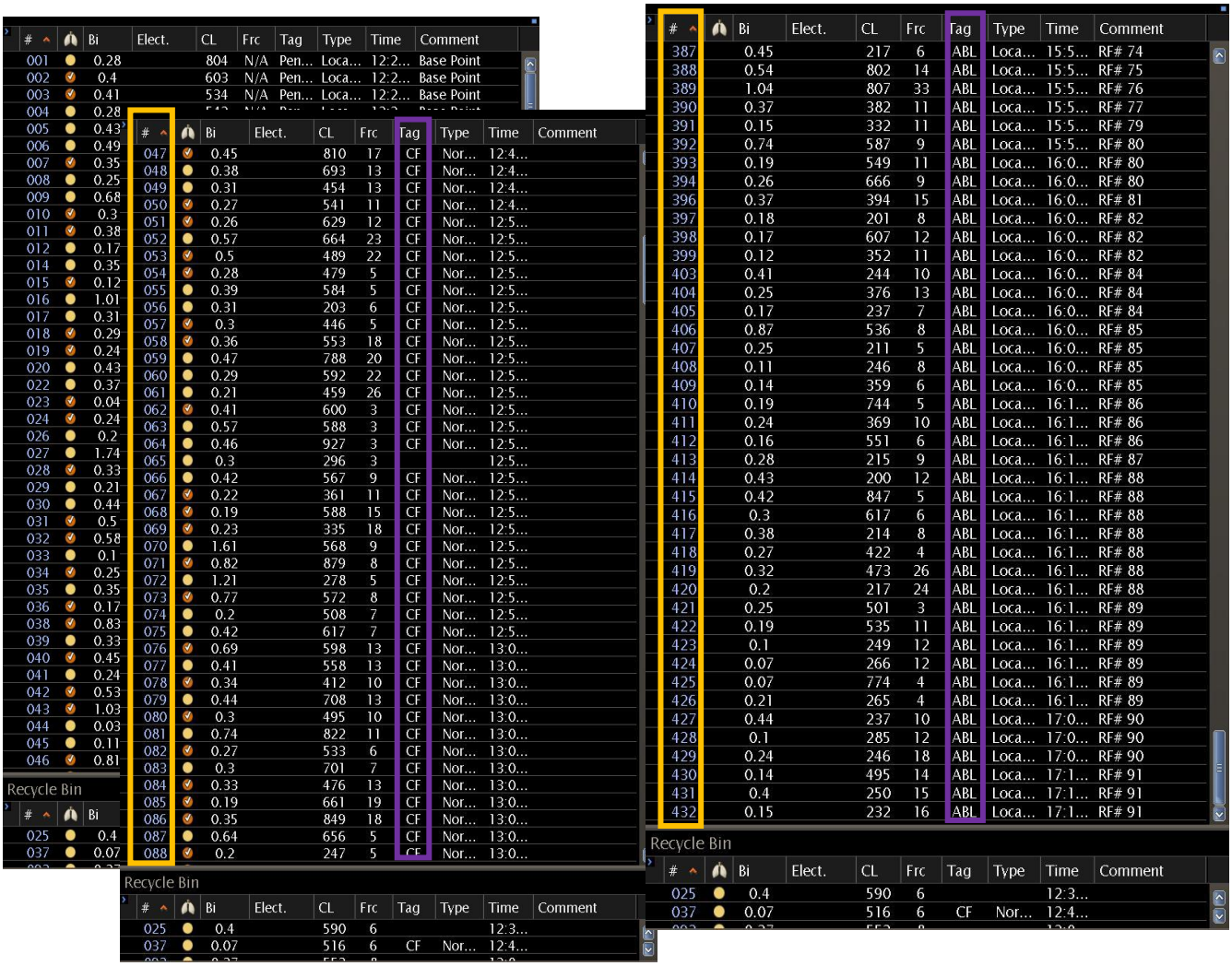

Figure 29: Screenshots of voltage data taken from Carto3 retrospectively after each ablation procedure of Bipolar voltage readings (mV). Data includes point number (#), Bipolar voltage reading (Bi = mV), force (Frc =g) at the point. The Carto 3 system tags the point for when it was taken (Tag), i.e during ablation (ABL), the purple boxes highlight the tag given

For each patient between 350-500 bipolar (mV) measures were collected. All bipolar voltage readings were manually added to excel, ensuring that they were matched with the correct location within the atria from which they were taken by the point# (highlighted orange in Figure 29).

Point#	Bi	Frc	Tag
001	0.18	1	frc
002	0.02	1	frc
003	0.04	3	frc
004	0.23	1	frc
005	0.05	1	frc
006	0.1	19	frc
007	0.44	9	frc
008	0.37	4	frc
009	2.51	15	frc

Figure 30: Example of the dataset containing bipolar voltage data from Carto3 for fibrosis analysis. The screenshot contains the point at which the reading was taken (highlighted orange, point #), bipolar voltage data (mV) collected by the ThermoCool® SmartTouch™ Biosense Webster (Diamond Bar, CA, USA), force data (Frc) at the time the point was acquired and is tagged by the system to say when the point was taken (frc = pre-ablation point).

Once added to excel, all data points with the Tag column marked ABL were removed, to ensure all data points were pre-ablation readings. Bipolar (mV) data points were then excluded if:

1. > 2mV - as this was considered too high a reading for the atria and therefore presumed to be taken from the ventricle.
2. The contact force at that point (Frc) < 5g - as this was deemed to be poor tissue contact.

In order to plot Figures 27 – 30 the biopolar data for each patient was quantified as mean percentage cover of the bipolar voltage reading. For Figure 31, the mean fibrosis reading for each patient was used to plot against compliance.

Data Analysis

Statistical analysis was performed using R Studio (V2.1 FOAS, Boston, MA, USA), Matlab V7.12 with Statistics Toolbox V7.5 and Microsoft Excel 2013 (Microsoft, WA). A p-value of <0.05 was taken to indicate statistical significance. All data was deemed as non-normally distributed by a Shapiro-Wilks test, and was analysed using Kruskal-Wallis test followed by a post hoc Dunn's test. Data was presented as mean±standard deviation or median [interquartile range]. Correlation was assessed for nonlinear relationship by Spearman rank correlation.

Results

Clinical characteristics of patients

36 patients were enrolled in the study, 75% were male. There were 20 PeAF patients in total and 16 PAF patients. The baseline characteristics of the study population are presented in Table .

Patient Population Characteristics (n=36)			
		Paroxysmal atrial fibrillation (PAF)	Persistent atrial fibrillation (PeAF <24)
	Total	(n=16)	(n=20)
Age, mean ± SD	62.8 ± 7.7	73.8 ± 48.2	62.4 ± 9.8
LVEF*, mean ± SD (%)	47.9 ± 17.3	60.8 ± 8.6	42 ± 12.5
LA^ area cm^2, mean ± SD	28.9 ± 5.9	25.4 ± 5.1	32.3 ± 4.0
Male, n (%)	27 (75)	11 (69)	16 (80)
Hypertension, n (%)	15 (42)	5 (25)	10 (50)
Diabetes mellitus, n (%)	2 (6)	1 (6)	1 (5)
Ischeamic heart disease, n (%)	1 (3)	1 (6)	0
Mitral valve disease, n (%)	2 (6)	1 (6)	1 (5)
Pacemaker in situ, n (%)	4 (11)	0	4 (20)
PeAF with a history of PAF, n (%)	9 (25)	-	9 (45)

Table 3: Study Population Baseline Characteristics. * Left ventricular ejection fraction, ^ Left atrial

Contact force applied by the catheter was the same for each group of patients, giving confidence in their comparison. Patients are separated into PAF and PeAF groups throughout this chapter rather than reviewing AF patients as a whole, as the difference in response is a key factor in this thesis.

Factors affecting compliance

Compliance Data

1,945 data points were collected across the 36 patients with either PAF (n=16, 864 data points) or PeAF (n=20, 1084 data points), and the spread of CFs is shown in Figure 31.

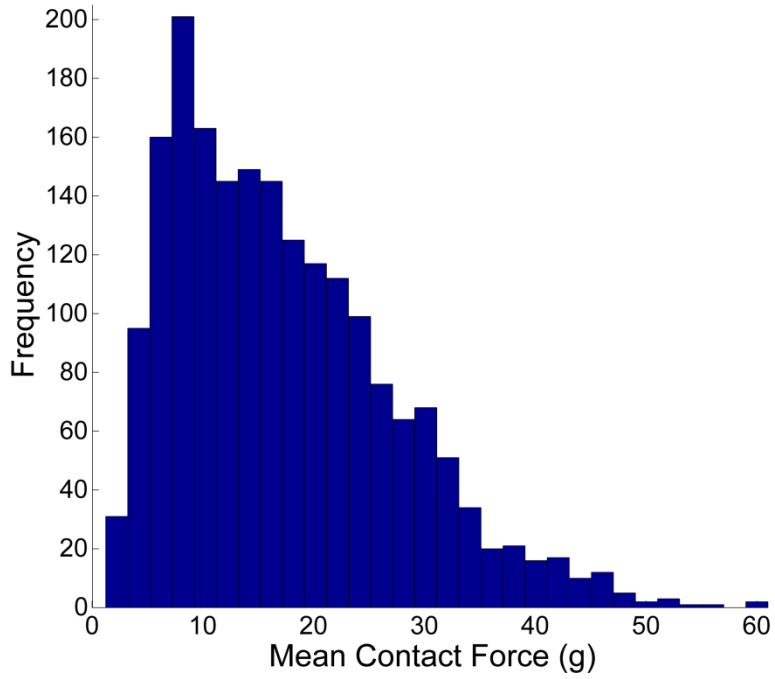

Figure 31: Histogram of mean CF of the study points.

The same number of vector location data points were collected across the same 36 patients, and the spread of displacement values is shown in Figure 32.

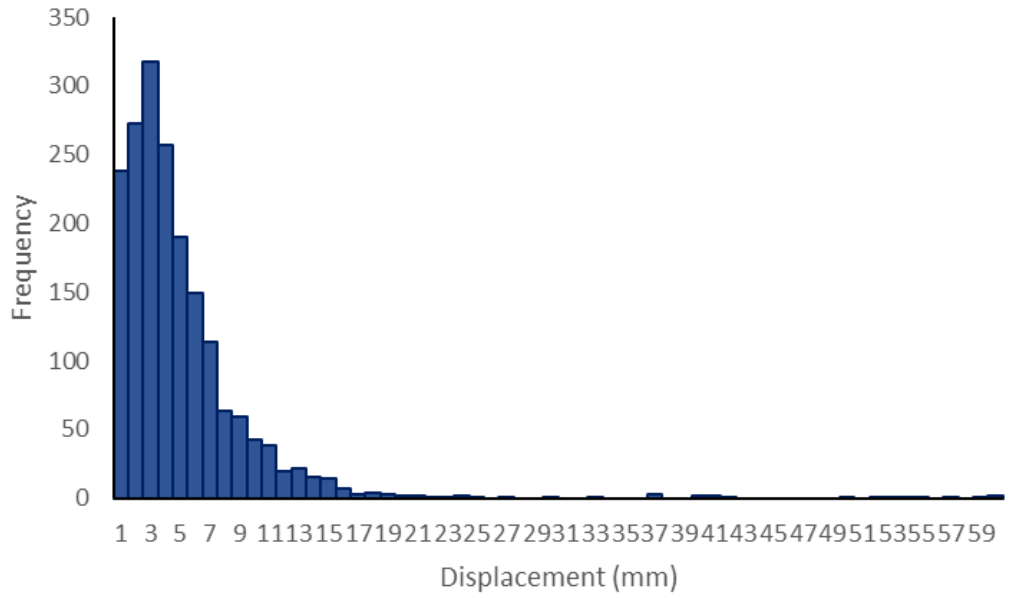

Figure 32: Histogram of displacement data of the study points.

These study points were used to calculate compliance as described previously. Establishing and calculating a suitable measure of compliance.

Differences in Compliance Measure between Types of AF

The compliance measure was compared between the different types of AF, PAF and PeAF. With the hypothesis that, the more severe the AF the lower the compliance value. (Figure 33 and Table 4)

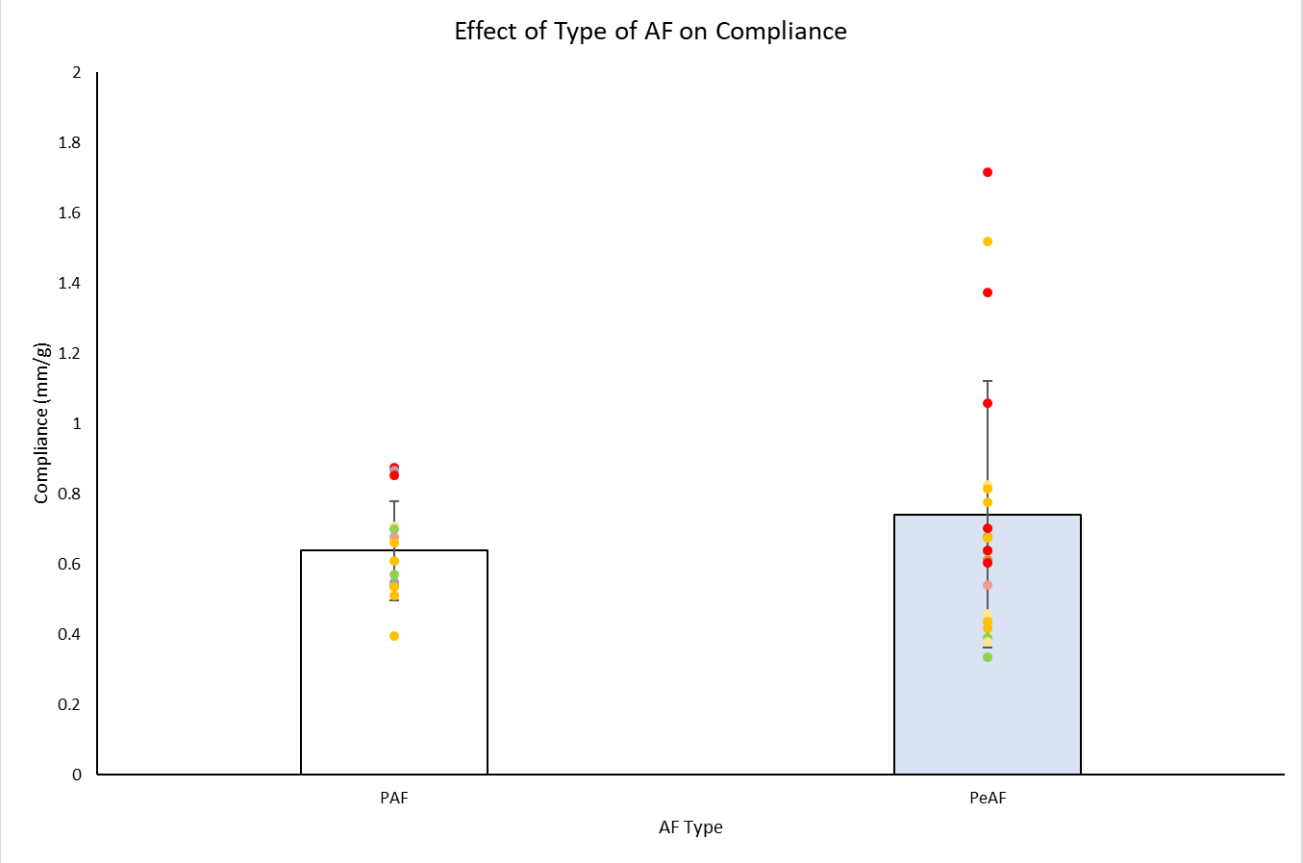

Figure 33: Effect of AF on Compliance Graph. Type of AF versus compliance. PAF = Paroxysmal atrial fibrillation; PeAF = Persistent Atrial Fibrillation. The colours of the individual data points represent the R^2 value of that point, Red = R^2 <0.5, Amber = R^2 = ≥ 0.5 < 0.7, Green = R^2 = >0.7. For females, the colour system remains the same except each colour is a slightly lighter shade.

	PAF		PeAF	
Compliance	Mean (mm/g)	SD	Mean (mm/g)	SD
All Data	0.64	0.14	0.74	0.38
Data removing R^2 below 0.7	0.60	0.07	0.45	0.16

Table 4: Effect of AF on Compliance .Mean and standard deviation in each AF type. Across all data points, and excluding data points with an R^2 Value below 0.7.

There was no significant difference seen in compliance between the two AF groups (P= 0.55). When data points with an R^2 value <0.7 were excluded compliance a decline compliance was visible, however, this again was not significant (P = 0.29).

Difference in Measure of Compliance between AF with and without comorbidities

The compliance measure was then compared between AF groups, with or without comorbidities, with the hypothesis that compliance would be lower in the AF with comorbidities cohort than the AF

cohort without. The comorbidities are listed in the Table 1: Study Population Baseline Characteristics. (Figure 34 and Table 5)

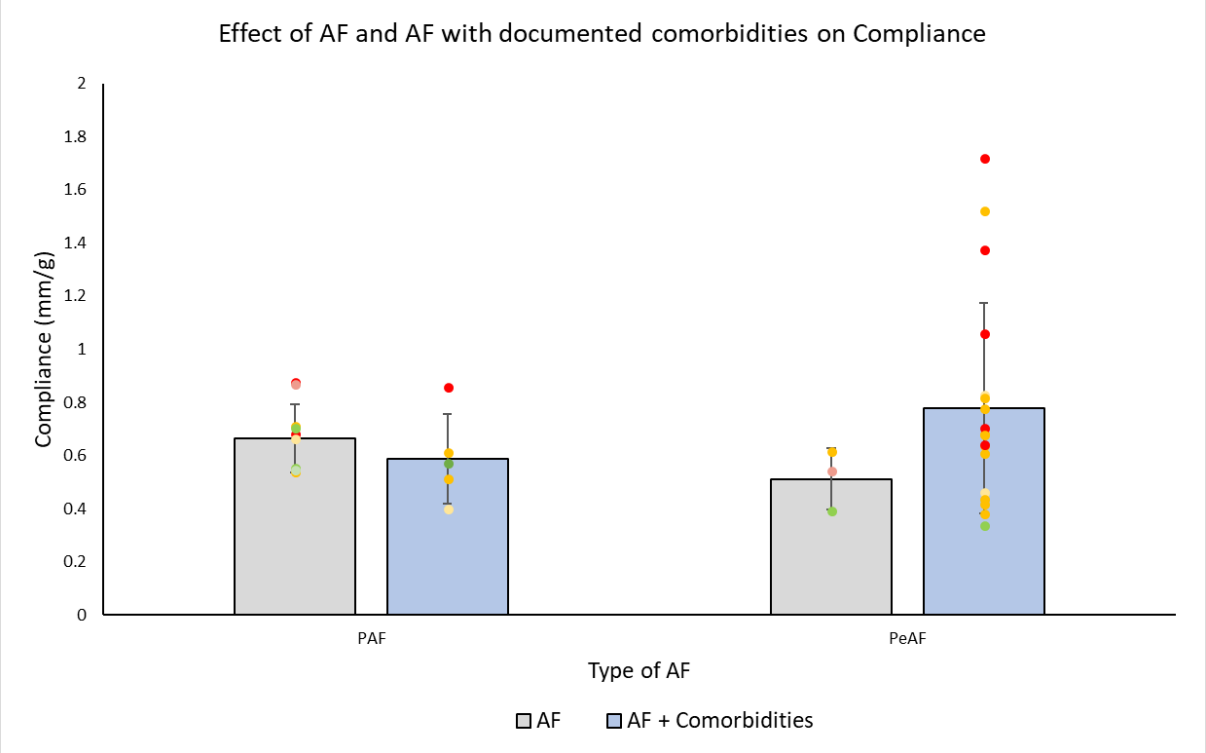

Figure 34: Effect of AF and AF with documented comorbidities on Compliance measure. PAF = Paroxysmal atrial fibrillation; PeAF = Persistent Atrial Fibrillation. The colours of the individual data points represent the R^2 value of that point, Red = R^2 <0.5, Amber = R^2 = ≥ 0.5 < 0.7, Green = R^2 = >0.7. For females, the colour system remains the same except each colour is a slightly lighter shade.

	PAF				PeAF			
	AF		AF + Comorbidities		AF		AF + Comorbidities	
Compliance	Mean (mm/g)	SD	Mean (mm/g)	SD	Mean (mm/g)	SD	Mean (mm/g)	SD
All Data	0.66	0.13	0.59	0.17	0.52	0.11	0.78	0.40
Data removing R^2 below 0.7	0.60	0.09	0.57		0.39		0.48	0.21

Table 5: Effect of AF and AF with documented comorbidities on Compliance measure. Mean and standard deviation in each AF type. Across all data points, and excluding data points with an R^2 Value below 0.7.

The results show that there was no difference between the AF group and the AF with comorbidities group, regardless of whether weak data points with an R^2 value of <0.7 were removed. Between the PAF cohorts with all data points included P = 0.13 (PAF with R^2 value <0.7 excluded: P = 0.65) , for the PeAF cohort with all data points included P = 0.12 (PeAF with R^2 value <0.7 excluded: P = 1).

When comparing all data points for the PAF without comorbidities and the PeAF cohort without comorbidities, although not significant there was a weak trend in compliance value decreasing (P = 0.09). The same trend was not seen between the PAF cohort with comorbidities and the PeAF group with comorbidities though (P = 0.09). When the less robust data points (R^2 value <0.5) no trend was seen, without comorbidities P = 0.18, with comorbidities P = 1.

Differences in Compliance Measure with time spend in AF

The compliance measure was compared between time spend in the two AF groups. Time was measured in years and was divided into three groups: ≤2 year, 3 years and > 4 years, with the hypothesis increased time spent in more severe AF type would result in a decrease in compliance. The results are displayed in Figure 35 and Table 6 below.

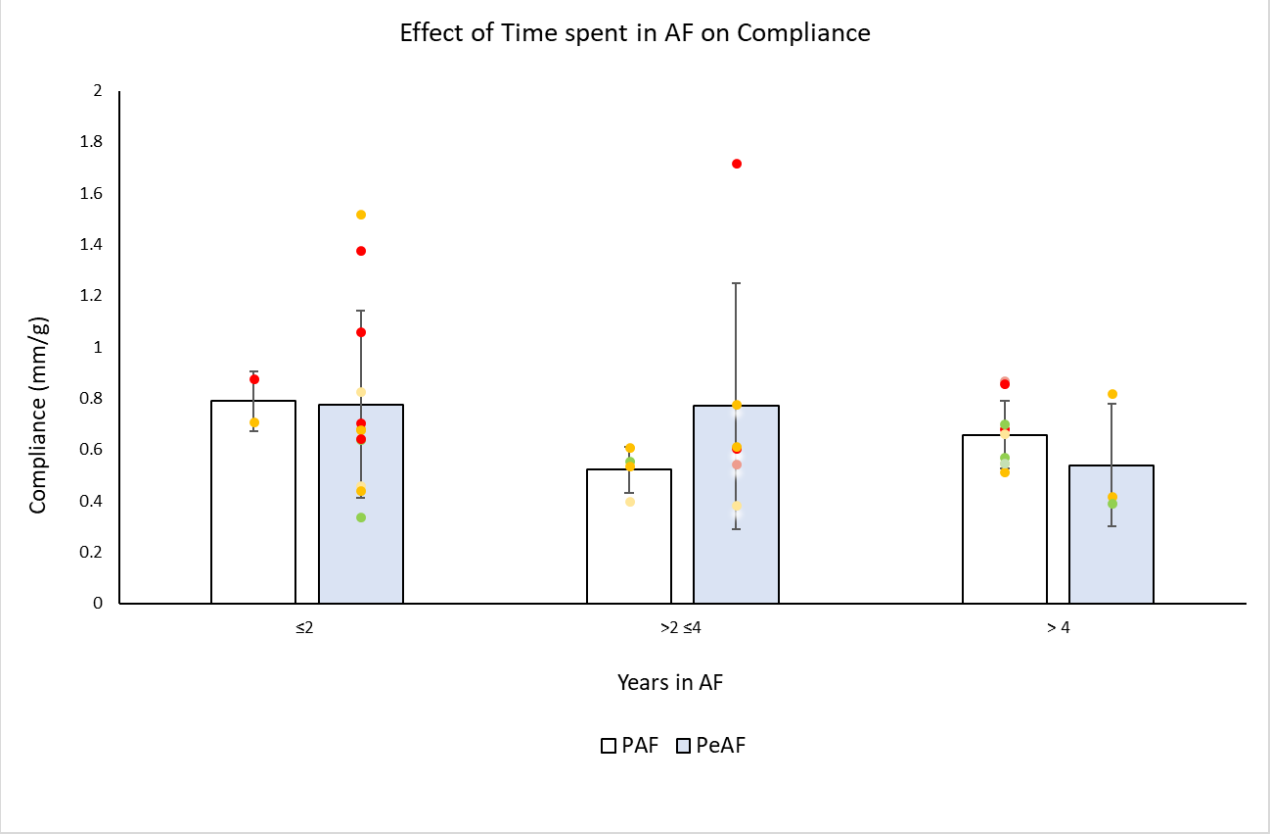

Figure 35: Effect of Time Spent in AF on Compliance Measure. PAF = Paroxysmal atrial fibrillation; PeAF = Persistent Atrial Fibrillation. The colours of the individual data points represent the R^2 value of that point, Red = R^2 <0.5, Amber = R^2 = ≥ 0.5 < 0.7, Green = R^2 = >0.7. For females, the colour system remains the same except each colour is a slightly lighter shade.

	PAF						PeAF					
Years in AF	≤2		>2 ≤4		> 4		≤2		>2 ≤4		> 4	
Compliance	Mean (mm/g)	SD	Mean (mm/g)	SD	Mean (mm/g)	SD	Mean (mm/g)	SD	Mean (mm/g)	SD	Mean (mm/g)	SD
All Data	0.79	0.12	0.52	0.09	0.65	0.13	0.78	0.36	0.77	0.48	0.53	0.24
Data removing R^2 below 0.7			0.54		0.60	0.08	0.48	0.21			0.39	0.60

Table 6: Effect of Time Spent in AF on Compliance Measure. Mean and standard deviation in each AF type. Across all data points, and excluding data points with an R^2 Value below 0.7.

Looking at all of the data points together indicates that there may be a steady decline in compliance associated with a greater amount of time spend in AF, a P of 0.08 in the PAF cohort supports that supports that, however, this is not significant. This same trend cannot be supported in the PeAF cohort as the P = 0.78. When data points with an R^2 value <0.7 are removed no trend can be seen (PAF: P = 0.65, PeAF P = 1).

Comparisons between the PAF cohort and the PeAF cohort at the same time showed no difference between measure of compliance. Patients in AF for ≤2 year: P = 0.36 (no patients within the PAF group had a compliance measure with an R^2 <0.7 therefore a p-value could not be calculated for this group), 3 years: P = 0.29 (no patients within the PeAF group had a compliance measure with an R^2 <0.7 therefore a p-value could not be calculated for this group), >4 years: P = 0.67 (data points with an R^2 <0.7 removed: P = 0.18).

Compliance Measure differences between Gender

The compliance measure of each of the 36 patients was then plotted by gender, in different types of AF, with the hypothesis compliance in the atria will be lower in females than males and that compliance reduces with severity of AF, therefore female patients in the PeAF cohort will have the lowest compliance measure. In actual fact no difference was seen between the male and female cohort. (Figure 36, Table 7).

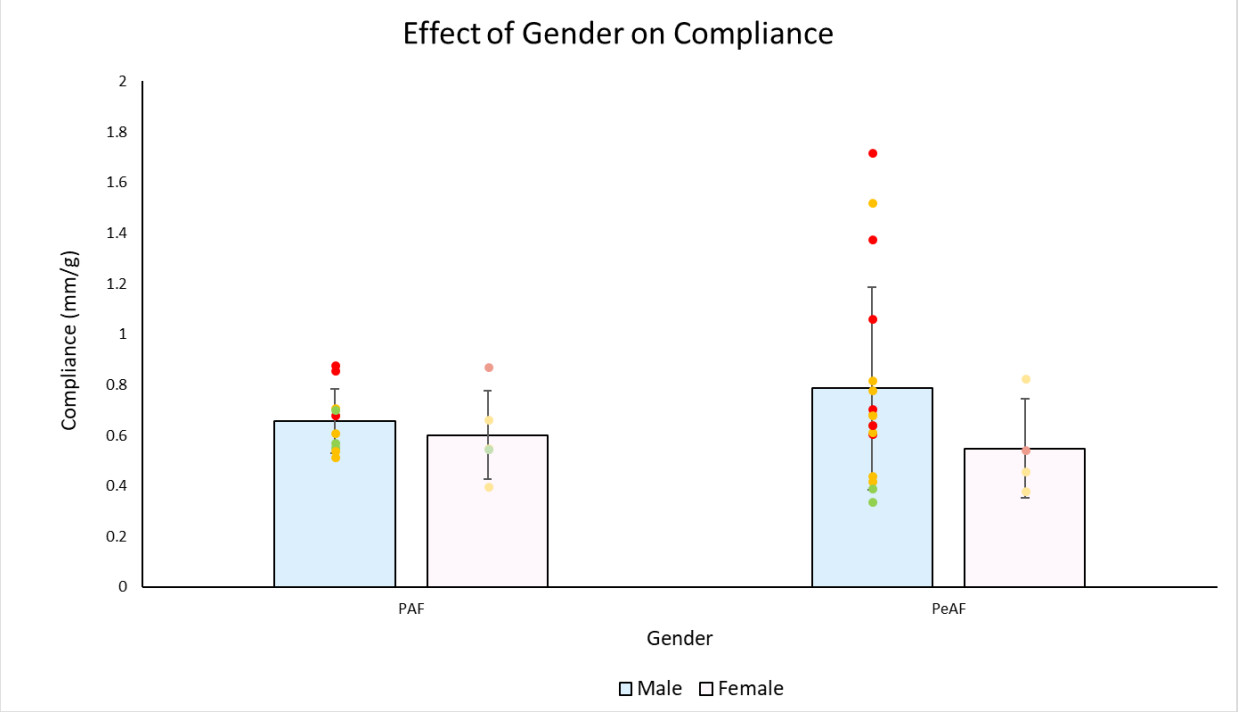

Figure 36: Change in compliance measure between genders. PAF = Paroxysmal atrial fibrillation; PeAF = Persistent Atrial Fibrillation. The colours of the individual data points represent the R^2 value of that point, Red = R^2 <0.5, Amber = R^2 = ≥ 0.5 < 0.7, Green = R^2 = >0.7. For females, the colour system remains the same except each colour is a slightly lighter shade.

	PAF				PeAF			
Gender	Male		Female		Male		Female	
Compliance	Mean (mm/g)	SD	Mean (mm/g)	SD	Mean (mm/g)	SD	Mean (mm/g)	SD
All Data	0.66	0.13	0.60	0.18	0.79	0.40	0.55	0.19
Data removing R^2 below 0.7	0.60	0.08	0.54		0.45	0.16		

Table 7: Change in compliance measure between genders. Mean and standard deviation in each AF type. Across all data points, and excluding data points with an R^2 Value below 0.7.

Although when looking at all of the data points, inclusive of those with an R^2 value <0.5 in Table 7, the measure of compliance is lower in females than that of males within the same group this is not significant. In the PAF group: P = 0.53 (excluding data points with R^2 value <0.7: P = 0.18) and in the PeAF group: P = 0.22 (excluding data points with R^2 value <0.7: P = 1).

In terms of change in compliance in gender with severity, again no trend could be seen Males: P = 0.35 excluding data points with R^2 value <0.7: P = 0.28), Females: P = 0.33 (too few points within the female cohort to calculate p-value for data points where the R^2 value <0.7).

Compliance measure change due to Ventricular Function

Compliance values were then compared between different groups to ventricular function, measured as a percentage of left ventricular ejection fraction. With the hypothesis lower ventricular function reduces compliance. Figure 37 and Table 8 indicate a trend in the PeAF group, that as LVEF decreases so to does compliance, which gives better confidence that there is a relationship between ventricular function and compliance, however this is not significant. PeAF: P = 0.23 (excluding data points with R^2 value <0.7: P = 0.22). As none of the PAF cohort had an LVEF % >50 it was not possible to calculate any difference.

Within the cohort of patients with an LVEF% ≥50, there was no significant difference between those with PAF and PeAF in terms of compliance: P = 0.16 (excluding data points with R^2 value <0.7: P = 0.48)

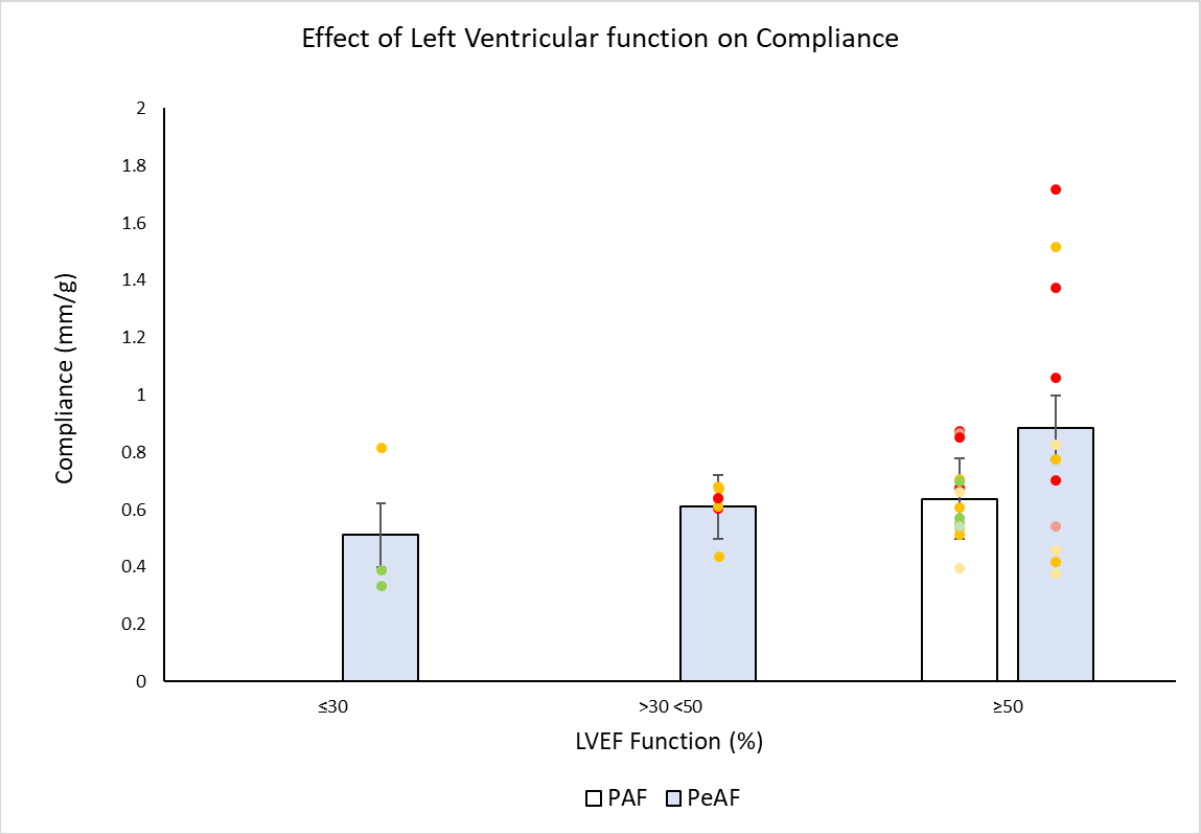

Figure 37: Ventricular function on Compliance measure. PAF = Paroxysmal atrial fibrillation; PeAF = Persistent Atrial Fibrillation. The colours of the individual data points represent the R^2 value of that point, Red = R^2 <0.5, Amber = R^2 = ≥ 0.5 < 0.7, Green = R^2 = >0.7. For females, the colour system remains the same except each colour is a slightly lighter shade.

	PAF						PeAF					
LVEF (%)	≤30		>30 ≤50		≥50		≤30		>30 ≤50		≥50	
Compliance	Mean (mm/g)	SD	Mean (mm/g)	SD	Mean (mm/g)	SD	Mean (mm/g)	SD	Mean (mm/g)	SD	Mean (mm/g)	SD
All Data					0.64	0.14	0.51	0.26	0.61	0.083	0.88	0.47
Data removing R^2 below 0.7					0.57	0.09	0.51	0.26	0.61	0.1	0.72	0.43

Table 8: Ventricular function on Compliance measure. Mean and standard deviation in each AF type. Across all data points, and excluding data points with an R^2 Value below 0.7.

Change in compliance dependent on Left Atrial size

Compliance values were compared between different sizes of LA, those ≤30 cm and those >30cm, with the hypothesis being as the size of the LA increases, compliance also increases. Although both Figure 38 and Table 9 show some indication that there is some relationship between an increase in size causing an increase in compliance, it is not significant. PAF cohort: P = 0.16 (excluding R^2 P = 1), PeAF: P = 0.62 (excluding R^2 value <0.7:, P = 0.22).

When comparing the size of the type of AF within the same size atria, to see if severity of AF regardless of the size of the atria had an impact on compliance, again no significant difference was seen between the two groups, ≤30cm : P = 0.46 (excluding R^2 value <0.7: P = 0.41), >30cm : P = 0.45 (excluding R^2 value <0.7: P = 0.32). Although not significantly different, the indication for the same relationship in both conditions, gives a better confidence that there is a link between LA size and compliance.

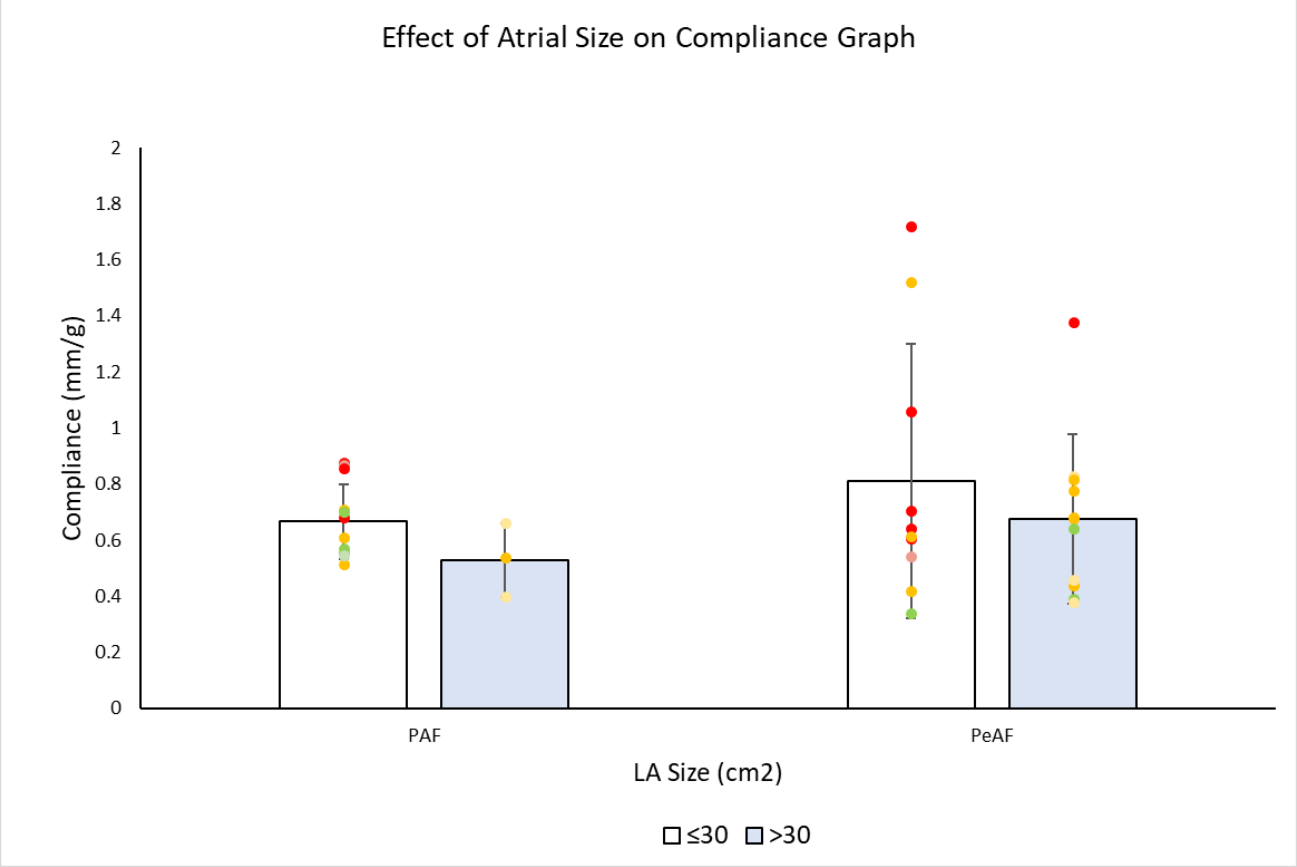

Figure 38: Differences in compliance measure due to size of the Left Atria. PAF = Paroxysmal atrial fibrillation; PeAF = Persistent Atrial Fibrillation. The colours of the individual data points represent the R^2 value of that point, Red = R^2 <0.5, Amber = R^2 = ≥ 0.5 < 0.7, Green = R^2 = >0.7. For females, the colour system remains the same except each colour is a slightly lighter shade.

	PAF				PeAF			
LA Size (cm)	≤30		>30		≤30		>30	
Compliance	Mean (mm/g)	SD	Mean (mm/g)	SD	Mean (mm/g)	SD	Mean (mm/g)	SD
All Data	0.67	0.14	0.53	0.68	0.81	0.49	0.68	0.30
Data removing R^2 below 0.7	0.59	0.07			0.33		0.51	0.18

Table 9: Differences in compliance measure due to size of the Left Atria. Mean and standard deviation in each AF type. Across all data points, and excluding data points with an R^2 Value below 0.7.

Change in compliance as a result of Age

An increase in age is believed to cause a decrease in compliance. To test this measure of compliance, it was compared in three different age groups: ≤60, >60 ≤70 and >70 years at the time of their first ablation procedure. In both Figure 39 and Table 10 no relationship was seen between age and

compliance, an increase in age was not seen to reduce compliance. This may suggest that age is not as relevant to compliance as time in AF.

In the PAF group: P = 0.79 (excluding R^2 value <0.7: P = 1), in the PeAF group: P = 0.16 (excluding R^2 value <0.7: P = 0.22).

When comparing PAF and PeAF in patients < 60 years old: P = 0.22 (excluding R^2 value <0.7: P = 0.22), >60 ≤70 years old: P = 0.48 (excluding R^2 value <0.7: P = 0.44) and >70 years old: P = 0.18 (no one >70 years old in either the PAF or PeAF cohorts had a compliance value with R^2 value <0.7, therefore unable to calculate).

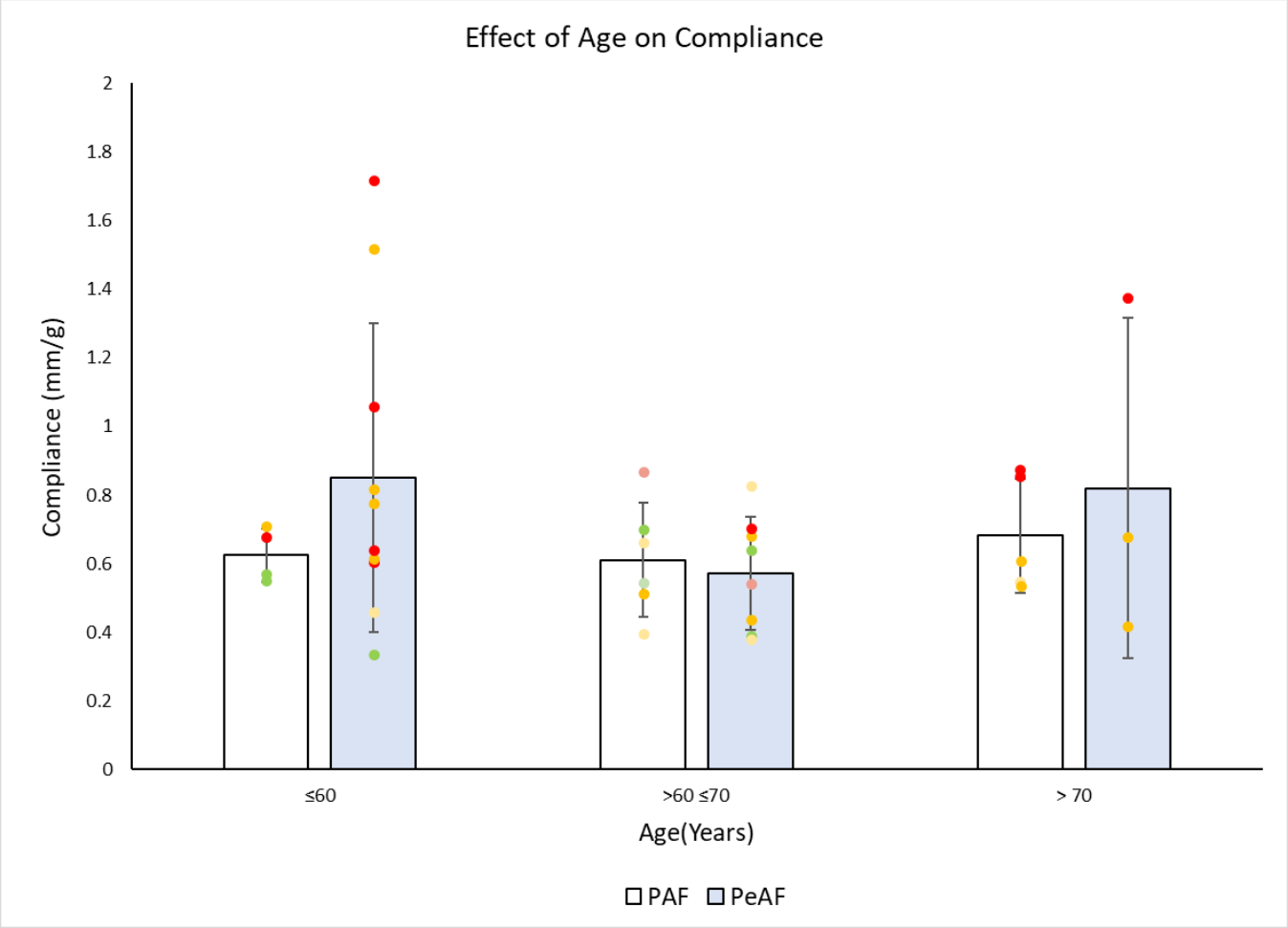

Figure 39: Differences in compliance measure due to Age. PAF = Paroxysmal atrial fibrillation; PeAF = Persistent Atrial Fibrillation. The colours of the individual data points represent the R^2 value of that point, Red = R^2 <0.5, Amber = R^2 = ≥ 0.5 < 0.7, Green = R^2 = >0.7. For females, the colour system remains the same except each colour is a slightly lighter shade.

	PAF						PeAF					
Age (years)	≤60		>60 ≤70		> 70		≤60		>60 ≤70		> 70	
Compliance	Mean (mm/g)	SD	Mean (mm/g)	SD	Mean (mm/g)	SD	Mean (mm/g)	SD	Mean (mm/g)	SD	Mean (mm/g)	SD
All Data	0.62	0.08	0.61	0.17	0.68	0.17	0.85	0.45	0.57	0.16	0.82	0.49
Data removing R^2 below 0.7	0.55	0.01	0.61	0.11			0.33		0.51			

Table 10: Differences in compliance measure due to Age. Mean and standard deviation in each AF type. Across all data points, and excluding data points with an R^2 Value below 0.7.

Compliance measures in different areas of the Left Atrium

Compliance measurements taken from 11 predefined areas across the LA and PVs were compared. With the hypothesis, higher levels of compliance would be seen in thinner, more elastic walled areas such as the LPV and RPV compared to thicker, more muscular walls of the atria such as the Anterior, posterior and lateral as well as the roof.

Figure 40 and Table 11 display this difference between areas. A slight trend could be seen in that generally the walls of the atria had the lower compliance values, the right lateral wall (RLW), anterior wall (AW) for example had the lowest measure of compliance recorded overall, however, this was not statistically this significant (RLW: p-value could not be calculated as there were too few values, AW: P = 0.16, excluding R^2 values <0.7: P = 0.28). The highest measure of compliance, lowest stiffness was recorded in the MVI, showing possible trend towards the hypothesis, however, statistical significance could not be calculated within this area owing to too few compliance values collected.

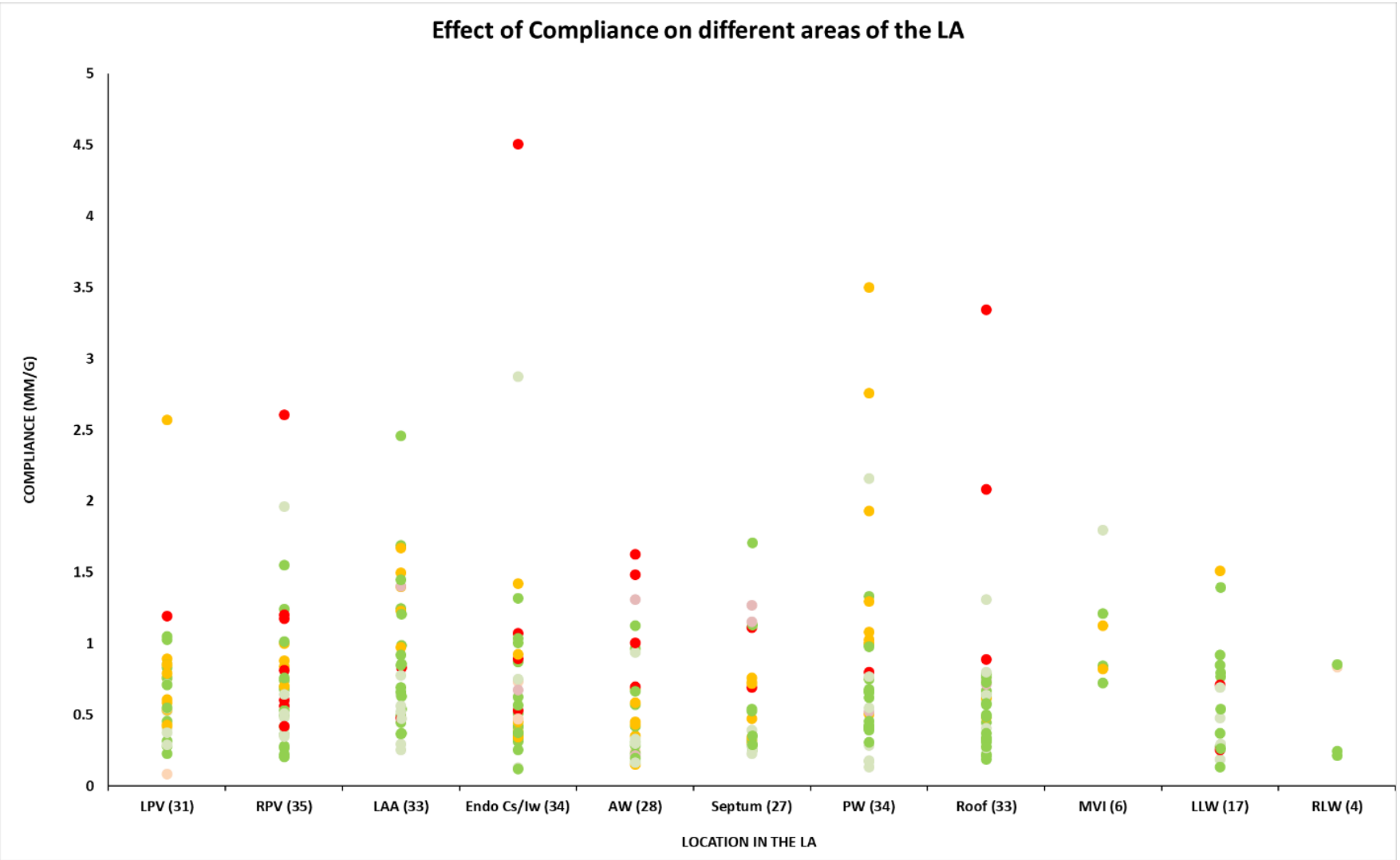

Figure 40: Differences in compliance measure between different areas of the Left Atrium. PAF = Paroxysmal atrial fibrillation; PeAF = Persistent Atrial Fibrillation. The colours of the individual data points represent the R^2 value of that point, Red = R^2 <0.5, Amber = R^2 = ≥ 0.5 < 0.7, Green = R^2 = >0.7. For females, the colour system remains the same except each colour is a slightly lighter shade.

Area	LPV		RPV		LAA		Endo Cs/Iw		AW		Septum		PW		Roof		MVI		LLW		RLW	
Compliance (mm/g)	Mean	SD	Mean	SD	Mean	SD	Mean	SD	Mean	SD	Mean	SD	Mean	SD	Mean	SD	Mean	SD	Mean	SD	Mean	SD
All Data	0.67	0.43	0.72	0.50	0.89	0.49	0.77	0.82	0.58	0.41	0.57	0.38	0.85	0.73	0.67	0.59	1.09	0.36	0.61	0.39	0.54	0.31
Data removing R^2 below 0.7	0.59	0.27	0.61	0.44	0.80	0.50	0.67	0.62	0.47	0.32	0.48	0.40	0.62	0.44	0.51	0.25	1.14	0.48	0.57	0.36	0.44	0.36

Table 11: Differences in compliance measure between different areas of the Left Atrium. Mean and standard deviation in each AF type. Across all data points, and excluding data points with an R^2 Value below 0.7.

Figure 41 and Table 12 Figure 42 and Table 13 show the difference between areas when compared between AF severity. For the PAF cohort no trends were seen between different areas of the LA (P = 0.4, excluding R^2 values < 0.7: P = 0.32), however for the PeAF cohort a difference was seen between the areas when looking at all compliance values (P = 0.01) when R^2 values <0.7 were removed however, this was no longer significant (P = 0.09).

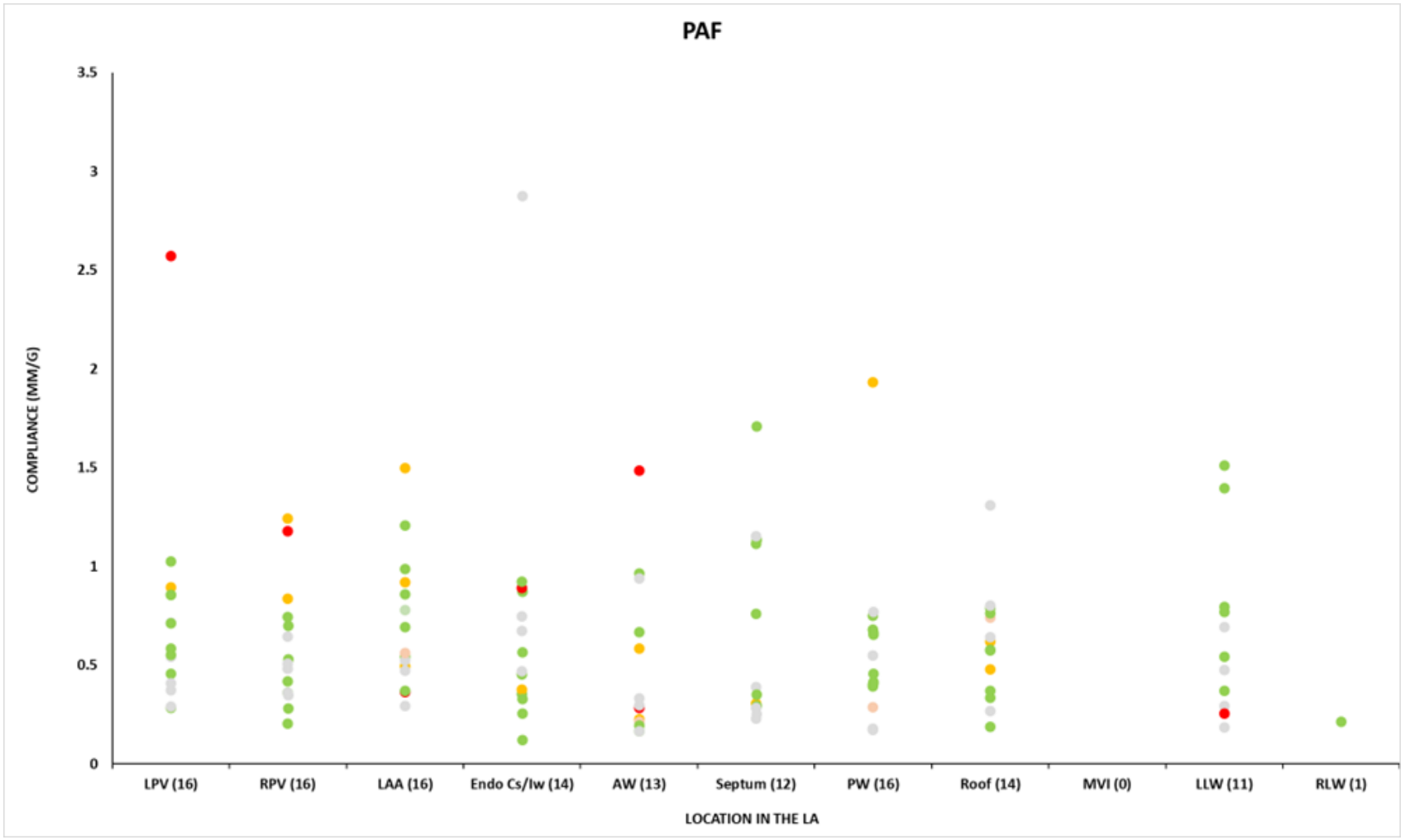

Figure 41: Differences in compliance measure between different areas of the Left Atrium in the PAF cohort. PAF = Paroxysmal atrial fibrillation. The colours of the individual data points represent the R^2 value of that point, Red = R^2 <0.5, Amber = R^2 = ≥ 0.5 < 0.7, Green = R^2 = >0.7. For females, the colour system remains the same except each colour is a slightly lighter shade.

Area	LPV		RPV		LAA		Endo Cs/Iw		AW		Septum		PW		Roof		MVI		LLW		RLW	
Compliance (mm/g)	Mean	SD	Mean	SD	Mean	SD	Mean	SD	Mean	SD	Mean	SD	Mean	SD	Mean	SD	Mean	SD	Mean	SD	Mean	SD
All Data	0.74	0.55	0.59	0.31	0.70	0.67	0.71	0.67	0.50	0.41	0.67	0.50	0.58	0.42	0.61	0.28			0.66	0.44		
Data removing R^2 below 0.7	0.57	0.25	0.65	0.27	0.65	0.27	0.77	0.89	0.42	0.31	0.58	0.54	0.49	0.20	0.60	0.32			0.61	0.36		

Table 12: Differences in compliance measure between different areas of the Left Atrium in the PAF cohort. Mean and standard deviation in each AF type. Across all data points, and excluding data points with an R^2 Value below 0.7.

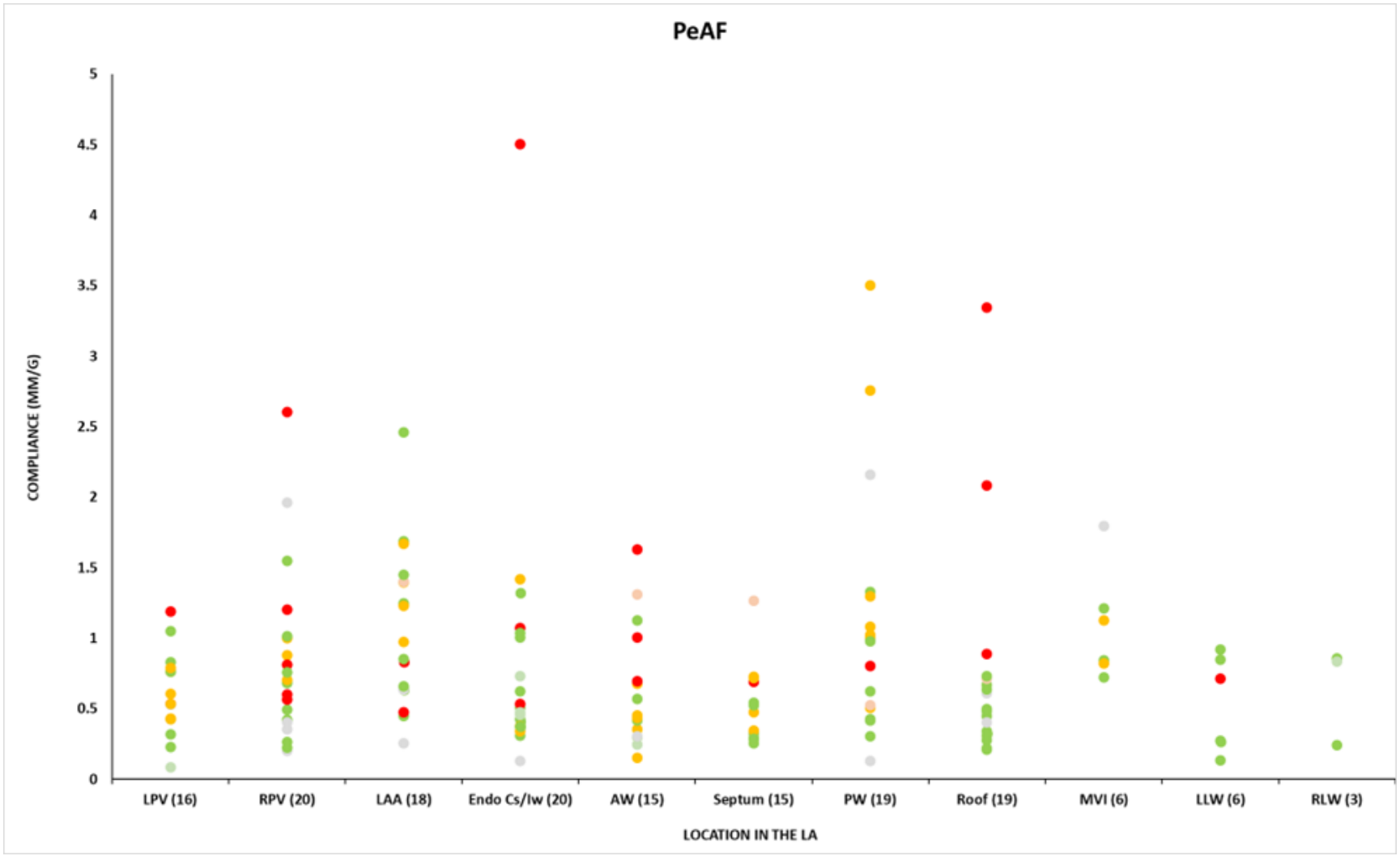

Figure 42: Differences in compliance measure between different areas of the Left Atrium in the PeAF cohort. PAF = Paroxysmal atrial fibrillation. The colours of the individual data points represent the R^2 value of that point, Red = R^2 <0.5, Amber = R^2 = ≥ 0.5 < 0.7, Green = R^2 = >0.7. For females, the colour system remains the same except each colour is a slightly lighter shade.

Area	LPV		RPV		LAA		Endo Cs/Iw		AW		Septum		PW		Roof		MVI		LLW		RLW	
Compliance (mm/g)	Mean	SD	Mean	SD	Mean	SD	Mean	SD	Mean	SD	Mean	SD	Mean	SD	Mean	SD	Mean	SD	Mean	SD	Mean	SD
All Data	0.59	0.29	0.84	0.61	1.05	0.56	0.82	0.94	0.64	0.43	0.49	0.27	1.07	0.87	0.72	0.75	1.09	0.40	0.53	0.34	0.64	0.35
Data removing R^2 below 0.7	0.62	0.31	0.69	0.56	1.00	0.65	0.59	0.37	0.54	0.37	0.36	0.12	0.82	0.63	0.44	0.17	1.14	0.48	0.49	0.37	0.55	0.43

Table 13: Differences in compliance measure between different areas of the Left Atrium in the PeAF cohort. Mean and standard deviation in each AF type. Across all data points, and excluding data points with an R^2 Value below 0.7.

Factors affecting levels of atrial fibrosis

The second aim of this section was to begin to explore the impact of fibrosis, through voltage on the measure of compliance calculated in the same cohort of patients.

Firstly, factors believed to have an impact of pre-ablation fibrosis levels were explored within this patient cohort to see whether they effected fibrosis as thought. Then the measure of compliance derived was compared to fibrosis.

Differences levels of fibrosis as a measure of voltage between Types of AF

Fibrosis levels between the two types of AF were compared, with the hypothesis the more severe AF type, the greater coverage of severe fibrosis (severe fibrosis being ≤0.1mV).

Figure 43 clearly shows that there is a significant difference between types of AF and severity of atrial fibrosis. The most significant difference being between the percentage coverage of normal tissue across the left atrium, in the PAF group normal, healthy tissue (>0.5mV) on average covered 47.7% of the LA, whereas in the PeAF group there was only 0.57% coverage (P=0.0003). The next most significant finding was the percentage of mild atrial fibrosis (<0.5mV) covering the LA of PAF and PeAF patients, mean percentage 46.7% and 82.58% respectively (P=0.02). The levels of severe atrial fibrosis also differed significantly between the PAF and PeAF groups, mean percentage cover 5.6% and 16.86% respectively (P=0.03).

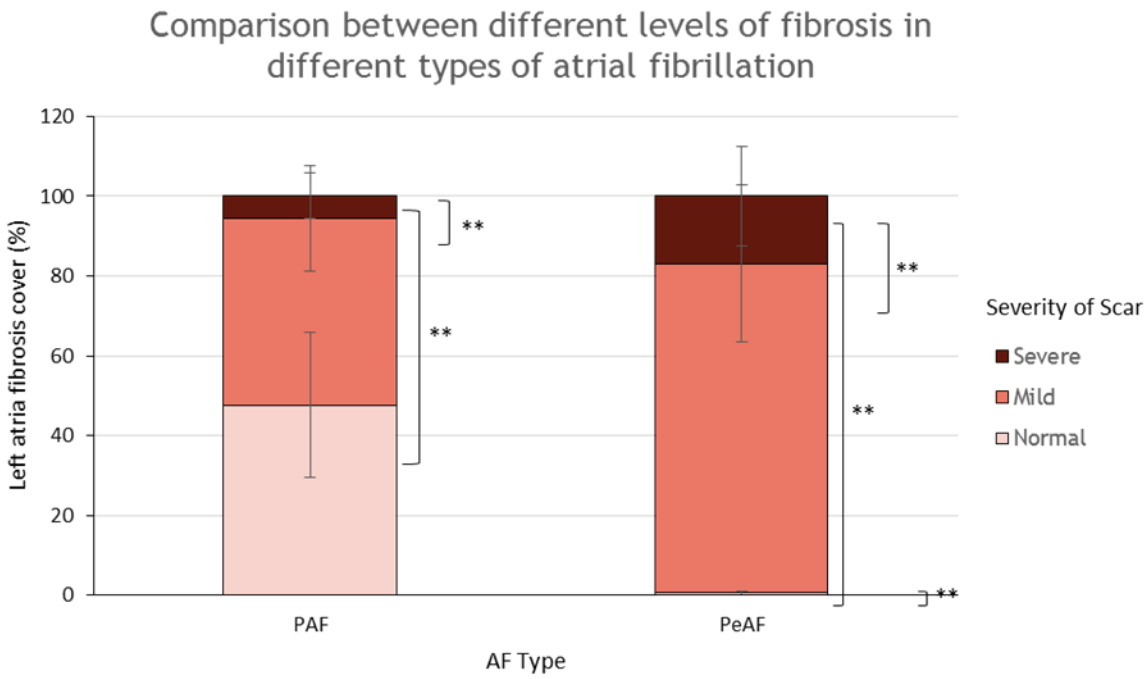

Figure 43: Levels of Fibrosis and Type of AF Graph. Comparison between different levels of atrial fibrosis and type of AF. PAF (n=16) = Paroxysmal atrial fibrillation, PeAF (n=20) = Persistent atrial fibrillation. Normal tissue = ≥0.5mV, mild atrial fibrosis = <0.5 but >0.1mV, severe atrial fibrosis = ≤0.1mV. * = P = 0.05, ** = P = <0.005, *** = P <0.0005.

Difference in Fibrosis coverage between AF with and without comorbidities

The percentage of fibrosis cover as a measure of bipolar voltage was then compared between AF groups, with or without comorbidities, with the hypothesis that the percentage of severe fibrosis (bipolar voltage <0.05mV) would be higher in the cohort with comorbidities, in both AF types. This more fully demonstrates the advancement of fibrosis (Figure 44) such advancement indicates a temporal development of fibrosis with AF; hence levels of fibrosis are affected by other clinically related disease.

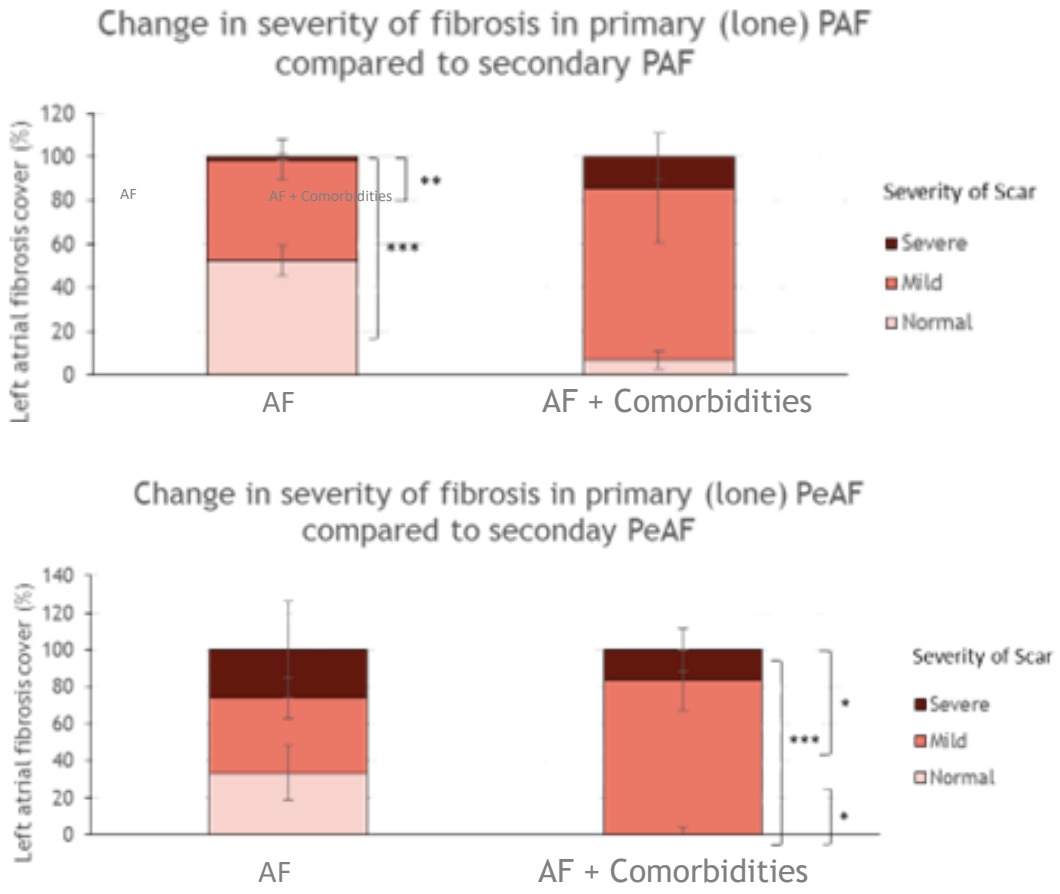

Figure 44: Severity of Fibrosis and Type of AF Graphs. Comparison between different types of AF, primary (lone) AF and secondary to other medically-related conditions. PAF (n=13, 1o=8, 2o=5) = Paroxysmal atrial fibrillation, PeAF (n=18, 1o=4, 2o=14) = Persistent atrial fibrillation. Normal tissue = ≥0.5mV, mild atrial fibrosis = <0.5 but >0.1mV, severe atrial fibrosis = ≤0.1mV. * = P = 0.05, ** = P = <0.005, *** = P <0.0005.

Differences in Fibrosis coverage with time spend in AF

The percentage of fibrosis cover as a measure of bipolar voltage (mV), was compared between time spent in the two AF groups, this was determined from the clinical notes. Time was measured in years

and was divided into three groups: ≤2 year, 3 years and > 4 years, with the hypothesis increased time spent in more severe AF type would result in increase in severity of fibrosis cover. The results are displayed in Figure 45.

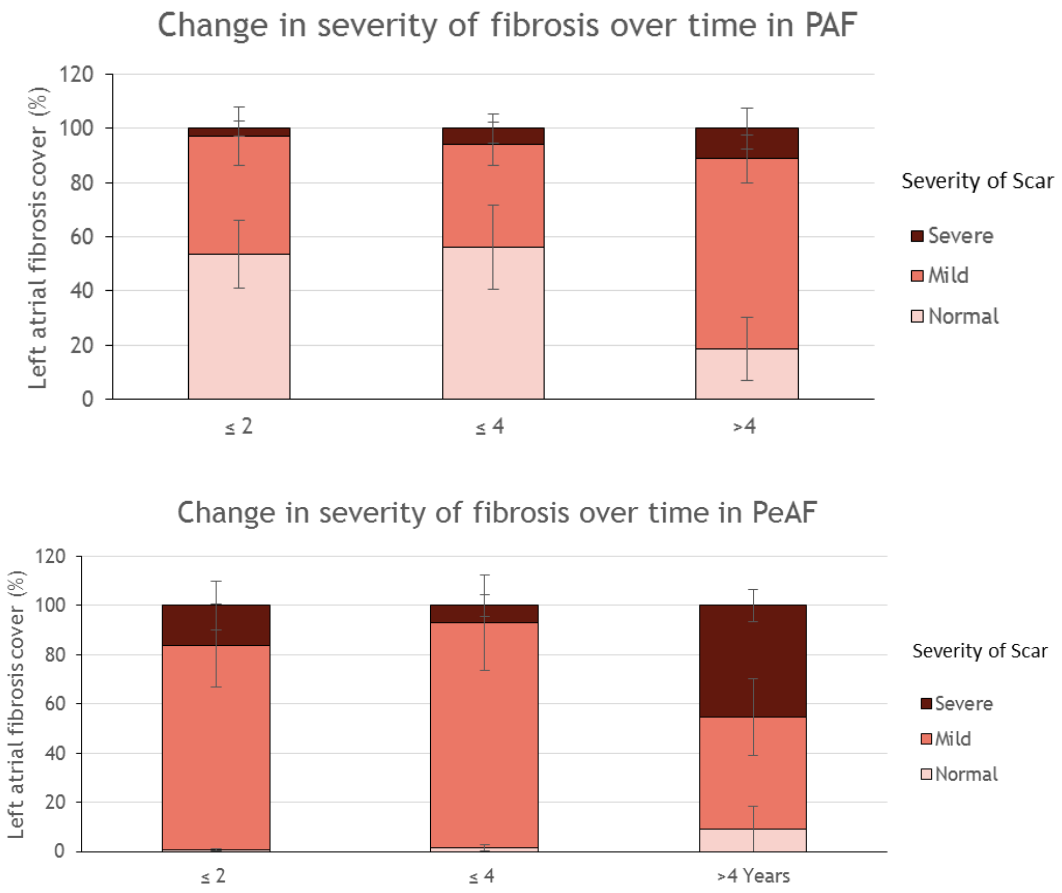

Figure 45: Severity of Fibrosis and Time in AF Graphs. Comparison between time in AF and percentage atrial fibrosis cover. PAF (n=13, ≤2 years =2, ≤4 years = 4, >4 years = 7) = Paroxysmal atrial fibrillation, PeAF (n=15, ≤2 years =9, ≤4 years = 4, >4 years = 2) = Persistent atrial fibrillation. Normal tissue = ≥0.5mV, mild atrial fibrosis = <0.5 but >0.1mV, severe atrial fibrosis = ≤0.1mV. * = P = 0.05, ** = P = <0.005, *** = P <0.0005.

Figure 45 shows that between the two AF groups there was a significant difference in the amount of healthy (normal) tissue up to four years of being in AF. In the PAF group at ≤2 years there was 53.49% mean coverage whereas in the PeAF group there was only 0.55% coverage (P=0.001). At ≤4 years in the PAF group there was 56.14% mean coverage whereas in the PeAF group there was 1.47% mean coverage (P=0.02). At ≤4 years there was also a significant difference in the percentage cover of mild atrial fibrosis tissue, in the PAF group the mean percentage coverage was 38.18% whereas in the PeAF group there was 91.58 % coverage (P = 0.04). At ≤2 years the PeAF group had

more severe atrial fibrosis coverage than the PAF group, mean percentage coverage 2.82% and 16.36% respectively (P=0.04), however, after more than four years this difference in the levels of severe atrial fibrosis between the two groups reduced mean percentage coverage 45.35% and 11.14% respectively (P=0.07).

Percentage of fibrosis coverage in different areas of the Left Atrium

Percentage of fibrosis coverage taken from 11 predefined areas across the LA. The data represented in Figure 30 only shows nine areas, due to data collected in both the RLW and MVI being excluded due to either contact force being less than 5g, or bipolar voltage being greater than 2mV.

Figure 46 shows that there is a difference in mean percentage cover between the different areas however, none of the results were statistically significant.

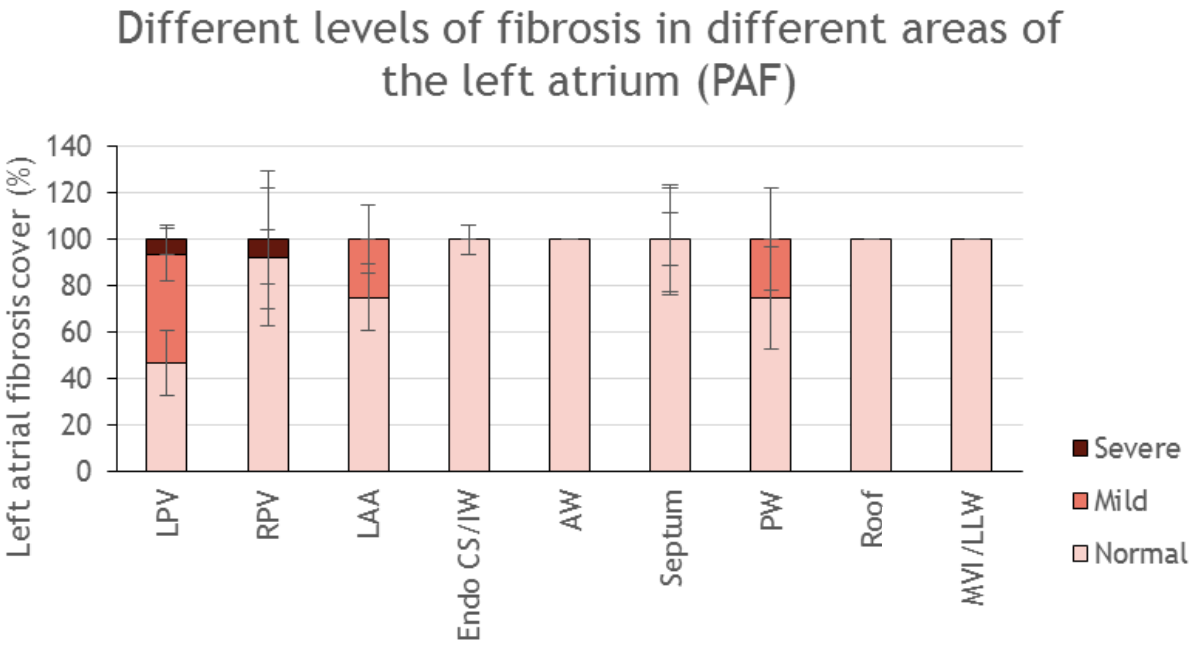

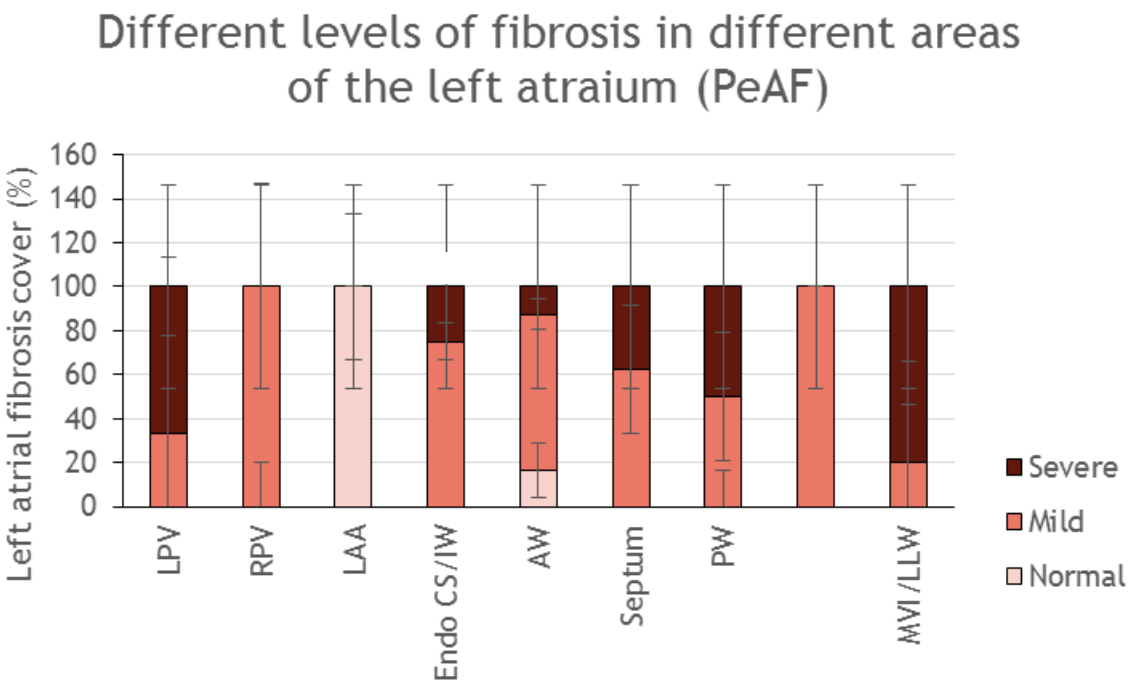

Figure 46: Fibrosis Levels in Different AF Areas Graphs. Comparison between different areas within the left atrium and percentage atrial fibrosis coverage. PAF (n=4, LPV n= 4, RPV n= 4, LAA n= 4, Endo Cs/Iw n= 4, AW n= 4, Septum n= 4, PW n= 4, Roof n= 4, MVI/LLW n= 4,) = Paroxysmal atrial fibrillation, PeAF (n=4, LPV n= 4, RPV n= 4, LAA n= 4, Endo Cs/Iw n= 4, AW n= 4, Septum n= 4, PW n= 4, Roof n= 4, MVI/LLW n= 4,) = Persistent atrial fibrillation. Normal tissue = ≥0.5mV, mild atrial fibrosis = <0.5 but >0.1mV, severe atrial fibrosis = ≤0.1mV. * = P = 0.05, ** = P = <0.005, *** = P <0.0005.

Impact of fibrosis on the measure of compliance calculated

The compliance measure (mm/g) calculated as previously described a suitable measure of compliance was plotted against mean fibrosis (mV) of the 29 patents fibrosis data was acquired from. With the hypothesis the lower the mean fibrosis value (mV), the lower the measure of compliance (mm/g). (Figure 47, Table 14).

A Spearman's rank correlation found no significant correlation between the two groups however, Figures 48 and 49, emphasises the difference in atrial fibrosis between PAF and PeAF patients, with the latter generally exhibiting higher atrial fibrosis levels.

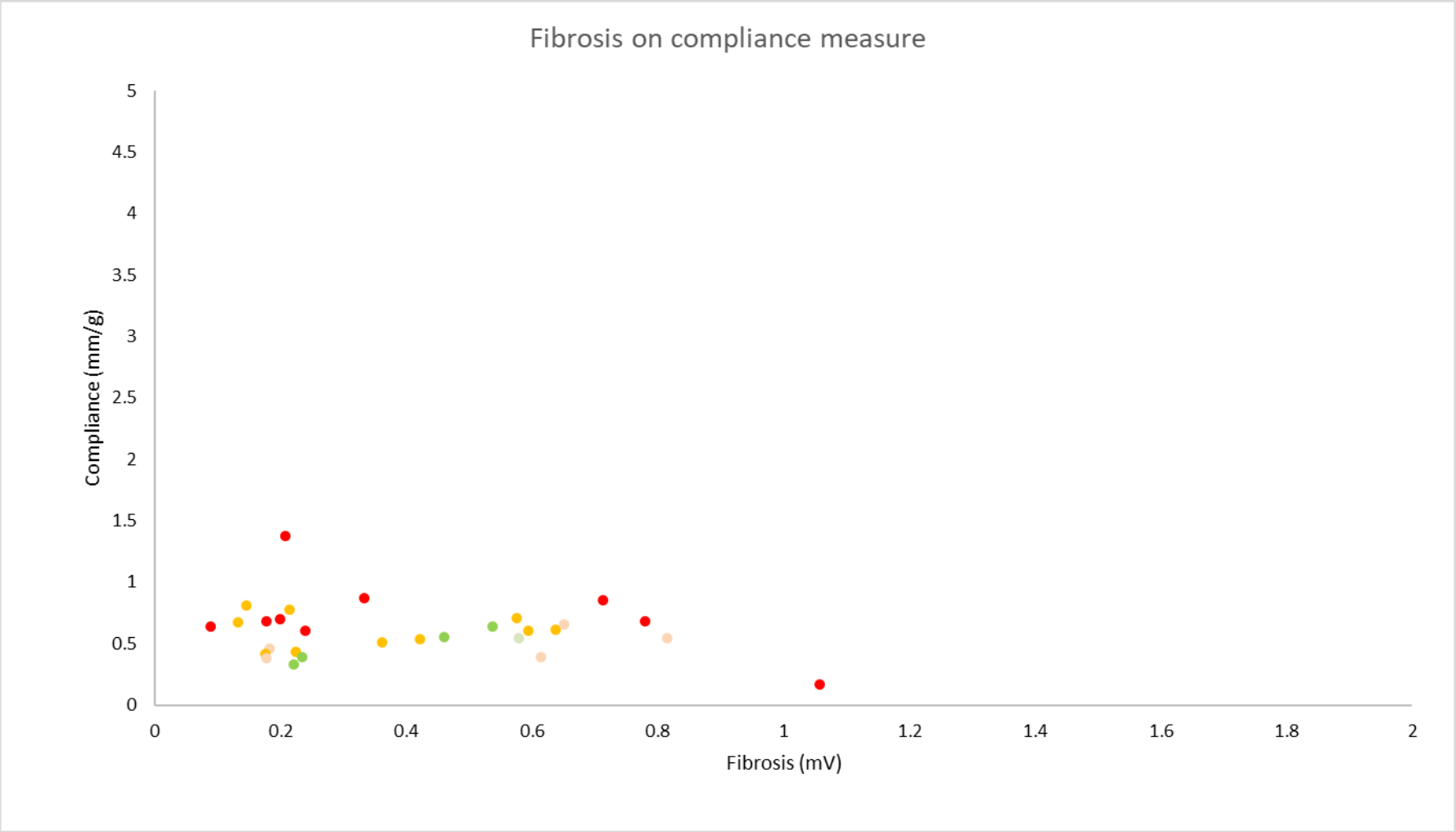

Figure 47: Differences in Compliance measure measured against mean fibrosis (as a measure of bipolar voltage (mV). Total number of patients = 29The colours of the individual data points represent the R^2 value of the compliance measure for that point, Red = R^2 <0.5, Amber = R^2 = ≥ 0.5 < 0.7, Green = R^2 = >0.7. For females, the colour system remains the same except each colour is a slightly lighter shade.

	PAF		PeAF	
Compliance	Mean (mm/g)	SD	Mean (mm/g)	SD
All Data	0.60435	0.14603	0.65886	0.26626
Data removing R^2 below 0.7	0.5454	0.00555	0.45194	0.16133

Table 14: Differences in compliance measure between the 29 patients for which fibrosis data was acquired represented as PAF and PeAF cohort. ***Number of patients in the PAF cohort = 13, Number of patients in the PeAF cohort = 16. Mean and standard deviation in each AF type. Across all data points, and excluding data points with an R^2 Value below 0.7.***

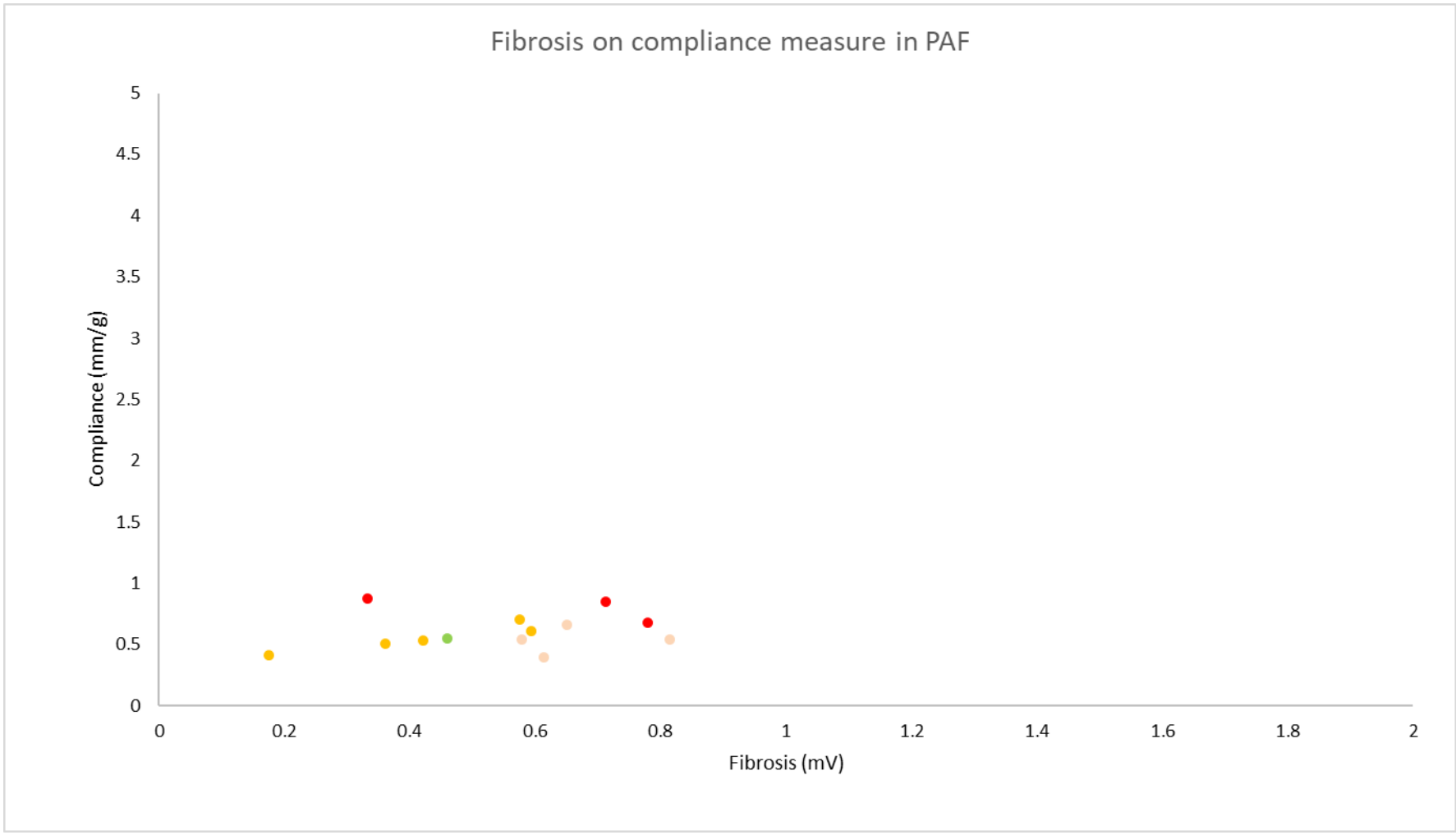

Figure 48: Differences in Compliance measure measured against mean fibrosis (PAF) (as a measure of bipolar voltage (mV) in the PAF cohort. Number of patients in the PAF cohort = 13. The colours of the individual data points represent the R^2 value of the compliance measure for that point, Red = R^2 <0.5, Amber = R^2 = ≥ 0.5 < 0.7, Green = R^2 = >0.7. For females, the colour system remains the same except each colour is a slightly lighter shade.

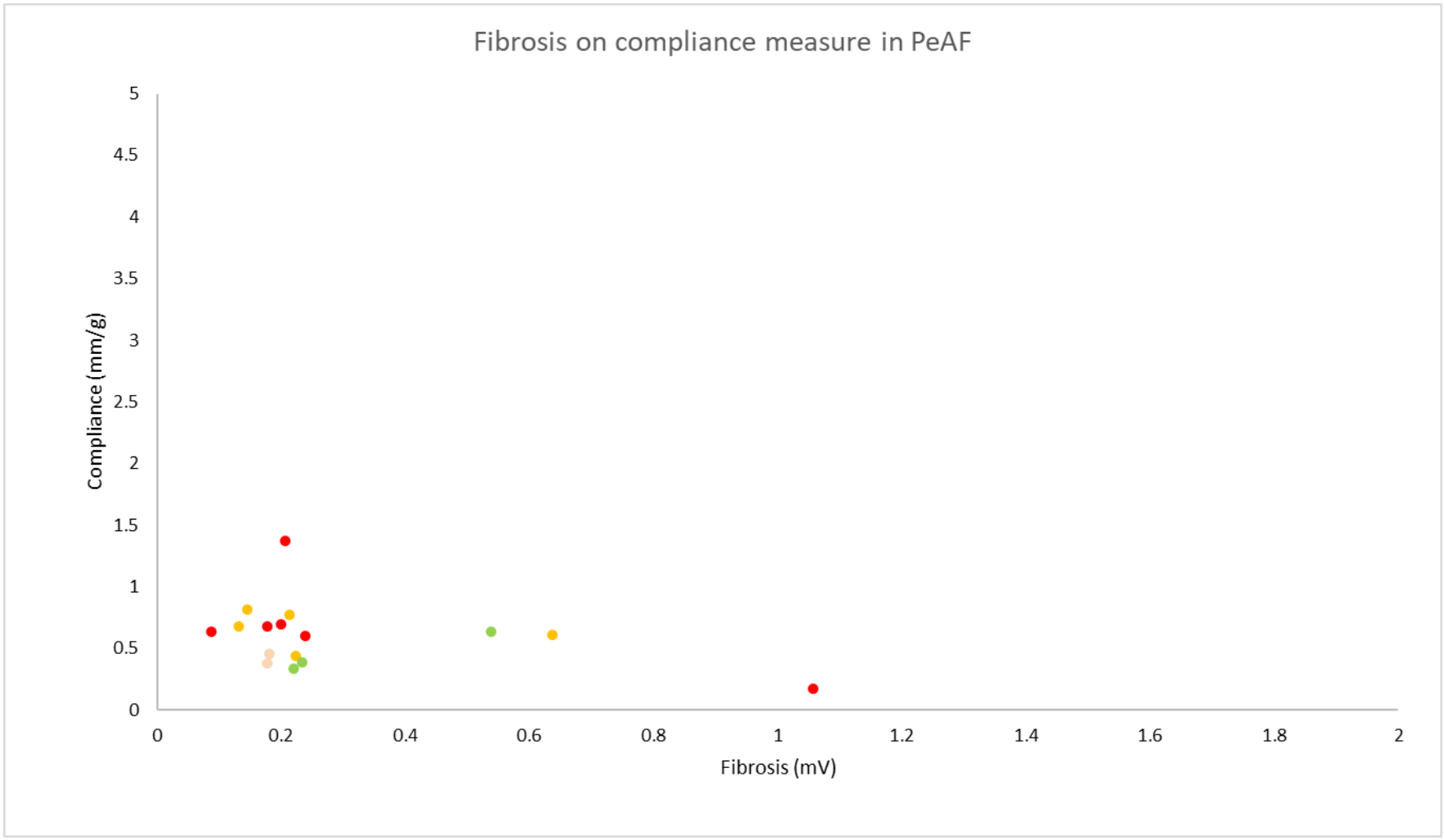

Figure 49: Differences in Compliance measure measured against mean fibrosis (PeAF) (as a measure of bipolar voltage (mV) in the PeAF cohort. Number of patients in the PeAF cohort = 16. The colours of the individual data points represent the R^2 value of the compliance measure for that point, Red = R^2 <0.5, Amber = R^2 = ≥ 0.5 < 0.7, Green = R^2 = >0.7. For females, the colour system remains the same except each colour is a slightly lighter shade.

Chapter 3:
Mechanical Tissue Testing of the Porcine Left Atria

This chapter will focus on the development of a system for testing left atrial tissue mechanics in multiple conformations. Firstly, methods for storing, samples and gripping the tissue during data acquisition will be reviewed, demonstrating development work to reach a final protocol used throughout this section. This will be followed by uniaxial and biaxial testing of the tissue, the basis of which has been used to develop a novel triaxial system that shall also be described in this chapter.

Introduction

The desired outcome of an AF ablation procedure is to create transmural lesions to terminate undesirable ectopic conductions. They are widely performed using radiofrequency (RF) energy, to transform electromagnetic energy into thermal energy by a process called resistive heating at the surface of tissue. There are two ways in which the RF current can be delivered, the first is between the catheter tip and electrode patch placed on the skin in unipolar fashion, and in the second, the current flows between two opposed small electrodes, in bipolar systems. Excellent catheter-tissue contact force (CF) is paramount to achieve either, as low electrode-tissue CF is associated with ineffective lesion formation and excessive CF may increase the risk of steam pop, perforation and injury outside the heart, such as oesophageal, pulmonary and phrenic nerve injury [214] [215]. Recent advances in catheter technologies have now made it possible to measure real-time catheter-tissue contact force during LA mapping prior to ablation [216]. One such catheter is the ThermoCool SmartTouch catheter, used by the clinicians at St Bartholomew's Hospital. This catheter uses a small spring between the ablation tip electrode and catheter shaft, with a tiny magnetic transmitter in the tip and magnetic sensors proximal to the tip to measure microdeflections of the spring, corresponding to tip force [216] [217].

Computer simulations using three-dimensional finite element models are usually performed in order to investigate advances in ablation technologies [218] [219]. Computer simulations have identified that lesion efficacy is mainly influenced by the thickness of LA tissue. However, for all finite element

analysis the LA models are uniformly 3mm thick. In a more recent study, finite element analysis was used to investigate wall stress distribution within the left atrium, to see whether there was a link to electrophysiological remodelling in persistent AF [220]. Again, the thickness of the LA was deemed to be 3mm throughout. Determining the amount of CF required to create effective lesions based on this these models could have implications on ablation success or even result in serious injury if there are any regions of the LA which are not 3mm thick. The aim of this chapter is to use porcine LA tissue to gain a better understanding of the left atrial local thickness and how this impacts, in order to improve selection of ablation forces and subsequently ablation success and reduce injury. The pig is commonly used as a model for cardiac studies, with far simpler availability. Prior to outlining experimental work, the key differences between porcine and human left atrial tissue are described.

Comparison between normal porcine and human left atria

The *Sus scrofa domesticus* or *Sus domesticus* (domestic pig) has long been used as a model in cardiac research, instead of human tissue. A number of studies have focused on comparing porcine and human coronary vascular anatomy [221] [222], each study reporting that not only was the porcine coronary anatomy very similar to that of man, but so too was the distribution of blood to different areas of the heart. Others concentrated on postnatal development [223] [224], finding that whilst there were large differences in the growth patterns of the heart from neonate to adult, the changes were proportionate between the two different mammals [225] [226], with studies concluding that the electrophysiological parameters of a pig heart were very similar to man. Indeed, similarities were more so than with any other species, making porcine cardiac tissue a useful and reliable model of human cardiac tissue for electrophysiological studies. Despite the general acceptance in the literature that the anatomy of the porcine heart is similar to that of man, knowledge of porcine cardiac anatomy is limited [227] [228]. However, without this information, regardless of the substantial evidence to suggest the cardiac structures of the two species are similar we cannot be certain.

The most extensive study to compare the anatomy of porcine and human heart structures carried out so far was by Crick et al. in 1998 [224]. They compared 27 healthy porcine hearts, with no known congenital heart defects or recognizable cardiovascular disease, aged from newborn – six months, weighing 1 – 50kg with human hearts referenced in Anderson & Becker's (1992) "The Heart – Structure in health and disease" [225].

They observed several important anatomical differences between the hearts of pig and man, the most notable being the difference in the shape of the respective hearts; the porcine heart has a classic "Valentine Heart" shape whereas the heart of man is trapezoidal in silhouette (Figure 50). This along with several other gross morphological differences, were attributed to the contrasting stances of the two different species. The unguligrade, quadrupedal stance of the pig clearly differs from the orthograde, bipedal stance of man, and it seems highly probable that gravity has an effect on the evolution of their respective cardiovascular systems. However, another factor that may also attribute to some of the anatomical differences between the porcine and human hearts is the location of the heart within the thorax. In pigs, the thorax is laterally compressed, whereas in man the thorax is dorsoventrally flattened. The location within the thorax and orientation of the pigs' body means that the porcine heart is suspended in the thoracic cavity by its major blood vessels, with its anterior surface resting near to the sternum, and the majority of the posterior surface adjacent to the diaphragm. As such, the porcine heart 'rests' on its apex, which is formed by only the left ventricular mass. By contrast, the orthograde stance along with dorsoventrally flattened thorax of man results in a markedly eccentric apex. The pig heart, nonetheless, retains an apex and a base, with upper and lower borders of dissimilar size; all features comparable with those of the human heart.

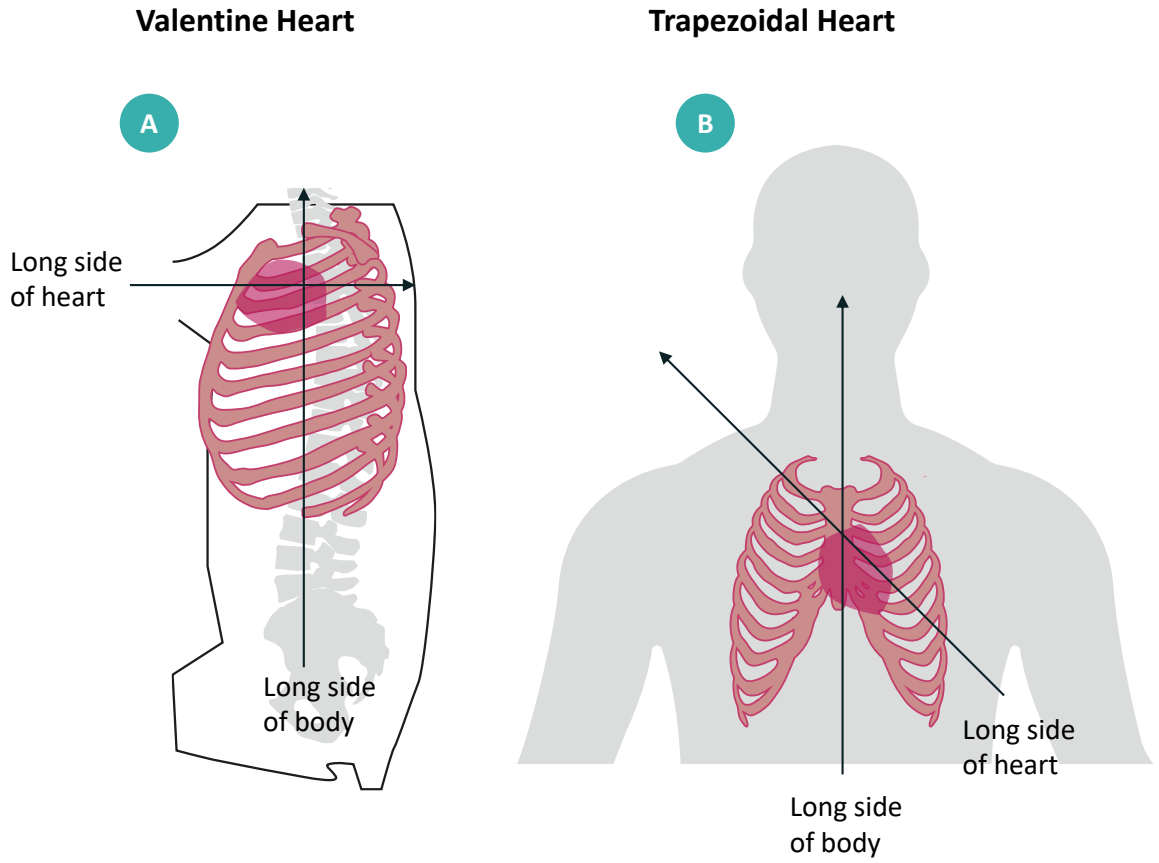

Figure 50: Porcine and Man Thoracic Cavities. Figure (A) is the cardiac silhouette of the heart within the rib cage of the pig, and (B) is a radiographic image of the porcine thoracic cavity, from the side. Adapted from *[224] [225]*.

The ventricular mass of the pig was found to have a basic conical morphology (Figure 51) with the caudal (or posterior) surface of the ventricle adjacent to the diaphragm, and the sternoventral (or anterior) surface resting against the sternum. In contrast, in the human heart the locations of these external surfaces were different, again associated with the difference in basic body orientation. Figure demonstrates the anterior direction in which the atrial appendages face, in the porcine heart, clearly showing its anterior-posterior orientation and how the left ventricle forms the entire apex of the heart.

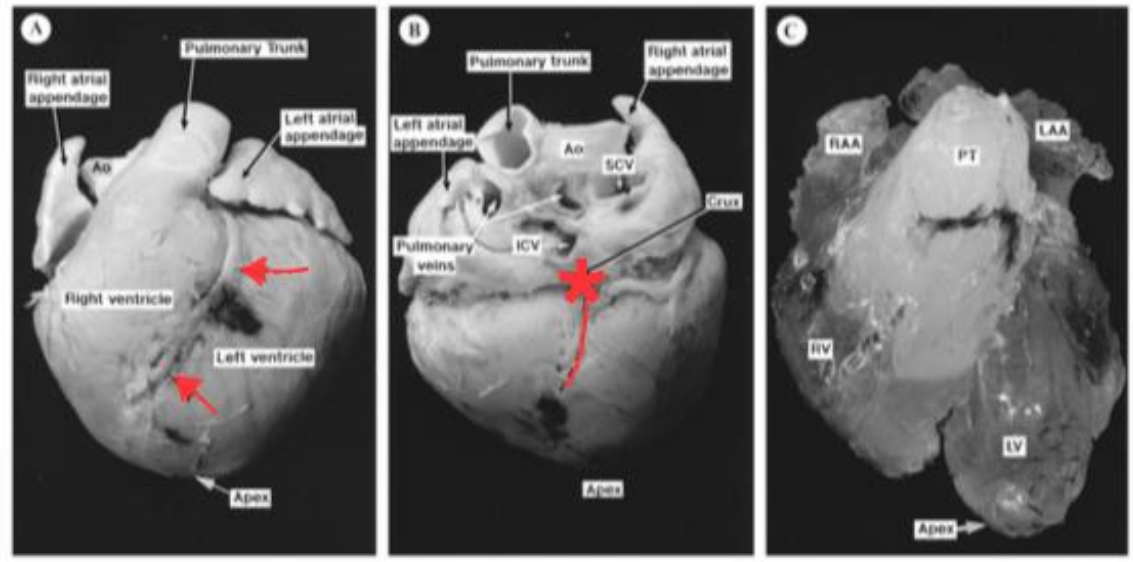

Figure 51: External Aspects of the Porcine Heart. Figure (A) is of the anterior aspect of the porcine heart and Figure (B) is of the posterior aspect. Figures (A) and (B) depict the characteristic valentine shape of the porcine heart. The orientation of the atrial appendage in Figure (A) confirms the anterior-posterior orientation of the porcine heart. The red arrows in Figure (A) point to the location of the anterior interventricular groove, which is situated towards the sloping leftward margin of the ventricular mass. The solid red line in Figure (B) that leads into the star (* = crux) is the posterior interventricular groove, this runs along the midpoint of the posterior surface and bisects the atrioventricular groove at the crux. Figure (C) is a cast of both the left and right sides of the porcine heart, which clarifies that the left ventricular musculature forms the apex. Ao, aorta; SCV, superior caval vein; ICV, inferior caval vein; RAA, right atrial appendage; LAA, left atrial appendage; PT, pulmonary trunk; RV, right ventricle; LV, left ventricle. Adapted from *[224]* .

Despite these differences the arrangement of the different regions within the heart is remarkably similar in pig and man. The anterior interventricular groove was located near to the sloping leftward margin of the ventricular mass, whereas the posterior interventricular groove spanned along the midpoint of the diaphragmatic surface, and bisected the atrioventricular groove at the crux. One difference however was that, the left and right atrial appendages located on the basal surface of the

porcine heart were of a similar size, whereas in humans the right atrial appendage is larger than the left (Figures 52 and 53).

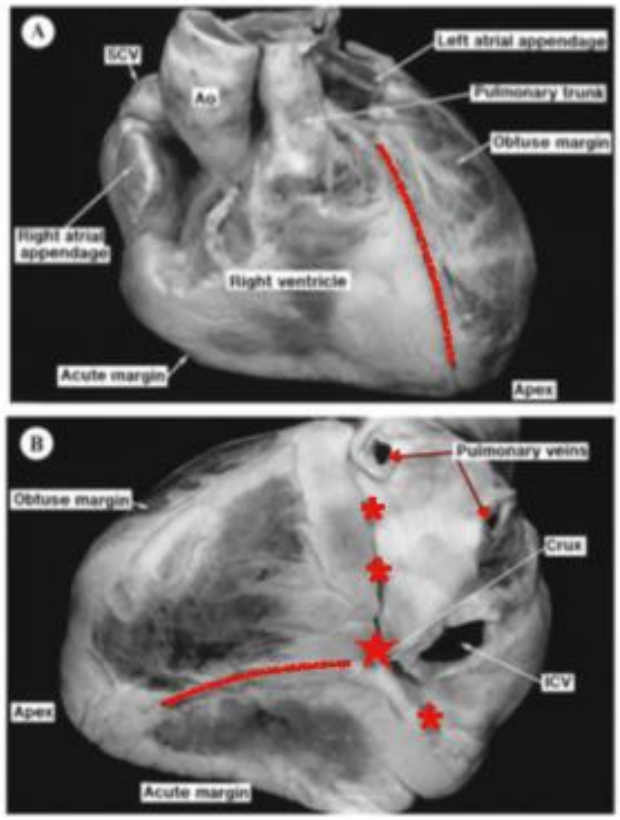

Figure 52: External Aspects of the Human Heart. Figure (A) is of the anterior surface of the human and Figure (B) is of the posterior surface. Both Figures (A) and (B) show the characteristic trapezoidal shape of the human heart, compared with Figure 7 (the porcine heart). In Figure (A) the solid red line represents the anterior interventricular groove, which is situated towards the sloping leftward border, close to the obtuse margin. The posterior interventricular groove (solid red line) in Figure (B) divides the diaphragmatic surface at its midpoint, the region between the acute and obtuse margins. Also bisecting the atrioventricular groove at the crux, which is represented by a star (*). Ao, aorta; SCV, superior caval vein; ICV, inferior caval vein. Adapted from *[224]* .

Atria

The atria of both pig and man have a venous component, an appendage and the vestibule of an atrioventricular valve, together with the septum whose function is to separate the two atriums. The porcine atrial appendages face either anteriorly towards the back, or posteriorly of the anterior thoracic wall (sternum) and have a triangular shape (Figures 51 and 53). The human left atrial appendage has a tubular appearance, the only difference is that the left and right atria in humans differ in size, 27-38mm and 34-53mm respectively (long axis dimension) [229].

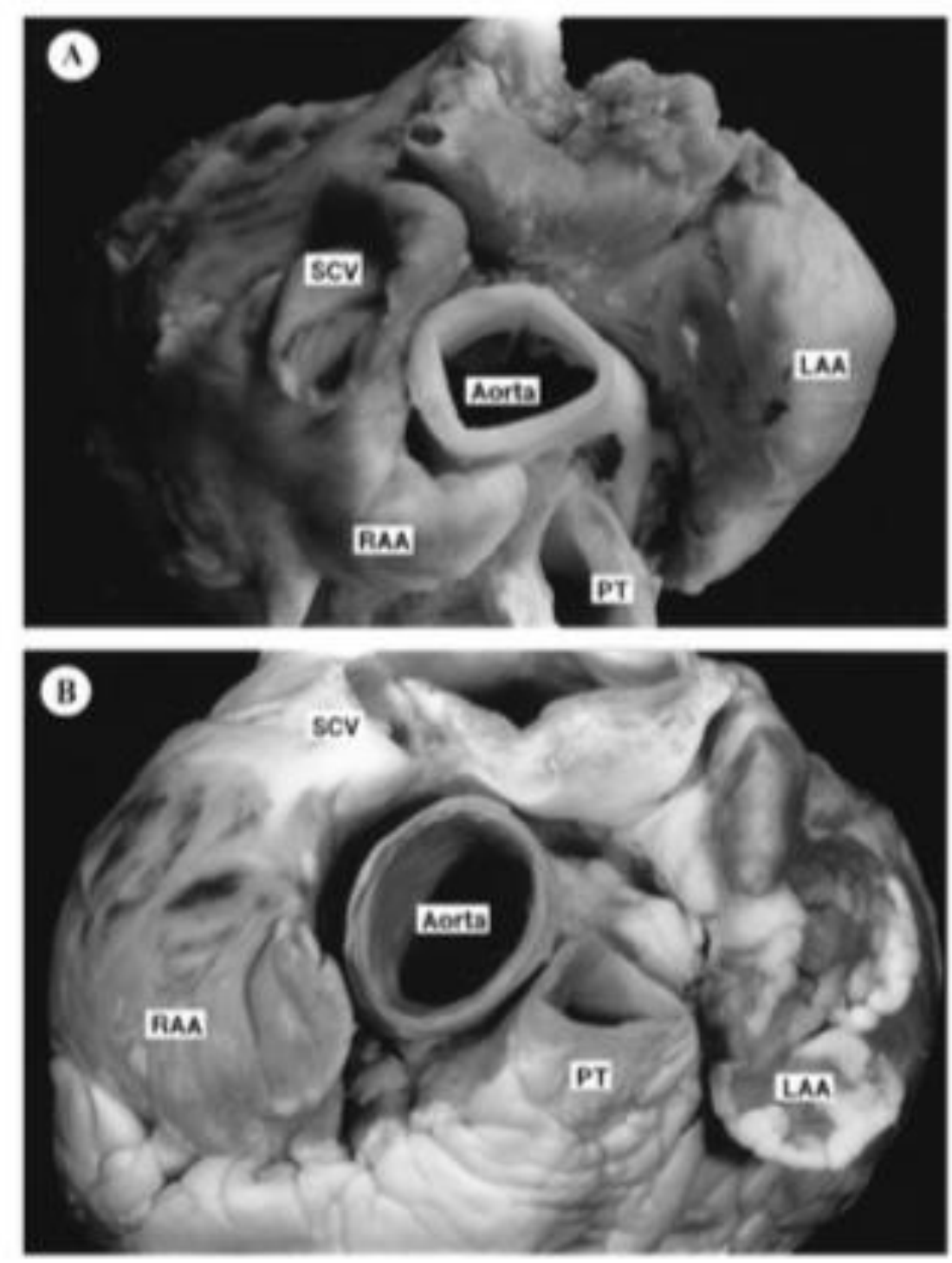

Figure 53: Basal Surface of the Heart. Figure (A) is an external view of the porcine basal surface, whereas (B) is an external view of the human basal surface for comparison. The main difference between the two images is the size of the left atrial appendages, the porcine left and right atrial appendages are of a similar size, whereas the human left atrial appendage (B) is smaller than the right atrial appendage. The positions of the pulmonary trunk and aorta are similar in both the porcine and human heart, with the pulmonary trunk located to the left of the aorta, and the aortic valve being the center point in both species of heart. RAA/LAA, right/left atrial appendage; SCV, superior caval vein; PT, pulmonary trunk. *[224]*

It is notable that the numbers of pulmonary veins that lead into left atrium differs between species; in humans there are generally four pulmonary veins that open into the human left atrium, whereas in pigs there are only two. Finally, as with the right atrial appendage the porcine left atrial appendage has a triangular shape, unlike the tubular appearance of the appendage seen in man (Figure 54).

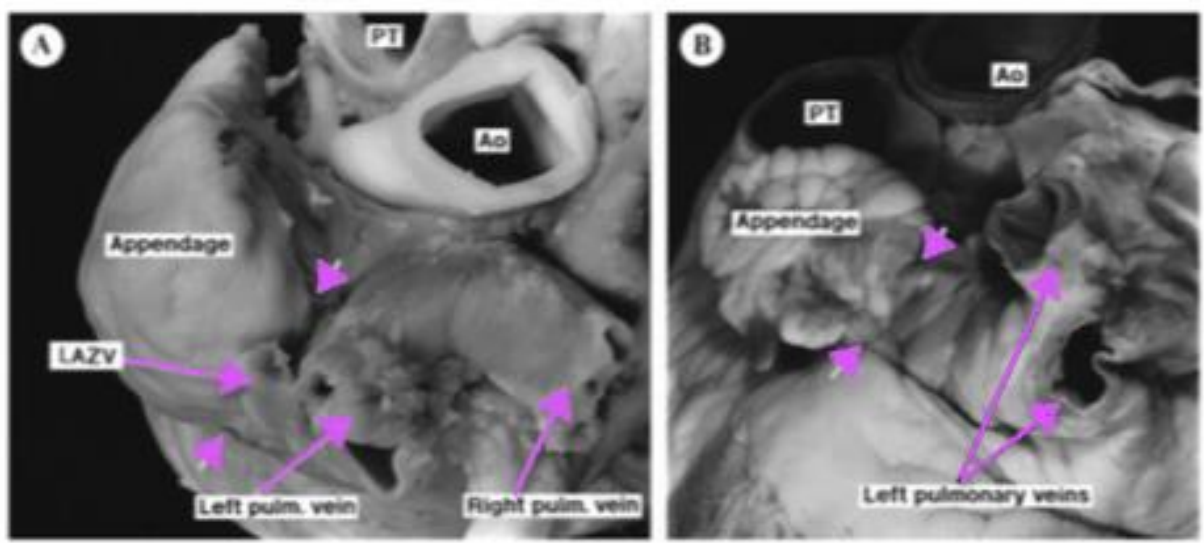

Figure 54: External Images of the Left Atrium. (A) is of the porcine left atrium and Figure (B) is of the human left atrium. The most notable difference between Figures (A) and (B) is the structure and appearance of the left atrial appendage, in Figure (A) the outer surface of the appendage appears smooth and has a triangular structure, whereas in Figure (B) the outer surface of the appendage looks rough and it has a narrow tubular appearance. The purple arrow heads in Figures (A) and (B) mark the junction at which the appendage meets the venous component of the left atrium, in Figure (A) (pig) the space between the two arrow heads is larger than the space between the two arrow heads in Figure (B) indicating that a large surface area of the appendage is attached to the venous component of the left atrium in the porcine heart when compared with the human heart. In Figure (A) the purple arrows mark the orifices of the one left and one right pulmonary veins that enter the left atrium, in Figure (B) only the two left pulmonary veins orifice locations are highlighted by the arrows, the two additional right pulmonary veins are not in the field of view of this image. Also in Figure (A) the location of the left azygous vein (LAZV) is highlighted by a purple arrow, however in Figure (B) of the adult human left atrium this vein is absent. PT, pulmonary trunk; Ao, aorta. Adapted from *[224]*.

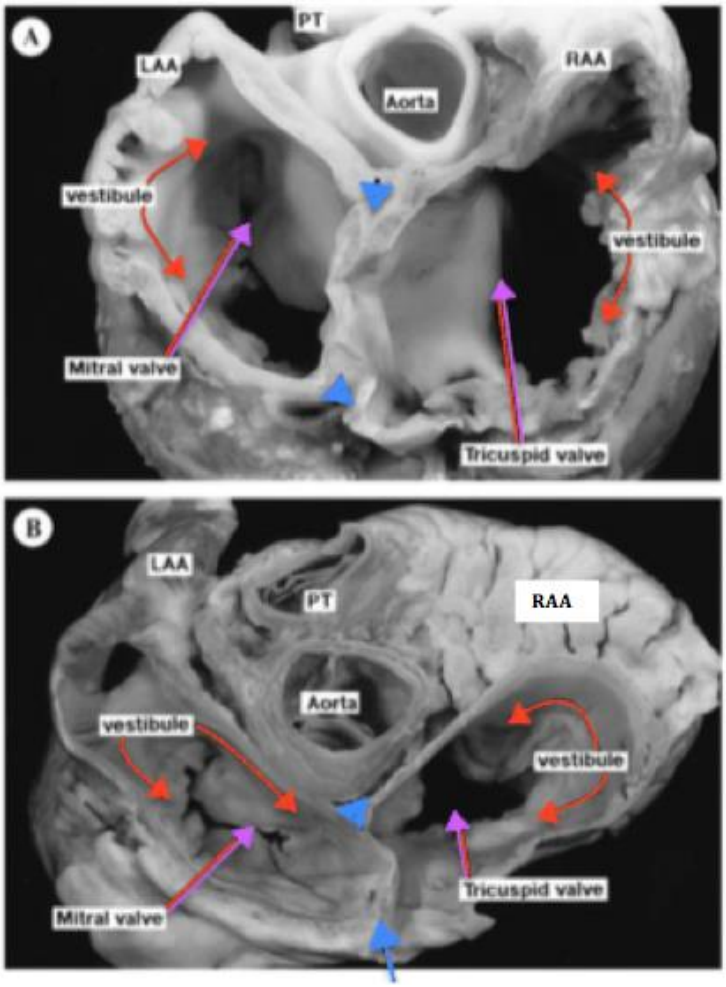

Figure 55: Basal view of the Heart. Basal view of short axis sections through the atriventricular junctions after removal of the atrial musculature to the level of the arterial valves. Figure (A) is porcine and Figure (B) is human for comparison. In both Figures (A) and (B) the rough, tubular appearance of the pectinate muscles can clearly be seen to be restricted to the right and left appendage sites, the structure of the appendage is most clearly visible in the human right atrial appendage (RAA) (B). In both Figures (A) and (B) the vestibule is smooth-walled and supports the mitral valve in the left atrium and the tricuspid valve in the right. The atrial septum, separating the right from left atrium (blue arrow heads) appears longer in Figure (A) (porcine) than in Figure (B) (human). LAA, left atrial appendage; RAA, right atrial appendage; PT, pulmonary trunk. Adapted from *[224]*.

The musculature of the left atrium in both species is the same, in that the pectinate muscle is restricted to the internal walls of the appendages, and the vestibule which supports the leaflets of the mitral valve is smooth-walled (Figure 55). The porcine septal region is longer than that of the human (Figure 55), believed to be a result of the different atrial morphology of the two species. While differences are evident, porcine tissue is still one of the most widely used models used in cardiac research [230] .

Mechanical Testing Method Development

Storage of Cardiac Tissue Samples

Cardiac tissue is commonly preserved by refrigerating or freezing it. This section will investigate the effects of common storage protocols on left atrial mechanics. Porcine left atrial tissue samples were prepared and uniaxially pulled to failure, implementing fresh, refrigerated, and frozen storage conditions. Fresh tissue samples were tested within 24 hours of sacrifice; refrigerated tissues were stored at +4 ^{o}C for 48 hours prior to testing, and frozen tissue samples were stored at -20 ^{o}C for 96 hours prior to testing.

Understanding the effects of storage protocols on left atrial tissue mechanics is not only vital for the experimental section of this thesis but could also have clinical applications. Human cardiac tissue specimens are usually harvested from cadavers stored in mortuary refrigerators for a limited period before they then get stored in freezers until required for testing. Specific storage protocols may not be effective at slowing tissue degradation, resulting in decreased accuracy with respect to the *in vivo* conditions. Previous experimental investigations have demonstrated the effects of cold or frozen storage on vessel structure [230] [231] [232] and physiological function [178] [233] [234]. However, no such work has been carried out to investigate the effect of these storage methods on left atrial tissue mechanics. The only closely related studies have investigated the effects on arterial tissue. One of those studies investigated the effects of freezing on rabbit carotid arteries frozen in Hank's solution for 10 to 15 days reported that elastic modulus and fracture strength were significantly decreased [235]. This could indicate that previously frozen tissue has increased susceptibility to tensile failure. However, in the other study, investigating human thoracic aorta segments refrigerated in Eurocollins solution for up to 31 days or frozen for up to 4 months, found no significant mechanical differences [182]. Neither of these studies reported or quantified arterial subfailures prior to complete vessel rupture. Further, both of these studies neglected to comprehensively quantify vessel mechanics, reporting only failure stress, a measure of vessel

strength, and elastic or high strain modulus, as a measure of vessel stiffness. Failure strain, a measure of vessel elasticity, is also an important metric in quantifying soft-tissue mechanics. It is also important to note that arterial and atrial tissue mechanics differ greatly. The hypothesis for this study is that refrigeration and freezing of left atrial tissue significantly affects the mechanical properties of the tissue.

Left atria were obtained from 16 adult pigs, and seven samples 30mm x 10mm cut from each atria. The resulting 112 samples were split into three test groups: fresh, refrigerated and frozen. Fresh samples were mechanically tested on the day of harvest. Refrigerated samples were stored for 24 hours at +4^{o}C and tested within one hour after being taken out of the fridge. Frozen samples were placed in a freezer at -20 ^{o}C and stored for 48 hours. At the time of testing, specimens were thawed to room temperature and tested within one hour of thawing.

As a result of this and for all further mechanical tests fresh samples shall be used.

Sample Preparation and Dissection

Nine porcine hearts were obtained from Cheale Meats abattoir, Brentwood, Essex, CM13 3EN, and delivered on ice to Queen Mary University Cell and Tissue laboratory the day of slaughter. The whole heart was stored intact at 4^{o}C overnight. The following morning the hearts were washed with cold running water to remove any visible residual blood from the heart structure, then placed on a dissection tray lined with paper soaked in phosphate buffered saline solution (PBS) (Figure 56A). The bottom third of the heart was removed in order to stably stand the heart on its short axis for further dissection (Figure 56B), after which handling of tissue, particularly left atrial tissue was done using non-toothed forceps, to minimise risk of damage. The pulmonary trunk and ascending aorta were dissected away, such that the left ventricle (LV) could be entered posteriorly to the origin of the aorta. If entering the LV could not be achieved by this method without damaging the anterior wall of the left atrium then the LV was entered laterally by identifying the circumflex coronary artery in the atrioventricular groove below the lateral wall of the LA and dissecting into the ventricle below the

coronary artery. On entering the LV, left and right ventricular tissue was cut away up to the plane of the atria, in a more gradual, controlled manner. Using a pair of scissors, the right atrium (RA) was then opened by cutting through the superior and inferior vena cavae, and the RA excluding the interatrial septum was then removed (Figure 56D).

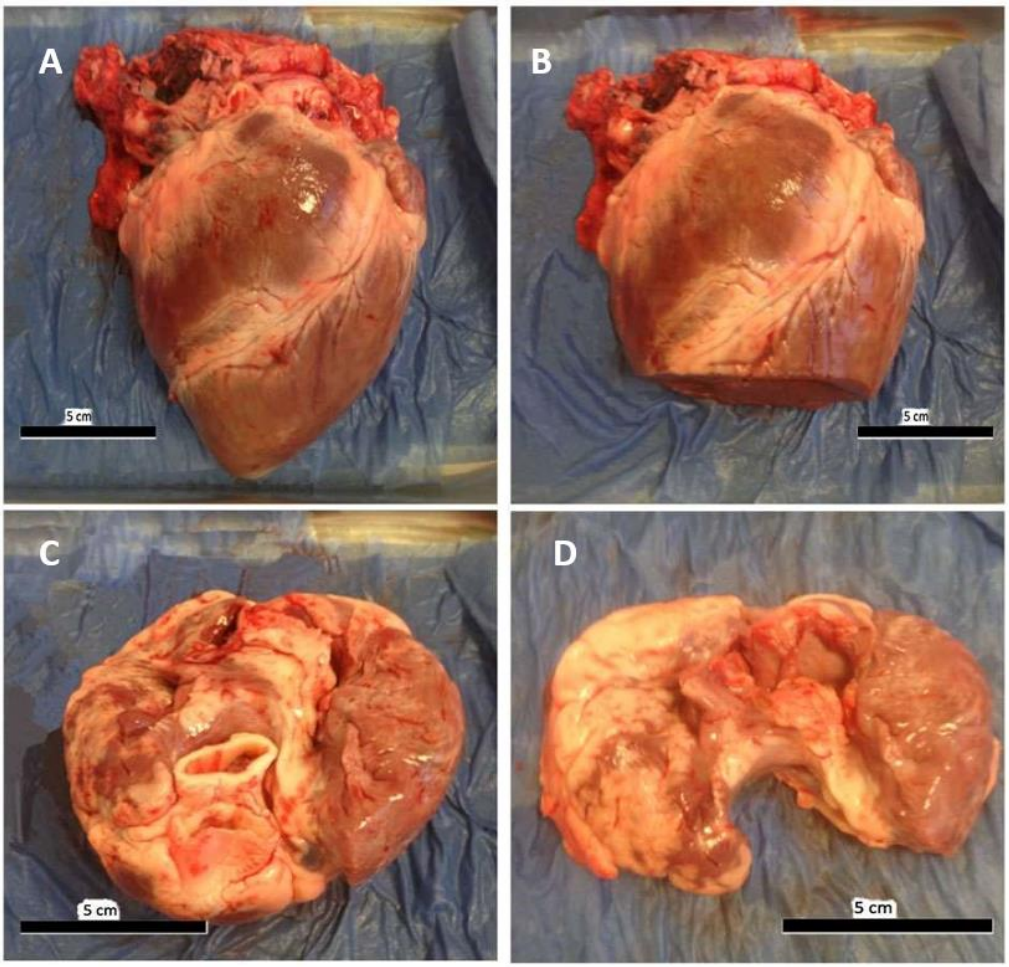

Figure 56: Heart Dissection Technique. A: heart ready for dissection. B: bottom third of the ventricle removed to form a stable base. C: Superior view of the heart. D: atria completely separate from ventricles ready for further dissection, right atria visible on the left of the image and left atria visible on the right of the image. Black scales represent 5cm.

A set of small scissors and a pair of non-toothed forceps were used to remove any fatty tissue surrounding the pulmonary veins and atrial tissue, after which the regional anatomy of the LA could be visualised and samples removed.

Porcine left atrial tissue sections identified by Hunter et al. [217], and Ullah et al [236] (Figure 57) were isolated from the left atrium and transferred to a petri dish lined with paper soaked in

phosphate buffered saline solution. Each atrial sample was cut to a target size of 30 x 10 mm where possible. If the available tissue was smaller, the longest possible length was used and dimensions recorded for later analysis. The samples were dissected and tested in the same order each time: anterior wall, lateral wall, roof (where possible), right pulmonary vein ostia, left pulmonary vein ostia, posterior wall (were possible), sinus wall, and septum.

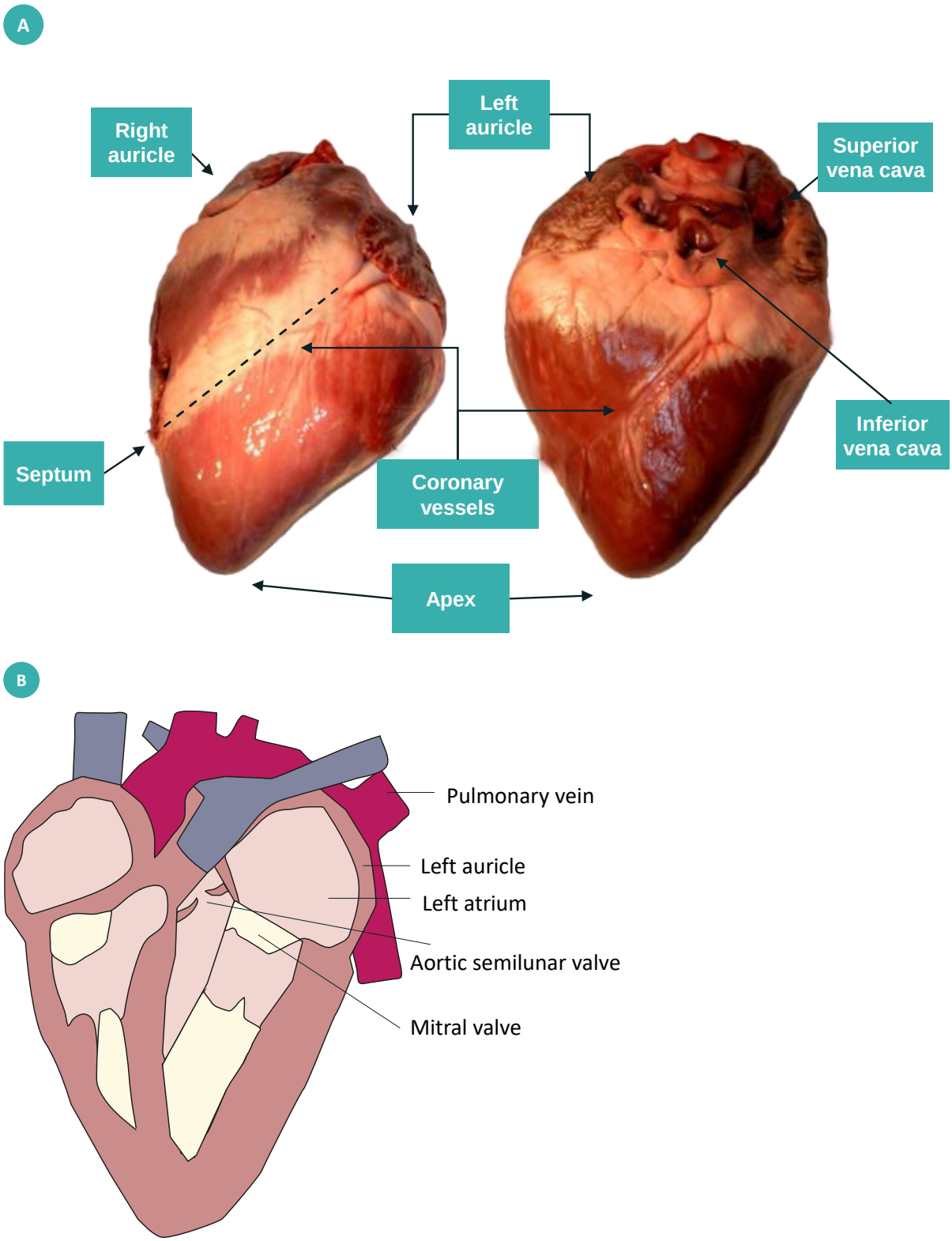

Figure 57: Anatomy of porcine heart. A – Frontal and posterior view of the heart B – Schematic drawing of fetal porcine heart

Sample Gripping

Uniaxial

Ideally tissue samples must be securely gripped in the rig without causing any damage to the tissue. In order to establish the best way to grip the samples a number of different methods were trialled, using the Instron 3300 (instron, Norwood, MA, USA) mechanical testing *machine and pneumatic grips working at 3 bar pressure as the basis for the tests.*

Firstly, the tissue was gripped directly into the pneumatic grips, by securing one end centrally in the top grip then using the forceps to position the sample and close the bottom clamp. Within each clamp there was 10 mm of tissue, leaving 10mm of tissue exposed for testing.

Gripping the tissue in this way, proved to be insufficient for testing as samples slipped out of the grips rapidly when loaded (Figure 58).

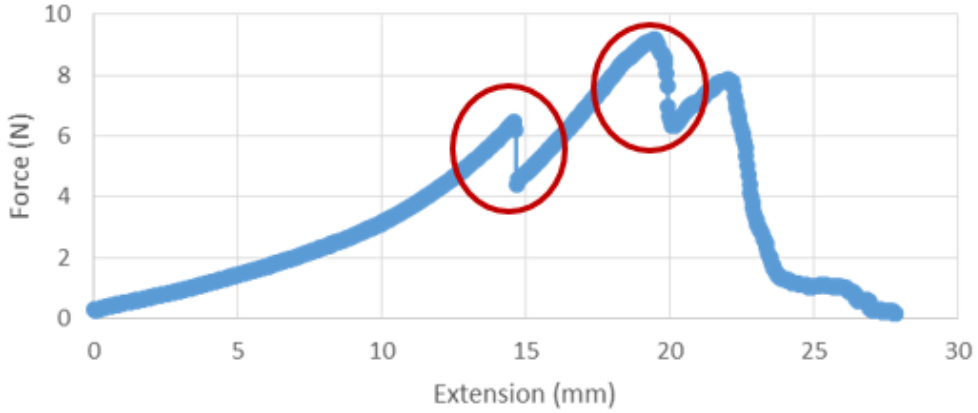

Figure 58: Force Extension Curve. For left pulmonary vein (LPV) sample that was gripped directly into the uniaxial rig and slipped during testing. Red circles highlight points of slippage.

Following on, fine grained sandpaper was employed to increase gripping friction. Four 25mm x 25mm squares of 100 grit sand paper were cut, and placed (rough side in) over the ends of the sample, leaving 10mm of tissue exposed for testing (Figure 59).

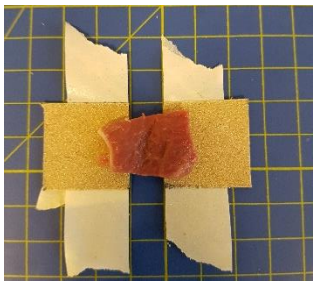

Figure 59: Tissue Gripping Method. Tissue placed on two pieces of 25mm^2, 100 grit sandpaper.

One each end of the sample was sandwiched between sandpaper, it was secured in place using autoclave tape (Figure 60),

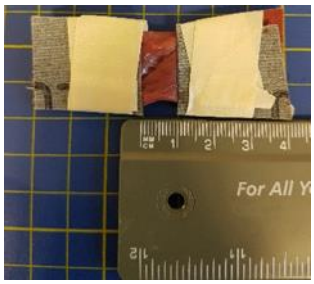

Figure 60: Tissue Gripping Method Progression. Left atrial tissue sandwiched between four pieces of sandpaper, with 10mm of tissue left exposed for testing.

and the sample placed between the grips in the same way as previously described (Figure 61).

Figure 61: Uniaxial Rig Set-Up. Tissue sandwiched between four pieces of sand paper and gripped within the uniaxial rig.

This method proved very successful with very little slippage, so was used for all further uniaxial tests.

Biaxial and Triaxial

Developing grips for biaxial testing is more complex as it is important to ensure the tissue is not constrained in either loading axis. Following previously published approaches, a method to suture samples, to allow strain application was explored using the Electroforce Planar Biaxial TestBench machine (TA Instruments, USA). For this method of testing, some tissue damage was unavoidable due to the tissue having to be suspended (Figure 62).

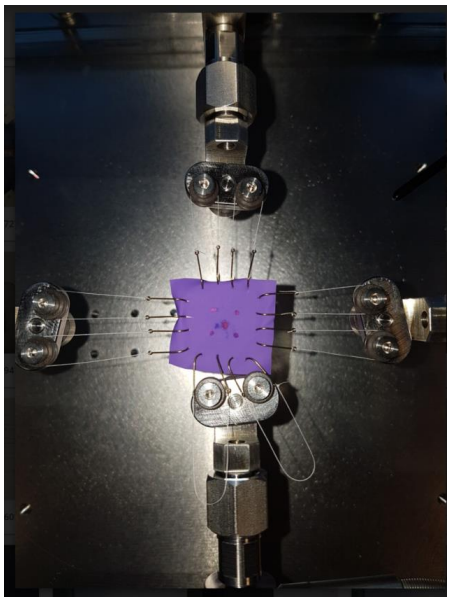

Figure 62: ElectroForce Biaxial Rig Set-Up. Example of the way a tissue sample would be suspended above the rig floor, using a section of glove instead of left atrial tissue.

In order to successfully grip the tissue causing as little damage as possible tissue samples were initially gripped following the Electroforce protocol. The tissue was placed on their tissue block (Figure 63A), then covered with the top cover (Figure 63B), holding tissue within the arrangement (Figure 63C). Four fishing hooks were then pierced through each side of the sample, and attached to wire, which can be connected to the biaxial loading arms in order to apply strain (Figure 64).

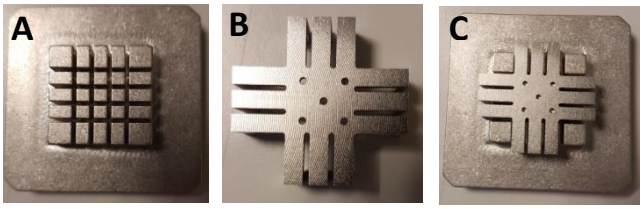

Figure 63: ElectroForce Biaxial Gripping Block. (A) Base of the block that tissue sits on, (B) the top of the block to secure the tissue in place, (C) how the top sits on the bottom of the block.

Unfortunately, the rectangular (not square) dimensions and notable thickness of the atrial tissue samples led to difficulties adopting the square attachment frame, thus a smaller top cover was built to fit the tissue.

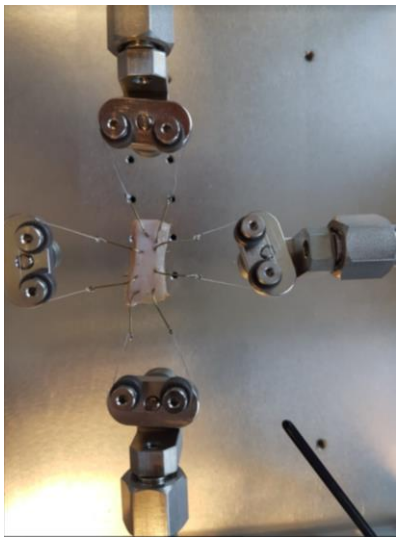

Figure 11: Tissue Gripping Method. Left atrial tissue sample hooked onto the grip surfaces.

Machine Development

Triaxial

Triaxial test combined the developed biaxial loading approach with a unidirectional compression test in the third axis, recapitulating atrial tissue under physiological tension subject to an ablation procedure (Figure 65).

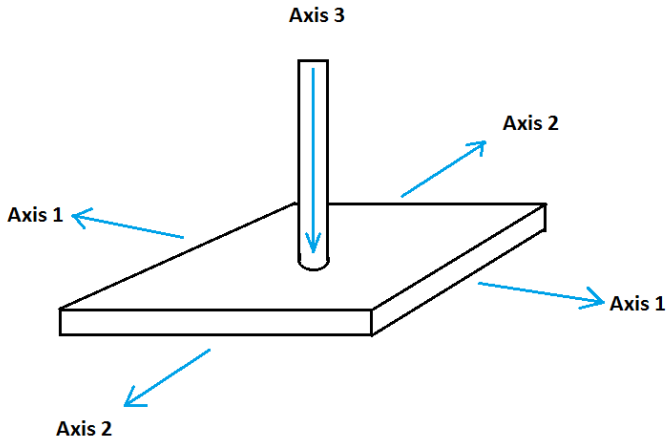

Figure 125: Triaxial test schematic: A schematic drawing showing the addition of the unidirectional compression test in the third axis.

Left atrial samples were dissected as described previously (*Sample Preparation and Dissection*), and sutured into the ElectroForce Biaxial Rig (TA Instruments, USA) as described above. The aim was to then integrate a machine to apply load or displacement in the third axis and record mechanical response in this direction. In order to achieve this, a Bose ElectroForce 5500 uniaxial rig (TA Instruments, USA) was attached to the ElectroForce Biaxial Rig (TA Instruments, USA) to create a Triaxial Rig.

The ElectroForce Biaxial Rig is stationed on an air table, and the uniaxial rig is held upright on a large base plate which would not fit onto the air table. A new base plate was therefore needed, to allow the uniaxial rig to be secured to the table and integrated into the setup, large enough to support the uniaxial rig but small enough to allow the biaxial motors to still be moved (Figure 66).

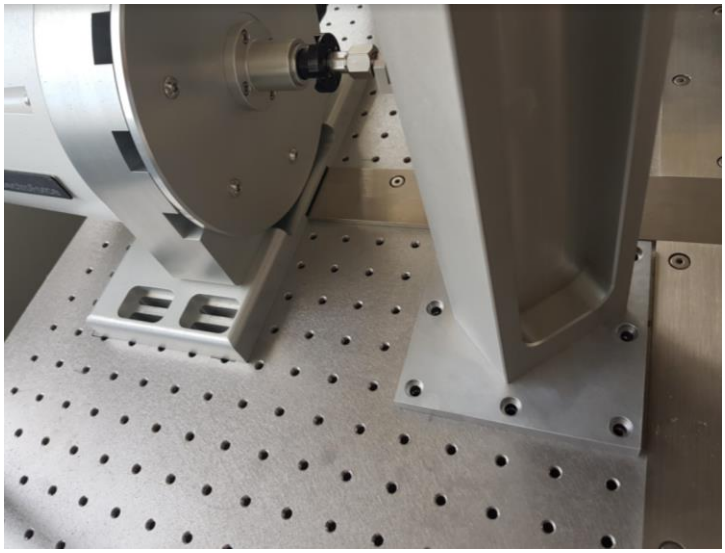

Figure 66: Custom Built Uniaxial Rig Base Plate.

The base plate was screwed onto the biaxial rig base to secure the uniaxial rig into place, with the third loading axis positioned above the sample area. In order for the loading arm to reach the sample and record force, and to attach the ablation catheter to recapitulate the physiological triaxial loading conditions, a connector needed to be made. (Figure 67A) The 250N load cell then screws onto the connector which is then screwed into place on the Bose system. (Figure 67B)

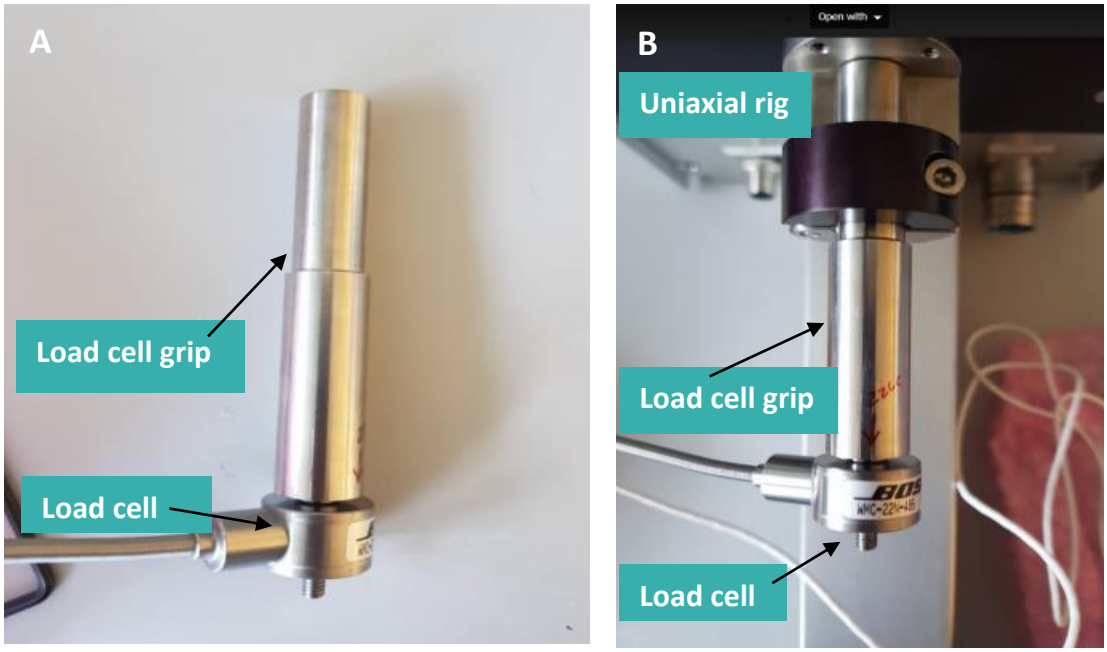

Figure 13: Load Cell Assembly. (A) 22N Load cell attached to the load cell grip, (B) the load cell – load cell grip assembly secured into the uniaxial rig.

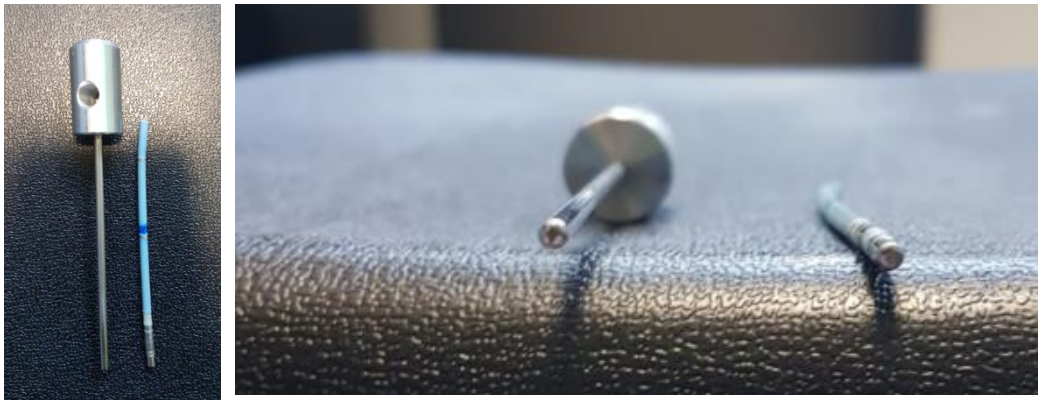

Figure 68: Custom Built Catheter. On the right in each of the above photos is the Biosense SmartTouch catheter, on the left is the stainless steel substitute built.

The ablation catheter used to compress the left atrial tissue was then attached to the bottom of the load cell. Initially, in order to keep the experiment a physiologically representable as possible an actual Biosense Thermacool SmartTouch (Biosense Webster Inc, CA, USA) catheter was going to be used, however, due to its ability to bend it could not be used to compress the tissue. Therefore, a piece of steel was fashioned to the same specifications as the catheter in order to replicate the precise contact area and tissue response to applied force (Figure 68). Figure 69 shows the overall triaxial rig set up.

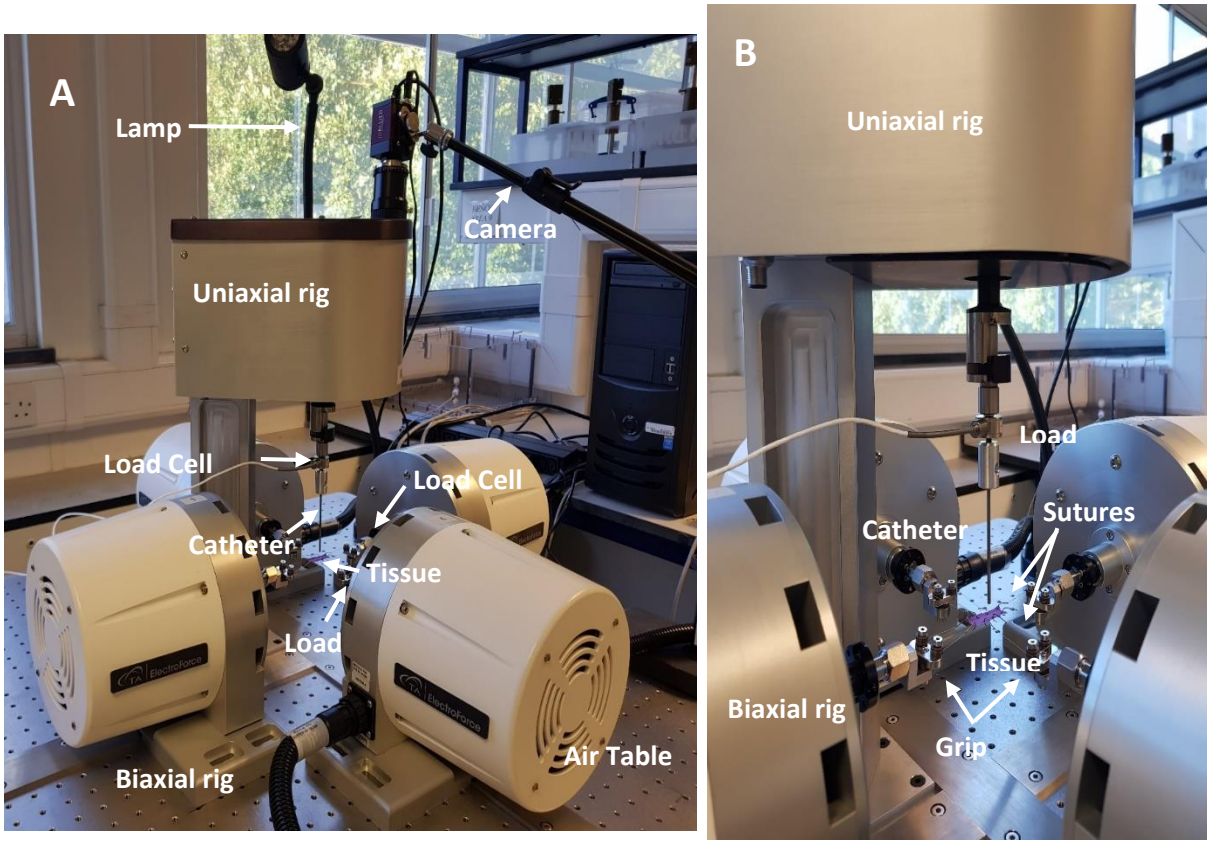

Figure 69: Triaxial Rig Set-Up. (A) Overall triaxial rig set-up. (B) Load cell assembly.

Statistical Analysis

Statistical analysis was performed using OriginPro (V9.0 OriginLab, Northampton, MA, USA) and R (V3.3.2, R Foundation for Statistical Computing, Vienna, Austria) with R studio (V2.1 FOAS, Boston, MA, USA). A p-value of <0.05 was taken to indicate statistical significance. A Shapiro-Wilks test for normality was carried out to establish if the data was normally distributed. Normally distributed data was then analysed for significance using a 2-way-ANOVA, followed by a post-hoc Tukey's HSD comparison of means to identify which groups were significantly different for the data which was not normally distributed a Mann-Whitney U or Kruskal-Wallis test was used. Data are presented as box plots showing the mean, median, interquartile range and 95% confidence interval error bars.

Uniaxial Testing

Uniaxial testing was adopted to determine the baseline characteristics of the left atrial tissue, and establish failure properties.

Methods

Uniaxial testing of the left atrial tissue sections was carried out using a materials test machine (*Instron, Norwood, MA, USA*), nine fresh porcine hearts were tested. Each heart was dissected as described in previously and the atria dissected into samples 30mm x 10mm from each of the seven regions. All samples were dissected and tested in a day, maintained in PBS during preparation and testing to retain hydration. The width of the samples was measured using calipers, thickness with the laser micrometre. Sample weight was also recorded prior to testing. Samples were loaded into the clamps of the pneumatic grips, at a grip to grip length of 10mm and gripping pressure of 3 bar. Each sample was subject to a pre-load of 0.2N, to remove slack and provide a consistent start point for tests. Sample length was then measured and taken as the test length for strain calculations. Tissue samples were stretched to failure at a speed of 0.05mm/s, with force and displacement data collected at 15Hz by Instron Bluehill Software *(Instron, Norwood, MA, USA)*. The test was considered complete once all of the tissue fibres had broken. The tissue was observed throughout the test and the location between the grips at which the tissue broke, as well as any observations such as visible sliding within the clamp was manually recorded.

Data was arranged by individual sample, collectively by region, and by heart for analysis. Regions were compared against one another for both thickness data and stress-strain data.

Elastic modulus and ultimate tensile strength (UTS) were calculated for each sample. From a stress-strain curve. To draw a stress-strain curve, stress (σ) was calculated by dividing force (F) by the cross-

Equation 1: $$\frac{F}{A} \text{ where } A = W \times h$$

Equation 2: $$\frac{\Delta l}{l^{\circ}} \text{ where } \Delta l = l - l^{\circ}$$

sectional area (A), where the cross-sectional area is equal to width (w) multiplied by thickness (h) (Equation 1). Strain (ε) was calculated by dividing the change in length (Δl) by initial length (l^o) (Equation 2).

Failure stress and strain were recorded at the point of maximum stress. Modulus was calculated by obtaining a five point moving average continual modulus from the stress-strain curve, and identifying the maximum value. Transition strain was also recorded as the point at which samples transitioned from the initial low stiffness toe region to the linear region. In order to find transition strain, the start of the linear region was identified from the continual modulus curve, and the stress-strain curve replotted to stop at this point. Two lines of best fit were then drawn relative to the x and y axes, and the point of intersection deemed the transition point (Figure 70). Data analysis was carried out using Excel, or Origin Pro (V9.0 OriginLab, Northampton, MA, USA) whereas curve generation was calculated using R (V2.1 FOAS, Boston, MA, USA).

Figure 70: Stress-Strain and Force-Extension Schematics. (A) Stress-strain curve, green circle indicates point of maximum stress, red line represents the five point moving average used to calculate modulus (σ/ε) and the purple circle at the point where the two black lines intersect represents the transition strain, the point at which the low stiffness toe region transitions to the linear region.

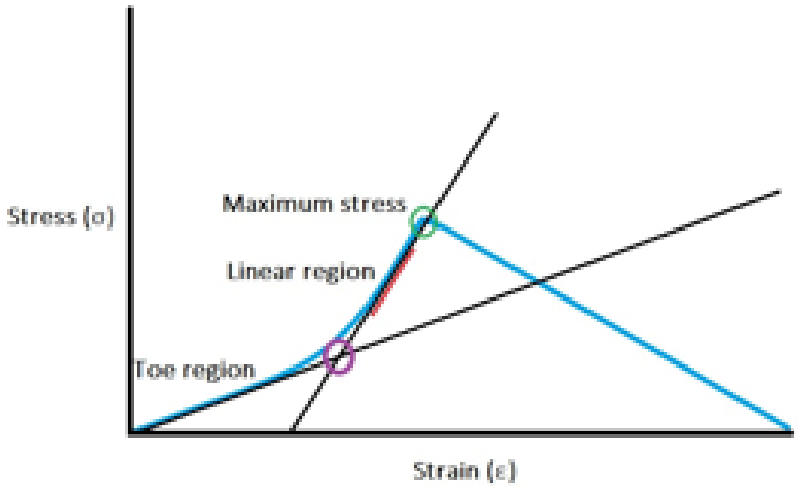

Results

*A total of 12 porcine hearts were dissected for testing, (*Table 15*). Owing to heart size and geometry there was a notable difference between the numbers of samples per region tested. The mean number of samples per region was 7.71 per region.*

Region	H1	H2	H3	H4	H5	H6	H7	H8	H9	H10	H11	H12	Total
Anterior	✔	✔	✔	✔	✔	✔	✔	✔	✔	✘	✘	✘	9
Lateral	✔	✔	✔	✔	✔	✔	✔	✔	✔	✘	✘	✘	9
Posterior	✘	✔	✘	✘	✘	✘	✘	✘	✘	✘	✘	✘	1
LPV	✔	✔	✔	✔	✔	✔	✔	✔	✔	✔	✘	✘	10
RPV	✔	✔	✔	✔	✔	✔	✔	✔	✔	✔	✘	✘	10
Roof	✔	✔	✔	✘	✘	✘	✘	✘	✘	✘	✘	✘	3
Sinus	✔	✔	✔	✔	✔	✔	✔	✔	✔	✔	✔	✔	12

Table 15 : LA Tissue Samples. Number of tissue samples taken from different regions within the left atrium for testing as well as total number of hearts these samples were obtained from.

The quality of data recorded for each sample was assessed by a single reviewer (RN) and graded via a traffic light system: red – data excluded, yellow – data had minor discrepancies but could still be used for analysis, and green – no abnormalities. Any issues were reviewed by a second reviewer (HS). Samples were assigned to the red category if they exhibited visual slipping during the test, failed at the gripping site, or failed immediately (<0.5N). Samples were assigned to the yellow category in the stress-strain curve displayed minor abnormalities, usually due to the tissue fibres breaking within the tissue sample but not visible on the surface of the tissue sample. Samples that showed no evidence of slipping either visibly or on assessment of the stress-strain curve were allocated to the green category. The number of samples assigned to each category can be seen in Table 16. Any area within the left atrium that had less than five viable samples for analysis were excluded from the study.

Atrial Region	Red Classification	Yellow Classification	Green Classification	No. Samples Included in mechanical analysis
Anterior Wall	2	3	4	7
Lateral Wall	1	1	7	8
Roof	2	-	1	1
RPV Ostia	2	3	5	8
LPV Ostia	1	2	7	9
Posterior Wall	-	1	-	1
Sinus Wall	1	4	7	11

Table 16: LA Tissue Sample Classification. Number of tissue samples assigned to each classification: red, yellow, green and the total number of samples used in the analysis.

Left Atrial Thickness

Previous studies have suggested that the left atrium has a uniform thickness of 2-3mm [237]*. Contrary to previous works, a large variation in atrial thickness was seen across the atria (Table 17), the thickest area being the roof measuring 6.06 ± 2.18 mm, and the thinnest area the RPV Ostia measuring, 3.45 ± 1.20 mm.*

Atrial Area	*Atrial Thickness Mean ± SD (mm)*
Anterior Wall	4.42±1.51
Lateral Wall	4.67±0.99
Roof	6.06±2.18
RPV Ostia	3.45±1.20
LPV Ostia	3.71±1.04
Posterior Wall	3.98±1.54
Sinus Wall	4.61±1.03

Table 17: Mean thickness of LA area. ± the standard deviation. The total number of samples tested in each area is also displayed. LPV = left pulmonary vein, RPV = right pulmonary vein.

The roof samples were significantly thicker than all other regions ($P<0.0001$). The RPV was thinner than all other regions except for the LPV. (Table 17 show that there is a difference in the thicknesses of the anterior, lateral, posterior and sinus walls, however, Table 18 shows that this difference wasn't significant.

	Anterior	Lateral	Posterior	RPV	LPV	Roof	Sinus
Anterior Wall	x	NS	NS	****	*	****	NS
Lateral Wall	NS	x	NS	****	****	****	NS
Posterior Wall	NS	NS	x	*	NS	****	NS
RPV Ostia	****	****	*	x	NS	****	****
LPV Ostia	*	****	NS	NS	x	****	***
Roof	****	****	****	****	****	x	****
Sinus Wall	NS	NS	NS	****	***	****	x

Key:	
*=	P<0.05
***=	P<0.001
****=	P<0.0001
NS=	Not Significant

Table 18: Variation in LA tissue thickness. Statistical significance in variation of thickness between different areas of the left atrium. LPV = left pulmonary vein, RPV = right pulmonary vein.

Mechanical Properties

Figure 71 shows failure force (Figure 71A) and the failure extension across all samples (Figure 71B), grouping the areas into regions of the wall (anterior, lateral and sinus) and vein (RPV and LPV), shown as red and green respectively in all Figures. Figure 71A shows that in terms of force, no significant difference was found between the two regions, however, the LPV and RPV within the vein region were significantly different, with a mean difference in force of 4.53 N (P=0.001). Figure 71B shows that the anterior wall extended significantly less than a number of areas before it failed, with wall regions generally appearing less extensible than vein regions.

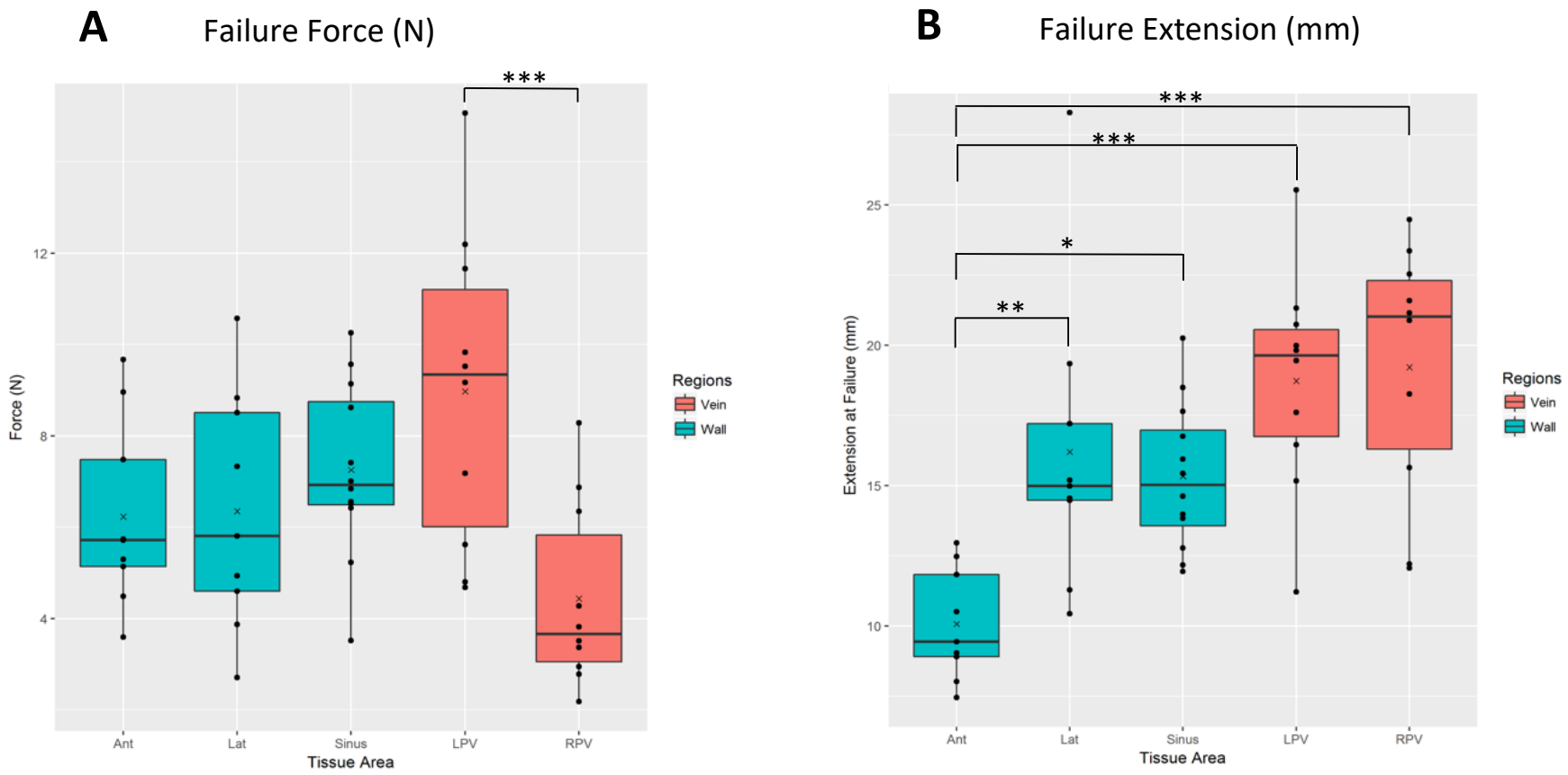

*Figure 7114: Failure Force and Extension Graphs. (*A) Displays the amount of force required for each atrial sample to fail. (B) Shows the corresponding extension value for each force per area. Ant = Anterior wall, Lat = Lateral wall, Sinus = Sinus wall, LPV = Left pulmonary vein, RPV = Right pulmonary vein. (*) = significance, (-) = median, box = interquartile range, lines above and below the box = 95% confidence interval, (x) = mean.

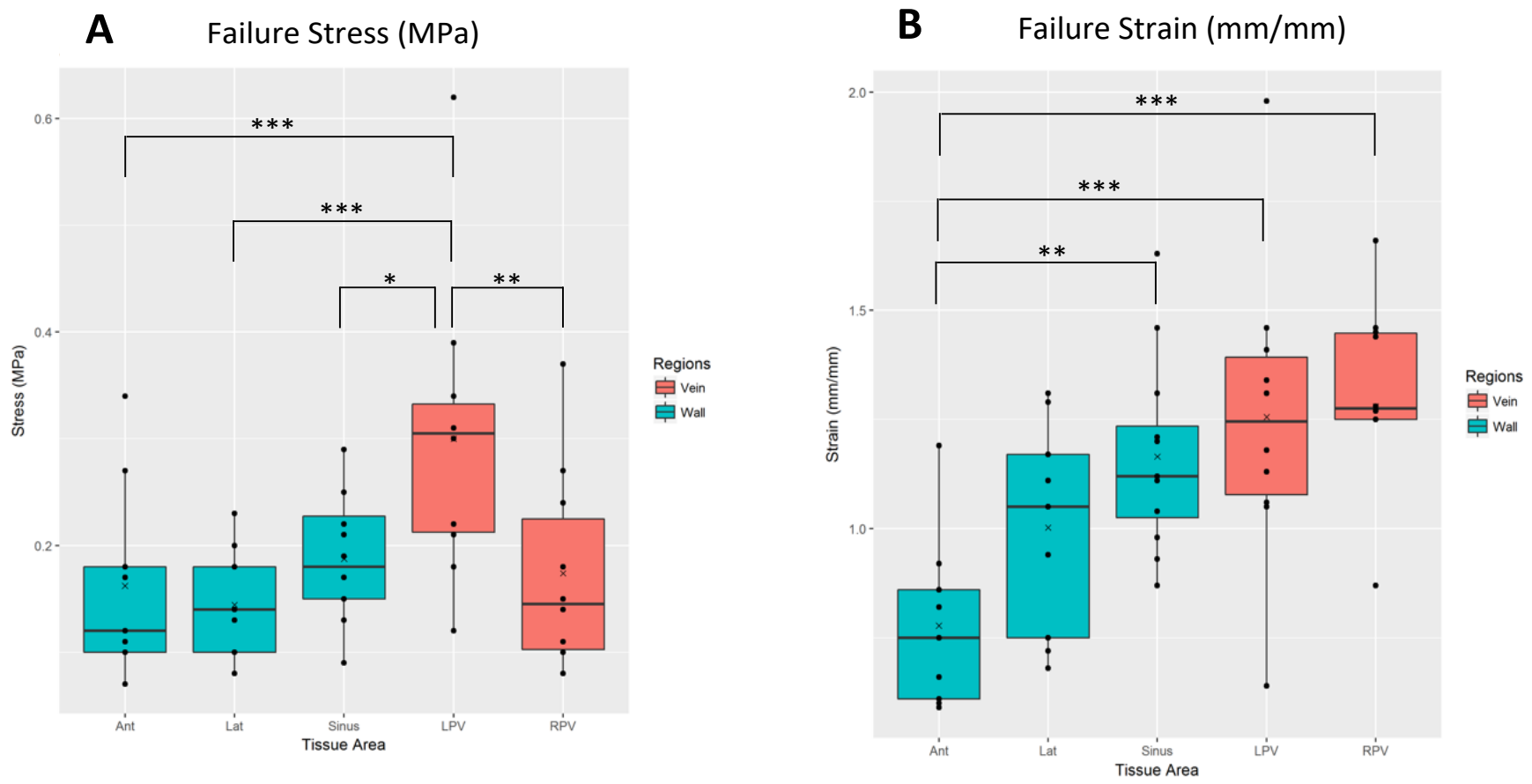

*Figure 72: Failure Stress and Strain Graphs. (*A) Shows the amount of stress required for each sample to fail, (B) shows the amount of strain applied to each sample for it to fail. Ant = Anterior wall, Lat = Lateral wall, Sinus = Sinus wall, LPV = Left pulmonary vein, RPV = Right pulmonary vein. (*) = significance, (-) = median, box = interquartile range, lines above and below the box = 95% confidence interval, (x) = mean.

A comparison of the max modulus (Figure 73A) and strain at max modulus (Figure 73B) showed no significant differences between regions, but trends which largely matched failure properties.

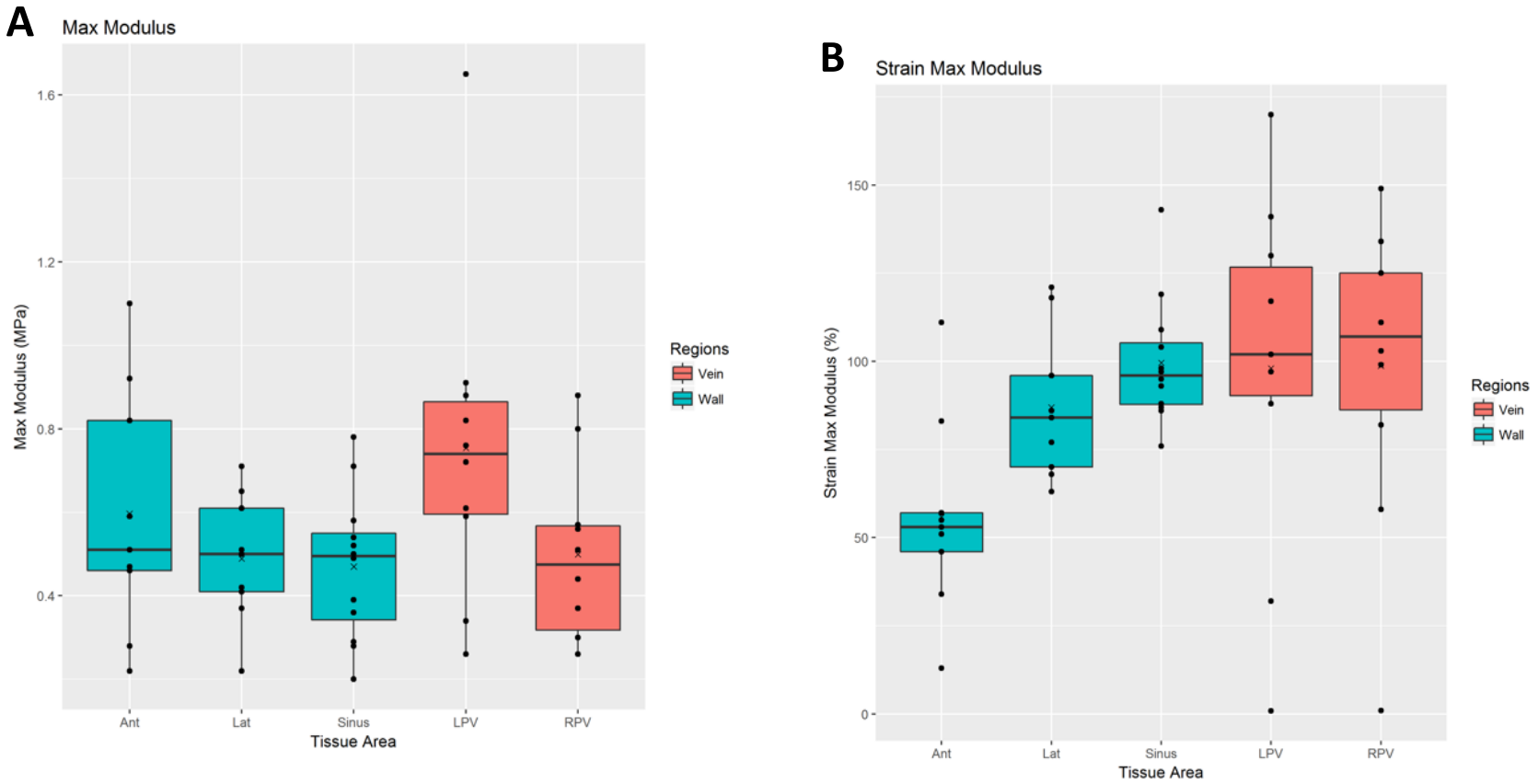

*Figure 73: Max Modulus and Strain at Max Modulus Graphs. (*A) Shows the Max modulus at failure, (B) show the strain max modulus at failure. Ant = Anterior wall, Lat = Lateral wall, Sinus = Sinus wall, LPV = Left pulmonary vein, RPV = Right pulmonary vein. (-) = median, box = interquartile range, lines above and below the box = 95% confidence interval, (x) = mean.

Interestingly, when the sample specific property of modulus was investigated, trends became more pronounced and the low stiffness of the RPV became significant (Figure 74).

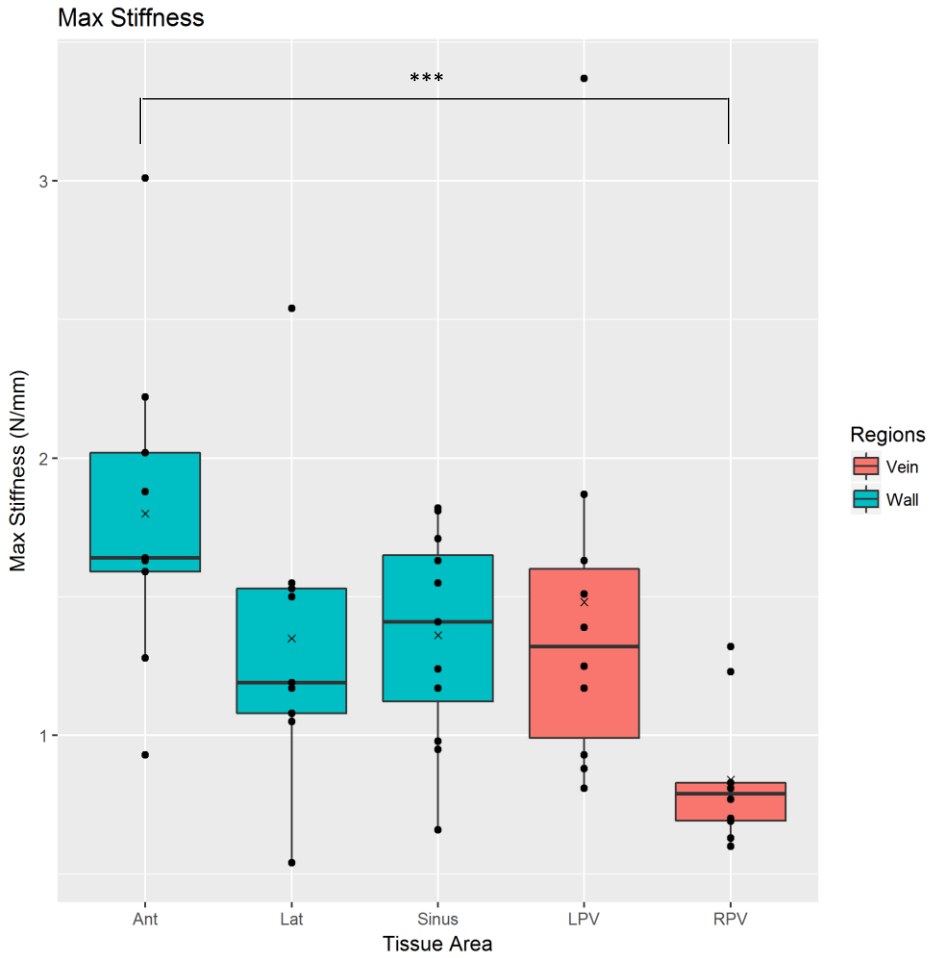

Figure 74: Max Stiffness Graph. Max stiffness at failure for each tissue sample. Ant = Anterior wall, Lat = Lateral wall, Sinus = Sinus wall, LPV = Left pulmonary vein, RPV = Right pulmonary vein. (*) = significance, (-) = median, box = interquartile range, lines above and below the box = 95% confidence interval, (x) = mean.

The final observation shown in Figure 75 looked at strain of the transition linear region of each area. While trends were similar to failure strain in most instances, it was notable that the toe region as a percentage of overall sample extension was markedly less in the RPV (Figure 75).

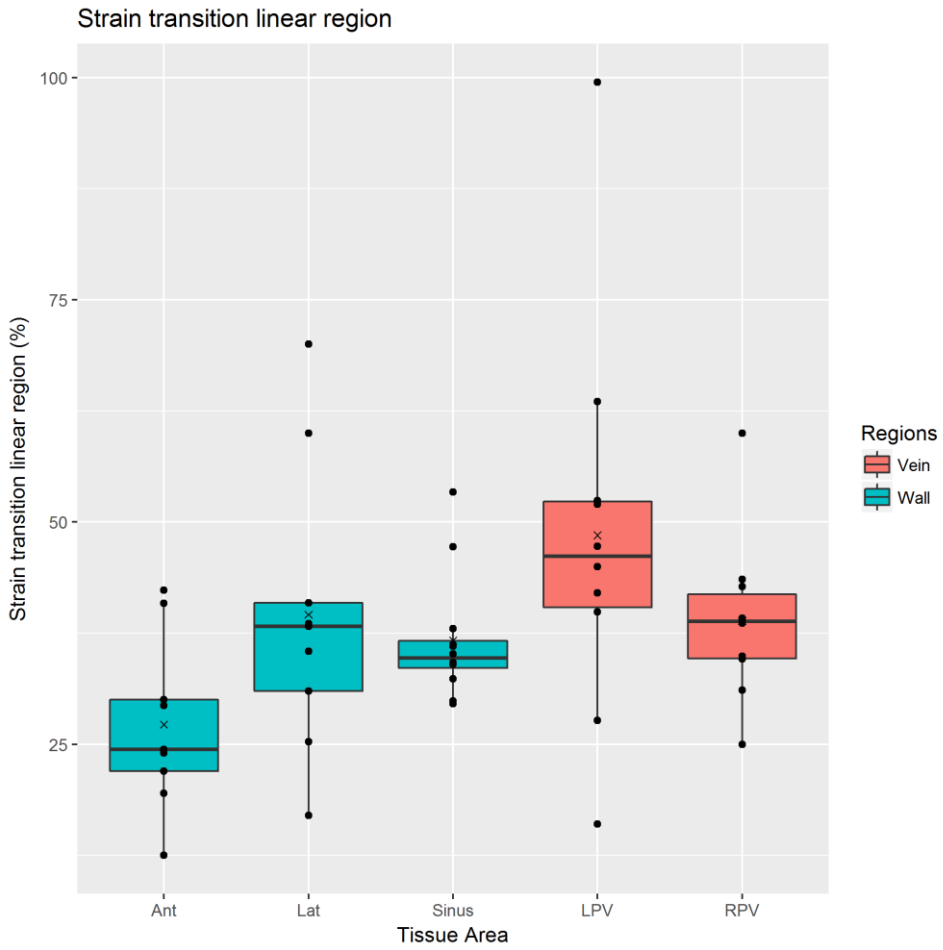

Figure 75: Strain at Transition Linear Region Graph. Strain at transition linear region for each atrial sample. Ant = Anterior wall, Lat = Lateral wall, Sinus = Sinus wall, LPV = Left pulmonary vein, RPV = Right pulmonary vein. (-) = median, box = interquartile range, lines above and below the box = 95% confidence interval, (x) = mean.

Biaxial Testing

In the present thesis, uniaxial studies of left atrium (LA) have shown that both sample thickness and local mechanical properties vary across the LA. Uniaxial testing provides a simple way in which LA mechanics can be investigated in a controlled environment. However, it does not reflect the complex multi-axial physiological loading conditions of the native functioning LA [237]. Biaxial testing more closely replicates the natural i*n vivo* physiological conditions of the LA, and is now considered.

Methods

Biaxial testing of the left atrial tissue sections was carried out using the ElectroForce Planar Biaxial TestBench (TA Instruments, USA), ten fresh porcine hearts were tested. Each heart was dissected and the atria dissected cutting samples as close to 30mm x 30mm as possible, depending on available tissue from each of the seven regions. All samples were dissected and tested in a day, maintained in PBS during preparation and testing to retain hydration. The length and width of the samples were measured using calipers, any sample in which either parameter was less than 10mm was discarded. The thickness of the tissue sections was measured using a laser micrometre, and weight recorded for each sample prior to testing. Samples were gripped using fishing wire hooked around the grip surfaces as sample gripping. Each sample was subject to a pre-load of around 0.2N on each axis to remove any slack, and final sample dimensions recorded.

Tissue samples then underwent a test protocol comprising 10 preconditioning cycles, between 0-8mm in axis 1 (long axis), and 0-4mm in axis 2 (short axis) (50% of the failure extension) at a frequency of 1Hz. Followed by a Ramp to 50% of the failure extension. Samples were then held under biaxial strain for 300 seconds to record stress relaxation behaviour. The change in peak stress between preconditioning cycles one to ten was used to indicate the amount of preconditioning stress relaxation, with further stress relaxation of the tissue determined for the specific stress relaxation test, peak load and stiffness properties were established from the quasi-static test (Figure 76).

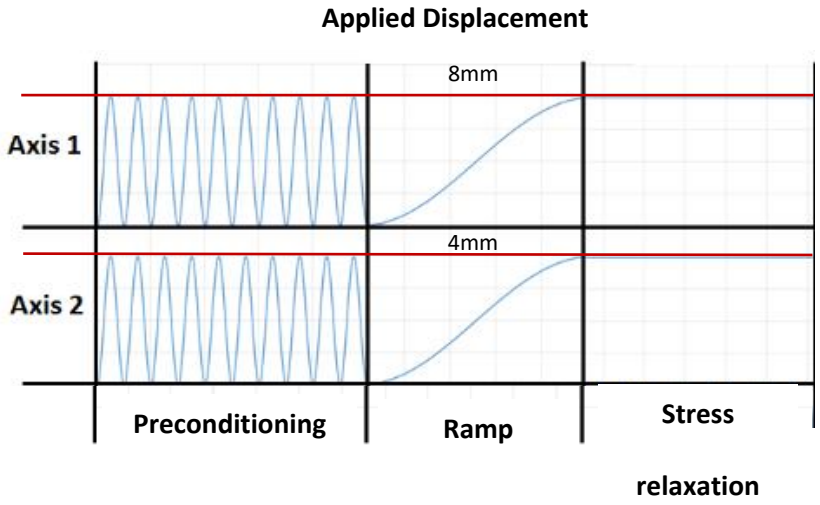

Figure 76: Biaxial rig applied displacement. Graphical representation of the biaxial test, 10 preconditioning cycles followed by the ramp to 50% failure extension and then hold for the stress relaxation test.

Data was arranged by individual sample, collectively by region, and by heart for analysis. Regions were compared against one another for both thickness data and mechanical properties.

Results

As described previously, owing to heart size and geometry not all samples were successfully acquired and tested from each heart, with details of available samples outlined in Table 19

Region (n)	H1	H2	H3	H4	H5	H6	H7	H8	H9	H10	H11	H12	H13	Total
Anterior	✔ (2)	✔	✘	✔	✔	✔	✘	✘	✘	✘	✔	✘	✔	8
Lateral	✔	✔	✘	✘	✔	✔	✔	✔	✔	✔	✔	✘	✘	9
Posterior	✘	✔	✔	✔ (2)	✔	✔	✘	✔	✔	✔	✔	✔ (2)	✘	12
PVO	✔	✘	✔ (3)	✔	✔	✔ (2)	✔	✘	✔	✘	✔	✔	✘	12
Roof	✘	✔	✔	✔	✔	✘	✘	✘	✔	✘	✔	✘	✘	6
Sinus	✘	✘	✔	✔	✘	✔	✔	✔	✔	✔	✔	✘	✘	8
Septum	✔	✘	✔	✔	✔	✔	✔	✔	✔	✔	✔	✘	✘	10

Table 19: LA Tissue Samples. Number of tissue samples taken from different regions within the left atrium for testing as well as total number of hearts these samples were obtained from.

Left Atrial Thickness

In keeping with the uniaxial findings, a large variation in atrial thickness was seen across the atria, the thickest area being the roof measuring 6.91 ± 1.5 mm to the thinnest area being the lateral wall measuring 5.18 ± 0.79 mm (Table 20).

Atrial Area	Atrial Thickness mean±SD (mm)	Total Number of Samples
Anterior Wall	4.52±0.61	8
Lateral Wall	5.18±0.79	9
Posterior Wall	3.5±1.49	12
Roof	6.91±1.5	6
PVO	3.52±1.22	12
Sinus Wall	4.77±0.53	8
Septum	4.33±1.94	10

Table 20: Mean thickness of LA area. ± the standard deviation. The total number of samples tested in each area is also displayed. LPV = left pulmonary vein, RPV = right pulmonary vein.

Viscoelastic Properties of Left Atrial Tissue

Mechanical test data are arranged to combine viscoelastic and quasi-static properties, to determine difference in the response across regions. Behavior of the two loading axes is shown side-by-side for ease of comparison of anisotropy.

Stress relaxation data demonstrates continual relaxation throughout the loading periods, with both axes generally reporting similar trends, suggesting isotropy in viscoelastic response. The overall amounts of relaxation were comparable across regions, but relaxation profiles varied somewhat. For example, the anterior region showed a notably more rapid initial relaxation rate, whilst relaxation of the PVO was more variable between samples, but more consistent in terms of rate over time.

Graph Type	Axis 1	Axis 2
Preconditioning Relaxation	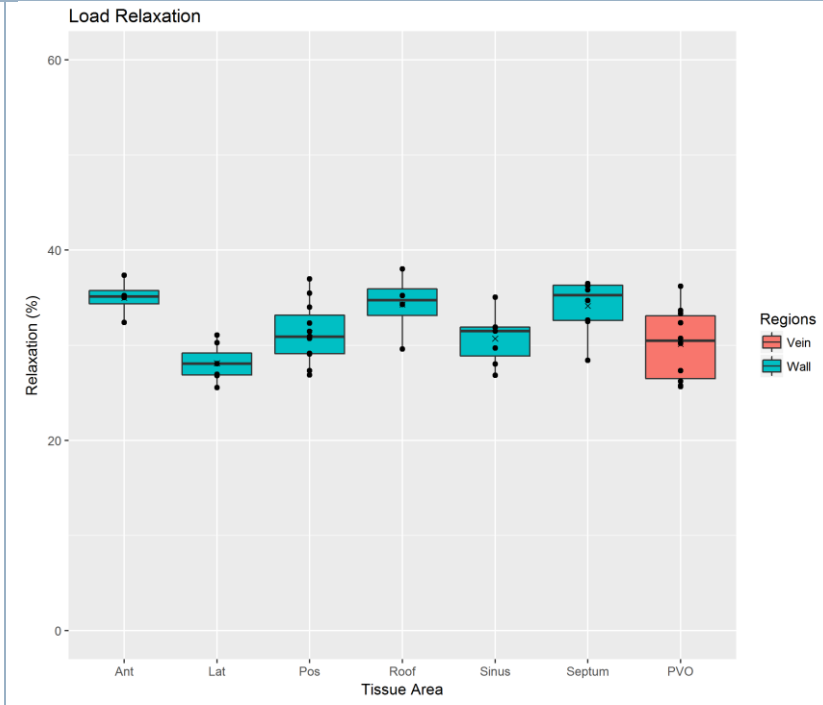	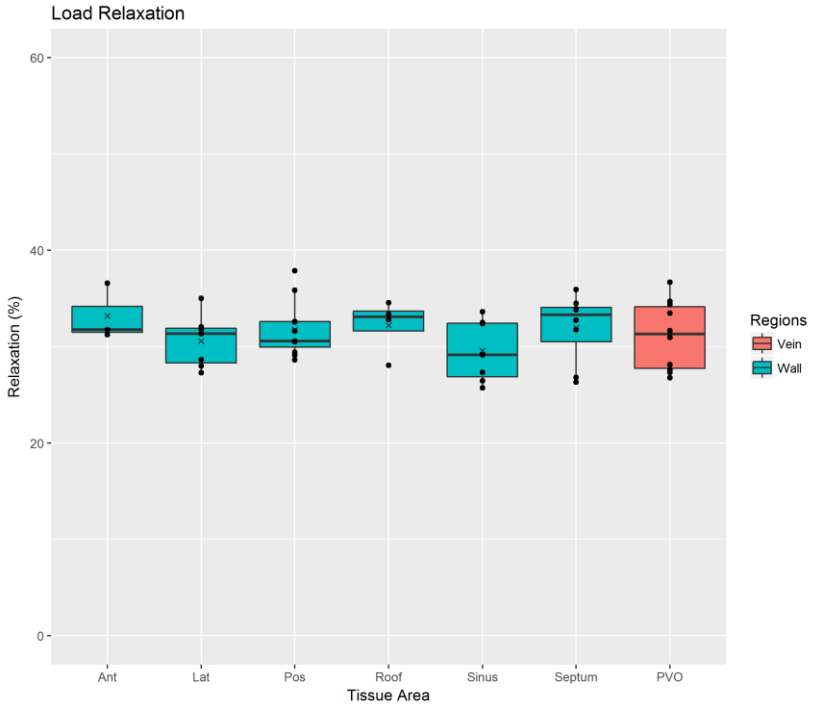

Stress- Relaxation at 150 seconds	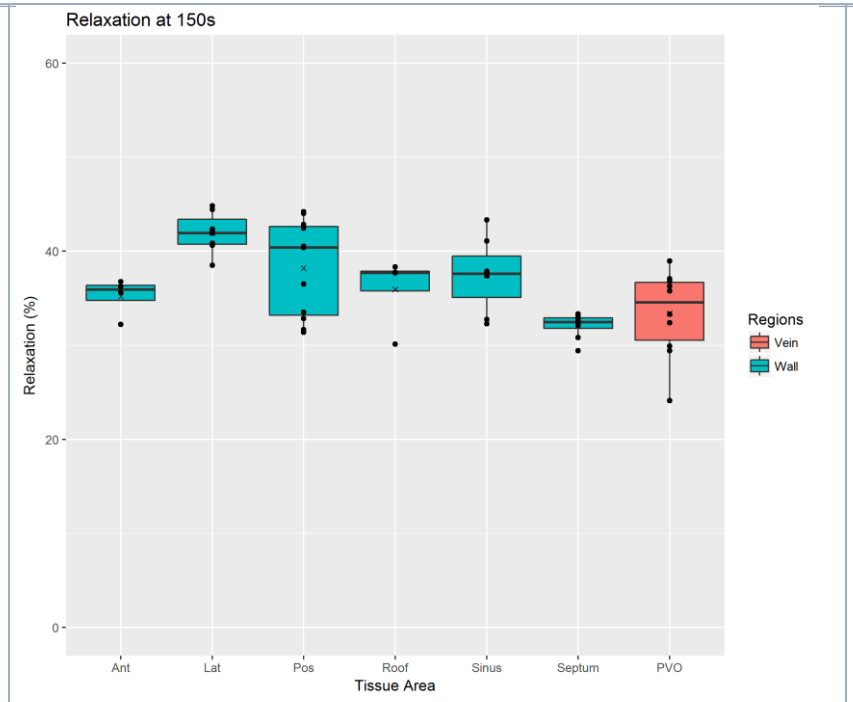	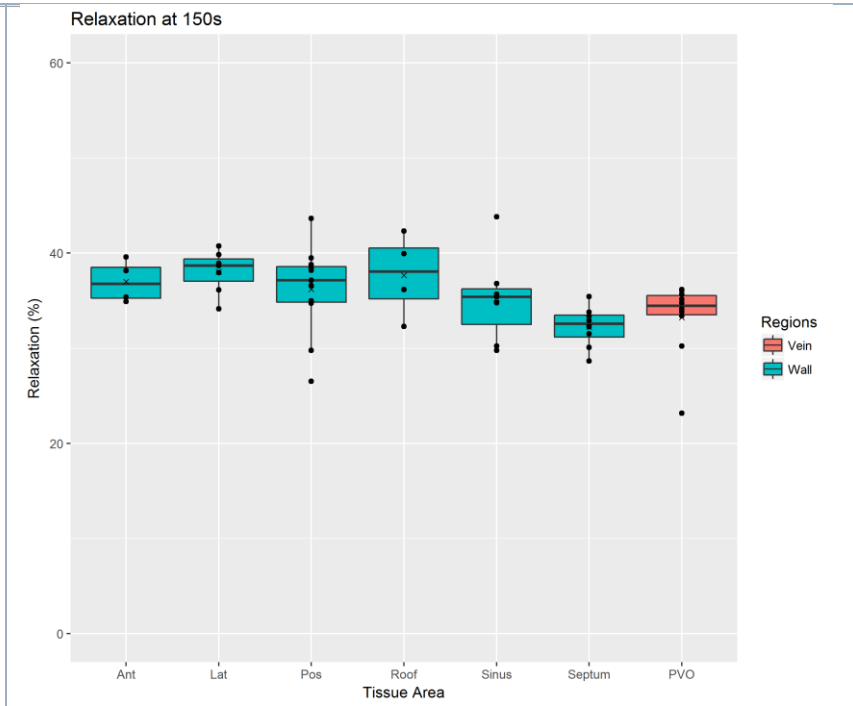

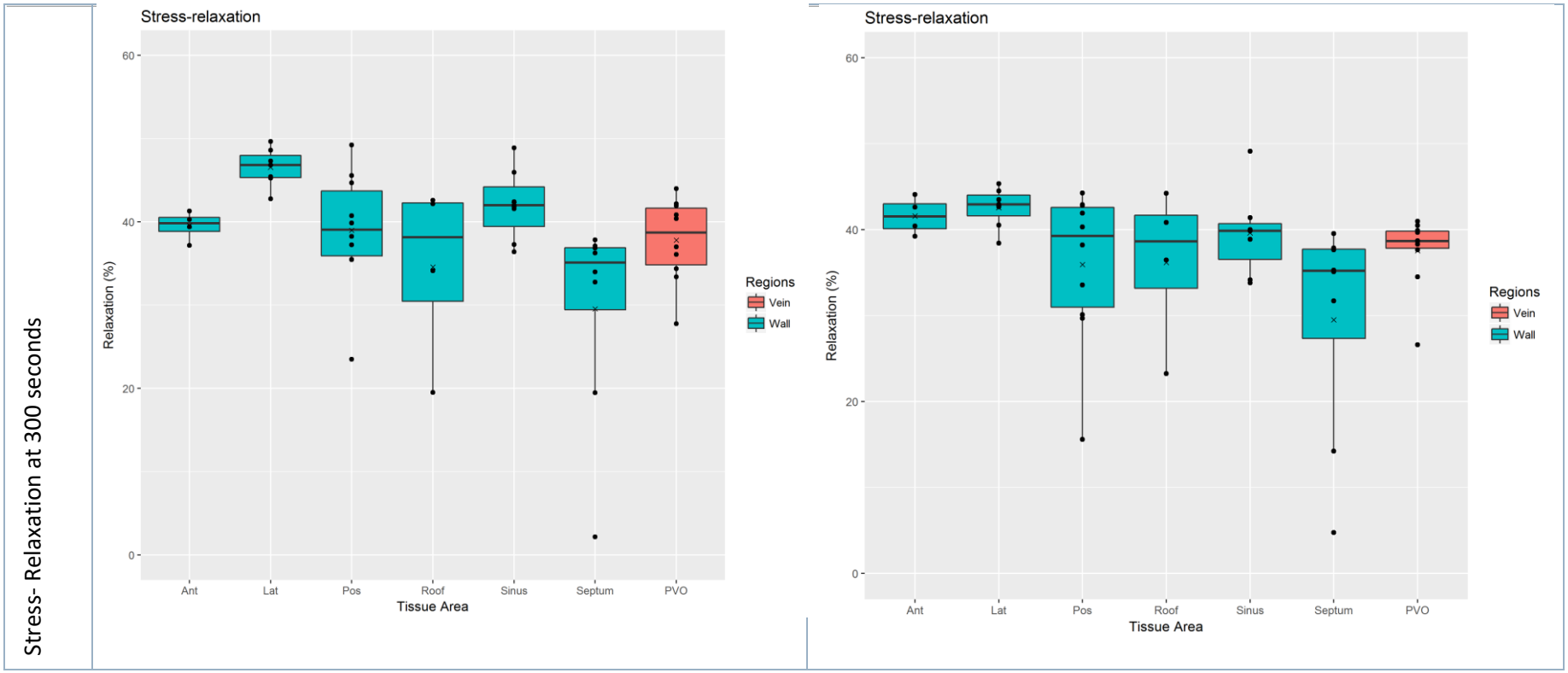

Table 21: Viscoelastic Properties of Porcine Left Atrial Tissue: Preconditioning relaxation, stress-relaxation at 150 seconds and at 300 seconds in both axis 1 and 2 for different areas within the left atrium. Ant = anterior wall, Lat = lateral wall, Pos = posterior wall, PVO = pulmonary vein ostia.

Quasi-Static Properties of Left Atrial Tissue

An analysis of quasi-static properties more clearly highlighted the anisotropy in the two axes, with opposing trends in load across axis 1 and 2. This was most evident in the lateral wall, where data indicates a stiffer response in axis 2. Variation in the transition point between axes was particularly prominent, and an extended toe region was seen in axis 1 in all regions, all regions were also more extensible in this plane.

Graph Type	Axis 1	Axis 2
Max Load at 50% strain	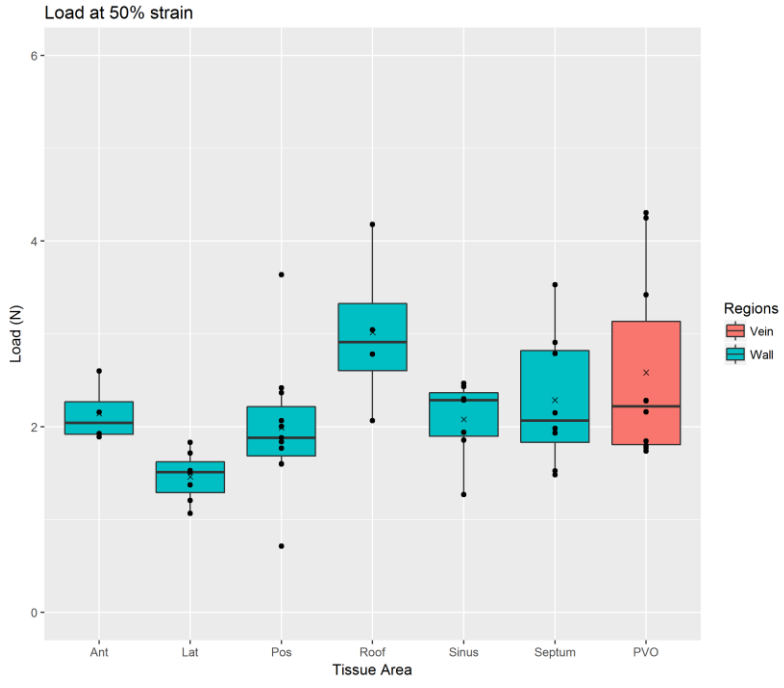	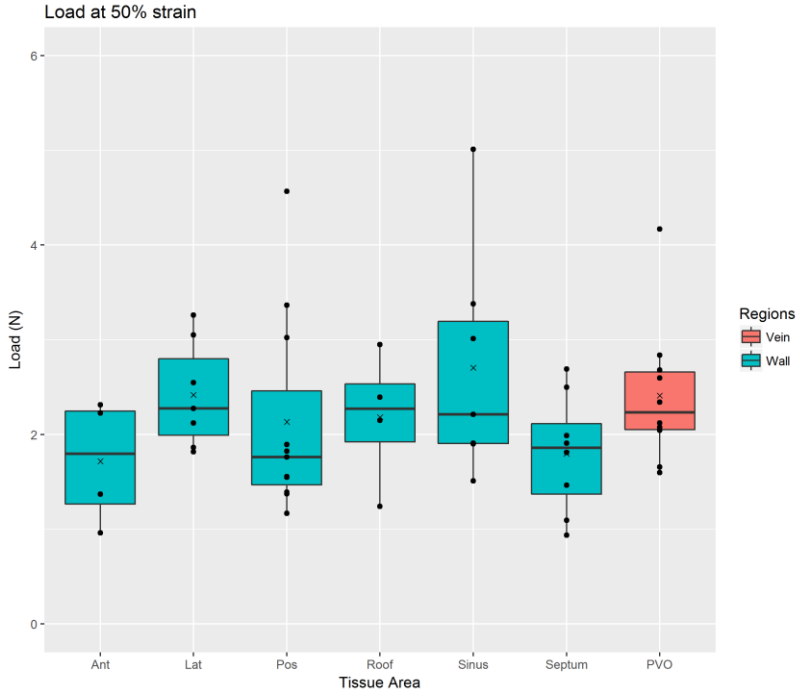

Max Stiffness	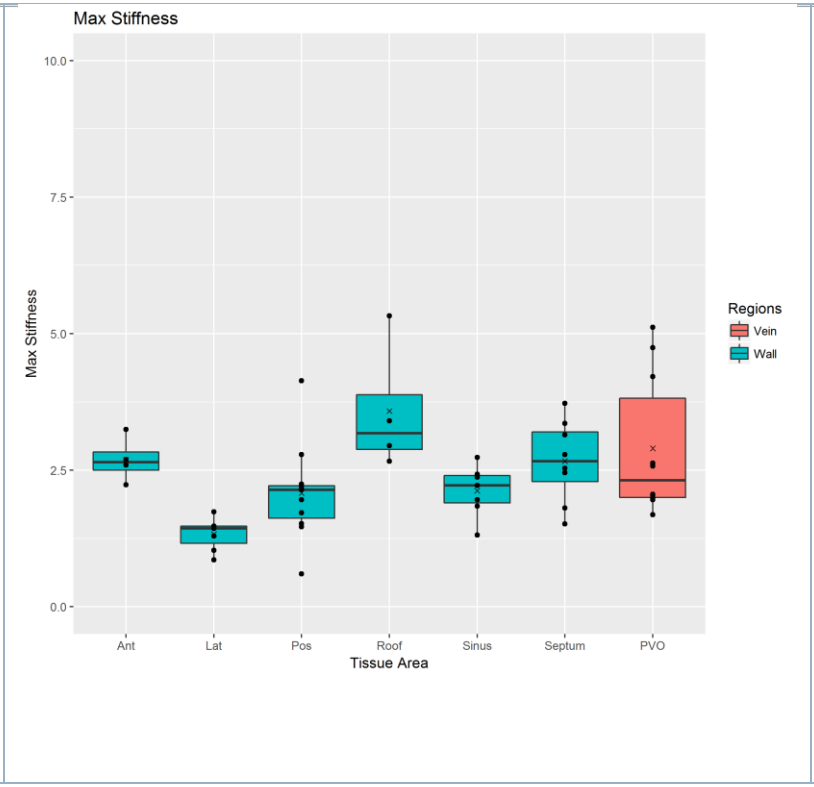	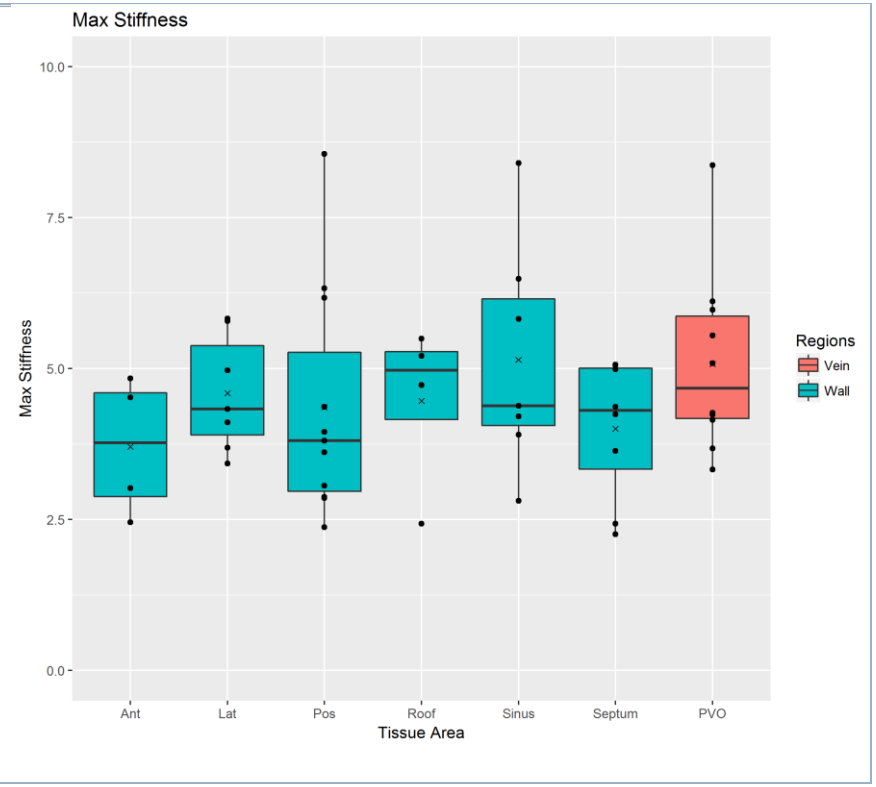

Transitio n Strain	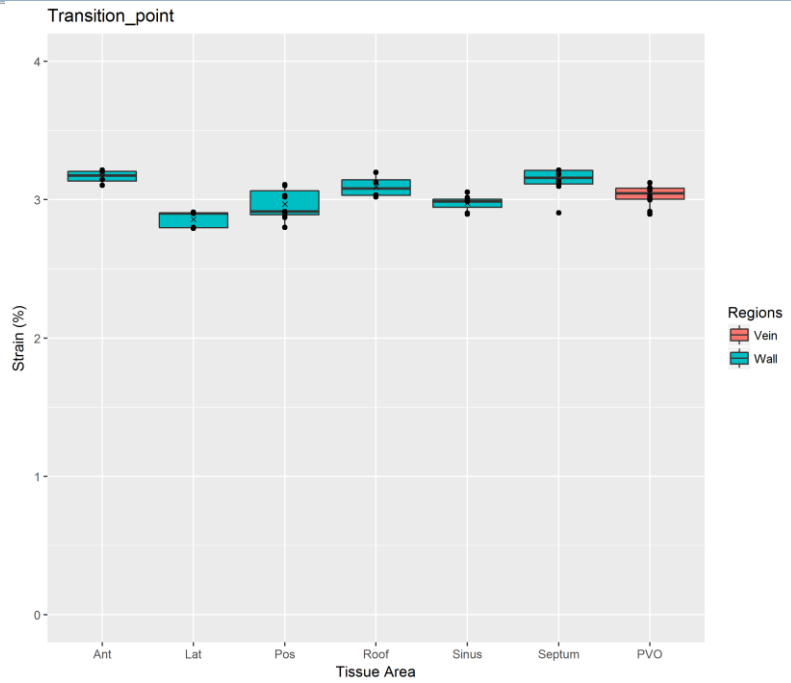	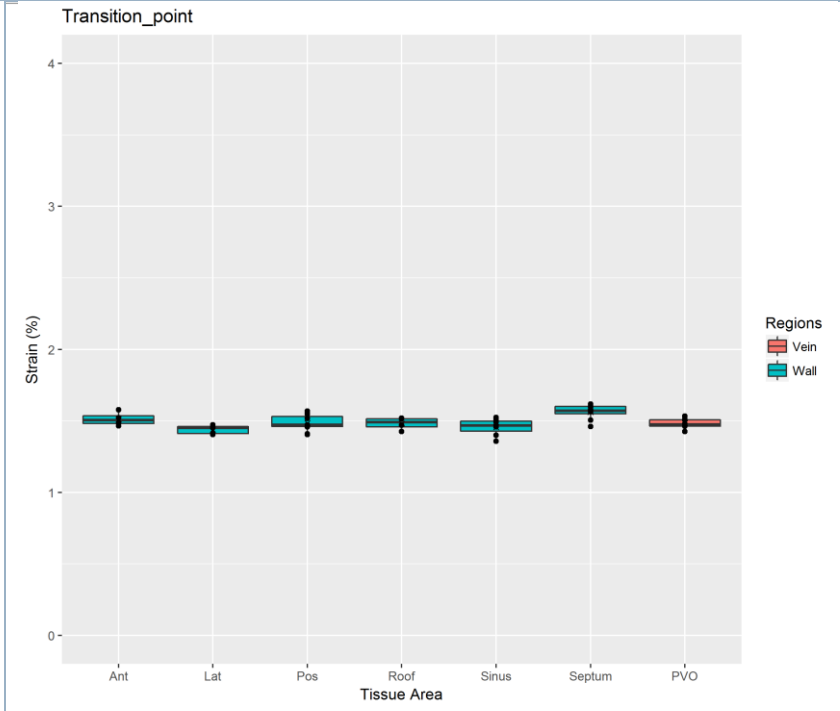

Table 22: Quasi-static Properties of Porcine Left Atrial Tissue: Maximum load at 50% strain (8mm in axis 1 and 4mm in axis 2), maximum stiffness (calculated as an average over one second of data, 10 data points), transition strain and stiffness after transition point. Ant = anterior wall, Lat = lateral wall, Pos = posterior wall, PVO = pulmonary vein ostia.

Triaxial Testing

Triaxial testing approaches were aimed at recreating the physiological condition of the ablation catheter applying force to the atrial wall, whilst it is subjected to in-plane stresses, as would result from the internal pressure acting on the atria.

Testing was carried out using the biaxial Electro Force equipment, with load in the third axis applied by incorporating a standard uniaxial Bose Electro Force 5500 rig (TA Instruments, USA) in a custom built arrangement.

Methods

The atria were extracted from the hearts of n = 13 healthy, young pigs (age range 18-24 months), and tissue specimens for mechanical characterisation excised from seven regions of the atria, following the dominant orientation of the fibre bundles. Sample length and width were measured will calipers and thickness with a laser micrometre, after which samples were loaded into the biaxial rig as sample gripping.

Tissue hydration was maintained by pipetting phosphate buffered saline solution on to the tissue samples at regular intervals. The Bose Electro Force 5500 was then secured to the platform of the Electro Force Biaxial Planar machine (TA Instruments, Eden Prairie, Minnesota, USA) ready to apply the out of plane third axis of loading, and the replica catheter tip secured to the loading arm.

Loading Protocol

A preload of around 0.2N was applied to both in plane axes of the tissue sample to remove any slack and obtain a consistent starting point. Samples were then subject to 10 preconditioning cycles to 50% max strain, in both inplane axes (axis1 and 2) at a frequency of 1Hz, followed by a ramp to 50% of the failure extension in both planes, at which the sample was held for 300 seconds to allow for stress relaxation to occur. After 300 seconds in plane stress relaxation period, the third out-of-plane loading condition was applied (Figure 77). The actuator was moved down until a small tare load of around 0.2N was detected, and a consistent starting condition defined. From this point the out-of-

plane actuator was displaced by 6mm, and held at this point for 10 seconds, recording force throughout the procedure at 100Hz in all three planes. Tissue displacement during the off axis loading period was additionally monitored by videoing the test on a Cannon EOS 7D camera.

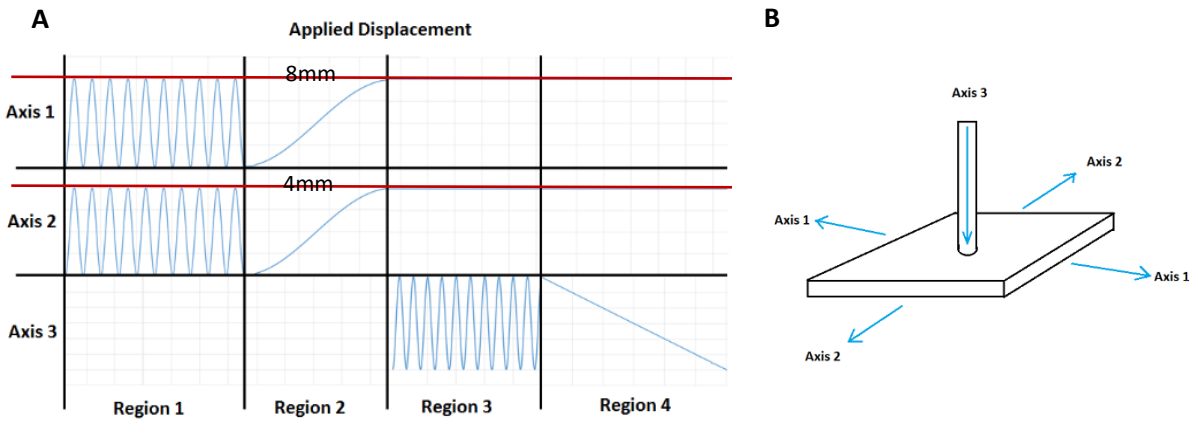

Figure 77: Triaxial rig applied displacement. (A) Graphical representation of the triaxial test, region 1, 10 preconditioning cycles followed by region to, the ramp to 50% failure extension in all three axis and then hold for the stress relaxation test in axes 1 and 2 (regions 3 and 4), meanwhile in axis 3 during region 3 10 preconditioning cycles take place, then ramp to maximum safe working load compression (6mm) and hold for 10 seconds. (B) Schematic to show the direction of all three axes.

Results

As described previously, owing to heart size and geometry not all samples were successfully acquired and tested from each heart, with details of available samples outlined in Table 23.

Region (n)	H8	H9	H10	H11	H12	H13	Total
Anterior	✗	✗	✗	✓	✗	✓	2
Lateral	✓	✓	✓	✓	✗	✗	4
Posterior	✓	✓	✓	✓	✓ (2)	✗	6
PVO	✗	✓	✗	✓	✓	✗	3
Roof	✗	✓	✗	✓	✗	✗	2
Sinus	✓	✓	✓	✓	✗	✗	4
Septum	✓	✓	✓	✓	✗	✗	4

Table 23: LA Tissue Samples. Number of tissue samples taken from different regions within the left atrium for testing as well as total number of hearts these samples were obtained from.

Visual Deformity Observation Test

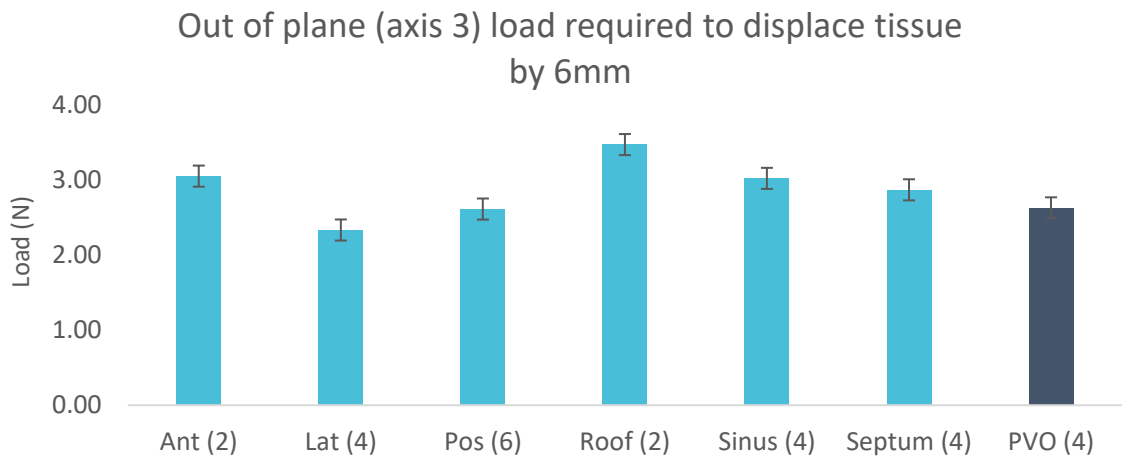

Figure 78 Uniaxial Compression: Graph showing the amount of force applied resulting from 6mm out of plane displacement across different regions of the left atria. Ant = anterior wall, Lat = lateral wall, Pos = posterior wall, PVO = pulmonary vein ostia.

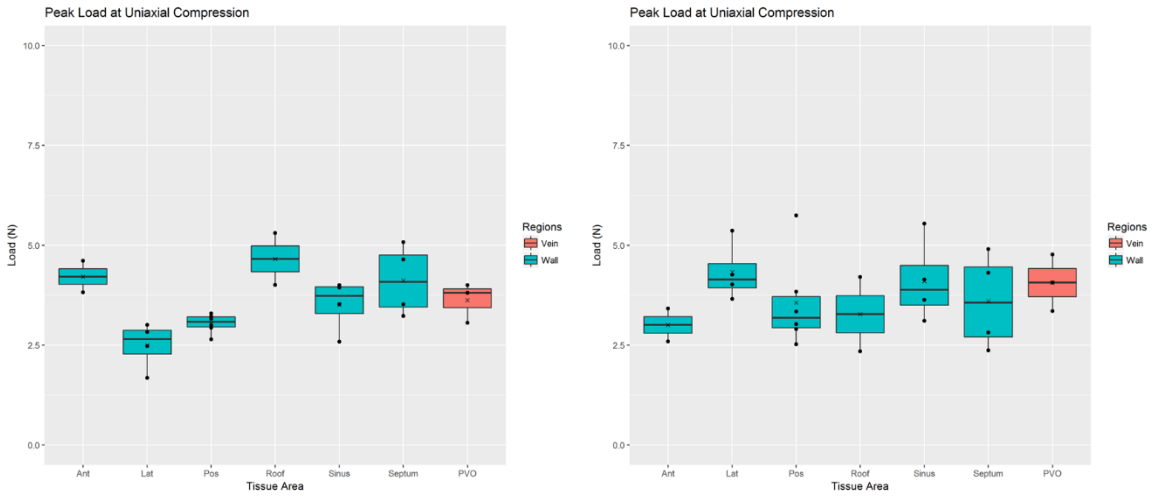

Figure 79: Uniaxial Compression Biaxial Readings: Corresponding graphs to show the effect of the out of plane force in load on in-plane axes 1 and 2. Ant = anterior wall, Lat = lateral wall, Pos = posterior wall, PVO = pulmonary vein ostia.

Visual Deformity Observation Test

In order to investigate the extent to which catheter ablation procedures deform the whole atria, or simply tissue directly beneath the catheter video footage of sample deformation during the off-axis loading protocol was analysed to investigate local deformation modes in the tissue.

Considering the sample in Figure 80, as an example, the schematics describe possible local modes through which the off-axis load may deform the tissue. Taking the video corresponding to off-axis loading in each sample, the frame at the point of peak off-axis deformation was cut, and stored as a single image ten people at random were asked to independently review each image and categorise local deformation on a scale of 1-5, as depicted in the schematic (Figure 80). Each person was allowed to look through the series of photos to get a feel for how the tissue deformed, then on their second viewing asked to rate each image.

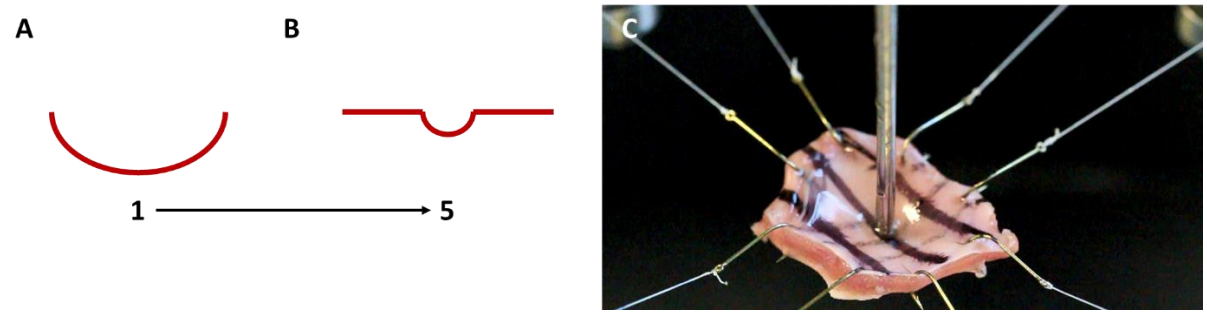

Figure 80: Left atrial tissue deformation. The grading scale used to rate deformation of LA tissue. (A) global deformation across the surface of the LA tissue, (B) local deformation at point of contact, and (C) an image used in the observational test deemed to globally deform.

Table 24 gives details of the most frequent answer given for each area along with its corresponding shape. Results suggest that the septum deforms more locally at the catheter contact site, whilst the anterior and lateral walls deform more globally. The posterior wall, roof and Pulmonary vein ostia were deemed to deform both globally and locally.

	Anterior	Lateral	Posterior	Roof	PVO	Sinus	Septum
Axis 3 Force (N)	3.05	2.33	2.61	3.47	2.63	3.02	2.87
Axis 1 Force (N)	2.08	1.04	1.05	2.25	1.02	1.43	1.83
Axis 2 Force (N)	1.29	1.91	1.43	1.37	1.65	1.4	1.8
Tissue Deformation	 2	 2	 3	 3	 3	 3	 4
Thickness (mm)	4.52	5.18	3.5	6.91	3.52	4.77	4.33

Table 24: Left atrial tissue deformation, thickness and force changes. PVO = Pulmonary vein ostia.

Discussion

In this study, a measure of compliance using only data collected routinely during first time radiofrequency catheter ablation procedures, in patients with atrial fibrillation was developed. This measure of compliance based of contact force and displacement data (mm/g), details of how this data was collected and this measure was developed can be found on page 80 (Establishing and calculating a suitable measure of compliance), was then preliminarily tested in 36 patients with atrial fibrillation against a multitude of factors associated with the disease. The main findings were as follows:

- A measure of compliance can be calculated using data routinely collected during ablation procedures.
- The results obtained when measuring compliance although slight follow expected trends, based on previous literature findings.
- Time could be suggested to have more of an effect on compliance than age.
- Left ventricular function appears higher in the PAF cohort when compared to the PeAF cohort, in women than in men.
- Healthy left atrial tissue coverage is significantly higher in the PAF group compared to the PeAF group.
- Atrial fibrosis coverage increases with time spent in both types of AF, with a higher percentage coverage in the PeAF however percentage coverage did not affect levels of compliance.

Over recent years, there has been increased interest in compliance, with many believing that a better understanding in the changes in compliance brought about by atrial fibrillation, the role compliance itself plays in the progression of atrial fibrillation, as well as to understand how

compliance is affected by catheter ablation may lead to higher success rates of ablation procedures [106] [174] [175] [176].

Even though the interest in compliance has grown, as yet there is still no standardised way of measuring compliance. Several attempts to measure compliance have been made. Each of these measures have had their limitation, usually owing to the highly selective cohort of patients enrolled in these trials [176] [108] [238]. Atrial fibrillation is a multifactorial disease associated with degenerative processes, with that in mind unlike other studies that have excluded Haemodynamic [108] [197] and metabolic [239] factors, in this study they have been included.

Both invasive and non-invasive attempts have been described to measure compliance however, further reading of the majority of the non-invasive methods for measuring compliance detail that only part of the method was non-invasive, some invasive measures were also being used [108] [177], therefore these measures are not entirely non-invasive. In this study, the method for measuring compliance, were similar to the method used in the Park et al. study [108] , involving the use of a catheter, in this case Thermocool SmartTouch catheter (Biosense Webster Inc., Diamond Bar, CA, USA) to collect both the force and displacement data (described on page 80 Establishing and calculating a suitable measure of compliance) that was inserted into the left atrium immediately after transseptal puncture, which in itself is invasive. Therefore, rather than being deemed as non-invasive, as it was in the Park et al. [108] , in this study it was deemed as invasive. However, all data collected and used to develop this measure was routinely collected as part of the ablation procedure, therefore no additional invasive procedures took place.

For all of the following results, only data where the p-value was found to be <0.05 was deemed statistically significant, any results that have p-values >0.05 but may show some trends have been described.

Developing the measure of compliance

Area selection

Before collecting any data, the areas this data was to be collected from must first be established. Eleven areas of interest were selected: Left Pulmonary Vein (LPV), Right Pulmonary Vein (RPV), Left Atrial Appendage (LAA), Coronary Sinus / Inferior Wall (Endo Cs/IW), Anterior Wall (AW), Septum, Posterior Wall (PW), Roof, Mitral Valve Isthmus (MVI), Left Lateral Wall (LLW), Right Lateral Wall (RLW). The LPV and RPV were included as isolation of the pulmonary veins (PVs) is the cornerstone of most atrial fibrillation (AF) procedures, as they are believed to play a crucial role in AF initiation and maintenance ([240]. [241]. The left atrial (LA) was then divided by a clock-face (Figure 81), as used for assigning ablation locations in wide areas circumferential ablation lines (WACA) [242]. The WACA technique, using radiofrequency ablation to perform circular lesions encompassing the ipsilateral PV away from the ostia, is used frequently, and has been shown to be more effective than ostial PVI [243] [244]. However, after point-by-point ablation, zones of residual connections can persist along the ablation lines, which can be difficult to identify precisely [245]. If compliance is affected by ablation, or compliance itself affects the ablation. Understanding if or how compliance differs within these areas could be key, hence why they were included.

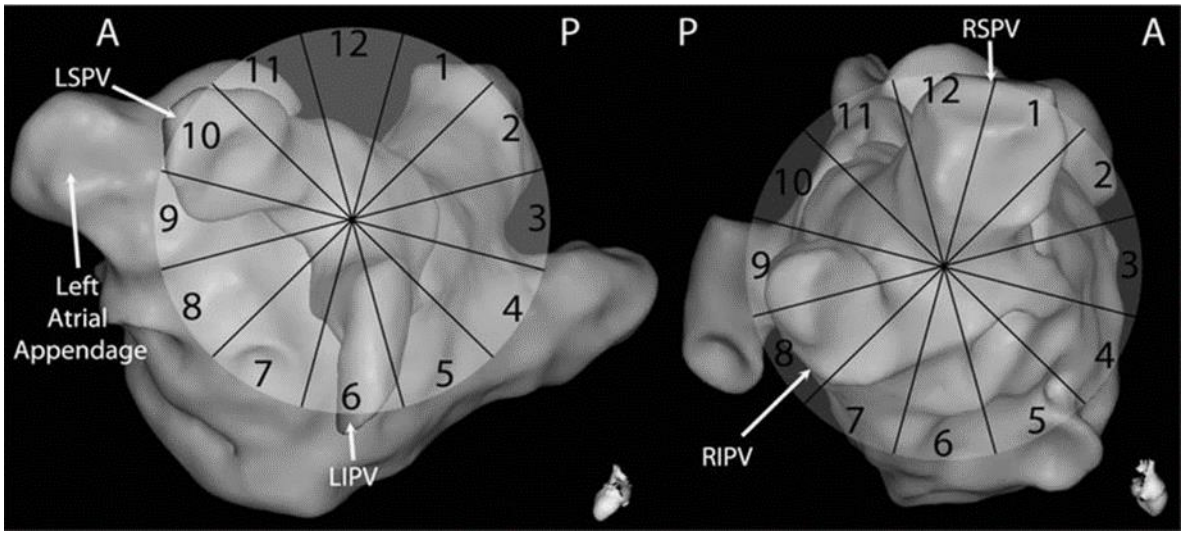

Figure 81: Clock face scheme used for assigning ablation location in wide area circumferential ablation lines. Left-hand side: Left pulmonary veins; Right-hand side: Right pulmonary veins. A = anterior; P = posterior; LIPV = left inferior pulmonary vein; LSPV = left superior pulmonary vein; RIPV = right inferior pulmonary vein; RSPV = right superior pulmonary vein.

Recently attention has been drawn to the function of the left atrial appendage (LAA) and the insight it may give into the mechanisms of atrial fibrillation and thromboembolism [246] [103]. Reduced left atrial appendage function has been found to be a cause of stroke in patients with sinus rhythm, therefore reduced left atrial appendage function may identify patients with unexplained stroke [246].Peak left atrial appendage velocity has also been found to be related to parameters of left ventricular and left atrial function [107], therefore understanding compliance in this area again could be key to better understanding left atrial compliance and factor into ablation success, which is why this area was also included.

Although data was collected from both the coronary sinus and the Inferior wall, owing to the close proximity of these areas (Figures 81 and 82) making it difficult to be certain a point was taken from a specific area, for all data analysis these two areas were combined (Endo Cs/Iw).

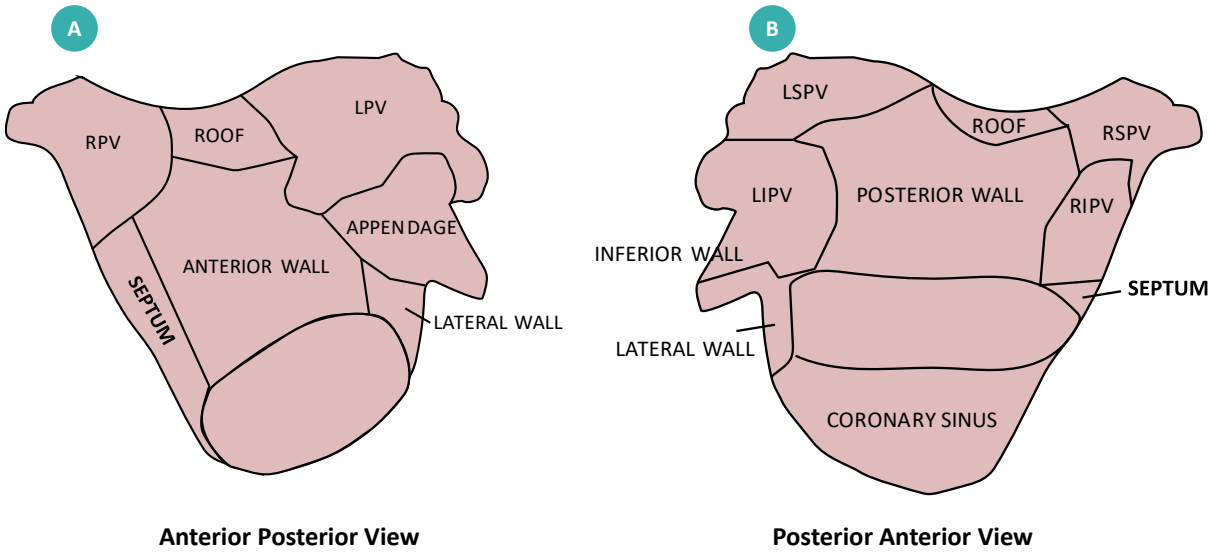

Figure 82: Left atrium divided into sections of interest

Contact Force and catheter Displacement Data Collection

Choice of Catheter

Contact force and catheter displacement data was collected using Thermocool SmartTouch catheter (Biosense Webster Inc., Diamond Bar, CA, USA). There are multiple ablation catheters available for use. Other catheters available include the EnSite NavX (Abbott, Abbott Park, IL, USA) catheter and

the TactiCath® from Endosense (Geneva, Switzerland), which was the first catheter-based technology to obtain a CE mark back in 2009.

This catheter utilises three optical fibres between the second and third electrode of the catheter and an elastic polymer catheter tip [247]. The elastic polymer tip undergoes microdeformations in response to changes of wavelength of reflected infrared light transmitted by optical fibres. From the wavelength of reflected light at the three fibres, the orientation and the magnitude of contact force is derived. Therefore, information regarding the catheter tip contact force and orientation of this is derived [247].

In comparison, the Thermocool SmartTouch catheter (Biosense Webster Inc., Diamond Bar, CA, USA) is the most recently CE marked of the contact force sensing technologies. The catheter tip electrode of the Thermocool SmartTouch catheter (Biosense Webster Inc., Diamond Bar, CA, USA) is mounted on a precision spring permitting a small amount of electrode deflection (Figure 16). Measuring this deflection using location sensor coils at the proximal end of the spring, the system is able to precisely calculate the force being exerted as well as the orientation of the catheter, using the known characteristics of the spring.

The Thermocool SmartTouch catheter (Biosense Webster Inc., Diamond Bar, CA, USA) catheter integrates with the Carto3 platform. During an ablation procedure, the magnitude of contact force and its vector are displayed in real-time on the Carto3 display screen as well as the contact force waveform.

The TactiCath® from Endosense (Geneva, Switzerland) and Thermocool SmartTouch catheter (Biosense Webster Inc., Diamond Bar, CA, USA) catheters are arguably the two most widely used catheters, a recent comparison between the between the measurements made by the two catheters demonstrated the measurements by the catheters were both highly sensitive and accurate (mean error ≤1g), and that there was little to distinguish between the two [211].

The reason the Thermocool SmartTouch catheter (Biosense Webster Inc., Diamond Bar, CA, USA) was selected for this study over other ablation catheters was not because it was considered to be

more accurate than the others, but rather largely down to operator choice, due to it integrating well with the CARTO® (Biosense Webster Inc., Irvine, CA, USA) electoanatomical mapping system, the mapping system of choice at St Bartholemews Hospital as well as being considered less stiff than both the EnSite NavX (Abbott, Abbott Park, IL, USA) catheter and the TactiCath® from Endosense (Geneva, Switzerland).

Catheter orientation

The data collected for the compliance measure was taken with the catheter in the perpendicular orientation. In terms of efficacy of Radiofrequency Catheter Ablation (RFCA) several studies have suggested that catheter to tissue orientation could play a significant role in lesion dimension [248] [236], with one study suggesting that a more perpendicular catheter contact orientation was associated with a lesser contact force, than a more parallel orientation [249]. As the measure of compliance developed was catheter displacement over contact force (mm/g), this may suggest that by orientating the catheter perpendicularly you could end up with a lesser over all compliance value than if it was orientated parallelly.

However, these were only the findings in one study, the lack of robust data and the heterogeneity of the existing studies [248] [250] have not yet entirely clarified the effects of catheter orientation on lesion size. For that reason. As orientation was beyond the scope of this project the orientation of the catheter was kept consistent, perpendicular for acquiring all data points. Future work could involve collecting the same data with the catheter in the parallel orientation and comparing, in order to better understand the effects of catheter orientation on compliance.

Catheter Contact

Preclinical studies, have found that the degree of contact between the ablation catheter and myocardium as well as the consistency of the contact influences the size of the subsequent lesion produced by a radiofrequency energy application [251] [252]. The importance of catheter contact force (CF) to clinical ablation has been investigated in studies looking at the reconnection of

segments in the wide area circumferential ablation (WACA) line during atrial fibrillation (AF) ablationWhat is the effect on the surrounding tissue [253] [254]. In clinical ablation, it is challenging to assess individual ablations due to a lack of access to histological lesion parameters [251]. All studies highlighted the complexities of catheter contact within the LA. Further highlighting the importance of establishing, target contact parameters to clinical ablation success. Although catheter contact could have an effect on contact force, which in turn could impact this measure of compliance the need to understand compliance of the left atria and develop a method for measuring it out ways the risk of poor contact. In order to minimise the risk of poor contact however, contact force readings >1g (the reported sensitivity by the manufacturer of the Thermocool SmartTouch catheter (Biosense Webster Inc., Diamond Bar, CA, USA) catheter) and above 40g the limit set by the operator were excluded from all data analysis.

Remote Robotic Navigation System

In 60% of the ablation procedures, a remote robotic navigation system, a type of steerable sheath technology was utilised (Table25). The advantage of this type of steerable sheath technology is believed to be its improved access and contact to ablation target sites, improving the efficacy of lesion delivery during radiofrequency catheter ablation.

		ALL (36)	PAF (16)	PeAF (20)
Hansen (Robot), n (%)				
Yes		22 (61)	6 (38)	16 (80)
No		14 (39)	10 (62)	4 (20)

Table 25: Percentage of procedures using steerable sheath technology.

The technology of choice for these procedures was the Sensei® Robotic Catheter System from Hansen Medical Inc. (Mountain View, California, USA). Obtaining its CE mark in 2007., the system incorporates an inner and outer sheath, each containing pull wires enabling deflection of the

sheaths, the Thermocool SmartTouch catheter (Biosense Webster Inc., Diamond Bar, CA, USA) is passed through the inner sheath. The advantage of this system is that the controls are placed outside of the radiation field (remote from the patient, Figure 83), and is used with the operator seated. The movements of the catheter are controlled using a 3D joystick (Figure 83).

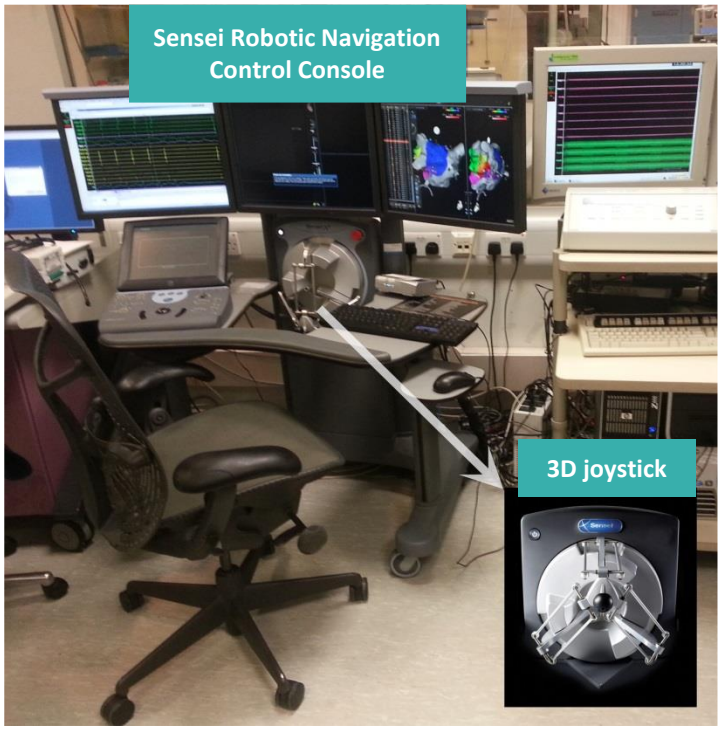

Figure 83: The Sensei Robotic Navigation System Control Console at St Bartholomew's Hospital. The console is placed outside of the radiation field and is therefore used without radiation protection equipment (and with the operator seated). The 3D joystick which is used to control the deflection of the steerable robotic trans-septal sheath is highlighted.

This system was selected as it was available for use at St. Bartholomew's Hospital and at the discretion of the operator. Although this was the system used, there is another type of steerable sheath technology currently available, a manual steerable sheath Agilis™ NxT (Abbott, USA) (Figure 84).

Figure 84: Agilis™ NxT (Abbott, USA) manual Steerable Trans-septal Sheath

The use of steerable sheath technologies may affect the quality of contact with the myocardium compared with manual non-steerable sheaths due to their increased stiffness ad potentially greater consistency of contact. One recent study that examined the impact of steerable sheath technology on contact force (CF), and its consistency, around the wide area circumferential ablation (WACA) lines, found that steerable sheaths are associated with an increase in CF during ablation. However, despite steerable sheath technologies increasing CFs in the WACA, the increase was not uniform, with some areas of the left atrium showing no increase in CF with steerable sheaths; additionally, these sheaths are also associated with a lower consistency of achieved CF in some areas of the left atrium [242]. Increasing CF could affect the compliance measure, the only way to determine the extent of this would be to compare compliance measures in patients where the steerable sheath technology (Sensei® Robotic Catheter System from Hansen Medical Inc. (Mountain View, California, USA) has been used against those where it has not. More interestingly, this same study found that the increase in contact force was not uniform across different areas across the left atrium, suggesting that there may be something else within these areas attributing to the different measures of contact force. Understanding, the compliance of tissue within these areas may help to better understand what this is. Highlighting the need to find a suitable compliance measure.

Cardiorespiratory motion

Catheter-tissue contact on a beating heart is subject to force variability, in terms of ablation making it difficult to optimally deliver consistently durable and transmural lesions [255]. With regards to this measure of compliance (displacement (mm) / force (g)) potentially resulting in poor contact force data points, owing to poor catheter-tissue contact. Adjustments made to compensate for this motion are made by either by the operator, limited by human factors, such as perception and reaction time as well as system adjustments and delays

A previous study [256] developed and evaluate a catheter contact-force controller with the ability to monitor catheter tissue-contact force in real-time whilst simultaneously adjusting the position of the ablation catheter within a sheath to compensate for variations in contact force that occur due to cardiorespiratory motion. With preliminary lab-bench tests demonstrating that using a catheter contact-force controller resulted in significant improvement in the stability and control of catheter-tissue contact force on moving tissue-mimicking material. Whilst this study demonstrated that a catheter contact-force controller could reduce the effects of motion on contact force during ablations in vivo and in vitro. It also found that typically for most target locations in the porcine heart used to test the catheter tissue contact-force controller, disturbances were dominated by systolic-diastolic cardiac motion, while disturbances caused by respiration were in comparison smaller. Whereas in most clinical settings, the opposite relationship is observed, in that contact-force profiles are dominated by respiration; contact-force disturbances caused by cardiac motion are often negligible in most targets. Leading the author to conclude that different tissue types within the left atrium may be affected differently by cardiorespiratory motion [255], which may suggest that another variable such as compliance of the tissue may contribute to these differences in findings. Again leading to question the potential impact of compliance on catheter-tissue contact, with that in mind Chapter 3: Mechanical Tissue Testing of the Porcine Left Atria of this thesis, stripping back the methods already validated by Gelman et al [256], aimed to develop a lab-bench method to recreate compliance measures displacement (mm) / force (N) for preliminary testing tissue compliance in porcine tissue removing force variability brought about by cardiorespiratory motion. Little is known about the individual tissue characteristics of different areas within the left atrium and their effect on compliance, as well as the effect of compliance on them [256]

Once a suitable method was developed, and a compliance measure calculated future work would involve testing this method on whole hearts rather than atrial segments and later recreating cardiorespiratory motion.

Once a suitable measure for compliance was determined, the next section of this study was to preliminary test this measure in a small cohort of patients to firstly validate this measure, by comparing it within different variabilities such as: type of AF, AF with and without comorbidities, time in AF, gender, ventricular function, left atrial size, age, and different areas within the left atrium. All though to affect compliance [176]. As well as to look for trends, that may determine factors that could reduce compliance (Figure 85).

	ALL	PAF	PeAF	p-vale (group)
PAF (%)	25		45	0.55 (PAF) 0.13 (PeAF)
Comorbidities total (%)	64	31	90	0.13 (PAF) 0.12 (PeAF) 0.09 (AF only) 0.14 (comorbidities)
Time in AF (years)	5 ± 2.60	6 ± 2.45	3 ± 2.11	0.08,(PAF) 0.78 (PeAF) 0.36 (≤2) 0.29 (3-4) 0.67 (>4)
Male (%)	75	69	80	0.53 (PAF) 0.22 (PeAF) 0.35 (Male) 0.33 (Female)
LV Ejection Fraction (%)	47.9 ± 17.3	60.8 ± 8.6	42 ± 12.5	0.23 (PeAF) 0.16 (LVEF ≥50)
LA area (cm^2)	28.9 ± 5.9	25.4 ± 5.1	32.3 ± 4.0	0.16 (PAF) 0.62 (PeAF) 0.46 (≤30) 0.45 (>30)
Age (years)	62.8 ± 7.7	73.8 ± 48.2	62.4 ± 9.8	0.79 (PAF) 0.16 (PeAF) 0.22 (<60) 0.48 (>60 ≤70) 0.18 (>70)

Figure 85: Clinical characteristics of patients including p-values for both between group and intergroup analysis, described further in sections below. PAF = Paroxysmal atrial fibrillation, PeAF = Persistent atrial fibrillation.

Differences in Compliance Measure between Types of AF

Atrial fibrillation (AF) type is determined by duration and treatment response, these are thought to be linked to stiffening of the atria [176] [238], therefore, could affect compliance.

There are slight variations in the duration of AF that determines the type, for the purpose of this thesis the type of AF was defined as:

- **Paroxysmal AF (PAF)** - the occurrence of two or more episodes of AF within the space of a year, which terminates spontaneously within a week.
- **Persistent AF (PeAF)** – continues AF lasting for more than seven days

These definitions were selected as they are in keeping with the majority of the literature [257].

Atrial fibrillation is known to induce fibrosis of the atria [258] [259]. With patients with PeAF found to show greater structural remodeling and endocardial fibroelastosis of the atria and appendage than PAF [259] [260]. Each of these factors could potentially affect compliance, however, most research looking into compliance of the left atrium in patients with atrial fibrillation tend to focus on PeAF patients [176] [108] [13]. This may be due to the majority of projects opting for an opportunistic approach to recruiting patients based on who presented for radiofrequency catheter ablation (RFCA) procedures within a given timeframe. Although catheter ablation for atrial fibrillation has been established as an effective, durable and safe way to manage arrhythmias, which has resulted in a huge increase in ablations being performed per year, one large study by Raymond-Paquin et al, [261] found the number of ablations performed on PAF patients has been found to be far fewer than on PeAF patients.

With that in mind in this study both PAF and PeAF patients were included, which to the best of the authors knowledge is the first to report an association between AF type and compliance.

At St. Bartholomew's hospital around 400 ablation procedures are performed per year to treat atrial fibrillation, with that in mine this project aimed to recruit a similar number of PAF and PeAF patients presenting for first time ablation procedures. In total, 16 PAF patients were recruited and 20 PeAF patients were recruited, the characteristics of these patients can be found in Table 3 and Figure 85 including the p-values for all studies. Throughout the results included in this thesis the PAF and PeAF patient groups have remained separated for analysis, so that for every factor though to impact compliance, the difference between AF type can be compared.

As PeAF was found to show greater structural remodeling and endocardial fibroelastosis of the atria and appendage than PAF [259] [260], it was hypothesized that in the PeAF cohort the AF would be less compliant than PAF patients, owing to great fibroelastosis caused by cardiomyocytes undergoing structural changes and show signs of degradation and apoptosis in order to maintain homeostasis [188], causing the tissue to become more scarred and stiffer, therefore less compliant.

The data indicates that there may be a slight trend to tentatively suggest that compliance maybe lower in PeAF patients than PAF patients, however, the data is also very variable, with between group analysis showing statistically little difference in the compliance measure (mm/g) between the two groups (p-value =0.55).

Previously, it has been though that low LA compliance could be a predictor of clinical recurrence after catheter ablation for AF in structurally and functionally normal hearts, independent of age and gender [108]. These result, not only suggest that this method for measuring compliance could be a suitable way to measure compliance, based on the similarity in trend shown to that hypothesized, albeit a tentative link based on variable data. It also provides better confidence there could potentially be a link between AF type and compliance. Understanding this difference in LA compliance between AF types, could provide further insight into predicting clinical recurrence of AF after catheter ablation.

Difference in Measure of Compliance between AF with and without comorbidities

A number of high recruiting studies have found that comorbidities have impacted success. One such study, that estimated the risk of in-hospital complications after left atrial appendage closure (LAAC) in relationship with comorbidity burden [262] found that patients with increased numbers of comorbidities (≥10) were at increased risk of complications following LAAC.

Although not directly related to AF, having looked at the effects of comorbidities on complications in LAAC, this is import to patients with AF in that, LAAC is a non-pharmacological approach for stroke prevention in AF patients. The left atrial appendage closure (LAAC) procedure, is also similar in

approach to the catheter ablation procedure it involves guiding catheters through blood vessels to the left atrial appendage, as with ablation. Identifying those comorbidities could cause complications to this procedure is clinically important because it may help identify patients at higher risk of complication.

Another study looking at the effects of both haemodynamic and metabolic comorbidities, such as obesity, anemia, diabetes mellitus, renal dysfunction as well as age in relation ventricular and vascular structure and function in patients with heart failure [263]. Finding that comorbidities were associated with unique clinical, structural and functional profiles. In diabetic patients, for example, they found that they had higher ventricular filling pressures and stiffer vasculature, even though they tended to be younger than the non-diabetic cohort.

Other studies have also linked diabetes mellitus to left ventricular hypertrophy (LVH), systolic and diastolic left ventricular (LV) dysfunction, endothelial dysfunction, and increased vascular stiffness [264] [265]. Others, have found associations between intrinsic renal disease and increased levels of apoptosis, fibrosis, hypertrophy, and LV dysfunction [266] [267]. Although, these findings were not observed within the left atrium, they are important as they suggest the potential for comorbidities to account for alterations in LA structure and function, which could in turn impact compliance.

With that in mind, it is surprising that most research into left atrial compliance are highly selective in their recruitment of patients, specifically excluding patients with hemodynamic factors such as: valvular disease, structural disease, and left ventricular systolic and diastolic dysfunction, and metabolic factors such as hypertension and diabetes [197] [176] [108].

In this study comorbidity conditions were identified each patients' medical notes, the list of individual comorbidities can be found in Table 3, with the grouped, comorbidity profile shown in Figure 85. The comorbidities selected were based of those identified as potential risk factors in previous studies, as well as the Charlston Comorbidity index (CCI) [268], the Elixhauser Comorbidity Score (ECS) [269] and the CHA_2DS_2-VASc score.

Each cohort was separated by type and compared to patients where no comorbidities were detailed within their medical notes. Of the 16 patients in the PAF cohort, five had recorded comorbidities listed in their medical notes; within the PeAF group, of the 20 patients, 17 of them had listed comorbidities.

Based on the works detailed above, it was hypothesized that compliance measured in the AF cohort with comorbidities would be lower than that without. Also, based on the results in the previous section looking at AF type. The second hypothesis, was that the lowest measure of compliance would be seen in the PeAF group with comorbidities, owing to both it being the more sever type of AF and the presence of comorbidities.

However, unlike those studies the results from this study however, suggest that there is no difference either within groups (PAF: p-value =0.13; PeAF: p-value-0.12), or between groups, when comparing the PAF cohort with comorbidities to the PeAF group with comorbidities (p-value=0.14). This difference in results however, may not be due to this method for measuring compliance being unsuitable but may instead be due to the AF groups without comorbidities not truly being without comorbidities. This would mar up, with recent studies suggesting the AF is never truly without comorbidities, but rather these comorbidities even with the scientific and technical advances in diagnosing these comorbidities, have not yet been identified [270]

Differences in Compliance Measure with time spend in AF

Time spent in AF was defined as the time since AF symptoms such as palpitations or chest discomfort started, as recorded in the patients' clinical notes.

The time spent in atrial fibrillation is clinically important because it has long been thought to determine the success of catheter ablation [271] [272] [273]. In animal experimental models it was found that during the first few days of induced AF, that electrical remodeling occurred, in that the atrial effective refractory period was considerably shortened [195] [274] [275] [276]. The contractility ability of the atria during the same time period, under the same conditions has also

been seen to be markedly reduced [277]. This same study by Schotten et al. [29] reported that if the time spend in AF was less than three days, both electrical and structural remodeling brough about by AF was seen to be reversible. However, other studies have found that after prolonged periods of time in AF, it takes a lot longer for electrical remodeling to be reversed [278] [279] [280], and even longer still for structural remodeling [274] [281] [282]. If at all.

Calcium has been identified as one of the common messengers in the signaling pathways involved in the complex regulation of electrical and structural remodeling of the atria. A number of studies have found that the calcium antagonist verapamil was able to inhibit the progression of both electrical [259] [182], and structural [281] [32] remodeling. In a study by Lee et al, however, after longer time spend in AF, the ability of verapamil in preventing progression of remodeling was no longer seen [283]. At the onset of AF, the high rate of atrial activation causes an excessive influx of calcium [173].As a result, calcium overload occurs and atrial contractile function becomes depressed. This reduced contractile function results in increased passive stretch, which in turn has been found to promote AF [284] [285].

What is interesting about this, is that patients with paroxysmal AF have been found to spend more time in AF than persistent AF [286] [287]. Therefore, one would expect to see lower compliance measures recorded within the Paroxysmal atrial fibrillation (PAF) cohort, due to the reduced contractile function recorded. This finding however, suggests that reduced compliance is not caused by severity of AF, as suggested by Park et al [238], but in fact is as a result of time spent in AF.

This makes assessing levels of compliance an interesting topic. Taking into account the above findings in relation to both AF type and time spent in AF, for this project the hypothesis was that increased time spent in AF would cause a decrease in compliance, additionally in line with the hypothesis stated in the previous findings: *Differences in Compliance Measure between Types of AF*, although the results only tentatively linked a decrease in compliance with more severe AF type. The overall hypothesis was, increased time spent in more severe AF type would result in a decrease in compliance.

In this project we compared patients with PAF or PeAF, grouping them into three groups of time spent in AF: ≤2, 3-4, and >4 years. The first observation was that of the 36 patients recruited, those in PAF had spent almost twice as long in AF as those in PeAF (Figure 85). Which is in line with the findings made by Ganesan et al [286] and Boriani et al [287]. In group analysis of time spent in AF suggests that there might be a steady decline with years spent in AF. However, when removing the values where R^2 is <0.7 (as highlighted by the colour grading system in the results), there is no clear trend. Between group analysis, comparing the two groups in the same time period also showed no clear trends (Figure 85).

These findings, although they only show a slight trend in decline of compliance between the two types of AF are important as they give confidence in the method derived for measuring compliance being a suitable method for measuring compliance and achieving expected trends in terms of age, albeit provisional. Making it worth exploring further.

Compliance Measure differences between Gender

Atrial fibrillation (AF) is the most commonly sustained arrhythmia in men and women worldwide, with the Framingham Heart Study [288] reporting the incidence to be as high as 1.1% women compared to 1.3% men in the UK. In a review by Ko et al, evaluating literature published by each county on differences in prevalence between males and females, it was found that this lower incidence in females was the same everywhere that reported incidence data except for Iran [289]. The prevalence findings from this study have been depicted in Figure 86.

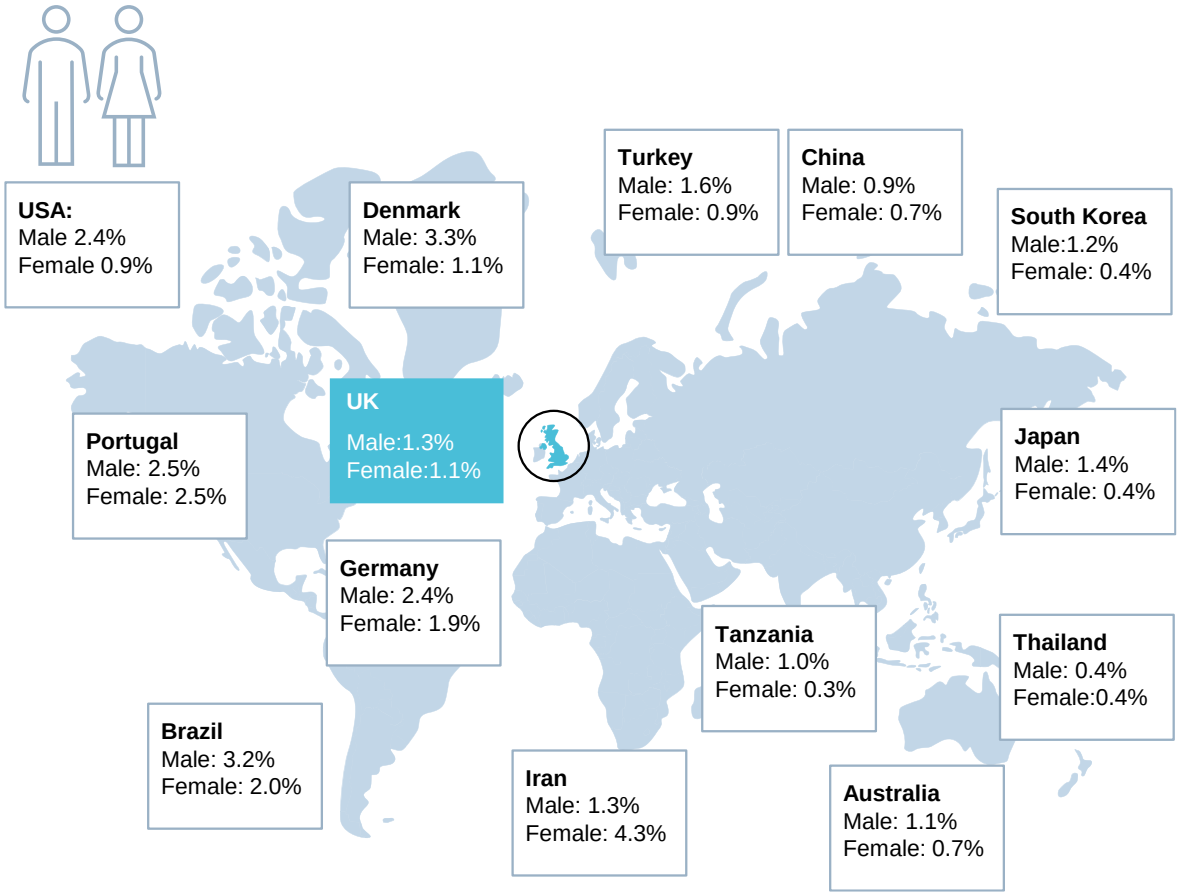

Figure86: Differences in prevalence of atrial fibrillation between men and women, based on data published by Ko et al. [289].

Although the prevalence of AF has been increasing steadily over the years, research into differences between women and men in relation to AF has not received as much attention as other diseases. With most research into epidemiological and pathophysiological changes in AF focusing on men [289]. The few studies that have focused on changes in females associated with AF have focused on difference in incidence and prevalence [290] [291] [292] [293], risk factors [294] [295], genetics [296] [297], prognosis [295] [298] and presentation [298] [295]. A summary of the findings from each of these studies in relation to women in presented in Figure 87.

High risk factors
- Older at diagnosis
- Higher prevalence of hypertension
- Higher prevalence of valvular heart disease
- Lower prevalence of coronary artery disease

Genetics
- No consistently reported differences

Prognosis
- Increased risk of stroke
- Increased risk of myocardial infarction
- *Increased mortality*

Incidence and prevalence
- Lower incidence
- Lower prevalence

Pathophysiology
- Minimally studied
- High left atrial dimension and atrial fibrosis
- More nonpulmonary foci
- Differences in membrane potential and action potential duration
- Oestrogen-associated electrical differences

Presentation
- More commonly symptomatic
- Atypical symptoms
- Higher heart rate

Figure 87: Overview of the differences in incidence and prevalence [290] [291] [292] [293], risk factors [294] [295], genetics [296] [297], prognosis [295] [298] and presentation [298] [295].of atrial fibrillation in women compared to men. The italicized differences under the pathophysiology header have been italicized as there is some differing results between the limited number of studies that reported on pathophysiological change.

Until now, only a small number of studies have investigated the underlying pathophysiological differences in AF between gender. A summary of these finding has been presented in Figure 87 Figure 88.

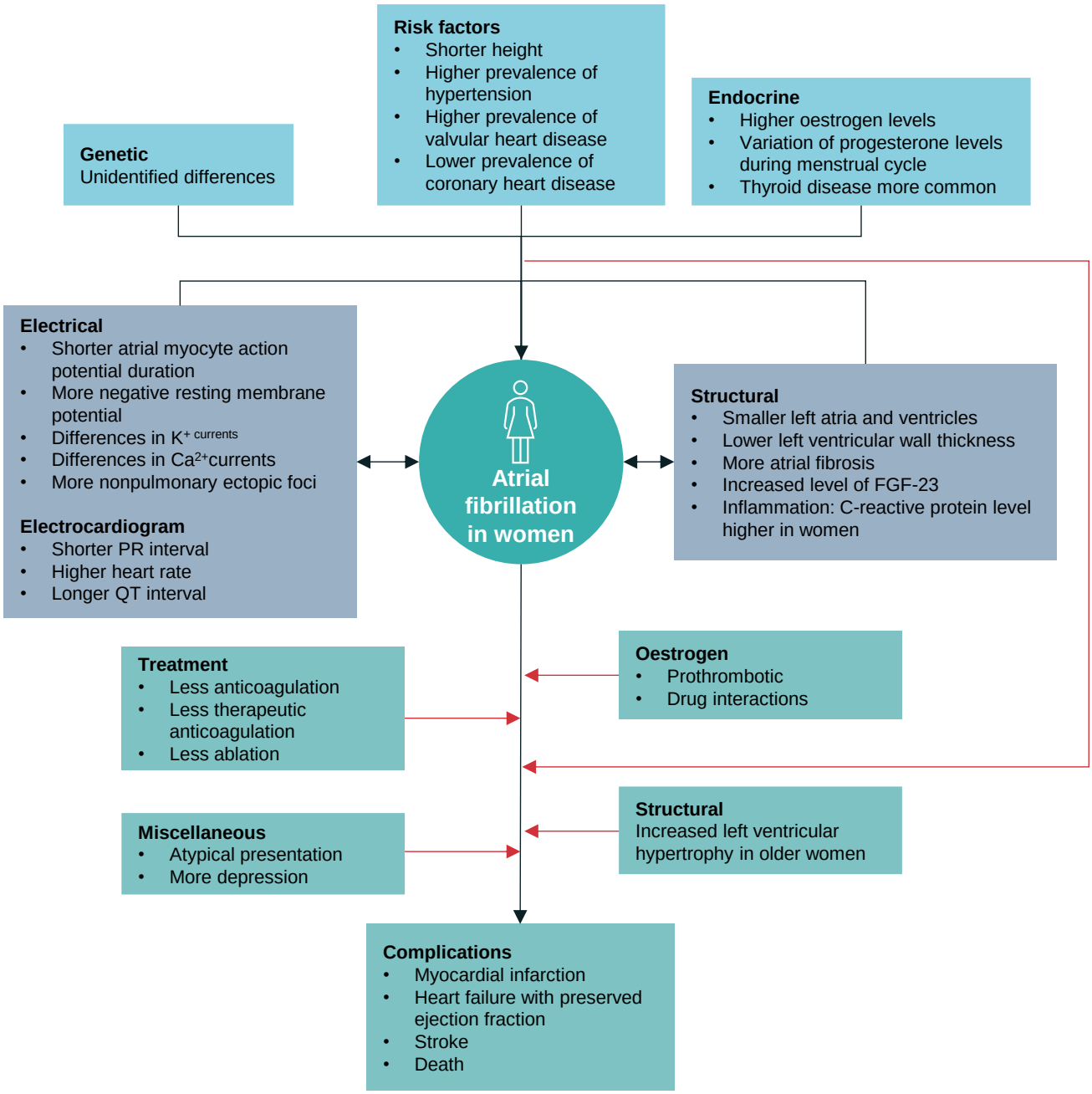

Figure 88: Summary of potential differences in pathophysiological mechanisms of atrial fibrillation between gender.

As described previously, structural and electrical remodeling is thought to be associated with increased risk of AF. Structural remodeling in particularly, may also lead to reduced atrial compliance. Larger left atria as a result of structural remodeling as well as increased ventricular wall thickness have been associated with increased risk of AF [299]. However, in general, women have, reduced ventricular wall thickness and smaller left atria and ventricles then men [300] [301]. Another difference that could lead to structural variations between male and female atria is the

levels of the plasma concentration of the inflammatory marker C-reactive protein [302] and fibroblast growth factor-23 [303], these, are known contributors in the development of fibrosis. Higher concentrations of both have been found in females [279] [302] [303], which may be associated with the increased risk of fibrosis in females [302] [303].

With levels of fibrosis though to differ between males and females, and increased fibrosis though to cause increased stiffness of the left atria [238] [108]. This study, thought to be the first if it's kind, aimed to compare differences in compliance measure between males and females. Owing to limited work carried out previously in gender differences associated with AF, this study was based of the hypothesis, measurements of compliance taken within the left atria will be lower in females than in males. Of the 36 patients to take part in this preliminary study to determine a suitable way of measuring compliance, however, 27 of them were male, and only 9 were female. From the previous work detailed above, this would be as expected, owing to a lower prevalence in females [289] (Figure 86).

As with all studies within this manuscript, the groups were divided by AF type, and then further divided by gender. There were 17 males recruited to the PAF cohort, compared to 4 females; in the PeAF group 10 males were compared with 5 females.

Although from the graph in Figure 36 there looks to be a slight trend in compliance levels being lower in females than in males in both the PAF and PeAF groups, a Dunn's test of nonparametric pairwise analysis following a Kruskal–Wallis one-way analysis of variance found the results to be statistically insignificant, with evidence to suggest there was no difference in compliance between males and females within the PAF cohort (p-value = 0.53), or PeAF group (p-value = 0.22). Within the male cohort, there was also no difference seen when comparing males in PAF with males in PeAF (p-value=0.35), the same was seen in the female cohort (p-value=0.33).

The initial trend, even though not statically significant follows the expected trend of the literature, which may suggest that the method for measuring compliance is still worth exploring.

Compliance measure change due to Ventricular Function

In recent years, a lot of evidence has been presented suggesting that AF could trigger or exacerbate left ventricular (LV) dysfunction [305] [306] [307] [308] [309]. LV dysfunction is usually measured by left ventricular ejection fraction (LVEF) percentage [305] [306]. According to the American heart Foundation, a normal ejection fraction is between 50% to 75% [310]. However, in an observation study of 282 patients with AF undergoing corrective ablation procedures, in 105 of them an LVEF of ≤40% was recorded [311].

Patients with reduced diastolic function as a result of left ventricular impairment, depend on filling by atrial contraction, requiring a longer diastolic period to fill the LV at normal atrial pressures [100], as described in the introduction of this Thesis: Structural remodeling. Following the onset of AF, left atrial pressures increase in order in order to maintain cardiac output, as a result of the loss of atrial contribution to filling due to rapid rate and fibrillating motion, as well as shortened diastolic filling times [100].

Follow-up studies of patients with abnormal LV diastolic function, have recorded diagnosis of new-onset AF in 10% of patients within 4 years [312]. Demonstrating that as well as LV dysfunction being a consequence of AF, LV dysfunction also attributes to AF. Once study by Tsang et al. [312] even reporting that the risk of AF is proportional to the severity of LV diastolic dysfunction, clinically this is important as it may provide a way of identifying AF at an earlier stage.

If a consequence of LV dysfunction is loss of contraction [100] as highlighted in the introduction of this thesis, and LV dysfunction could potentially be a novel way of identifying AF. Then being able to measure this loss of contraction, as a measure of compliance could be clinically important in the early diagnosis resulting in earlier treatment, potentially leading to better outcomes of patients with AF. Which is why in this thesis LV functional differences between different types of AF at different measures of LVEF were compared. This is, to the best of the authors knowledge the first time such

comparisons have been made. Building on the literature surrounding LV function, the hypothesis for this section was that lower ventricular function would reduce compliance.

For the purpose of this comparison, LV function was characterized as left ventricular ejection fraction, one of the most commonly reported measures of left ventricular (LV) systolic function [313] and in line with the previous studies detailed above. The two AF types (PAF and PeAF) were then subdivided into three groups of LVEF measure: ≤30 % (defined as severely impaired [310]), >30 <50% (as anything below 50% has been deemed as abnormal by the American Heart Association [310], this group was included to see if any comparisons could be made between less severe and the more severe LV functional groups in terms of compliance), ≥50% (as this is defined as the lower limit of normal LVEF function [310]).

All patients underwent transthoracic echocardiography, from this a measure of LVEF was obtained. There is currently no universally accepted gold standard from measuring LVEF, with several invasive and non-invasive methods available [313]. Each of the different methods for measuring LVEF are subject to factors that may introduce error and/or variability into the calculated ejection fraction [313]. However, comparing different modalities of measuring LVEF was beyond the scope of this project. The choice of method was based solely of local resources.

The first thing to note from the results of this comparison, is that within the PAF cohort, there was no measure of LVEF less than 50%, this is interesting as it could potentially support the work by Tsang et al. [312] in that the risk of AF may be proportional to the severity of LV diastolic dysfunction and furthermore, that a reduction in LV function may identify severity of AF. Another interesting observation, was that out of the 9 females included in this preliminary study, none of them had an LVEF% <50, which could be clinically relevant in that in previous studies described above it was found that in general, women have, reduced ventricular wall thickness and smaller left atria and ventricles then men [300] [301]. However, this preliminary study although limited in sample size due to the fact it was to develop and validate a method for measuring compliance rather than test it. May suggest that although the ventricles are generally small and the walls less thick, the LV function

is still better than in males, therefore the ventricles may be more compliant. Which may provide a better understanding of why the prevalence of AF in women was lower than me. Again, emphasizing the clinical need to develop a suitable measure for compliance.

Having only LVEF >50% in all PAF patients, although interesting, made it difficult to compare compliance within the AF types. With the only comparison able to be made between PAF and PeAF cohorts with an LVEF >%50, although not statistically significant based of off a Kruskal-Wallis non-parametric test, followed by a Dunn nonparametric pairwise test (p-value= 0.16) a slight trend in reduction of compliance based on severity of AF at the same LVEF% was observed which may suggest that LV function may be proportional to AF severity. Within the PeAF cohort, a slight trend in the reduction of compliance with reduction in LVEF % was also seen, although again not statistically significant (p-value = 0.23).

Although this may demonstrate that this method for measuring compliance is a viable method, in that some expected trends based on previous works have been observed. The variability of the compliance values, both within different AF types and different levels of LV function recorded would need to display greater differences in compliance measures to have confidence that they are real.

Change in compliance dependent on Left Atrial size

Left atrial size is an important risk factor in the development, as described in the introduction of this Thesis: Structural remodeling, with the AFFIRM trial, suggesting that it is also a risk factor in the recurrence of atrial fibrillation [314]. Conversely atrial enlargement can occur as a consequence of AF [107]. The pathophysiological mechanism associated with LA size being a factor in the development of AF is that with chronic haemodynamic burden comes left atrial enlargement, which in turn leads to atrial fibrillation [271]. A recent study found that patients with PeAF had more enlarged left atria (LA) size, using spontaneous echo contract (SEC) than those in PAF (27.5±15.9 vs. 20.1±10.3, p=0.033) [315]. Which interestingly contradicts work carried out previously by Stefanadis et al. that found the LA size to be more enlarged in PAF patients [107]. It has also long been thought,

that left atrial enlargement is also believed to be a factor in predicting the risk of stroke. With Caplan et al. [316] first identifying that increased LA size correlated with increased risk of stroke back in 1989. With Moulton et al. [317] a few years later demonstrating that LA enlargement could in fact be considered independent factor for stoke in AF patients.

Although the pathophysiological mechanisms for atrial size variation are not completely understood, it is believed that even though haemodynamic burden results in atrial enlargement [107], more recent studies by Kim et al. [315] suggest that this may not be associated with atrial fibrosis. Making understanding variations in compliance in relation to LA size all the more interesting. With that in mind, for this study, it was hypothesised that: as atrial size increases, so too does compliance.

There are a number of different ways of measuring LA size, which usually involve some method of imaging. Studies have previously used magnetic resonance imaging to measure the LA [107], which is considered the most accurate non-invasive technique for measuring LA size, however, due to its relatively long times required to acquire an image, as well as the cumbersome data analysis required to calculate LA size, this method of measuring LA size is not usually performed on a daily basis in clinical practise [318]. The most widely used method for measuring LA size is via echocardiography imaging [319]. There are a number of echocardiographic techniques currently available for measuring LA size [319], including transthoracic, transoesophageal and intracardiac echocardiography, with Transoesophageal and intracardiac echocardiography mainly used during interventions for AF, as it provides good views of both the LA as well as the LAA, both believed to be involved with the initiation and recurrence of AF [98]. One limitation of this method however, is that visualisation of the LA may be hindered by the close proximity of the transoesophageal probe to the LA and obstructed by the variable position of the oesophagus to the posterior wall of the LA [319].

The size of the left atrium for this project was taken from the patient's clinical notes. It was measured using transesophageal echocardiography, despite of its limitations, as this is still considered the most widely used method of imaging during AF interventions. A summary of findings between the sizes of LA between AF-type can be found in Figure 85.

Left atrial size for the purpose of this study was referenced as a measure of left atrial length (cm^2), using reference values from Otto et al, textbook of clinical echocardiography [320] (Figure 89).

LA size values	
Normal (cm2)	≤20
Mild (cm2)	20 - 30
Moderate (cm2)	30 - 40
Severe (cm2)	>40

Figure 89: Reference values for Left atrial (LA) size based on LA length, as referenced in The Sixth Edition Textbook of Clinical Echocardiography [320]

Initially the groups were separated as referenced above however, within the limited patient cohort of this preliminary study, no patients were seen to have a normal LA size (≤ 20 cm^2), and only one male patient within the PeAF cohort recorded severe LA enlargement (>40cm^2). For that reason, in order to be able to compared compliance readings obtained by this method for measuring compliance, the groups were adapted to compare mildly enlarged atria (defined as ≤30 cm^2) and moderately/severely enlarged atria combined (>30cm^2). Although not in line with the referenced ranges, the aim of this section was to validate the method used to measure compliance, by comparing results obtained for difference LA sized groups. Therefore, being separated into distinct referenced size was not as important, but should be made clear when evaluating any results that these results are only for the purpose of testing the method used for measuring compliance and providing an understanding of compliance in relation to LA size. In order to be confident of compliance measure in relation to LA size, further work in a much larger cohort of patients, grouped into the specific referenced ranged values for LA size should be carried out.

Within the LA size ≤30cm 12 had PAF, whereas 9 had PeAF. Given that the total number of PAF patients was 16 and the total number of PeAF patients was 20, this supports previous recent works in that the size of the LA was found to be smaller overall in PAF patients. Table 9, also shows a small trend in compliance in both cohorts as atrial size increases when comparing compliance points when removing R^2 values below 0.7. Although not statistically significant, (PAF p-value=0.16, PeAF: p-value

= 0.62) nor can this data be provided answers on compliance changes with LA size. It does suggest that this measure for measuring compliance do show the expected relationship between compliance and LA size based on previous literature. Therefore, may also with further work, give better confidence of link between LA size and compliance.

Change in compliance as a result of Age

Advancing age has been found to be an important factor for the risk of developing AF [321] [322]. The pathological and functional changes in the atria that enhance the risk of AF are not well understood. Although current theories suggest that left atrial triggers are crucial to the initiation of AF, with the theory that age is related to increased levels of myocardial fibrosis, resulting in atrial fibrillation documented in a number of studies [321] [322].

In general, structurally, myocardial thickness is believed to increase with age as a result of cardiomyocyte size [321]. In the arterial wall, an area where more extensive work into age-related differences has been carried out, collagen content and collagen cross-linking, which provides the strength of the arteries have been to increase, resulting in the arteries becoming stiffer. And the elastin fibrils, which provide elasticity have been seen to fray in the medial layer of the artery. Resulting in remodeling of the arteries [323]. With stiffness being the inverse of compliance, if may be inferred that increased stiffness may result in decreased compliance.

Already in this thesis the critical role of myocardial fibrosis in atrial remodeling has been discussed, however, it is not known to what extent the prevalence of age impacts left atrial compliance. Having previously discussed the importance of compliance in maintaining homeostatic within the heart, being able to measure compliance affectively could be important to better understand how it is affected in relation to age.

Based on the theory that age is related to myocardial fibrosis [321] [322] as well as the theory that fibrosis increases stiffness (as detailed previously) [323]. The hypothesis for this section was that an increase in age causes a decrease in compliance.

Patient age was taken from the clinical notes. As well as being divided into groups based on AF type, patients were subdivided into age groups: ≤60 years (PAF n = 4; PeAF n = 10), >60 ≤70 years (PAF n= 6; PeAF n=8), > 70 years (PAF n= 5; PeAF n=3). Generally following the trend observed previously, whereby patients with PeAF tend to present for ablactation procedures at an earlier age than those in PAF [288].

When observing the graph (Figure 23) and Table 8, no relationship was seen between age and compliance. This was statistically supported by no p-value =<0.05, either within groups or between groups.

This does not necessarily suggest that this method of measuring compliance is inadequate, instead it may suggest that age is not as relevant in relation to compliance as time in AF is. In order to understand which, it is, further studies would need to take place on a larger cohort.

Compliance measures in different areas of the Left Atrium

Abnormalities in the left atrial (LA) structure and function may develop in patients with paroxysmal atrial fibrillation (AF), however, to the best of the authors knowledge so far all research into mechanical and structural abnormalities have been looked at in terms of the whole atria [324] [325] [176] [238]. This thesis has demonstrated findings that AF is a progressive condition that begins with hemodynamic and/or structural changes in the left atrium (LA) and evolves through the paroxysmal and persistent stage, yet structural changes vary between individuals' multiple variants. Better understanding of the LA structure and function has been made over the years; however, this understanding is based on the LA structure as a whole. Within the LA and surrounding, the tissue structure may vary as demonstrated previously at the beginning of this chapter

With that in mind a better understanding of differences in structure and compliance could be instrumental in better understanding the progression of AF. With that in mind, for this section not only was compliance measured and compared between different areas of the LA, building on the work carried out by Gelmann et al. [255] but a method for mechanical testing porcine left atrial

tissue was in the lab was developed. With the aim to better understand the functional and mechanical properties of different areas of interest within the left atrium as described in the beginning of this chapter.

Building on conclusions from work carried out by Diez et al. [323], reviewed during the section on age-related differences in compliance, found within arterial walls. Whereby collagen content and collagen cross-linking and elastin fibrils seen to change in relation to age. And due to the lack of seminar information related to LA structure, it was hypothesized for this section that, which provides the strength of the arteries have been to increase, resulting in the arteries becoming stiffer. And the elastin fibrils, which provide elasticity have been seen to fray in the medial layer of the artery. Resulting in remodeling of the arteries higher levels of compliance would be seen in thinner, more elastic walled areas such as the LPV and RPV compared to thicker, more muscular walls of the atria such as the Anterior, posterior and lateral as well as the roof.

Although Figure 39 and Table 10 show that there may be some true to this hypothesis, during statistical analysis of the results no statistically significant (p-value <0.05) differences were achieved. With some expected trends being seen, these results suggest that this method for measuring compliance may be suitable. However, further work would need to be carried out both on a larger number of patients, as well as building on the lab based mechanical tissue method developed

The discussion for the novel development of a method for testing mechanical tissue function of the atria in porcine tissue based on the works by Diaz et al [323]. Is as follows

To the best of the authors knowledge all methods for testing and validating the measure of compliance as well as designing and evaluating a method for testing left atrial tissue mechanics are unique.

Porcine left atrial samples were dissected and tested within 24 hours of slaughter due to preliminary evidence that refrigerating or freezing the tissue samples once dissected into their individual areas had a detrimental impact on the mechanical properties of the tissue.

The results of this project have revealed some interesting findings, with regards to mechanical properties within different areas of the left atrium, notably the variation in thickness within different areas of the LA. Contrary to popular belief, in this study the left atrium was not found to have a uniform thickness of between 2-3 mm. Instead, there was found to be large variations; regionally the veins were thinner than the walls, with the RPV being the thinnest area and almost half the thickness of the thickest area, the roof.

Mechanical properties of the regions were first investigated with uniaxial loading. Whilst some studies have documented variations in tissue thickness in the past there is still no determined ideal density and duration of ablation energy to be applied to achieve safe and optimal ablation lesions [222].

Similar trends indicate consistent packing of tissue and correlation between sample and material properties and also highlight that the difference in properties between regions are not solely a result of variable tissue thickness. Accounting for thickness differences, mechanical differences were still seen.

Failure extension displayed statistically significant variations most notably between the anterior wall and other areas of the LA. As the difference was only found in failure extension and not in failure strain, it can be summarised that the mechanical properties of atrial tissue as a biological material extends to a similar degree in all areas relative to the regions size prior to failure. Failure force displayed much less variation than failure extension with only one statistically significant variation between areas; the LPV and RPV ostia and no significant difference between regions. This is interesting as it suggests that different areas of left atria wall tissue have similar mechanical properties.

This relates importantly to the process of atrial ablation therapy; the advent of contact force sensing catheters enables careful monitoring of the forces being applied to the atrial wall. Knowledge that the various regions display similar stretch properties, if applicable to human hearts, would confirm that the force applied can be similar for each region enabling confident usage of these catheters.

Additionally, the knowledge of the varied thickness of each region could be combined with substantial data to allow modelling of patient's atria prior to the ablation process. This modelling could be used to allow varied usage of energy to electrically isolate tissue from different atrial regions, thus improving efficacy of full thickness ablation. This could be used to reduce the error generated from tissue oedema clouding the ability to judge if tissue has been isolated without local inflammation contributing towards the observed electrical isolation, a commonly hypothesized cause of ablation failure [223].

Cardiovascular tissue is viscoelastic, exhibiting behaviours that combine features of elastic solids and viscous fluids. Viscoelastic materials dissipate energy upon deformation, which can be observed through hysteresis or time-dependent tests. The structural basis of myocardial viscoelasticity can be attributed to a combination of cardiac cells and extracellular matrix proteins, but the nature and extent of each components contribution to viscoelasticity are still debated. Clinically this could play a vital role in the success rate of AF ablation procedures in terminating AF. This project aimed to investigate the viscoelastic properties of left atrial cardiac tissue in conjunction with quasi-static behaviour under physiologically relevant biaxial loading conditions.

The reported test areas do not directly match those shown in the uniaxial tests for direct comparison. However, variations between regions under biaxial loading was less pronounced and no significant differences were evident. This could be due to samples not being loaded to failure, or due to the difference in boundary conditions which restricted fiber reorientation. This provides more confidence in uniformity of tissue properties. However, it was notable that the toe region and quasi-static properties varied across axes 1 and 2 indicating anisotropy in the tissue.

The viscoelastic properties of left atrial tissue showed that the roof relaxed the most overall, and particularly rapidly to begin with. The roof was also the thickest area and required the highest force to displace the tissue by 6mm, particularly in axis 1, indicated highly aligned fibers in this direction. A visual of its response to out-of-plane triaxial loading suggests it deformed both globally and locally.

The pulmonary vein ostia and the septum on the other hand were distinctly different, both displayed more elastic than viscoelastic behaviour and were a lot thinner, requiring less force to displace the tissue samples by 6mm in the third axis. Both were equally as stiff in both axes and relaxed at a consistent rate, suggesting reasonable isotropic behaviour in these regions.

In contrast, both the sinus and the lateral wall were stiffer in axis 2, but relaxed at a similar rate. This would suggest that unlike the roof where the fiber alignment visible on the surface of the tissue denoted the stiffer direction, the predominant fiber direction was deeper in the tissue. Despite these anisotropic behaviours, the regions showed similar viscoelastic properties, showing little correlation between quasi-static and viscoelastic behaviour throughout the atria.

The most interesting find was that despite the veins being notably thinner than the walls, they showed similar quasi-static and viscoelastic properties (max stiffness, relaxation) to the septum, suggesting no clear correlations between atrial tissue mechanical properties and wall thickness. Whilst some studies have documented variations in tissue thickness in the past there is still no determined ideal density and duration of ablation energy to be applied to achieve safe and optimal ablation lesions [222]. The current evidence of variability in the porcine atria suggests a similar study should be carried out in human hearts to see whether they correlate.

Under biaxial loading conditions, the PVO was the least stiff of all tissue samples tested overall in both axis, which corresponds with it also being the thinnest sample tested. This finding is as expected due to the veins elastin rich interstitial matrix [224]. Again, it must be noted that this preliminary work has been carried out in porcine hearts, to ensure the same mechanical properties apply these same tests would now have to be repeated using human heart tissue.

Overall, this data has displayed that the viscoelastic and quasi-static properties of the LA wall is comparable across all regions.

However, despite relative consistency in tissue response to biaxial loading, of possible concern for ablation procedures, triaxial testing indicates considerable variation in tissue response to out-of-plane loading. Forces required to apply equivalent out-of-plane displacement to different regions of

the atria varied significantly and imaging of local tissue deformation suggest that in some regions the catheter deforms all surrounding tissue, whilst in other regions the local compressive properties of the tissue are lower and it deforms directly under the catheter. This is of concern, as it implies that the same ablation force used throughout the atria will have very different outcomes in different regions. This variability may explain some of the variability in ablation procedure success, and further studies to quantify regionally appropriate contact forces may be warranted.

Factors affecting levels of atrial fibrosis

Throughout this discussion, it has been demonstrated that atrial fibrosis may result in low LA compliance and poor clinical outcomes of AF catheter ablation in patients without hemodynamic burden or LA enlargement, which is consistent with the findings from the DECAAF (Delayed Enhancement– MRI determinant of successful Catheter Ablation of Atrial Fibrillation) study [329]. Which showed poor clinical outcomes of AF ablation in the group with extensive atrial scarring. Earlier on in this chapter, the method used for measuring fibrosis was detailed. Endocardial voltage was used as a measure of fibrosis, Low endocardial voltage has been known to be an indicator of changes in the cardiac matrix or myocardial scars [330] [73].

In this section, the impact of fibrosis, through voltage on compliance was explored. Factors believed to effect fibrosis as identified (AF type, comorbidities, time, gender, LV function, LA size, age and area) above were looked at too seen what effect fibrosis had on these and whether any trends could be identified between the compliance data and fibrosis data that may suggest a link between fibrosis and compliance. Followed by directly comparing compliance to fibrosis. With the hypothesis the lower the mean fibrosis value (mV), the lower the measure of compliance (mm/g).

When directly comparing compliance to fibrosis, now links could be drawn and now statistically significant values were seen (Figure 47, Table 14).

Atrial fibrosis was measured in terms of percentage coverage across the left atrium for all comparison data (AF type, comorbidities, time, gender, LV function, LA size, age and area). CF-force

sensing catheters were used to collect electrical activity measures across all regions of the left atrium, and data manually copied from the Carto electrical-anatomical mapping software (Biosense Webster, Inc) by screenshotting images of the electrical activity measures shown on screen and inputting into Excel. The measure of electrical activity was divided into three categories, normal tissue coverage: the percentage of tissue measuring greater than 0.5mV; mild atrial fibrosis tissue coverage: the percentage of tissue in the left atrium measuring less than 0.5mV but greater than 0.1mV; and severe atrial fibrosis coverage, measuring less than 0.1mV. Only when determining the effect of atrial fibrosis on ablation success was the total amount of atrial fibrosis used as a measure (mild and severe atrial fibrosis combined).

Fibrotic tissue is well known to be stiffer than healthy tissue [73], such that increased fibrosis would be expected to be correlated with reduced compliance. Figure 61 highlights the surprising lack of such correlation. However, figures 56 to 60, which identify how fibrosis is influenced by time in AF and severity of condition, show the anticipated advancement of damage and accumulation of fibrosis, which was expected when looking at compliance data.

These findings directly support previous studies, showing more atrial fibrosis was detected in patients with persistent AF compared to paroxysmal AF [73]. Furthermore, when the type of AF (PAF and PeAF) was further divided into lone (primary) AF and AF secondary to other clinically related conditions such as high blood pressure, diabetes etc, the worsening of fibrosis in patients with other conditions became very apparent. A comparison between time in AF and amount of fibrotic tissue also showed a clear positive correlation. Taken together, data all point to a direct fibrotic tissue response to the presence of fibrillation, such that time in AF and its level of persistence all augment the damage. This is in line with predictions from previous studies [330] [73] .

It has previously been hypothesised that greater amounts of atrial fibrosis increase the number of ablation procedures required to terminate AF, a theory arising from evidence that in order to effectively isolate atrial areas capable of initiating electrical signals that result in AF, effective ablation lesions needed to be made around these sites [73] . Following on from that, in this study

the aim was to investigate the hypothesis that increased atrial fibrosis coverage of the left atrium increases the likelihood of suboptimal catheter tip-to-tissue contact force during lesion delivery, and therefore reducing the clinical efficacy of first-time ablation procedures.

A comparison between atrial fibrosis and number of ablation procedures required to terminate AF, showed that patients with more scar before their procedure seemed to be more likely to require more ablation procedures This certainly supports the hypothesis, but sample numbers are too small to be conclusive and in order to be sure larger multicentre trials would need to be carried out. The percentage coverage of scar was also compared in different areas of the left atrium; however, this did not yield any significant regional differences. This uniformity of damage over time across all regions of the atria, which may indicate that it is the direct mechanical perturbations resulting from fibrillation that led to damage. This uniformity of scar tissue developing in the atria has implications for voltage conduction, and may mean that conduction pathways remain minimally disrupted despite the large levels of fibrotic tissue.

Chapter 4:
Limitations

Despite some promising results from the hypothesis and the dataset presented, to suggest that the method could be a suitable measure for compliance within the left atrium using only data routinely as part of ablation procedures, it is important to note that the study is limited by a number of factors.

Patient population

Although this was a preliminary study within a small sample size of patients AF affects large number of individuals. To test this measure properly would require testing in a much larger cohort. To determine the size of this cohort a power calculation would be needed. This data could be used to calculate this. This study did not excluded patients with haemodynamic and metabolic factors, as has been done in other studies related to compliance, however it was highly selective in that all Patients

Method of data collection

Data was collected using a single type of catheter. Although this catheter is one of the most widely used catheters on the market, there are other catheters are available. Results from this Thesis cannot be standardised for other catheter types and therefore further work using a variation of catheters would need to be carried out. All data points were collected with the catheter electrode in the perpendicular orientation. Electrode orientation is thought to affect lesion size, however, in this study the catheter orientation was not included in the analysis and my therefore have contributed to some of the variances observed. Further work could be carried out taking orientation of the catheter into account.

Carto was the electroanatomical mapping system of choice used in this study. Although this is one of the most widely used electroanatomic mapping systems and the one available locally, there are other electroanatomical mapping systems available. To enhance the findings of this study, now a measure of compliance has been established future work could be carried out to collect the same contact force (g) and displacement (mm) data using other systems to see if it is reliable.

In over 60% of the 36 cases included in this study, steerable sheath technology in the form of remote robotic navigation system was used, steerable sheaths are thought to also affect lesion size, with this in mind, they could also affect catheter-tissue contact force. This may also have influenced the contact force readings acquired, and therefore impacted the overall measure of compliance.

Data collected from the Coronary sinus and the Inferior wall, were grouped and analysed together. This was due to the close proximity in these areas. Having grouped and analysed both areas together could impact contact force and displacement reading within these areas, should properties vary between these areas. Therefore, in order to be confident, the measure is taken from either the coronary sinus or Inferior wall a better way to distinguish the two areas must be developed.

This method used to calculate compliance although using data collected during a planned ablation procedure an invasive parameter, and non-invasive tests should have been validated as alternatives, for wider clinical application of LA compliance.

Fibrosis was quantified based on endocardial voltage, although this is an acceptable widely used method for quantifying fibrosis, other measures should have been explored. Data was measured by point-by-point contact mapping (350-500 points), the voltage map may not represent a specially homogeneous distribution of endocardial voltage.

The second section of this thesis, a method for testing mechanical tissue properties within the left atrium in vitro was developed, while this study demonstrates some insight into the mechanical properties of different areas of the left atrium in a limited set of experiments, a number of limitations have been identified.

Most notably, this study looked at independent areas within the left atrium, small tissue segments were used. Typical contact-force profiles observed in the clinical setting are dominated by respiration; however from this model, it was not possible to witness the effects of respiration.

In relation to the samples collected, very few of roof and posterior wall tissue samples were collected. This was due to a difficulty in isolating and testing these samples. Which resulted in data from these areas having to be excluded.

The use of porcine hearts instead of human tissue. Whilst porcine hearts are often used as analogues in research, chapter one of this thesis shows that there are number of structural differences between the two. In order to validate these results further investigation would need to occur using human heart tissue.

Another limitation is the use of 10mm test sample areas. Dissecting the tissue into different areas before testing, will cause local damage. This, together with the gripping method adopted will all influence sample response. Although for this study the tissue had to be tested in this way future studies could look at testing the tissue with the atrium still intact, or better still, still within the heart structure. Such an approach would require an inflation set up to apply physiological, multiaxial loading to the tissue, and was beyond the scope of this study but would provide a better representation as to the mechanics within a healthy functioning heart system. In a further iterative improvement method to recreate pulsatile pressures could be explored.

Chapter 5:
Conclusion and Future Work

This study was designed to develop a method for measuring compliance using data routinely collected during ablation procedures. Data showed some trends between the compliance measure and expected outcomes from previous literature suggesting that this method of measuring compliance may be suitable. It highlights that compliance is a very variable measurement and this pilot study indicates it might be difficult to draw clear relationships, but with some trends or values indicating there may be a relationship, significant results might be seen with a much larger cohort. Future work should involve testing this method in a large cohort of people, using these initial findings to build into the power ratio to determine recruitment numbers.

Additional tests should be carried our using different electroanatomical mapping systems, catheters and comparing steerable sheath technology.

The second part of this project aimed to investigate regional, mechanical and viscoelastic properties of the left atrium with the intention of understanding if mechanical properties may influence first-time ablation efficacy. This study demonstrates that one potential cause for ineffective transmural electrical isolation of the atrial tissue could be due to the variation in thickness of different areas within the LA. This study produced data that suggests there is variation between different areas of the LA with statistical significance. Future work could assess whether there is any correlation between the porcine analogues within this study and human samples, to confirm these variations and assist with ensuring transmural lesions in lone ablative procedures by carefully matching force applied with area in which lesions are being generated.

There were no significant regional differences found in this study between the walls and the veins, however a number of significant observations were seen between different areas of the LA. After further work using human tissue to confirm these findings, this knowledge could be implemented into the ablative process to ensure optimal tissue-catheter contact to produce optimal lesions, leading to electrical isolation of troublesome areas within the atria.

In summary, this project investigated the left atrial regional and area thickness, as well as mechanical properties with the aim to generate research avenues to improve the efficacy of first-

time ablations. This project has been a success and has provided additional focus points for research into the improvement of ablation procedures and pathways for future research and progression of the project to obtain more accurate and reliable regional and area data.

Following on from this project an important future direction would be to assess the viscoelastic behaviour in healthy versus diseased left atrial tissue to determine the effect of viscoelastic properties. Therefore, it may be important to investigate the effect of collagen accumulation on myocardium viscoelasticity during arrhythmia progression. Differences in viscoelastic properties between atria and ventricles as well as looking at a more cellular level could be important directions for future research to understand the role of viscoelasticity in healthy and diseased myocardium function.

References

[1] A. Go and e. al, "Executive summary: heart disease and stroke statistics: 2013 update: a report from the American Heart Association," *Circulation,* vol. 127, no. 1, pp. 143-146, 2013.

[2] S. Chugh and e. al, "Worldwide epidemiology of atrial fibrillation: a Global Burden of Disease 2010 Study," *Circulation,* vol. 129, p. 837–847, 2014.

[3] D. Lloyd-Jones and e. al, "Lifetime risk for development of atrial fibrillation in adults: national implications for rhythm management and stoke prevention: the AnTicoagulation and Risk Factors in Atrial Fibrillation (ATRIA) Study," *JAMA,* vol. 285, no. 18, pp. 2370-2375, 2004.

[4] A. Go and e. al, "Prevalence of diagnosed atrial fibrillaion in adults: national implications for rhythm management and stroke prevention: the AnTicoagulation and Risk Factors in Atrial Fibrillation (Atria) Study," *JAMA,* vol. 18, pp. 2370-2375, 2001.

[5] N. Wineinger and e. al, "Identification of paroxysmal atrial fibrillation subtypes in over 13,000 individuals," *Heart Rhythm,* vol. 16, p. 26–30, 2019.

[6] C. Groh and e. al, "Patient-reported triggers of paroxysmal atrial fibrillation," *Heart Rhythm,* vol. 16, p. 996–1002, 2019.

[7] S. Blum and e. al, "Incidence and predictors of atrial fibrillation progression: a systematic review and meta-analysis," *Heart Rhythm,* vol. 16, p. 502–510, 2019.

[8] M. Middeldorp and e. al, "PREVEntion and regReSsive Effect of weight-loss and risk factor modification on Atrial Fibrillation: the REVERSE-AF study," *Europace,* vol. 20, p. 1929–1935, 2018.

[9] A. Goette and e. al, "EHRA/HRS/APHRS/SOLAECE expert consensus on atrial cardiomyopathies: definition, characterization, and clinical implication," *Europace,* vol. 18, p. 1455–1490, 2016.

[10] P. Wolf and e. al, "Atrial fibrillation: a major contributor to stroke in the elderly. The Framingham Study," *Arch Intern Med,* vol. 147, no. 9, pp. 1561-1564, 1987.

[11] R. Taylor and e. al, "Home-based versus centre-based cardiac rehabilitation," *Cochrane,* vol. 8, no. 8, 2015.

[12] NHS, "Estimating the direct costs of atrial fibrillation to the NHS in the constituent contries of the UK and at SHA level in England," NHS, London, 2009.

[13] J. Andrade and e. al, "The clinical profile and pathophysiology of atrial fibrillation: relationships among clinical features, epidemiology, and mechanisms," *Circ. Res,* vol. 114, p. 1453–1468, 2014.

[14] K. Odening and e. al, "Mechanisms of sex differences in atrial fibrillation: role of hormones and differences in electrophysiology, structure, function, and remodelling," *Europace,* vol. 21, p. 366–376, 2019.

[15] H. Ezekowitz and e. al, "Atrial fibrillation: are there gender differences?," *JGSM,* vol. 3, no. 6, pp. 44-49, 2000.

[16] C. Lip and e. al, "Atrial Fibrillation and ethnicicy," *Circulation,* vol. 100, p. 153, 1999.

[17] D. Wyse and e. al, "Lone atrial fibrillation: Does it exist?," *J. Am. Coll. Cardiol,* vol. 63, p. 1715–1723, 2014.

[18] B. Weijs and e. al, "The occurrence of cardiovascular disease during 5-year follow-up in patients with idiopathic atrial fibrillation," *Europace,* vol. 15, p. 18–23, 2013.

[19] R. De With and e. al, "Atrial fibrillation progression and outcome in patients with young-onset atrial fibrillation," *Europace,* vol. 20, p. 1750–1757, 2018.

[20] J. Steinberg, "Atrial fibrillation: an emerging epidemic?," *Heart,* vol. 90, p. 239–240, 2004.

[21] S. Stewart and e. al, "Cost of an emerging epidemic: an economic analysis of atrial fibrillation in the UK," *Heart,* vol. 90, pp. 286-292, 2004.

[22] S. Nattel and e. al, "Controversies about atrial fibrillation mechanisms: aiming for order in chaos and whether it matters," *Circ Res,* vol. 120, p. 1396–1398, 2017.

[23] E. Diker and e. al, "Dispersion of repolarization in paroxysmal atrial fibrillation," *Int. J. Cardiol,* vol. 63, p. 281–286, 1998.

[24] J. Eckstein and e. al, "Time course and mechanisms of endo-epicardial electrical dissociation during atrial fibrillation in the goat," *Cardiovasc. Res,* vol. 89, p. 816–824, 2011.

[25] A. Gharaviri and e. al, "Epicardial fibrosis explains increased endo–epicardial dissociation and epicardial breakthroughs in human atrial fibrillation," *Front. Physiol,* vol. 11, 2020.

[26] S. Nattel, "New ideas about atrial fibrillation 50 years on," *Nature,* vol. 415, no. 6868, pp. 219-226, 2002.

[27] J. Jalife and e. al, "Mother rotos and fibrillatory conduction: a mechanism of atrial fibrillation," *Cardiovascular research,* vol. 54, no. 2, pp. 204-216, 2002.

[28] D. Dobrev and e. al, "The ryanodine receptor channel as a molecular motif in atrial fibrillation: pathophysiology and therapeutic implications," *Cardiovascular research,* vol. 89, no. 4, pp. 734-743, 2011.

[29] U. Schotten and e. al, "Pathophsiological mechanisms of atrail fibrillation: a translational appraisal," *Physiological reviews,* vol. 911, pp. 265-270, 2011.

[30] T. Heart, "Atrial fibrillation: Current understandngs and research imperatives," *Journal of American college of cardiology,* vol. 22, no. 7, pp. 1830-1834, 1993.

[31] J. Cox, "The surgical treatment of atrial fibrillation IV Surgical Technique," *The Journal of thoracic and cardiovascular surgery,* vol. 101, no. 4, pp. 584-592, 1991.

[32] C. Morillo and e. al, "Chronic rapid atrial pacing structural, functional, and electrophysiological characteristics of a new model of sustained atrial fibrillation," *Circulaion,* vol. 91, no. 5, pp. 1588-1595, 1995.

[33] G. van Loon and e. al, "Pacing induced sustained atrial fibrillation in a pony," *Canadian Journal of Veterinary Research,* vol. 64, no. 4, p. 254, 2000.

[34] M. Haissaguerre and e. al, "Radiofrequency catheter ablation in unusual mechanisms of atrial fibrillation," *Journal of cardiovascular electrophysiology,* vol. 5, no. 9, pp. 743-751, 1994.

[35] P. Jai and e. al, "A focal source of atrial fibrillation treated by discrete radiofrequency ablation," *Circulation,* vol. 95, no. 3, pp. 572-576, 1997.

[36] M. Haissaguerre and e. al, "Spontaneous intiation of atrial fibrillation by ectopic beats originating in the pulmonary veins," *New England Journal of Medicine,* vol. 339, no. 10, pp. 659-666, 1998.

[37] D. Scherf, "Studies on auricular tachycardia caused by aconitine admistration," *Experimental Biology and Medicine,* vol. 64, no. 2, pp. 223-229, 1947.

[38] M. Haissaguerre and e. al, "Right and left atrial radiofrequency catheter therapy of paroxysmal atrial fibrillation," *Journal of cardiovascular electrophysiology,* vol. 7, no. 12, pp. 1132-1144, 1996.

[39] S. Ho and e. al, "Architecture of the pulmonary veins: relevance to radiofrequency ablation," *Heart,* vol. 86, no. 3, pp. 265-270, 2001.

[40] C. Pappone and e. al, "Atrial fibrillation ablation: state of the art," *The American journal of cardiology,* vol. 96, no. 12, pp. 59-64, 2005.

[41] F. Morady, "Cardiac arrhythmias: mechanisms and catheter ablation therapy of atrial fibrillation," *Texas heart institute Journal,* vol. 32, no. 2, p. 199, 2005.

[42] H. Nathan and e. al, "The junction between the left atrium and the pulmonary veins an anatomic study of human hearts," *Circulation,* vol. 34, no. 3, pp. 412-422, 1966.

[43] R. Wakili and e. al, "Recent advances in the molecular pathophysiology of atrial fibrillation," *The journal of clinical investigation,* vol. 121, no. 8, p. 2955, 2011.

[44] S. Ho and e. al, "Anatomy of the left atrium: implications for radiofrequency ablation of atrial fibrillation," *Journal of cardiovascular electrophysiology,* vol. 10, no. 11, pp. 1525-1544, 1999.

[45] C. Weiss and e. al, "Impact of the distribution and structure of myocardium in the pulmonary veins for radiofrequency ablation of atrial fibrillation," *Pacing and clinical elcetrophysiology,* vol. 25, no. 9, pp. 1352-1356, 2002.

[46] A. Gittenberger-de Groot and e. al, "The role of neural crest and epicardium-derived cells in conduction system formation," *Novatis Found Symp,* 2003:2003b.

[47] M. Jongloed and e. al, "Embryonic conduction tissue," *Journal of cardiovascular electrophysiology,* vol. 15, no. 3, pp. 349-355, 2004.

[48] A. Perez-Lugones and e. al, "Evidence of specialized conduction cells in human pulmonary veins of patients with atrial fibrillation," *Journal of cardiovascular elecrophysiology,* vol. 14, no. 8, pp. 803-809, 2003.

[49] J. Ehrlich and e. al., "Cellular electrophysiology of canine pulmonary vein cardiomyocytes: action potential and ionic current properties," *The journal of physiology,* vol. 551, no. 3, pp. 801-813, 2003.

[50] Y. Chen and e. al, "Heterogenous expression of potassium currents and pacemaker currents potentially regulates arrhythmogenesis of pulmonary vein cardiomyocytes," *Journal of cardiovascular electrophysiology,* vol. 9, pp. 1039-1045, 2009.

[51] S. Verheule and e. al, "Tissue structure and connexin expression of canine pulmonary veins.," *Cardiovascular research,* vol. 4, no. 55, pp. 727-738, 2002.

[52] Honjo and a. e. H, "pacing-induced spontaneous activity in myocardial sleeves of pulmonary veins after treatment with ryanodine," *Circulation.,* vol. 104, no. 14, pp. 1937-1943, 2003.

[53] V. Patel and e. al, "Melanocyte-like cells in the heart and pulmonary veins contribute to atrial arrhythmia triggers," *The FASEB Journal,* vol. 24, no. 1, pp. 180-184, 2010.

[54] W. Wongcharoen and e. al, "Effects of a Na+/Ca2+ exchanger inhibitor on pulmonary vein electrical activity and ouabain-induced arrhythmogenicity," *Cardiovascular research,* vol. 70, no. 3, pp. 497-508, 2006.

[55] R. Mandapati and e. al, "Stable microreentrant sources as a mechanism of atrial fibrillation in the isolated sheep heart.," *Circulation,* vol. 101, no. 2, pp. 194-199, 2000.

[56] M. Hocini and e. al, "Electrical conduction in canine pulmonary veins electrophysiological and anatomic correlation," *Circulation,* vol. 105, no. 20, pp. 2442-2448, 2002.

[57] R. Arora and e. al, "Arrhythmogenic substrate of the pulmonary veins assessed by high-resolution optical mapping.," *Circulation,* vol. 107, no. 13, pp. 1816-1821, 2003.

[58] J. Kalifa and e. al, "Intra-atrial pressure increases rate and organization of waves emanating from the superior pulmonary veins during atrialfibrillation," *Circulation,* vol. 108, no. 6, pp. 668-671, 2003.

[59] K. Kumagai and e. al, "Electrophysiologic properties of pulmonary veins assessed using a multielectrode basket catheter.," *Journal of the American college of Cardiology,* vol. 43, no. 12, pp. 2281-2289, 2004.

[60] J. Armour, "Intrinsic cardiac neurons involved in cardiac regulation possess alpha 1-, alpha 2-, beta 1- and beta 2-adrenoceptors.," *The canadian journal of cardiology,* vol. 13, no. 3, pp. 277-284, 1997.

[61] D. Pauza and e. al, "Morphology distribution, and variability of the epicardiac neural ganglionated subplexuses in the human heart," *The anatomical record,* vol. 259, no. 4, pp. 353-382, 2000.

[62] H. Hoff and e. al, "The maintenance of experimental atrial fibrillation by cholinergic factors," *Cardiovascular research centre bulletin,* vol. 49, pp. 117-129, 1964.

[63] S. Po and e. al, "Experimental model for paroxysmal atrial fibrillation arising at the pulmonary vein-atrial junctions," *Heart rhythm,* vol. 3, no. 2, pp. 201-208, 2006.

[64] B. Scherlag and e. al, "Autonomically induced conversion of pulmonary vein focal firing into atrial fibrillation," *Journal of the American College of Cardiology,* vol. 45, no. 11, pp. 1875-1886, 2005.

[65] E. Patterson and e. al, "Spontaneous Pulmonary Vein Firing in Man: Relationship to Tachycardia-Pause Early Afterdepolarizations and Triggered Arrhythmia in Canine Pulmonary Veins In Vitro," *Journal of cardiovascular electrophysiology,* vol. 18, no. 10, pp. 1067-1075, 2007.

[66] E. Patterson and e. al, "Triggered firing in pulmonary veins initiated by in vitro autonomic nerve stimulation," *Heart rhythm,* vol. 2, no. 6, pp. 624-631, 2005.

[67] E. Patterson and e. al, "Sodium-calcium exchange initiated by the Ca2+ transient: an arrhythmia trigger within pulmonary veins," *Journal of the American College of Cardiology.,* vol. 47, no. 6, pp. 1196-1206, 2006.

[68] A. Burashnikov and e. al, "Reinduction of atrial fibrillation immediately after termination of the arrhythmia is mediated by late phase 3 early afterdepolarization-induced triggered activity," *Circulation,* vol. 107, no. 18, pp. 2355-2360, 2003.

[69] M. Platt and e. al, "Limiting the number and extent of radiofrequency applications to terminate atrial fibrillation and subsequently prevent its inducibility," *Heart Rhythm,* vol. 1, p. s11, 2004.

[70] E. Pokushalov and e. al, "Left atrial ablation at the anatomic areas of ganglionated plexi for paroxysmal atrial fibrillation," *Pacing and clinical electrophysiology,* vol. 33, no. 10, pp. 1231-1238, 2010.

[71] J. Heijman and e. al, "Cellular and molecular electrophysiology of atrial fibrillation initiation, maintenance, and progression," *Circ. Res,* vol. 114, p. 1483–1499, 2014.

[72] C. Schmidt and e. al, "Inverse remodelling of K2P3.1 K+ channel expression and action potential duration in left ventricular dysfunction and atrial fibrillation: implications for patient-specific antiarrhythmic drug therapy," *Eur. Heart J,* vol. 38, p. 1764–1774, 2017.

[73] M. Allessie and e. al, "Electrical, contractile and structural remodeling during atrial fibrillation," *Cardiovasc. Res,* vol. 54, p. 230–246, 2002.

[74] A. Goette and e. al, "Electrical remodeling in atrial fibrillation. Time course and mechanisms," *Circulation,* vol. 94, pp. 2968-2974, 1996.

[75] N. Voigt and e. al, "Cellular and molecular mechanisms of atrial arrhythmogenesis in patients with paroxysmal atrial fibrillation," *Circulation,* vol. 129, pp. 145-156, 2014.

[76] C. Molina and e. al, "Profibrotic, electrical, and calcium-handling remodeling of the atria in heart failure patients with and without atrial fibrillation," *Front. Physiol,* vol. 9, p. 1383, 2018.

[77] W. Hobbs and e. al, "Reversal of atrial electrical remodeling after cardioversion of persistent atrial fibrillation in humans," *Circulation,* vol. 101, p. 1145–1151, 2000.

[78] A. De Jong and e. al, "Mechanisms of atrial structural changes caused by stretch occurring before and during early atrial fibrillation," *Cardiovasc. Res,* vol. 89, p. 754–765, 2011.

[79] K. Ohtani and e. al, "High prevalence of atrial fibrosis in patients with dilated cardiomyopathy," *J Am Coll Cardiol,* vol. 25, p. 1162–1169, 1995.

[80] G. Bailey and e. al, "Relation of left atrial pathology to atrial fibrillation in mitral valvular disease," *Ann Intern Med,* vol. 69, p. 13–20, 1968.

[81] J. Ausma and e. al, "Time course of atrial fibrillation-induced cellular structural remodeling in atria of the goat," *J Mol Cell Cardiol,* vol. 33, pp. 2083-2094, 2001.

[82] A. Frustaci and e. al, "Histological substrate of atrial biopsies in patients with lone atrial fibrillation," *Circulation,* vol. 96, pp. 1180-1184, 1997.

[83] K. Thiedemann and e. al, "Left atrial ultrastructure in mitral valvular disease," *Am J Pathol,* vol. 89, pp. 575-604, 1977.

[84] W. Anne and e. al, "Matrix metalloproteinases and atrial remodeling in patients with mitral valve disease and atrial fibrillation," *Cardiovasc Res,* vol. 67, pp. 655-666, 2005.

[85] W. Han and e. al., "Nitric oxide overproduction derived from inducible nitric oxide synthase increases cardiomyocyte apoptosis in human atrial fibrillation," *nt J Cardiol,* vol. 130, pp. 165-173, 2008.

[86] S. Eiras and e. al., "Alterations in contractile protein composition and function in human atrial dilatation and atrial fibrillation," *J Mol Cell Cardiol,* vol. 41, pp. 467-477, 2006.

[87] C. Aime-Sempe and e. al., "Myocardial cell death in fibrillating and dilated human right atria," *J Am Coll Cardiol,* vol. 34, pp. 1577-1586, 1999.

[88] C. Rucker-Martin and e. al, "Dedifferentiation of atrial myocytes during atrial fibrillation: role of fibroblast proliferation in vitro," *Cardiovasc Res,* vol. 55, pp. 38-52, 2002.

[89] V. Polyakova and e. al, "trial extracellular matrix remodelling in patients with atrial fibrillation," *J Cell Mol Med,* vol. 12, pp. 189-208, 2008.

[90] L. Ke and e. al., "Calpain mediates cardiac troponin degradation and contractile dysfunction in atrial fibrillation," *J Mol Cell Cardiol,* vol. 45, pp. 685-693, 2008.

[91] S. Nattel and e. al, "Molecular and cellular mechanisms of atrial fibrosis in atrial fibrillation," *ACC Clin. Electrophysiol,* vol. 3, p. 425–435, 2017.

[92] S. Verheule and e. al., "Loss of continuity in the thin epicardial layer because of endomysial fibrosis increases the complexity of atrial fibrillatory conduction," *Circ. Arrhythm. Electrophysiol,* vol. 6, p. 202–211, 2013.

[93] S. Ricksten and e. al, "Distensibility of the left atrial wallin spontaneously," *Clin Sci Lond Engl,* pp. 1980(59 Suppl):6:361s-3s, 1979.

[94] B. Hoit and e. al, "Regional atrial distensibility," *Am J Physiol,* vol. 262, pp. H1356-H1360, 1992.

[95] C. Davis and e. al, "Compliance of left atrium with and without left atrial," *Am J Physiol,* vol. 259, pp. H1006-H1008, 1990.

[96] B. Hoit and e. al, "Altered left atrial compliance after atrial," *Circ Res,* vol. 72, pp. 167-175, 1993.

[97] Y. Ko and e. al, "Effects of left atrial compliance on left atrial pressure in pure mitral stenosis," *Catheter Cardiovasc Interv,* vol. 52, pp. 328-333, 2001.

[98] C. Stefanadis and e. al, "Effects of balloon mitral valvulplasty on left atrial function in mitral stenosis as assessed by pressure-area relation," *J Am Coll Cardiol,* vol. 32, pp. 159-168, 1998.

[99] F. Flachskampf and e. al, "Calculation of atrioventricular compliance from the mitral flow profile: analytic and in vitro study," *J Am Coll Cardiol,* vol. 19, pp. 998-1004, 1992.

[100] Y. Güray and e. al, "Left atrial compliance and pulmonary venous flow velocities are related to functional status in patients with moderate-to-severe mitral stenosis," *Echocardiography,* vol. 26, no. 10, pp. 1173-1178, 2009.

[101] H. Masugata and e. al, "Evaluation of left atrial wall elasticity using acoustic microscopy," *Angiology,* vol. 50, pp. 583-590, 1999.

[102] C. White and e. al, "The effects of atrial fibrillation on atrial pressure-volume and flow relationships," *Circ Res,* vol. 51, pp. 205-215, 1982.

[103] C. Stefanadis and e. al, "Assesment of left atrial pressure-area relation in humans by means of retrograde left atrial catheterization and echocardiographic automatic

boundary detection: effects of dobutamine," *J Am Coll Cardiol,* vol. 31, pp. 426-436, 1998.

[104] E. Leistad and e. al, "Effects of atrial fibrillation on left and right atrial dimensions, pressures, and compliances," *Am J Physiol,* vol. 264, pp. H1093-H1097, 1993.

[105] C. White and e. al, "Effects of acute atrial fibrillation on the vasodilator reserve of the canine atrium," *Cardiovasc Res,* vol. 20, pp. 683-689, 1986.

[106] E. Leistad and e. al, "Effects of atrial fibrillation on left and right atrial dimensions, pressures, and compliances," *Am J Physiol,* vol. 264, p. 1093–1097, 1993;.

[107] C. Stefanadis and e. al, "Assessment of left atrial pressure–area relation in humans by means of retrograde left atrial catheterization and echocardiographic automatic," *JACC,* vol. 31, no. 2, pp. 426-436, 1998.

[108] J. Park and e. al, "Low Left Atrial Compliance Contributes to the Clinical Recurrance of Atrial Fibrillation after Catheter Ablation in Patients with Structurally and Functionally Normal Heart," *PLoS ONW,* vol. 10, no. 12, 2015.

[109] S. Corley and e. al, "elationships between sinus rhythm, treatment, and survival in the Atrial Fibrillation Follow-Up Investigation of Rhythm Management (AFFIRM) Study," *Circulation,* vol. 109, p. 1509–1513, 2004.

[110] H. Bhatt and e. al, "Atrial Fibrillation: Pathophysiology and Therapeutic Options," *Journal of Cardiothoracic and Vascular Anaesthesia,* vol. 29, no. 5, pp. 1333-1340, 2015.

[111] A. Camm and e. al, "A proposal for new clinical concepts in the management of atrial fibrillation," *American Heart Journal,* vol. 164, no. 3, pp. 292-302, 2012.

[112] A. Camm and e. al, "Guidelines for the management of atrial fibrillation: the Task Force for the Management of Atrial Fibrillation of the European Society of Cardiology (ESC)," *European heart journal,* vol. 31, no. 19, pp. 2369-2429, 2010.

[113] H. Calkins and e. al, "2012 HRS/EHRA/ECAS Expert consensus statement on catheter and surgical ablation of atrial fibrillation: recommendations for patient selection, procedural techniques, patient management and follow up, definitions endpoints, and research trial design," *Europace,* vol. 14, no. 4, pp. 528-606, 2012.

[114] J. Tamai and e. al, "Delayed Improvement in Exercise Capacity with Restoration of Sinoatrial node Response in Patients After Combined Treatment With Surgical Repair for Organic Heart Disease and the Maze Procedure for Atrial Fibrillation," *Circulation,* vol. 91, pp. 2392-2399, 1995.

[115] A. Ganesan and e. al, "Long-term outcomes of catheter ablation of atrial fibrillation: A systematic review and meta-analysis," *Journal of the American Heart Association,* vol. 2, p. e004549, 2013.

[116] C. McKenna and e. al, "Cost-effectiveness of radiofrequency catheter ablation for the treatment of atrial fibrillation in the United Kingdom," *Heart,* vol. 95, pp. 542-549, 2009.

[117] R. Kobza and e. al, "Late recurrent arrhythmias after ablation of atrial fibrillation: incidence, mechanisms, and treatment," *Heart Rhythm,* vol. 1, no. 6, pp. 676-683, 2004.

[118] J. Dong and e. al, "Integrated electroanatomic mapping with three dimensional computed tomographic images for real time guided ablations," *Circulation,* vol. 113, no. 2, pp. 186-194, 2006.

[119] C. Piorkowski and e. al, "First in human validation of impedance based catheter tip to tissue contact assessment in the left atrium," *Journal of Cardiovascular Electrophysiology,* vol. 20, no. 12, pp. 1366-1373, 2009.

[120] R. Hunter and e. al, "Point-by-point Radiofrequency ablation versus the Cryoballoon or a Novel Combined Approach: A randomized trial comparing 3 methods of pulmonary vein isolation for paroxysmal atrial fibrillation (the cryo versus RF trial)," *Journal of Cardiovascular Electrophysiology,* vol. 26, no. 12, pp. 1307-1314, 2015.

[121] D. Haines and e. al, "Tissue heating during radiofrequency catheter ablation: A thermodynamic model and observations in isolated perfused and superfused canine right ventricular free wall.," *Pacing Clin Electrophysiol,* vol. 12, pp. 962-976, 1989.

[122] W. Haverkamp and e. al, "Coagulation of ventricular myocardium using radiofrequency alternating current: bio-physical aspects and experimental findings," *Pacing Clin Electrophysiol,* vol. 12, pp. 187-195, 1989.

[123] D. Haines and e. al, "Electrode radius predicts lesion radius during radiofrequency energy heating. Validation of a proposed thermodynamic model," *Circ Res,* vol. 67, pp. 124-129, 1990.

[124] D. Haines and e. al, "Observations on electrode-tissue interface temperature and effect on electrical impedance during radiofrequency ablation of ventricular myocardium," *Circulation,* vol. 82, pp. 1034-1038, 1990.

[125] H. Nakagawa and e. al, "Comparison of In Vivo Tissue Temperature Profile and Lesion Geometry for Radiofrequency Ablation With a Saline-Irrigated Electrode Versus Temperature Control in a Canine Thigh Muscle Preparation," *Circulation,* vol. 91, pp. 2264-2273, 1995.

[126] C. Weiss and e. al, "Radiofrequency catheter ablation using cooled electrodes: impact of irrigation flow rate and catheter contact pressure on lesion dimensions," *Pacing Clin Electrophysiol,* vol. 25, pp. 463-469, 2002.

[127] H. Nakagawa and e. al, "Inverse relationship between electrode size and lesion size during radiofrequency ablation with active electrode cooling," *Circulation,* vol. 98, pp. 458-465, 1998.

[128] D. Haines and e. al, "Determinants of lesion size during radiofrequency catheter ablation: The role of electrode-tissue contact pressure and duration of energy delivery," *J Cardiovasc Electrophysiol,* vol. 2, pp. 509-515, 1991.

[129] H. Petersen and e. al, "Temperature-controlled radiofrequency ablation of cardiac tissue: an in vitro study of the impact of electrode orientation, electrode tissue contact pressure and external convective cooling," *J Interv Card Electrophysiol,* vol. 3, pp. 257-262, 1999.

[130] M. Wood and e. al, "Effect of electrode orientation on lesion sizes produced by irrigated radiofrequency ablation catheters," *J Cardiovasc Electrophysiol,* vol. 20, pp. 1262-1268, 2009.

[131] V. Reddy and e. al., "The relationship between contact force and clinical outcome during radiofrequency catheter ablation of atrial fibrillation in the TOCCATA study," *Heart rhythm,* vol. 9, no. 11, pp. 1789-1795, 2012.

[132] V. Reddy and e. al, "The relationship between contact force and clinical outcome during radiofrequency catheter ablation of atrial fibrillation in the TOCCATA study," *Heart Rhythm,* vol. 9, pp. 1789-1795, 2012.

[133] S. Haldar and e. al, "Contact force sensing technology identifies sites of inadequate contact and reduces acute pulmonary vein reconnection: A prospective case control study," *Int J Cardiol,* vol. 168, pp. 1160-1166, 2013.

[134] S. Kumar and e. al, "Effect of respiration on catheter-tissue contact force during ablation of atrial arrhythmias," *Heart Rhythm,* vol. 9, pp. 1041-1047, 2012.

[135] P. Neuzil and e. al, "Electrical Reconnection Following PVI is Contingent on Contact Force during Initial Treatment - Results From the EFFICAS I Study," *Circ Arrhythm Electrophysiol,* vol. 6, pp. 327-333, 2013.

[136] C. Sohns and e. al, "Quantitative Magnetic Resonance Imaging Analysis of the Relationship Between Contact Force and Left Atrial Scar Formation After Catheter Ablation of Atrial Fibrillation," *J Cardiovasc Electrophysiol,* vol. 25, pp. 138-145, 2014.

[137] W. Ullah and e. al, "Contact Force and Atrial Fibrillation Ablation," *Journal of atrial fibrillation.,* vol. 8, no. 5, 2016.

[138] L. Gepstein and e. al, "Atrial Linear Ablations in Pigs : Chronic Effects on Atrial Electrophysiology and Pathology," *Circulation,* vol. 100, pp. 419-426, 1999.

[139] J. Sanchez and e. al, "Identification of transmural necrosis along a linear catheter ablation lesion during atrial fibrillation and sinus rhythm," *J Interv Card Electrophysiol.,* vol. 8, pp. 9-17, 2003.

[140] K. Rajappan and e. al, "Acute and chronic pulmonary vein reconnection after atrial fibrillation ablation: a prospective characterization of anatomical sites," *Pacing Clin Electrophysiol,* vol. 31, pp. 1598-15605, 2008.

[141] C. Pappone and e. al, "Circumferential radiofrequency ablation of pulmonary vein ostia: A new anatomic approach for curing atrial fibrillation," *Circulation,* vol. 102, pp. 2619-2628, 2000.

[142] D. Schwartzman and e. al, "Electrogram-guided radiofrequency catheter ablation of atrial tissue comparison with thermometry-guide ablation: comparison with thermometry-guide ablation," *J Interv Card Electrophysiol,* vol. 5, pp. 253-266, 2001.

[143] K. Otomo and e. al, "Local unipolar and bipolar electrogram criteria for evaluating the transmurality of atrial ablation lesions at different catheter orientations relative to the endocardial surface," *Heart Rhythm,* vol. 7, pp. 1219-1300, 2010.

[144] S. Kumar and e. al., "Catheter-Tissue Contact Force Determines Atrial Electrogram Characteristics Before and Lesion Efficacy After Antral Pulmonary Vein Isolation in Humans," *J Cardiovasc Electrophysiol,* 2013.

[145] C. McGann and e. al, "New Magnetic Resonance Imaging-Based Method for Defining the Extent of Left Atrial Wall Injury After the Ablation of Atrial Fibrillation," *J Am Coll Cardiol,* vol. 52, pp. 1262-1271, 2008.

[146] T. Badger and e. al, "Evaluation of Left Atrial Lesions After Initial and Repeat Atrial Fibrillation Ablation Lessons Learned From Delayed-Enhancement MRI in Repeat Ablation Procedures.," *Circ Arrhythm Electrophysiol,* vol. 3, pp. 249-259, 2010.

[147] R. Hunter and e. al, "Diagnostic Accuracy of Cardiac Magnetic Resonance Imaging in the Detection and Characterization of Left Atrial Catheter Ablation Lesions: A Multicenter Experience," *J Cardiovasc Electrophysiol,* vol. 24, pp. 394-403, 2013.

[148] J. Harrison and e. al, "Cardiac magnetic resonance and electroanatomical mapping of acute and chronic atrial ablation injury: a histological validation study," *Eur Heart J,* p. eht560, 2014.

[149] P. Maury and e. al, "Three-dimensional mapping in theelectrophysiological laboratory," *Archives of Cardiovascular Disease,* vol. 111, p. 456—464, 2018.

[150] D. Packer and e. al, "Three-dimensional mapping in interventional electrophysiology: techniques and technology," *Journal of Cardiovascular Electrophysiology,* vol. 16, no. 10, p. 1110–1116, 2005.

[151] S. Sporton and e. al, "Electroanatomic versus fluoroscopic mapping for catheter ablation procedures: a prospective randomized study," *Journal of Cardiovascular Electrophysiology,* vol. 15, no. 3, p. 310–315, 2004.

[152] P. Della Bella and e. al, "2009," *Image integration-guided catheter ablation of atrial fibrillation: a prospective randomized study,* vol. 20, no. 3, p. 258–265, Journal of Cardiovascular Electrophysiology.

[153] M. Casella and e. al, "Near-zero” fluoroscopic exposure in supraventricular arrhythmia ablation using the EnSite NavX mapping system: personal experience and

review of the literature," *Journal of Interventional Cardiac Electrophysiology,* vol. 31, no. 2, p. 109–118, 2011.

[154] M. Earley and e. al, "Radiofrequency ablation of arrhythmias guided by non-fluoroscopic catheter location: a prospective randomized trial," *European Heart Journal,* vol. 27, no. 10, p. 1223–1229, 2006.

[155] M. Shurrab and e. al, "Three-dimensional localization versus fluoroscopically only guided ablations: a meta-analysis," *Scandinavian Cardiovascular Journal,* vol. 47, no. 4, p. 200–209, 2013.

[156] C. Schmitt and e. al, "Recent advances in cardiac mapping techniques," *Curr Cardiol Rep,* vol. 1, pp. 149-156, 1999.

[157] R. Hunter and e. al, "Comparisons for mapping technologies for cardiac electrophysiology," in *Cardiac Mapping (4th ed.)*, Hoboken, Wiley Blackwell, 2012, pp. 36-45.

[158] S. Ben-Haim and e. al, "Nonfluoroscopic, in vivo navigation and mapping technology," *Nat Med,* vol. 2, pp. 1393-1395, 1996.

[159] F. Wittkampf and e. al, "Accuracy of the LocaLisa system in catheter ablation procedures," *J Electrocardiol,* vol. 32, pp. 7-12, 1999.

[160] J. Romero and e. al, "Electroanatomic mapping systems (CARTO/EnSite NavX) vs. conventional mapping for ablation procedures in a training program," *J Interv Card Electrophysiol,* vol. 7, p. 71–80, 2016.

[161] D. Bhakta and e. al, "Principles of electroanatomic mapping Indian Pacing," *Electrophysiol J,* vol. 8, pp. 32-50, 2008.

[162] H. DeSena and e. al, "Future Diagnostic Strategies—Pediatric," in *Cardioskeletal Myopathies in Children and Young Adults*, Cininnati, Academic Press, 2017, pp. 361-379.

[163] P. Douglas and e. al, "Electroanatomical Mapping for Arrhythmias," in *Cardiac Electrophysiology: From Cell to Bedside (Seventh Edition)*, Philadelphia, Elsevier, 2018, pp. 574-587.

[164] R. Kabra and e. al, "Recent trends in imaging for atrial fibrillation ablation," *Indian Pacing Electrophysiol J,* vol. 10, pp. 215-227, 2010.

[165] Z. Issa and e. al, "A Companion to Braunwald's Heart Disease," in *Clinical Arrhythmology and Electrophysiology*, Philadelphia, Elsevier Science, 2009, pp. 157-176.

[166] S. Shpun and e. al, "Guidance of radiofrequency endocardial ablation with real-time three-dimensional magnetic navigation system," *Circulation,* vol. 96, pp. 2016-2021, 1997.

[167] G. Hayam and e. al, "Accuracy of the in vivo determination of location using a new nonfluoroscopic electroanatomical mapping system," *PACE,* vol. 19, p. 712, 1996.

[168] S. Shpun and e. al, "Guidance of radiofrequency endocardial ablation with real-time three-dimensional magnetic navigation system," *Circulation,* vol. 96, pp. 2016-2021, 1997.

[169] J. Smeets and e. al, "New method for nonfluoroscopic endocardial mapping in humans. Accuracy assessment and first clinical results," *Circulation,* vol. 97, pp. 2426-2432, 1998.

[170] K. Klabunde and e. al, "Complinace," in *Cardiovascular Physiology Concepts*, Philadelphia, Wolters Kluwer Health, 2021, p. 103.

[171] K. Toutouzas and e. al, "Echocardiographic features of left atrium in elite male athletes.," *The American journal of cardiology,* vol. 78, no. 11, pp. 1314-1317, 1996.

[172] Y. Kihara and e. al, "Role of the left atrium in adaptation of the heart to chronic mitral regurgitation in conscious dogs," *Circulation research,* vol. 62, no. 3, pp. 543-553, 1988.

[173] E. Leistad and e. al, "Effects of atrial fibrillation on left and right atrial dimensions, pressures, and compliances.," *American Journal of Physiology-Heart and Circulatory Physiology,* vol. 264, no. 4, pp. 1093-2007, 1993.

[174] D. Gibson and e. al, "Stiff left atrial syndrome after catheter ablation for atrial fibrillation: clinical characterization, prevalence, and predictors," *Heart Rhythm,* vol. 8, p. 1364–1371, 2011.

[175] C. Elayi and e. al, "Ablation for longstanding permanent," *Heart Rhythm,* vol. 5, p. 1658–1664, 2011.

[176] J. Park and e. al, "High left atrial pressures are associated with advanced electroanatomical remodeling of left atrium and independent predictors for clinical recurrence of atrial fibrillation after catheter ablation," *Heart Rhythm,* vol. 11, pp. 953-960, 2014.

[177] C. Hammerstingl and e. al, "Left atrial deformation imaging with ultrasound based two-dimensional speckle-tracking predicts the rate of recurrence of paroxysmal and

persistent atrial fibrillation after successful ablation procedures," *Journal of Cardiovascular Electrophysiology,* vol. 23, no. 3, pp. 247-255, 2012.

[178] C. Morillo and e. al, "Atrial fibrillation: the current epidemic," *J Geriatr Cardiol,* vol. 14, no. 3, pp. 195-203, 2017.

[179] D. Lane and e. al, "Temporal Trends in Incidence, Prevalence, and Mortality of Atrial Fibrillation in Primary Care," *JAMA,* vol. 6, no. 5, p. https://doi.org/10.1161/JAHA.116.005155, 2017.

[180] J. Donahue and e. al, "urrent state of the art for cardiac arrhythmia gene therapy," *Pharmacology & Therapeutics,* vol. 176, pp. 60-65, 2017.

[181] V. Robinson and e. al, "Basic Electrophysiology," in *Cardiac Arrhythmias, Pacing and Sudden Daeth*, London, Springer, 2017, pp. 1-13.

[182] E. Daoud and e. al, "Identification of Repetitive Activation Patterns Using Novel Computational Analysis of Multielectrode Recordings During Atrial Fibrillation and Flutter in Humans," *JACC,* vol. 3, no. 3, pp. 207-216, 2017.

[183] H. Tsao and e. al, "Functional Remodeling of Both Atria is Associated with Occurrence of Stroke in Patients with Paroxysmal and Persistent Atrial Fibrillation," *Acta Cardiol Sin,* vol. 33, no. 1, pp. 50-57, 2017.

[184] B. Hoit and e. al, "Left Atrial Remodeling More Than Just Left Atrial Enlargement," *Circulation: Cardiovascular Imaging,* vol. 10, p. e006036, 2017.

[185] M. Flannery and e. al, "State of the Art Review: Atrial Fibrillation in Athletes," *Heart and Lung Circulation,* vol. 26, no. 9, pp. 983-989, 2017.

[186] Q. Zhao and e. al, "Median nerve stimulation prevents atrial electrical remodelling and inflammation in a canine model with rapid atrial pacing," *Europace,* p. https://doi.org/10.1093/europace/eux003, 2017.

[187] H. Lim and e. al, "Complexity and Distribution of Drivers in Relation to Duration of Persistent Atrial Fibrillation," *JACC,* vol. 69, no. 10, pp. 1257-1569, 2017.

[188] J. Guichard and e. al, "Atrial Cardiomyopathy: A Useful Notion in Cardiac Disease Management or a Passing Fad?," *JACC,* vol. 70, no. 6, pp. 756-765, 2017.

[189] Y. Wang and e. al, "Electrophysiological remodelling in heart failure," *JMCC,* vol. 48, no. 4, pp. 619-632, 2010.

[190] S. Nattel and e. al, "Atrial Remodeling and Atrial Fibrillation: Mechanisms and Implications," *Circulation: Arrhythmia and Electrophysiology,* vol. 1, no. 1, pp. 62-73, 2008.

[191] S. Nattel and e. al, "New ideas about atrial fibrillation 50 years on," *Nature,* vol. 415, p. 219–226, 2002.

[192] M. Wijffels and e. al, "Atrial fibrillation begets atrial fibrillation: a study in awake chronically instrumented goats.," *Circulation,* vol. 92, pp. 1954-1968, 1995.

[193] S. Nattel and e. al, "Arrhythmogenic ion-channel remodeling in the heart: heart failure, myocardial infarction, and atrial fibrillation.," *Physiol Rev,* vol. 87, p. 425–456, 2007.

[194] G. Michael and e. al, "emodelling of cardiac repolarization: how homeostatic responses can lead to arrhythmogenesis.," *Cardiovasc Res,* vol. 81, p. 491–499, 2009.

[195] M. Wijffels and e. al, "Atrial Fibrillation Begets Atrial Fibrillation: A Study in Awake Chronically Instrumented Goats," *Circulation,* vol. 92, p. 1954–1968, 1995.

[196] L. Yue and e. al, "Ionic remodeling underlying action potential changes in a canine model of atrial fibrillation," *Circ Res,* vol. 81, pp. 512-525, 1997.

[197] T. Cha and e. al, "Kir3-based inward rectifier potassium current: potential role in atrial tachycardia remodeling effects on atrial repolarization and arrhythmias.," *Circulation,* vol. 113, pp. 1730-1737, 2006.

[198] D. Dobrev and e. al, "Molecular basis of downregulation of G-protein-coupled inward rectifying K+ current (IK,ACh) in chronic human atrial fibrillation: decrease in GIRK4 mRNA correlates with reduced IK,ACh and muscarinic receptor-mediated shortening of action potentials.," *Circulation,* vol. 104, p. 2551–2557, 2001.

[199] D. Dobrev and e. al, "The G-protein gated potassium current IK,ACh is constitutively active in patients with chronic atrial fibrillation," *Circulation,* vol. 112, p. 3697–3706, 2005.

[200] H. Sun and e. al, "Cellular mechanisms of atrial contractile dysfunction caused by sustained atrial tachycardia," *Circulation,* vol. 98, pp. 719-727, 1998.

[201] Y. Shi and e. al, "Remodeling of atrial dimensions and emptying function in canine models of atrial fibrillation," *Cardiovasc Res,* vol. 52, p. 217–225, 2001.

[202] B. Burstein and e. al, "Atrial fibrosis: mechanisms and clinical relevance in atrial fibrillation," *J Am Coll Cardiol,* vol. 61, p. 802–809, 2008.

[203] S. Nattel and e. al, "Atrial remodeling and atrial fibrillation: mechanisms and implications," *Circulation: Arrhythmia and Electrophysiology,* vol. 1, no. 1, pp. 62-73, 2008.

[204] A. Katz and e. al, "Proliferative signaling and disease progression in heart failure," *Circ J,* vol. 66, p. 225–231, 2002.

[205] L. Martinez-Lemus and e. al, "The Plastic Nature of the Vascular Wall: A Continuum of Remodeling Events Contributing to Control of Arteriolar Diameter and Structure," *APS,* vol. 24, no. 1, pp. 45-57, 2009.

[206] S. Kuppahally and e. al, "Left atrial strain and strain rate in patients with paroxysmal and persistent atrial fibrillation: relationship to left atrial structural remodeling detected by delayed-enhancement MRI," *Circulation: Cardiovascular Imaging,* vol. 3, no. 3, pp. 231-239, 2010.

[207] G. Casaclang-Verzosa and e. al, "Structural and functional remodeling of the left atrium: clinical and therapeutic implications for atrial fibrillation.," *Journal of the American College of Cardiology,* vol. 51, no. 1, pp. 1-11, 2008.

[208] R. Inciardi and e. al, "Mitral regurgitation, left atrial structural and functional remodelling and the effect on pulmonary haemodynamics," *European Journal of Heart Failure,* vol. 22, no. 3, pp. 499-506, 2020.

[209] F. D'Ascenzi and e. al, "Increased left atrial size is associated with reduced atrial stiffness and preserved reservoir function in athlete's heart," *The international journal of cardiovascular imaging,* vol. 31, no. 4, pp. 699-705, 2015.

[210] T. Lin, F. Ouyang, K. Kuck and R. Tilz, "ThermoCool® SmartTouch® Catheter – The Evidence So Far For Contact Force Technology And The Role Of VisiTag™ Module," *AER,* vol. 3, no. 1, p. 44, 2014.

[211] K. Yokoyama and e. al, "Novel contact force sensor incorporated in irrigated radiofrequency ablation catheter predicts lesion size and incidence of steam pop and thrombus," *Circ Arrhythm Electrophysiol,* vol. 1, pp. 354-362, 2008.

[212] L. Gepstein and e. al, "A novel method for nonfluoroscopic catheter-based electroanatomical mapping of the heart in vitro and in vivo assuracy results," *Circulation,* vol. 95, pp. 1611-1622, 1997.

[213] R. Kabra and e. al, "Recent trends in imaging for atrial fibrillation ablation," *Indian Pacing Electrophysiol J,* vol. 10, pp. 215-227, 2010.

[214] H. Nakagawa and e. al, "Controlling Lesion Size and Incidence of Steam Pop by Controlling Contact Force and Radiofrequency Power in Canine Beating Heart," *Circulation,* vol. 122, p. A15777, 2010.

[215] F. Perna and e. al, "Assessment of catheter tip contact force resulting in cardiac perforation in swine atria using force sensing technology," *Circ Arrhythm Electrophysiol,* vol. 2, pp. 218-224, 2011.

[216] F. Berjano and e. al, "A cooled intraesophageal balloon to prevent thermal injury during endocardial surgical radiofrequency ablation of the left atrium: a finite element study," *Physics in medicine & Biology,* vol. 20, p. 50, 2005.

[217] R. Hunter and e. al, "Left Atrial Wall Stress Distribution and Its Relationship to Electrophysiologic Remodeling in Persistent Atrial Fibrillation," *Circulation: Arrhythmia and Electrophysiology,* vol. 5, pp. 351-360, 2012.

[218] L. Alvarez and e. al, "The swine heart: the papillo-tendino-valvular system of the right ventricle," *Anatomia Histologia Embryologia,* vol. 22, pp. 319-323, 1993.

[219] R. Hamlin and e. al, "The QRS electrocardiogram, epicardiogram, vectrocardiogram, and ventricular excitation in swine," *American Journal of Physiology,* vol. 198, pp. 537-542, 1960.

[220] T. Bowman and e. al, "Swine as an in vivo model for electrophysiologic evaluation of cardiac pacing parameters," *PACE,* vol. 7, pp. 187-194, 1984.

[221] T. Opthof and e. al, "Functional morphology of the pig sinoatrial node," *Journal of Molecular and Cellular Cardiology,* vol. 19, pp. 1221-1236 , 1987.

[222] G. Lumb and e. al, "Experimentally induced cardiac failure in swine:pathological changes," in *Swine in Biomedical Research*, Seattle, Elsevier, 1966, pp. 389-403.

[223] D. Cooper and e. al, "The pig as potential organ donor for man," in *Xenotransplantation: The Transplantation of Organs and Tissues Between Species*, Berlin, Springer, 1991, pp. 480-500.

[224] S. Crick and e. al, "Anatomy of the pig heart: comparisons with normal human cardiac structure," *JAnt,* vol. 193, pp. 105-119, 1998.

[225] R. Anderson and e. al, The Heart: Structure in Health and Disease, London: Gower Medical, 1992.

[226] X. Feng and e. al, "Effects of storage temperature and fetal calf serum on the endothelium of porcine aortic valves," *The Journal of thoracic and cardiovascular surgery,* vol. 11, no. 1, pp. 218-230, 1996.

[227] J. Corner and e. al, "Preservation of vascular tissue under hypothermic conditions," *Journal of Surgical Research,* vol. 113, no. 1, pp. 21-25, 2003.

[228] H. Piepot and e. al, "Cold storage sensitizes rat femoral artery to an endotoxin-induced decrease in endothelium-dependent relaxation," *Journal of Surgical Research,* vol. 105, no. 2, pp. 189-194, 2002.

[229] C. Bellini and e. al, "Mechanical behaviour of human atria," *Annals of biomedical engineering,* vol. 41, no. 7, pp. 1478-1480, 2013.

[230] B. Hall and e. al, "Variation in left atrial transmural wall thickness at sites commonly targeted for ablation of atrial fibrillation," *Journal of Interventional Cardiac Electrophysiology,* vol. 17, no. 2, pp. 127-132, 2006.

[231] R. Kobza and e. al, "Late recurrent arrhythmias after ablation of atrial fibrillation: incidence, mechanism, and treatment," *Heart Rhythm,* vol. 1, no. 6, pp. 676-683, 2004.

[232] M. Townsley and e. al, "Structure and composition of pulmonary arteries, capillaries and veins," *Compr Physiol,* vol. 1, no. 2, pp. 675-709, 2012.

[233] J. Donahue and e. al, "Current state of the art for cardiac arrhythmia gene therapy," *Pharmacology & Therapeutics,* vol. 176, pp. 60-65, 2017.

[234] V. Robinson and e. al, "Basic Electrophysiology," in *Cardiac Arrhythmias, Pacing and Sudden Daeth*, London, Springer, 2017, pp. 1-13.

[235] D. Lane and e. al, "Temporal Trends in Incidence, Prevalence, and Mortality of Atrial Fibrillation in Primary Care," *JAMA,* vol. 6, no. 5, 2017.

[236] W. Ullah and e. al, "Factors affecting catheter contact in the human left atrium and their impact on ablation efficacy," *J Cardiovasc Electrophysiol,* vol. 26, pp. 129-136, 2015.

[237] G. Holzapfel and e. al, "Anisotropic mechanical properties of tissue components in human atherosclerotic plaques," *Journal of biomechanical engineering,* vol. 126, no. 5, pp. 657-665, 2004.

[238] J. Park and e. al, "Low left atrial compliance contributes to the clinical recurrence of atrial fibrillation after catheter ablation in patients with structurally and atrial fibrillation after catheter ablation in patients with structurally and functionally normal heart.," *PLoS One,* vol. 10, no. 12, 2015.

[239] E. Benjamin and e. al, "Independent risk factors for atrial fibrillation in a population-based cohort. The Framingham Heart Study," *JAMA,* vol. 271, pp. 840-844, 1994.

[240] A. Camm and e. al, "Guidelines for the management of atrial fibrillation: the Task Force for the Management of Atrial Fibrillation of the European Society of Cardiology (ESC)," *European Heart Journal,* vol. 31, no. 19, pp. 2369-2429, 2010.

[241] M. Haissaguerre and e. al, "Spontaneous initiation of atrial fibrillation by ectopic beats originating in the pulmonary veins.," *New England Journal of Medicine,* vol. 339, no. 10, pp. 659-666, 1998.

[242] W. Ullah and e. al, "Impact of steerable sheaths on contact forces and reconnection sites in ablation for persistent atrial fibrillation.," *Journal of Cardiovascular Electrophysiology,* vol. 26, no. 3, pp. 266-273, 2015.

[243] T. Arentz and e. al, "Small or large isolation areas around the pulmonary veins for the treatment of atrial fibrillation? Results from a prospective radomized study," *Circulation,* vol. 115, no. 24, pp. 3057-3063, 2007.

[244] R. Proietti and e. al, "Comparative effectiveness of wide antral versus ostial pulmonary vein isolation: a systematic review and meta-analysis," *Circulation: Arrhythmia and Electrophysiology,* vol. 7, no. 1, pp. 39-45, 2014.

[245] R. Bacquelin and e. al, "A novel method for localization and ablation of conduction gaps after wide antral circumferential ablation of pulmonary veins," *Archives of cardiovascular diseases,* vol. 111, no. 5, pp. 340-348, 2018.

[246] R. Grimm and e. al, "Characterization of left atrial appendage Doppler flow in atrial fibrillation and flutter by Fourier analysis," *American heart journal,* vol. 132, no. 2, pp. 286-296, 1996.

[247] K. Yokoyama and e. al, "Novel contact force sensor incorporated in irrigated radiofrequency ablation catheter predicts lesion size and incidence of steam pop and thrombus," *Circ Arrhymia Electrophysiol,* vol. 1, pp. 354-362, 2008.

[248] M. Wood and e. al, "ffect of electrode orientation on lesion sizes produced by irrigated radiofrequency ablation catheters," *J Cardiovasc Electrophysiol,* vol. 20, pp. 1262-1268, 2009.

[249] A. DeBortoli and e. al, "Ablation Effect Indicated by Impedance Fall is Correlated with Contact Force Level During Ablation for Atrial Fibrillation.," *J. Cardiovasc. Electrophysiol,* vol. 24, p. 1210–1215, 2013.

[250] S. Knecht and e. al, "Contact force and impedance decrease during ablation depends on catheter location and orientation: insight from pulmonary vein isolation using contact force-sensing catheter.," *J interv Card Electrophysiol.,* pp. 433-442, 2015.

[251] O. Eick and e. al, "Popping phenomena in temperature-controlled radiofrequency ablation: When and why do they occur?," *Pacing Clin Electrophysiol,* pp. 253-258, 2000..

[252] D. Shah and e. al, "Area under the real-time contact force curve (force-time integral) predicts radiofrequency lesion size in an in vitro contractile model," *J Cardiovasc Electrophysiol,* pp. 1038-1043, 2010.

[253] S. Haldar and e. al, "Contact force sensing technology identifies sites of inadequate contact and reduces acute pulmonary vein reconnection: A prospective case control study.," *Int J Cardiol,* pp. 1160-1166, 2013.

[254] P. Neuzil and e. al, "Electrical reconnection following PVI is contingent on contact force during initial treatment—Results from the EFFICAS I study.," *Circ Arrhythm Electrophysiol,* pp. 327-333, 2013.

[255] D. Gelman and e. al, "liminating the effects of motion during radiofrequency lesion delivery using a novel contact-force controller.," *Journal of Cardiovascular Electrophysiology,* vol. 30, no. 9, pp. 1652-1662, 2019.

[256] D. Gelman and e. al, "Design and evaluation of a catheter contact-force controller for cardiac ablation therapy," *IEEE Trans Biomed Eng.,* vol. 63, no. 11, pp. 2301-2307, 2016.

[257] O. Inaba and e. al, "trial fibrillation type matters: greater infarct volume and worse neurological defects seen in acute cardiogenic cerebral embolism due to persistent or permanent rather than paroxysmal atrial fibrillation," *EP Europace,* vol. 20, no. 10, pp. 1591-1597, 2018.

[258] A. Boldt and e. al, "Fibrosis in left atrial tissue of patients with atrial fibrillation with and without underlying mitral valve disease," *Heart,* vol. 90, pp. 400-405, 2004.

[259] A. Goette and e. al, "EHRA/HRS/APHRS/SOLAECE expert consensus on atrial cardiomyopathies: definition, characterization, and clinical implication," *Europace,* vol. 18, pp. 1455-1490, 2016.

[260] J. Shirani and e. al, "Structural remodeling of the left atrial appendage in patients with chronic non-valvular atrial fibrillation: Implications for thrombus formation, systemic embolism, and assessment by transesophageal echocardiography," *Cardiovasc Pathol,* vol. 9, pp. 95-101, 2009.

[261] A. Raymond-Paquin and e. al, "Catheter ablation: An ongoing revolution," *Journal of thoracic disease,* vol. 11, no. 3, 2019.

[262] S. Sanjoy and e. al, "omorbidity burden in patients undergoing left atrial appendage closure," *Heart,* vol. 107, no. 15, pp. 1246-1253., 2021.

[263] S. Mohammed and e. al, "omorbidity and ventricular and vascular structure and function in heart failure with preserved ejection fraction: a community-based stud," *Circulation: Heart Failure,* vol. 5, no. 6, pp. 710-719, 2012.

[264] R. Dhingra and e. al, "Diabetes and the risk of heart failure," *Heart Fail Clin,* vol. 8, pp. 125-133, 2012.

[265] S. Murarka and e. al, "Diabetic cardiomyopathy," *J Card Fail,* vol. 16, pp. 971-979, 2010.

[266] P. Pateinakis and e. al, "Cardiorenal syndrome type 4-cardiovascular disease in patients with chronic kidney disease: epidemiology, pathogenesis, and management.," *Int J Nephrol,* vol. 2011:938651, 2011.

[267] F. Martin and e. al, "Experimental mild renal insufficiency mediates early cardiac apoptosis, fibrosis, and diastolic dysfunction: a kidney-heart connection," *m J Physiol Regul Integr Comp Physiol,* vol. 302, pp. 292-299, 2012.

[268] M. Charlson and e. al, "A new method of classifying prognostic comorbidity in longitudinal studies: development and validation," *J Chronic Dis,* vol. 40, pp. 373-83, 1987.

[269] A. Elixhauser and e. al, "Comorbidity measures for use with administrative data," *Med Care,* vol. 36, pp. 8-27, 1998.

[270] D. Wyse and e. al, "Lone atrial fibrillation: does it exist?," *Journal of the American College of Cardiology,* vol. 63, no. 17, pp. 1715-1723, 2014.

[271] W. Henry and e. al, "Relation between echocardiographically determined left atrial size and atrial fibrillation," *Circulation,* vol. 53, pp. 273-279, 1976.

[272] J. Goy and e. al, "Restoration of sinus rhythm with flecainide in patients with atrial fibrillation," *m J Cardiol,* vol. 62, pp. 38-40, 1988.

[273] M. Brodsky and e. al, "Factors determining maintenance of sinus rhythm after chronic atrial fibrillation with left atrial dilatation," *Am J Cardiol,* vol. 63, pp. 1065-1068, 1989.

[274] W. Manning and e. al, "Impaired left atrial mechanical function after cardioversion: relation to the duration of atrial fibrillation," *J Am Coll Cardiol,* vol. 23, pp. 1535-1540, 1994.

[275] J. Ausma and e. al, "Structural changes of atrial myocardium due to sustained atrial fibrillation in the goat," *Circulation,* vol. 96, pp. 3157-3163, 1997.

[276] R. Gaspo and e. al, "Functional mechanisms underlying tachycardia-induced sustained atrial fibrillation in a chronic dog model," *Circulation,* vol. 96, pp. 4027-4035, 1997.

[277] U. Schotten and e. al, "Electrical and contractile remodeling during atrial fibrillation go hand-in-hand," *PACE,* vol. 24, p. 572, 2001.

[278] A. Elvan and e. al, "Pacing-induced chronic atrial fibrillation impairs sinus node function in dogs. Electrophysiological remodeling,," *Circulation,* vol. 94, pp. 2953-2960, 1996.

[279] E. Manios and e. al, "Changes in atrial electrical properties following cardioversion of chronic atrial fibrillation: relation with recurrence," *Cardiovasc Res,* vol. 47, pp. 244-253, 2000.

[280] P. Sparks and e. al, "lectrical remodeling of the atria associated with paroxysmal and chronic atrial flutter," *Circulation,* vol. 102, pp. 1807-1813, 2000.

[281] E. Daoud and e. al, "Short-term effect of atrial fibrillation on atrial contractile function in humans," *Circulation,* vol. 99, pp. 3024-3027, 1999.

[282] S. Fareh and e. al, "Importance of refractoriness heterogeneity in the enhanced vulnerability to atrial fibrillation induction caused by tachycardia-induced atrial electrical remodeling," *Circulation,* vol. 98, pp. 2202-2209, 1998.

[283] S. Lee and e. al, "ffect of verapamil on long-term tachycardia-induced atrial electrical remodeling,," *Circulation,* vol. 101, pp. 200-206, 2000,.

[284] D. Sideris and e. al, "Atrial pressure and experimental atrial fibrillation," *Pacing Clin Electrophysiol,* vol. 18, pp. 1679-1685, 1995.

[285] F. Ravelli and e. al, "Effects of atrial dilatation on refractory period and vulnerability to atrial fibrillation in the isolated Langendorff-perfused rabbit heart," *Circulation,* vol. 1695, p. 1686, 1997.

[286] A. Ganesan and e. al, "The impact of atrial fibrillation type on the risk of thromboembolism, mortality, and bleeding: a systematic review and meta-analysis," *Eur Heart J,* vol. 37, pp. 1591-1602, 2016.

[287] G. Boriani and e. al, "Optimizing indices of atrial fibrillation susceptibility and burden to evaluate atrial fibrillation severity, risk and outcome," *Cardiovascular research,* vol. 117, no. 7, pp. 1-21, 2021.

[288] S. Mahmood and e. al, "The Framingham Heart Study and the epidemiology of cardiovascular disease: a historical perspective," *The Lancet,* vol. 383, no. 9921, pp. 999-1008, 2014.

[289] D. Ko and e. al, "Atrial fibrillation in women: epidemiology, pathophysiology, presentation, and prognosis," *Nature Reviews Cardiology,* vol. 13, no. 6, pp. 321-332, 2016.

[290] S. Chugh and e. al, "Worldwide epidemiology of atrial," *Circulation,* vol. 129, pp. 837-847, 2014.

[291] K. Chien and e. al, "Atrial fibrillation prevalence,incidence and risk of stroke and all-cause death among Chinese," *Int. J. Cardiol,* vol. 139, pp. 173-180, 2010.

[292] Y. Miyasaka and e. al, "Secular trends in incidence of atrial fibrillation in Olmsted County, Minnesota 1980 to 2000, and implications on the projections for future prevalence," *Circulation,* vol. 114, pp. 119-125, 2006.

[293] T. Wilke and e. al, "Incidence and prevalence of atrial fibrillation: an analysis based on 8.3 million patients," *Europace,* vol. 15, pp. 486-493, 2013.

[294] T. Wang and e. al, "Obesity and the risk of new-onset atrial fibrillation," *JAMA,* vol. 292, pp. 2471-2477, 2004.

[295] T. Potpara and e. al, "Gender-related differences in presentation, treatment and long-term outcome in patients with first-diagnosed atrial fibrillation and structurally normal heart: the Belgrade atrial fibrillation study," *Int. J. Cardiol,* vol. 161, pp. 39-44, 2012.

[296] I. Christophersen and e. al, "Familial aggregation of atrial fibrillation: a study in Danish twins," *Circ. Arrhythm Electrophysiol,* vol. 2, pp. 378-383, 2009.

[297] P. Ellinor and e. al, "Familial aggregation in lone atrial fibrillation," *Hum. Genet,* vol. 118, pp. 179-184, 2005.

[298] J. Ball and e. al, "Women versus men with chronic atrial fibrillation: insights from the Standard versus Atrial Fibrillation spEcific managemenT studY (SAFETY)," *PLoS ONE,* vol. 8, p. e65795, 2013.

[299] S. Vaziri and e. al, "Echocardiographic predictors of nonrheumatic atrial fibrillation. The Framingham Heart Study," *Circulation,* vol. 89, pp. 724-730, 1994.

[300] S. Kishi and e. al, "Race-ethnic and sex differences in left ventricular structure and function: the Coronary Artery Risk Development in Young Adults (CARDIA) Study," *J. Am. Heart Assoc,* vol. 4, p. e001264, 2015.

[301] T. Tsang and e. al, "Left atrial volume: important risk marker of incident atrial fibrillation in 1655 older men and women," *Mayo Clin. Proc,* vol. 76, pp. 467-475, 2001.

[302] A. Khera and e. al, "Race and gender differences in C-reactive protein levels," *J. Am. Coll. Cardiol,* vol. 46, pp. 464-469, 2005.

[303] J. Mathew and e. al, "Fibroblast growth factor-23 and incident atrial fibrillation: the Multi-Ethnic Study of Atherosclerosis (MESA) and the Cardiovascular Health Atherosclerosis (MESA) and the Cardiovascular Health Study (CHS)," *Circulation,* vol. 130, pp. 298-307, 2014.

[304] H. e. a. Cochet, " Age, atrial fibrillation, and structural heart disease are the main determinants of left atrial fibrosis detected by delayed-enhanced magnetic resonance imaging in a general cardiology population," *J. Cardiovasc. Electrophysiol.,* vol. 26, pp. 484-492, 2015.

[305] J. Diez and e. al, "Losartan-dependent regression of myocardial fibrosis is associated with reduction of left ventricular chamber stiffness in hypertensive patients," *Circulation,* vol. 280, pp. 554-561, 2002.

[306] R. Pai and e. al, "Mitral A velocity wave transit time to the outflow tract as a measure of left ventricular diastolic stiffness: hemodynamic correlations in patients with coronary artery disease," *Circulation,* vol. 89, pp. 553-557, 1994.

[307] S. Solomon and e. al, "Left-ventricular diastolic function of remodeled myocardium in dogs with pacing-induced heart failure," *Am J Physiol,* vol. 43, pp. 944-945, 1998.

[308] J. Stulak and e. al, "Left ventricular dysfunction in atrial fibrillation: restoration of sinus rhythm by the Cox-maze procedure significantly improves systolic function and functional status.," *The Annals of thoracic surgery,* vol. 82, no. 2, pp. 494-501, 2006.

[309] S. Pabel and e. al, "Atrial fibrillation impairs ventricular function by altering excitation-contraction coupling in the human heart," *European Heart Journal 41.Supplement_2,* pp. ehaa946-3711, 2020.

[310] S. Hudson and e. al, "What is ‘normal’left ventricular ejection fraction?," *Heart,* 2020.

[311] C. Ozcan and e. al, "Significant effects of atrioventricular node ablation and pacemaker implantation on left ventricular function and long-term survival in patients with atrial fibrillation and left ventricular dysfunction," *Am J Cardiol,* vol. 92, pp. 33-37, 2003.

[312] T. Tsang and e. al, "Left ventricular diastolic dysfunction as a predictor of the first diagnosed nonvalvular atrial fibrillation in 840 elderly men and women," *J Am Coll Cardiol,* vol. 40, pp. 1636-1644, 2002.

[313] T. Foley and e. al, "Measuring left ventricular ejection fraction-techniques and potential pitfalls," *ur Cardiol,* vol. 8, no. 2, pp. 108-114, 2012.

[314] B. Olshansky and e. al, "Are transthoracic echocardiographic parameters associated with atrial fibrillation recurrence or stroke? Results from the Atrial Fibrillation Follow-Up Investigation of Rhythm Management (AFFIRM) study," . *J Am Coll Cardiol,* vol. 45, pp. 2026-2033, 2005.

[315] H. Kim and e. al, "eft atrial dysfunction, fibrosis and the risk of thromboembolism in patients with paroxysmal and persistent atrial fibrillation," *International Journal of Heart Failure,* vol. 4, no. 1, pp. 42-53, 2022.

[316] L. Caplan and e. al, "Atrial size, atrial fibrillation, and stroke," *Ann Neurol,* vol. 19, pp. 158-161, 1986.

[317] A. Moulton and e. al, "Risk factors for stroke in patients with nonrheumatic atrial fibrillation," *Am J Med,* vol. 91, pp. 156-161, 1991.

[318] J. Anderson and e. al, "trial dimensions in health and left ventricular disease using cardiovascular magnetic resonance," *J Cardiovasc Magn Reson,* vol. 7, no. 4, pp. 671-675., 2005.

[319] L. Tops and e. al, "Multi-modality imaging to assess left atrial size, anatomy and function," *Heart,* vol. 93, no. 11, pp. 1461-1470, 2007.

[320] C. Otto and e. al, Textbook of clinical echocardiography., Elsevier Health Sciences, 2013.

[321] E. Anyukhovsky and e. al, "ge-associated changes in electrophysiologic remodeling: a potential contributor to initiation of atrial fibrillation," *Cardiovascular research,* vol. 66, no. 2, pp. 353-363, 2005.

[322] M. Redfield and e. al, "Age-and gender-related ventricular-vascular stiffening: a community-based study," *Circulation,* vol. 112, no. 15, pp. 2254-2262, 2005.

[323] J. Díez and e. al, "Arterial stiffness and extracellular matrix," *Atherosclerosis, Large Arteries and Cardiovascular Risk,* vol. 44, pp. 76-95, 2007.

[324] Y. Yoon and e. al, "Left atrial mechanical function and stiffness in patients with paroxysmal atrial fibrillation," *ournal of cardiovascular ultrasound,* vol. 20, no. 3, pp. 140-145, 2012.

[325] M. Demir and e. al, "Left atrial mechanical function and stiffness in patients with atrial septal aneurysm: a speckle tracking study.," *Cardiology Journal,* vol. 22, no. 5, pp. 535-540, 2015.

[326] B. Hall and e. al, "Variation in left atrial transmural wall thickness at sites commonly targeted for ablation of atrial fibrillation," *Journal of Interventional Cardiac Electrophysiology,* vol. 17, no. 2, pp. 127-132, 2006.

[327] R. Kobza and e. al, "Late recurrent arrhythmias after ablation of atrial fibrillation: incidence, mechanism, and treatment," *Heart Rhythm,* vol. 1, no. 6, pp. 676-683, 2004.

[328] M. Townsley, "Structure and composition of pulmonary arteries, capillaries and veins," *Compr Physiol,* vol. 1, no. 2, pp. 675-709, 2012.

[329] N. Marrouche and e. al, "Association of atrial tissue fibrosis identified by delayed enhancement MRI and atrial fibrillation catheter ablation: the DECAAF stud," *JAMA,* vol. 311, no. 5, pp. 498-506, 2014.

[330] S. Kapa and e. al, "Contact Electroanatomic Mapping Derived Voltage Criteria for Characterizing Left Atrial Scar in Patients Undergoing Ablation for Atrial Fibrillation.," *J Cardiovasc Electrophysiol,* 2014.

[331] D. Lloyd-Jones, T. Wang, E. Leip, M. Larson, D. Levy, R. Vasan and e. al, "Lifetime risk for development of atrial fibrillation in adults: national implications for rhythm management and stoke prevention: the AnTicoagulation and Risk Factors in Atrial Fibrillation (ATRIA) Study," *JAMA,* vol. 285, no. 18, pp. 2370-2375, 2004.

[332] A. Go, E. Hylek, K. Phillips, Y. Chang, L. Henault, J. Selby and e. al, "Prevalence of diagnosed atrial fibrillaion in adults: national implications for rhythm management and stroke prevention: the AnTicoagulation and Risk Factors in Atrial Fibrillation (Atria) Study," *JAMA,* vol. 18, no. 2370-2375, p. 285, 2001.

[333] O. J. W. J. C. W. Duff H.J., "lass I and IV antiarrhythmic drugs and cytosolic calcium regulate mRNA encoding the sodium channel α subunit in rat cardiac muscle," *Mol Pharmacol,* vol. 42, pp. 570-574, 1992.